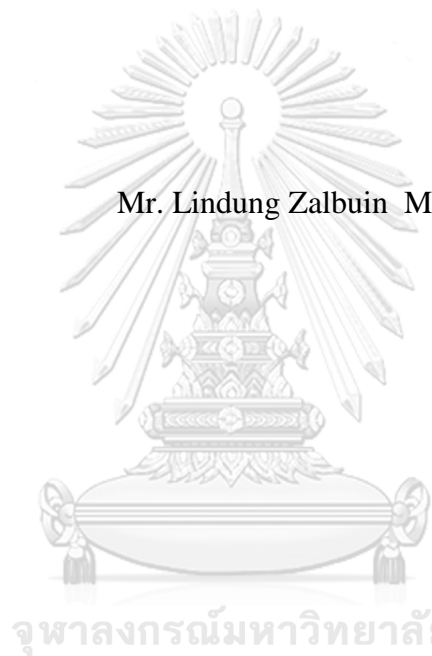


STUDY OF LIQUEFACTION MECHANISM IN CHIANG RAI PROVINCE

Mr. Lindung Zalbuin Mase



บทคัดย่อและแฟ้มข้อมูลฉบับเต็มของวิทยานิพนธ์ตั้งแต่ปีการศึกษา 2554 ที่ให้บริการในคลังปัญญาจุฬาฯ (CUIR)
เป็นแฟ้มข้อมูลของนิสิตเจ้าของวิทยานิพนธ์ ที่ส่งผ่านทางบัณฑิตวิทยาลัย

The abstract and full text of theses from the academic year 2011 in Chulalongkorn University Intellectual Repository (CUIR)
are the thesis authors' files submitted through the University Graduate School.

A Dissertation Submitted in Partial Fulfillment of the Requirements
for the Degree of Doctor of Philosophy Program in Civil Engineering
Department of Civil Engineering
Faculty of Engineering
Chulalongkorn University
Academic Year 2017
Copyright of Chulalongkorn University

การศึกษากลไกการเกิดทรายเหลวที่จังหวัดเชียงราย



วิทยานิพนธ์นี้เป็นส่วนหนึ่งของการศึกษาตามหลักสูตรปริญญาวิศวกรรมศาสตรดุษฎีบัณฑิต

สาขาวิชาวิศวกรรมโยธา ภาควิชาวิศวกรรมโยธา

คณะวิศวกรรมศาสตร์ จุฬาลงกรณ์มหาวิทยาลัย

ปีการศึกษา 2560

ลิขสิทธิ์ของจุฬาลงกรณ์มหาวิทยาลัย

Thesis Title STUDY OF LIQUEFACTION MECHANISM IN
 CHIANG RAI PROVINCE
By Mr. Lindung Zalbuin Mase
Field of Study Civil Engineering
Thesis Advisor Professor Suched Likitlersuang

Accepted by the Faculty of Engineering, Chulalongkorn University in
Partial Fulfillment of the Requirements for the Doctoral Degree

..... Dean of the Faculty of Engineering
(Associate Professor Dr. Supot Teachavorasinskun)

THESIS COMMITTEE

..... Chairman
(Associate Professor Dr. Supot Teachavorasinskun)

..... Thesis Advisor
(Professor Suched Likitlersuang)

..... Examiner
(Associate Professor Dr. Tirawat Boonyatee)

..... Examiner
(Associate Professor Dr. Boonchai Ukritchon)

..... External Examiner
(Associate Professor Dr. Tetsuo Tobita)

จุฬาลงกรณ์มหาวิทยาลัย
CHULALONGKORN UNIVERSITY

ลินดุง ซาบูอิน เมส : การศึกษากลไกการเกิดทรายเหลวที่จังหวัดเชียงราย (STUDY OF LIQUEFACTION MECHANISM IN CHIANG RAI PROVINCE) อ.ที่ปรึกษา
วิทยานิพนธ์หลัก: สุเชษฐ์ ลิขิตเลอสรวง, หน้า.

ทางภาคเหนือของประเทศไทยได้เผชิญภัยแผ่นดินไหวครั้งใหญ่ถึง 2 ครั้งคือ แผ่นดินไหวที่ศูนย์กลางอยู่ที่เมืองทาร์เลย์ในประเทศเมียนมาปี ค.ศ. 2011 และแผ่นดินไหวที่อ.แม่ลาว จ. เชียงรายในปี ค.ศ. 2014 งานวิจัยนี้จึงดำเนินการศึกษาการเกิดทรายเหลวระหว่างการเกิดแผ่นดินไหวโดยเฉพาะในจังหวัดเชียงราย งานวิจัยนี้เริ่มจากการวิเคราะห์ด้วยสูตรเชิงประสบการณ์โดยใช้ข้อมูลในหลายพื้นที่ในภาคเหนือ การศึกษาผลตอบสนองแผ่นดินไหวสามารถนำไปใช้ประเมินผลของการแผ่ขยายของคลื่นแผ่นดินไหวในชั้นดินได้ นอกเหนือจากนี้ มีการสำรวจพื้นที่ด้วยการทดสอบไมโครทริบเมออร์และการวิเคราะห์สเปกตรัมคลื่นผิวดินบริเวณพื้นที่ที่เคยเกิดทรายเหลวในระหว่างแผ่นดินไหวทั้งสองครั้ง การวิเคราะห์ผลตอบสนองต่อการเกิดทรายเหลวแบบหนึ่งมิติเพื่อสังเกตพฤติกรรมพลศาสตร์ของชั้นดินพบว่า ชั้นทรายชั้นแรกและชั้นที่สองของบริเวณที่ทำการศึกษามีโอกาสการเกิดทรายเหลวก่อนข้างสูง นอกเหนือจากนี้ ผลวิเคราะห์การแผ่ขยายของคลื่นพบว่า ที่บริเวณอ.แม่สาย ชายแดนไทย-เมียนมา อาจเกิดความเสียหายต่ออาคารความสูงปานกลางจากการขยายตัวของคลื่นแผ่นดินไหวได้ เนื่องจากการสั่นพ้องระหว่างดินและโครงสร้าง ส่วนผลการสำรวจพื้นที่ยังพบว่าสภาพทางธรณีวิทยาประกอบไปด้วยชั้นดินตะกอนของแม่น้ำที่มีความต้านทานต่อแรงเฉือนค่อนข้างต่ำ พฤติกรรมของดินพวกนี้ระหว่างการแผ่ขยายคลื่นน่าจะโอกาสเกิดทรายเหลวได้ง่าย การศึกษานี้มาใช้แนะนำวิศวกรท้องถิ่นเพื่อให้ตระหนักถึงความไม่ปลอดภัยต่อแผ่นดินไหวและการเกิดทรายเหลวในพื้นที่ภาคเหนือ โดยเฉพาะในจังหวัดเชียงรายได้

CHULALONGKORN UNIVERSITY

ภาควิชา วิศวกรรมโยธา

ลายมือชื่อนิลิขิต

สาขาวิชา วิศวกรรมโยธา

ลายมือชื่อ อ.ที่ปรึกษาหลัก

ปีการศึกษา 2560

5771481921 : MAJOR CIVIL ENGINEERING

KEYWORDS: EARTHQUAKE, LIQUEFACTION, LOCAL SITE INVESTIGATION, GROUND RESPONSE ANALYSIS, SOIL BEHAVIOUR

LINDUNG ZALBUIN MASE: STUDY OF LIQUEFACTION MECHANISM IN CHIANG RAI PROVINCE. ADVISOR: PROF. DR. SUCHED LIKITLERSUANG, pp.

Learning from the Tarlay Earthquake in 2011 and Mae Lao Earthquake in 2014, the intensive study of soil liquefaction in Northern Thailand, particularly in Chiang Rai Province, was performed. This study was initiated by conducting the empirical analysis to the several sites in Northern Thailand. Furthermore, the seismic ground response analysis was performed to investigate the effect of wave propagation through the soil layers. Local site investigations including microtremor and spectral analysis of surface waves tests were performed to the liquified locations during both earthquakes. One-dimensional liquefaction site response analysis was performed to observe soil behaviour during the earthquake. The results showed that the first and second sand layers in the study area were possible to liquefy. The propagating wave at the ground surface showed that at the border of Thailand-Myanmar could gain the serious impact due to the amplifying wave, which was predicted to contribute to the medium-high rise buildings damage. Soil behaviour under dynamic load also indicated liquefaction could happen. The resonance between ground structure and ground motion was occurred and possibly increased a worse damage in the study area. The local site investigation showed that the existence of low shearing resistance in the liquified site dominated by alluvial deposits in the study area. Generally, this study could give a recommendation to the local engineers to reconsider the earthquake and liquefaction impacts to structure design in Northern Thailand.

Department: Civil Engineering Student's Signature

Field of Study: Civil Engineering Advisor's Signature

Academic Year: 2017

ACKNOWLEDGEMENTS

Alhamdulillah, finally this research had been completed. The research would not have been possible without the support from many people whom it is appropriate to acknowledge and thank. Firstly, I would like to express my high gratitude to my scholarship sponsor, AUN/SEED-net Project (JICA), who has financially and technically supported me during the doctoral program in Chulalongkorn University and Kyoto University.

I would like to express my gratitude to Prof. Suched Likitlersuang for giving the valuable suggestion and guidance through my research. I also would like to extend my gratitude to Associate Prof. Dr. Tetsuo Tobita for his guidance and valuable suggestion during my study at Kyoto University. They gave me the best supervision which could lead me to finish my study successfully with a credit of knowledge.

I owe many helpful discussions with Dr. Suttisak Soralump and Dr. Susit Chaiprakaikeow, for the geotechnical earthquake engineering aspect in the Northern Thailand. I also owe some helpful discussions with Dr. Kyohei Ueda for the application of finite element simulation in liquefiable layers and laboratory tests in liquefaction cases. I am deeply thankful to all lecturers in Civil Engineering Department of Chulalongkorn University and Disaster Prevention Research Institute, Kyoto University, for providing the valuable knowledge during my doctoral studies in Thailand-Japan. Most importantly friends in Geotechnical Research Group at Chulalongkorn University and Kyoto University, I would like to thank for many help during my study.

Finally, I owe the greatest debt of gratitude to my parents for their unlimited support, advice, encouragement, endorsement, and believe. My wife, Novaria Frety and my son, Elang Alzadewa Lino Mase for the understanding, love, and motivation during the tough time. Most of all, they are my strength to struggle against every obstacle in my life. This thesis is dedicated to My Wife and My Son.

CONTENTS

	Page
THAI ABSTRACT	iv
ENGLISH ABSTRACT.....	v
ACKNOWLEDGEMENTS	vi
CONTENTS.....	vii
LIST OF FIGURES	1
LIST OF TABLES	8
CHAPTER I. INTRODUCTION.....	9
1.1. Background.....	10
1.2. Problems Formulation	12
1.3. Research Objectives and Scopes	12
1.4. Benefits of Research.....	13
1.5. Research Methodology.....	13
1.6. Thesis Structure	14
CHAPTER II. LITERATURE REVIEW	19
2.1. Liquefaction	19
2.1.1. Introduction	19
2.1.2. Preliminary evaluation of liquefaction potential	20
2.1.3. Empirical approach of soil liquefaction potential	23
2.1.4. Liquefaction study in Thailand.....	28
2.1.5. Subsoils and seismic characteristic of study area.....	31
2.1.6. Liquefaction mitigation efforts.....	32
2.2. Numerical Modelling of Finite Element Liquefaction Program (FLIP).....	35
2.2.1. Introduction	35
2.2.2. Constitutive modelling of soil liquefaction	35
2.2.3. Background of the model	38
2.2.4. Shear mechanism.....	39
2.2.5. Volumetric mechanism.....	40
2.2.6. Liquefaction study using FLIP	42

	Page
2.3. Experimental Test of Soil Liquefaction.....	45
2.3.1. Shaking table test.....	45
2.3.2. Cyclic triaxial test.....	48
2.3.3. Cyclic simple shear test.....	54
2.4. Seismic Response Analysis and Ground Motion Prediction.....	57
2.4.1. Overview of one dimensional seismic response analysis.....	57
2.4.2. Equivalent linear model.....	58
2.4.3. Nonlinear model.....	60
2.4.4. Computation method of one-dimensional seismic response analysis	72
2.5. Next Generation Attenuation Model.....	82
2.6. Geophysical Survey.....	85
2.6.1. Ambient noise using microtremor.....	85
2.6.2. Spectral analysis surface wave (SASW).....	89
2.6.3. Site classification.....	91
CHAPTER III. EMPIRICAL ANALYSIS OF LIQUEFACTION POTENTIAL	93
3.1. Introduction.....	93
3.2. Study Area and Geological Characteristic.....	93
3.3. Research Methodology.....	95
3.4. Result and Discussions.....	99
3.5. Concluding remarks.....	103
CHAPTER IV. SITE RESPONSE ANALYSIS	104
4.1. Introduction.....	104
4.2. Study Area and Geologic Characteristic.....	106
4.3. Attenuation Model.....	106
4.4. Research Methodology.....	111
4.5. Result and Discussions.....	112
4.5.1. Attenuation model analysis of Tarlay Earthquake.....	112
4.5.2. PGA of suitable attenuation model.....	115
4.5.3. Spectral acceleration of seismic response analysis.....	117

	Page
4.5.4. PGA of seismic response analysis	123
4.6. Concluding remarks.....	128
CHAPTER V. LOCAL SITE INVESTIGATION TO THE LIQUEFIED LOCATIONS DURING THE MAE LAO AND TARLAY EARTHQUAKES	130
5.1. Local Site Investigation in Mae Lao	130
5.1.1. Introduction	130
5.1.2. Study area	133
5.1.3. Analysis procedures.....	136
5.1.4. Result and discussions for the local site investigation in Mae Lao	139
5.2. Local Site Investigation in Mae Sai.....	150
5.2.1. Introduction	150
5.2.2. Study area	151
5.2.3. Result and discussions for the local site investigation in Mae Sai	154
5.3. Concluding Remarks	161
CHAPTER VI. LIQUEFACTION SITE RESPONSE ANALYSIS.....	164
6.1. Introduction.....	164
6.2. Site Location	165
6.3. Research Methodology	165
6.3.1. Ground attenuation models	166
6.3.2. Liquefaction resistance curve	166
6.4. Result and Discussions	167
6.4.1. Generated Wave Forms	167
6.5.2. Element Simulation Result	167
6.5.3. Cyclic Stress-strain Response from FLIP	168
6.6. Concluding Remarks	172
CHAPTER VII. CONCLUSIONS AND RECOMMENDATIONS	173
7.1. Conclusions.....	173
7.2. Recommendations.....	174
REFERENCES	176

VITA.....189



จุฬาลงกรณ์มหาวิทยาลัย
CHULALONGKORN UNIVERSITY

LIST OF FIGURES

Chapter 1. Introduction

Figure 1.1.	Liquefaction evidences in Northern Thailand reported by GERD (2014)	11
Figure 1.2.	Methodology of Research	16
Figure 1.3.	Interaction of each chapter in this research	17

Chapter II. Literature Review

Figure 2.1.	Liquefaction phenomenon (a) sand boil reproduced from (reproduced from Castro (1995)) and (b) lateral spread (reproduced from Bartlett and Youd (1992))	20
Figure 2.2.	Grain size distribution of liquefaction soil (Tsuchida, 1970).....	21
Figure 2.3.	Modified Chinese Criteria (Seed et al., 2003).....	21
Figure 2.4.	Recommendations graph for liquefaction criteria (Seed et al., 2003)..	22
Figure 2.5.	Comparison of laboratory test results from the test results of several criteria (a) Tsuchida (1970) (b) Modified Chinese Criteria, (c) Andrews and Martin (2000), (d) Seed et al. (2003)	23
Figure 2.6.	Variation of $\Delta(N_1)_{60}$ with fines content (Idriss and Boulanger, 2010) ..	25
Figure 2.7.	A sand boiling phenomenon caused by 24 th March 2011 Earthquake (Ruangrassamee et al., 2012)	32
Figure 2.8.	Drainage for liquefaction control (reproduced from Seed and Booker (1977)).....	33
Figure 2.9.	Soil columns with jet grouting reinforcement (Yilmaz et al., 2008)....	34
Figure 2.10.	Dynamics compaction method (Kumar, 2001)	34
Figure 2.11.	Air injection testing scheme (Yasuhara et al., 2008)	34
Figure 2.12.	Systematic Mechanism of Shear Plane in FLIP (Iai, 1993)	37
Figure 2.13.	The schematic figure of contact normal n_k , tangential direction t_k and contact force increment dP_k (Iai et al., 1993).....	38

Figure 2.14.	The Schematic figure of liquefaction front, state variable S and shear stress ratio r (reproduced from Iai et al. (1992b)).....	42
Figure 2.15.	Relationship between normalized plastic shear work w and liquefaction front parameter S_o (Iai et al., 1992b).....	43
Figure 2.16.	Shaking table equipment (Mase, 2017).....	45
Figure 2.17.	Modelling earth dam using a shaking table (reproduced from Gopalakrishna and Namdar (2009)).....	46
Figure 2.18.	Effect of relative density to the volumetric strain (reproduced from Özener et al. (2009)).....	47
Figure 2.19.	The mini shaking table and the increase in pore water pressure (Singh et al., 2008).....	47
Figure 2.20.	Liquefaction curve of loose Toyoura sand in large triaxial sample, relative density ($D_r = 65\%$) and sample diameter of 30 cm (Towhata, 2008).....	49
Figure 2.21.	Sketch of typical results of three undrained cyclic simple shear strain-controlled test for the saturated sand with definition of cyclic threshold shear strain pore pressure (Hsu and Vucetic, 2006).....	51
Figure 2.22.	The effect of relative density on liquefaction for Sacramento River Sand (reproduced from Lee and Seed (1960)).....	52
Figure 2.23.	The effect of relative density on liquefaction for Sacramento River Sand (reproduced from Lee and Seed (1960)).....	53
Figure 2.24.	The effect of deviatoric stress on liquefaction resistance for Sacramento River Sand (reproduced from Lee and Seed (1960)).....	53
Figure 2.25.	The effect of over consolidated ratio on liquefaction (reproduced from Campanella and Lim (1981)).....	54
Figure 2.26.	Initial liquefaction in cyclic simple shear on Monterey Sand (reproduced from Peacock and Seed (1968)).....	55

Figure 2.27.	The effect of over consolidated ratio on liquefaction (reproduced from Seed and Peacock (1971))	56
Figure 2.28.	Rate of pore pressure build up cyclic simple shear test	58
Figure 2.29.	The assumption implemented in equivalent linear method (reproduced from Bardet and Tobita (2001) (a) estimating secant shear modulus and (b) Kelvin-Weight model	59
Figure 2.30.	Variation of material behaviour for clayey soils (reproduced from (Vucetic and Dobry, 1991)) and sandy soils (reproduced from (Seed and Idriss, 1970)))	61
Figure 2.31.	The illustration of nonlinear IM model applied in seismic response analysis (reproduced from Bardet and Tobita (2001)), (a) idealism of stress-strain in IM model (b) backbone curve and hysteresis loop generated during cyclic loading	62
Figure 2.32.	Areas A_i , I_i , and J_i calculated for hysteresis loop during the cyclic loading based on IM model (reproduced from Bardet and Tobita (2001)).....	64
Figure 2.33.	Hyperbolic, non-linear model with extended Masing's rule to define loading and unloading behaviour (reproduced from Hashash and Park (2001)).....	66
Figure 2.34.	Schematic of constitutive model response showing shear stress, effective confinement, and shear-strain relationship (reproduced from Elgamal et al. (2006))	71
Figure 2.35.	Multi-yield surfaces in principal stress space and deviatoric plane (reproduced from Parra (1996) and Yang (2000))	71
Figure 2.36.	The backbone curves and yield surfaces (reproduced from Elgamal et al. (2006))	72
Figure 2.37.	One dimensional layered soil deposit system and its spatial discretization (reproduced from Bardet and Tobita (2001))	73

Figure 2.38.	Terminology used in seismic response analysis and shear wave velocity at various location (reproduced from Bardet and Tobita (2001)).....	74
Figure 2.39.	Definition of displacement, strain, and stress in finite difference formulation (reproduced from Bardet and Tobita (2001)).....	76
Figure 2.40.	Definition of fictitious nodes 0 and N+1 at (a) ground surface and (b) at bottom of soil column (reproduced from Bardet and Tobita (2001)).....	77
Figure 2.41.	Illustration of lumped mass system (reproduced from Hashash and Park (2001)).....	80
Figure 2.42.	Soil column model subjected to earthquake in finite element method (modified from Mase et al. (2016)).....	83
Figure 2.43.	Description of geology structure (a) strike-rake-dip (b) foot wall and hanging wall (Courtesy Jenifer Donahue (with modification))	86
Figure 2.44.	Fault types in active tectonic region (Courtesy Jenifer Donahue (with modification) (a) slip strike, (b) reverse strike for foot wall, (c) reverse strike for hanging wall	87
Chapter III. Empirical Analysis of Liquefaction Potential		
Figure 3.1.	Study area of liquefaction empirical analysis	94
Figure 3.2.	Site investigation results of BH-1	96
Figure 3.3.	Site investigation results of BH-4	97
Figure 3.4.	Examples of FS-depth on the investigated sites.....	100
Figure 3.5.	CSR versus $(N_1)_{60}$ or $(N_1)_{60cs}$ (a) based on FC , (b) clean sand criteria, (c) based on magnitude	101
Figure 3.6.	Probability of liquefaction versus FS	102
Chapter IV. Site Response Analysis		
Figure 4.1.	Locations of Nam Ma Fault, epicentre of Tarlay Earthquake in 2011, site investigations, and surrounding seismic stations TMD (2015)..	104

Figure 4.2.	Acceleration record at Mae Sai station due to Tarlay earthquake on March 24, 2011 (TMD, 2015).....	105
Figure 4.3.	Site investigation results at study area, (a) BH-1, (b) BH-2, (c) BH-3, and (d) BH-4.....	110
Figure 4.4.	Location of earthquake stations recording the ground motion of Tarlay Earthquake (TMD, 2015).....	116
Figure 4.5.	NGA attenuation model analysis (medians) to the ground motion recorded during Tarlay Earthquake, (a) peak ground acceleration, (b) spectral acceleration at 0.2s, and (c) spectral acceleration at 1s.	119
Figure 4.6.	Comparison of Abrahamson and Silva (2008) and Boore and Atkinson (2008) models analysis to the ground motion recorded during Tarlay Earthquake for (a) peak ground acceleration (PGA), (b) spectral acceleration (SA) at 0.2s, and (c) SA at 1s	120
Figure 4.7.	Residual of ground motion parameters from recorded ground motions relative to predictions for (a) peak ground acceleration (PGA), (b) spectral acceleration (SA) at 0.2s, and (c) SA at 1s.....	121
Figure 4.8.	Comparison between PGA of the Boore and Atkinson (2008) model and maximum recorded ground motion at surrounding stations.....	122
Figure 4.9.	Comparison of ground surface spectral acceleration of seismic response analysis and spectral acceleration of input motion and local design spectral acceleration (TDS, 2009), and ground surface acceleration of both equivalent linear and non-linear approach on study area, (a) BH-1, (b) BH-2, (c) BH-3), and (d) BH-4.....	127
Figure 4.10.	Comparison of PGA of seismic response analysis obtained from both equivalent linear and non-linear approaches the on the study area....	128
Figure 4.11.	Comparison of amplification factor of seismic response analysis obtained from both equivalent linear and non-linear approaches on the study area.....	128

Chapter V. Local Site Investigation to Liquefied Soils during Mae Lao and Tarlay Earthquakes

Figure 5.1.	Focused areas of local site investigation.....	132
Figure 5.2.	Geological setting of study area (TDMR, 2016).....	138
Figure 5.3.	Location of seismic stations recorded Mae Lao earthquake ground motion.....	139
Figure 5.4.	Comparison of recorded ground motion and ground motion prediction during Mae Lao Earthquake to median and median \pm one standard deviation from NGA models.	140
Figure 5.5.	Soil boring log data and downhole seismic test at BH.....	141
Figure 5.6.	Interpretation of amplitude versus frequency for the investigated locations.	144
Figure 5.7.	Comparison of measured H/V and inversed H/V	145
Figure 5.8.	Comparison of V_s from both geophysical surveys in the study area. .	146
Figure 5.9.	Equipment used for SASW measurement (a) a sledge hammer, (b) a drop weight, and (c) two geophone receivers.	147
Figure 5.10.	The dispersion curves of phase velocity in the measurement of SASW in the study area.	149
Figure 5.11.	Comparison of V_{s30} of both measurements in the study area.	150
Figure 5.12.	Research area and epicentre of the 6.8 M_w Tarlay Earthquake rupture hit the border of Thailand-Myanmar.....	152
Figure 5.13.	Geology map (TDMR, 2016) and investigated location.....	153
Figure 5.14.	Typical subsoil condition of Mae Sai Basin.....	156
Figure 5.15.	H/V ratio corresponding to frequency obtained from microtremor measurements.	157
Figure 5.16.	Comparison of H/V measured and H/V inversion.	157
Figure 5.17.	Shear wave velocity profile from inversion H/V ratio	159

Figure 5.18.	V_{s30} -vulnerability index (K_g) interpretation on each site	160
Figure 5.19.	Comparison of predominant frequency between ground structure and Tarlay Earthquake ground motion.....	161
Figure 5.20.	Spectral acceleration design between the recorded ground motion in Tarlay Earthquake and Thai Design Code for earthquake resistance building.....	161

Chapter VI. Liquefaction Site Response Analysis

Figure 6.1.	Generated input motion based on attenuation model analysis	167
Figure 6.2.	Liquefaction Resistance Curve.....	169
Figure 6.3.	Soil behaviour of sand layers on BH-1	170
Figure 6.4.	Soil behaviour of sand layers on BH-2.	171
Figure 6.5.	Soil behaviour of sand layers on BH-3	171
Figure 6.6.	Soil behaviour of sand layers on BH-4.	172

LIST OF TABLES

Chapter II. Literature Review

Table 2. 1.	Vulnerability criteria and silt loam soil against liquefaction according to Andrews and Martin (Seed et al., 2003).....	22
Table 2.2.	Equivalent number of cycles (Seed and Idriss, 1982).....	50
Table 2.3.	Model applicability of NGA	84
Table 2.4.	Strain dependence of soil dynamic properties (Ishihara, 1978).....	88
Table 2.5.	Site classification for seismic hazard analysis (BSSC, 1997).....	92

Chapter III. Empirical Analysis of Liquefaction Potential

Table 3.1.	Soil investigation data	99
------------	-------------------------------	----

Chapter IV. Site Response Analysis

Table 4.1.	Attenuation models used for earthquake studies in Thailand	114
Table 4.2.	The 6.8 M_w Tarlay earthquake event data on March 24, 2011 (TMD, 2015).....	117

Chapter V. Local Site Investigation to Liquefied Soils during Mae Lao and Tarlay Earthquakes

Table 5.1.	Location of investigated location and earthquake epicentres (TMD, 2015).....	134
Table 5.2.	Observed ground motion within 200 km from the 6.1 Mae Lao Earthquake (TMD, 2015)	135
Table 5.3.	Initial model for H/V inversion	141
Table 5.4.	Comparison of shear wave velocities measured from seismic downhole, SASW and microtremor tests	144
Table 5.5.	Location of investigated location and earthquake epicentre (TMD, 2015).....	154
Table 5.6.	Modelling parameter of analysis	156
Table 5.7.	Vulnerability indices of investigated sites	156

CHAPTER I. INTRODUCTION

Liquefaction is a phenomenon of loss of shear strength of saturated sandy soil, due to excess pore water pressure caused by dynamic loads such as earthquakes. Liquefaction occurred when high pore pressure was developed in saturated sandy soil due to the ground shaking and resulting in the soil-water system into liquefied condition. Soils having liquefaction potential are sand deposits with relatively loose to medium condition and the ground water table close to the ground surface. During an earthquake, the sand deposit is propagated by shear wave which brings the soil to be contracted and producing excess pore water pressure. The rapid shaking of earthquake occurs and no chance for water in soil to drain, hence the saturated soil is subjected to undrained condition. This soil-water mass with water pressure tends to push the surrounding mass. Significant movement occurs in the weak mass such as sand boils on the ground surface when an upward flow could not be resisted by upper soil layer because of the increase of pore water pressure. At liquefied condition, the soil effective stress becomes zero, no more inter particle stress left and soil particles behave as floating elements in water.

Since the Good Friday in Alaska (1992), Niigata Earthquake (1964), and Kobe (1995), liquefaction has been being a topic, which was seriously investigated by many researchers. This research is an effort to study liquefaction phenomenon. This research focuses on Northern Thailand that in 2011 and 2014 hit by two strong earthquakes with the magnitude larger than 6.0 M_w . This study aims to determine the liquefaction potential based on preliminary analysis, seismic ground response analysis, and experimental study. The results of this research are expected to give more explanations about liquefaction phenomena. The results are expected to contribute to geotechnical earthquake engineering study focused on North of Thailand area. In the future, the outcomes of this research would be contributed as a consideration to design the countermeasure and mitigation plan of the liquefaction disaster.

1.1. Background

In recent decades, liquefaction is a phenomenon that is often appointed as a research topic. Liquefaction is a phenomenon of loss of shear strength in saturated sandy soil, due to excess pore water pressure caused by dynamic loads, such as earthquakes. Liquefaction is a natural disaster, which causes many losses, among of them are sand boils and lateral spreadings. There are several factors that influence liquefaction occurrence in a region. The factors include the earthquake maximum acceleration, soil type, depth of water table, building load, drainage conditions, confining pressure, particle size, cementation and age of sand, and the past history of soil deposit (Day, 2002).

March 24, 2011, the strong earthquake happened in the border of North of Thailand and Myanmar, which was called as the Tarlay Earthquake. This earthquake had a magnitude of 6.8 M_w with maximum Peak Ground Acceleration (PGA_{max}) of 0.207g (recorded at Mae Sai Station). Tarlay earthquake triggered liquefaction phenomena as reported by GERD (Geotechnical Engineering Research Development Centre) in Figure 1.1, such as sand boils and lateral spreads in some areas of Northern Thailand Area. In May 4, 2014, another strong earthquake also happened in the Northern Thailand. This earthquake had a magnitude of 6.1 M_w with maximum PGA of 0.3g (recorded at Mae Suai Dam Station). The epicentre of this earthquake was in Mae Lao District, Chiang Rai Province, and was known as the Mae Lao Earthquake. This earthquake also resulted in the extensive damage to the ground, especially liquefaction in several locations. In general, the area that experienced the earthquakes and liquefaction impacts was Chiang Rai Province that is dominated by sandy soils. According to geological condition, Chiang Rai consists of loose to medium dense layer of sand on shallow depth, therefore the liquefaction had been widely observed during the earthquakes. The liquefaction phenomenon on 2011 and 2014 were recorded as the first liquefaction ever witnessed in the last decade in Thailand (Soralump and Feungaugorn, 2013) and the most destructive earthquake in Thailand (Soralump et al., 2014), respectively. Learning from this event, intensive studies were conducted to study liquefaction phenomena, especially in the North of Thailand.

Several researchers conducted many studies about liquefaction potential, particularly in Northern Thailand. Most of them used the secondary data based on site investigation, such as SPT and CPT data combined with empirical analysis. The method used in the liquefaction potential analysis in those areas was the simplified procedure proposed by [Seed and Idriss \(1971\)](#). The method is still being a choice to analyse liquefaction susceptibility until now, even some researchers used the updated version of the CPT analysis method that was recommended by [Robertson and Wride \(1998\)](#). Although these methods are easy to use and more practical in application, it cannot model the condition when liquefaction happens, especially related to soil behaviours during earthquakes. The behaviour of excess pore water pressure it cannot be observed using these methods. Therefore, the experimental methods are needed to be used to study liquefaction in detail. Several experimental methods known in Geotechnical Earthquake Engineering are shaking table test, cyclic simple shear test, cyclic triaxial test, and centrifuge test, which can be simulated in the laboratory to determine the liquefaction potential. The concept of determining liquefaction used is not only the cyclic stress concept, but also the excess pore water pressure ratio (r_u). r_u is used as liquefaction signal. Liquefaction potentially occurred when $r_u \geq 1$, and on the other hand, $r_u < 1$ indicates that liquefaction did not potentially occur.



Figure 1.1. Liquefaction evidences in Northern Thailand reported by [GERD \(2014\)](#)

Numerical modelling of liquefaction soil is also used in liquefaction analysis. The method gives a depiction of strain-stress when pore water pressure builds up. The sophisticated numerical modelling method provides a more complete explanation than

the simplified procedure. However, the method should be validated by the experimental method or field measurement, which is expected to give the best understanding of soil liquefaction phenomenon.

Liquefaction potential in Northern Thailand is still needed to be more intensively investigated. Based on the explanation that is elaborated in the previous paragraphs, the research of liquefaction in experimental and numerical studies is important to study liquefaction potential. Therefore, the preliminary analysis, the ground response analysis, and the local site investigation, and the numerical modelling are being the selected parts in this research to study the liquefaction potential in Northern Thailand.

1.2. Problems Formulation

Based on the introduction, several problem formulations are addressed as follows,

1. How are the sandy soil properties of Northern Thailand related to liquefaction potential?
2. How is the seismic ground response happening when the maximum earthquake ground motion of recorded during Tarlay Earthquake is applied in site area?
3. How is the local site interpretation of the liquefiable layers in the Northern Thailand?
4. How is the behaviour of sandy soils when undergo cyclic loading?
5. How is the behaviour of sandy soils when undergo cyclic loading by using numerical modelling concept in one-dimensional problem?

1.3. Research Objectives and Scopes

Based on the problem formulations shown in Section 1.2., some highlights have been pointed out such as,

1. The preliminary analysis of liquefaction potential in the Northern Thailand.
2. The one-dimensional seismic response analysis during earthquake in Northern Thailand.

3. The local site condition of the liquefiable spots during the recent earthquakes in Northern Thailand.
4. The soil behaviour of sand under the dynamic load.
5. One-dimensional finite element simulation on the horizontally layered soil under the earthquake shaking.

Based on the points listed above, the aim of this doctoral research is to investigate the liquefaction potential in Northern Thailand due to the earthquake. The points that are studied in this research can be divided as follows,

1. To analyse the liquefaction potential analysis based on the empirical approach for the investigated location in Northern Thailand, which in this case is Chiang Rai Province.
2. To carry out the site response analysis in one-dimensional problem to the investigated soil profile.
3. To observe the local site condition of the investigated spots which underwent liquefaction during Tarlay and Mae Lao Earthquakes.
4. To observe the soil behaviour of the horizontally layered soils during the actual earthquake in the Northern Thailand.

1.4. Benefits of Research

The benefits of this research are as follows:

1. Collecting the necessary data for earthquake study in the Northern Thailand.
2. Theoretical verification of liquefaction potential in the Northern Thailand.
3. Provide the site investigation data related to local site condition.
4. Understanding seismic ground response analysis due to the earthquake in Northern Thailand.

1.5. Research Methodology

The systematic steps have been constructed in advance to reach the successful and the smooth-running research work. Based on this research, there are three steps of the research framework, which are listed as bellow (Figure 1.2).

- Research preparation

Research preparation is the preliminary step in conducting the research, which is performed after the problem statements are defined. At this step, the literature review and secondary data collection are performed to get the better understanding to the focus of the research. The data collected in this study includes soil boring log for several locations in the Northern Thailand and the ground motion records during the Tarlay Earthquake and Mae Lao Earthquake.

- Site Visit

After the data collection and literature review, the site visits to the location where liquefaction found in 2011 and 2014 is conducted. The locations are Mae Lao District and Mae Sai District in Chiang Rai Province, the Northern Thailand. In the site, the measurement of ambient noise using the microtremor is performed to investigate the local site condition of the liquefied site.

- Studio Work

The boring log and the earthquake ground motion data are combined to analyse the seismic response analysis in the study area especially during the Tarlay Earthquake. The analysis of measurement result is also performed to obtain the information of the local site undergoing liquefactions in 2011 and 2014. The analysis of soil behaviour under the dynamic load was also performed to investigate the effect of the Tarlay Earthquake to the sub-soils.

1.6. Thesis Structure

The thesis is systematically composed based on the schematics of the research interacting between various parts of the thesis (shown in Figure 1.3). The brief explanation of the content in each chapter is elaborated below,

- Chapter I

In Chapter I, the backgrounds motivated the author to compose a study of liquefaction potential in the Northern Thailand is explained. The problem definition, the objective of the study, the benefit of the study, the research methodology, and the systematics of thesis, are presented in this chapter.

- Chapter II

Chapter II presents the literature review of the study related to the focus of the research. In this chapter, there are five main parts. This first one includes the liquefaction definition, the updated empirical approach of soil liquefaction, the liquefaction experimental test, and the previous study of soil liquefaction in the Northern Thailand. The second one talks about the theory of one dimensional site response analysis to the liquefiable layer based on Finite Element Liquefaction Program (FLIP) ([Iai et al. \(1992a\)](#) and [Iai et al. \(1992b\)](#)), the previous studies of one-dimensional liquefaction site response analysis in the Northern Thailand. The third part talks about the experimental test of soil liquefaction. The fourth part presents the theory of site response analysis to the horizontally layered soil. The attenuation model analysis based on next generation attenuation (NGA) models is presented in the fifth part. The last part presents the theory of ambient noise measurement (microtremor) and SASW (Spectral Analysis of Surface Wave), the previous study of local site investigation in Northern Thailand.

- Chapter III

Chapter III presents the preliminary analysis of soil liquefaction in the study area due to Tarlay Earthquake. In this chapter, the analysis of the liquefaction analysis based on the updated empirical method is presented. The vulnerability of liquefaction in terms of safety factor (FS) and liquefaction probability (PL) is performed. In addition, the comparison to the previous study is performed.

- Chapter IV

Chapter IV presents the one-dimensional site response analysis to the horizontally layered soil of the investigated area. In this chapter, not all investigated locations from data collection are simulated, but only the several sites investigated where sandy soils are dominant. In this chapter, the one-dimensional seismic response analysis based on scaled ground motion is performed. The scaled ground motion is considered based on the maximum peak ground acceleration and attenuation model analysis. In this chapter, the comparison of non-linear and equivalent linear method is performed as well as the comparison of spectral acceleration to the design of spectral acceleration in the investigated area. The estimation of ground motion

prediction based on attenuation model analysis is also compared to the recorded ground motion surrounded the study area.

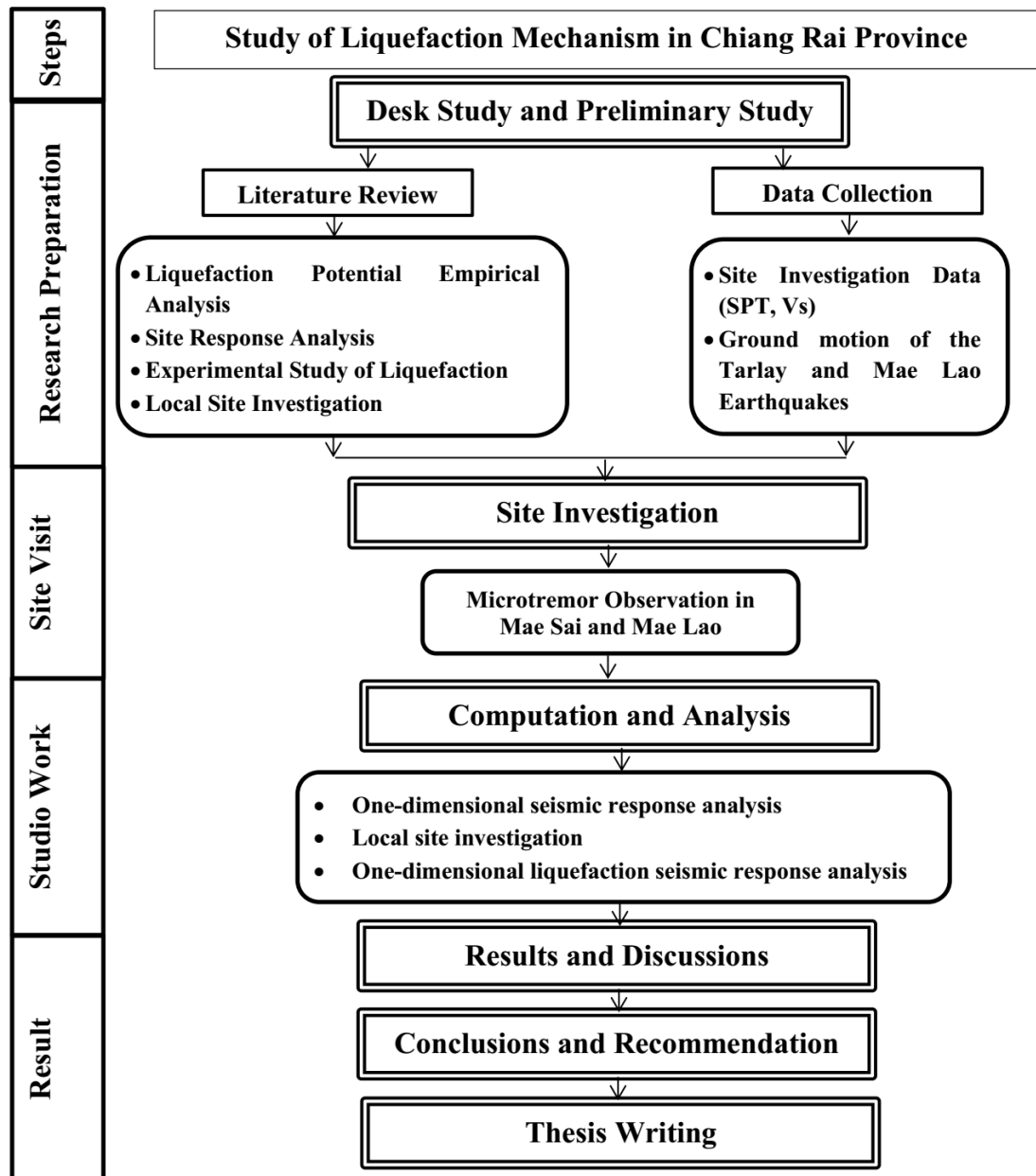


Figure 1.2. Methodology of Research

- Chapter V

Chapter V presents the local site investigation result performed in Mae Sai District which undergo the serious impact of liquefaction during the Tarlay Earthquake in 2011 and Mae Lao District where liquefaction is massively found during the Mae

Lao Earthquake in 2014. In this chapter, the interpretation of the H/V Ratio and predominant frequency is presented. The interpretation of site characterization in the investigated location is also performed. The attenuation model analysis is performed to confirm PGA at the investigated location is higher than the minimum standard of PGA triggering liquefaction. The vulnerability indices and the comparison of the ground motion H/V observed at Mae Sai Station and the observed H/V are also presented. In this chapter, the comparison to the previous study is also presented especially related to vulnerability indices and the first 30 m shear wave velocity average (V_{s30}) are also presented.

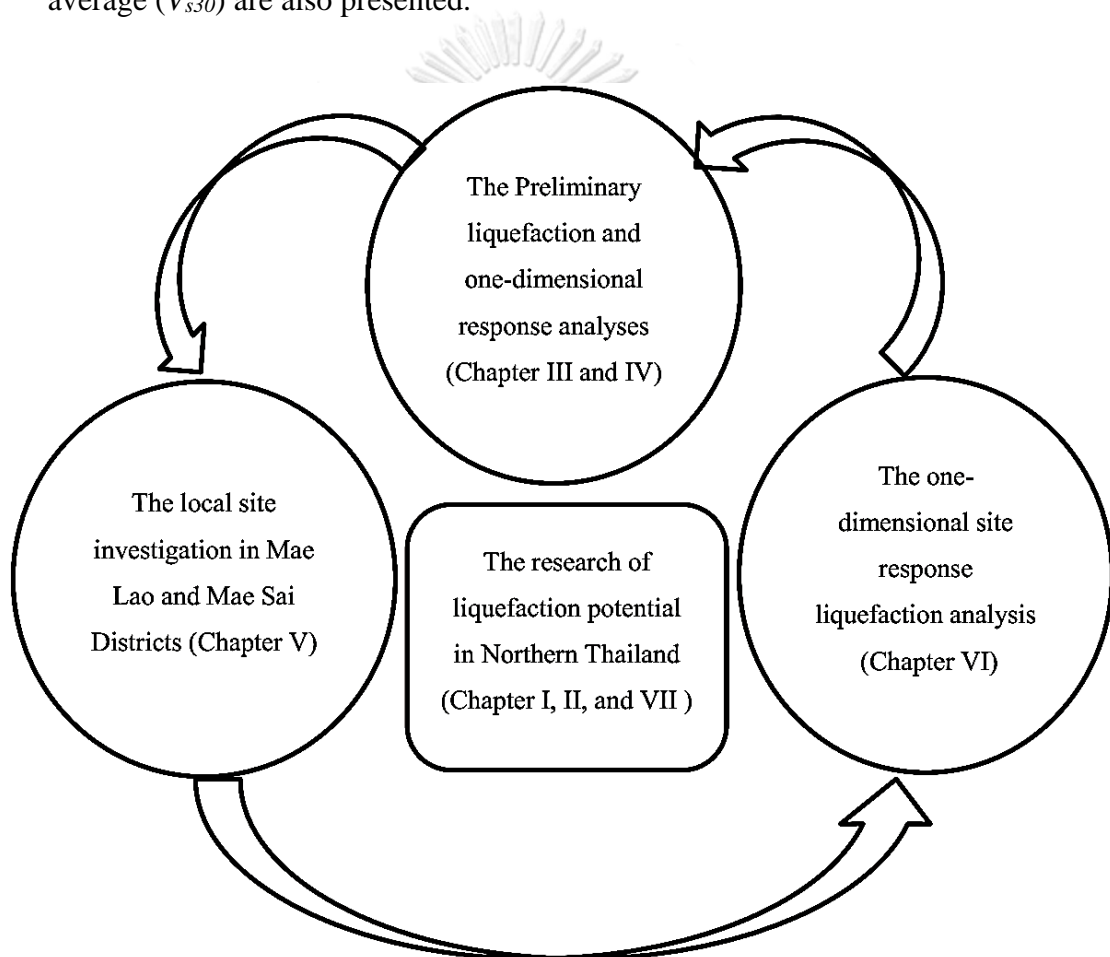


Figure 1.3. Interaction of each chapter in this research

- Chapter VI

In Chapter VI, the implementation of one-dimensional liquefaction site response analysis using FLIP (Iai et al. (1992a) and Iai et al. (1992b)) is performed. This chapter as the further study presents in Chapter 4. In this chapter, only several sites

are simulated based on the Tarlay Earthquake event. The interpretation of soil behaviour under the dynamic load of the Tarlay Earthquake is presented.

- Chapter 7

Conclusions and recommendations are presented in this chapter. This chapter is the closing of the research report, where the concluding remarks, final judgement, ideas for the further research, and comments are quantitatively presented based on the research results. The recommendation as the first step to improve the weak points in this research for the further study is also presented.



CHAPTER II. LITERATURE REVIEW

2.1. Liquefaction

2.1.1. Introduction

Liquefaction is a phenomenon of the loss of sand saturated soil shear strength due to dynamic loads such as earthquakes. One of the first attempts to explain the liquefaction phenomenon in sandy soils was made by [Casagrande \(1936\)](#) and is based on the concept of critical void ratio. Casagrande explained that deposits of sand that have a void ratio larger than the critical void ratio tend to decrease in volume when subjected to vibration by a seismic effect. If drainage is not provided, the pore water pressure will increase. Based on the effective stress approach at any depths of soil deposit, the relationship is shown as follows:

$$\sigma_v = \sigma_v' + u \quad (2.1)$$

where σ_v' = effective stress

σ_v = total stress

u = pore pressure

If the magnitude of σ_v remains practically constant, and the pore water pressure gradually increases, a time may come when σ_v will be equal to u . At that time, σ_v' or effective stress will be equal to zero. Under this condition, the sand does not have any shear strength, and it behaves as liquid material.

According to [Day \(2002\)](#), there are at least 12 factors that influence liquefaction, such as the intensity and duration of an earthquake, ground water table, soil type, relative density, grain size gradation, environmental conditions and placement of soil, drainage conditions, particle size, restraint stress, age and cementation, environmental history, and building load. Liquefaction phenomena that often occur are sand boiling and lateral spreading. According to [Castro \(1995\)](#), sand boiling is caused by an increase of pore water pressure triggering the grains of sand lifted and it comes out through the cracks or soil fissures. [Kramer \(1996\)](#) explained that lateral spreading occurs due to a gradual shift during earthquake period when the strength of the saturated soil less than

that required to resist lateral forces acting on unsaturated soil above it. The mechanism of lateral spreading and sand boiling is depicted in Figure 2.1.

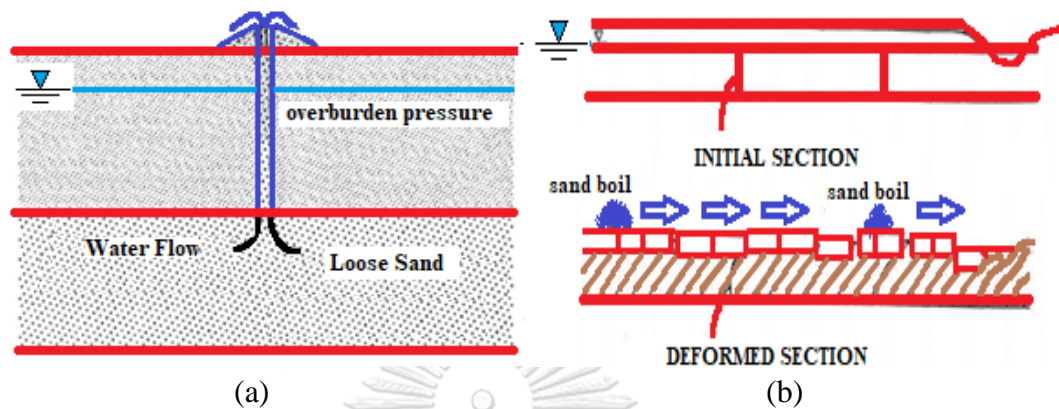


Figure 2.1. Liquefaction phenomenon (a) sand boil reproduced from (reproduced from Castro (1995)) and (b) lateral spread (reproduced from Bartlett and Youd (1992))

2.1.2. Preliminary evaluation of liquefaction potential

According to Tsuchida (1970), the diameter size of soil particle can be used as the preliminary investigation to evaluate the liquefaction potential. The preliminary evaluation of liquefaction potential can be determined by using the graph as shown in Figure 2.2.

Wang (1979), Seed and Idriss (1982) in Seed et al. (2003) stated that the ground that is vulnerable to liquefaction has the criteria as shown in Figure 2.3. The criteria are known as Modified Chinese Criteria. Then, that criteria are modified by Andrews and Martin in Seed et al. (2003), which converts fine particle size criteria to be 0.002 mm and the results are listed in Table 2.1.

To the criteria according to Andrews and Martin, there was another criterion that was proposed by the 24 experts. The criterion was proposed because Modified Chinese Criteria did not provide satisfactory results. The criteria in liquefaction investigation are shown in Figure 2.4.

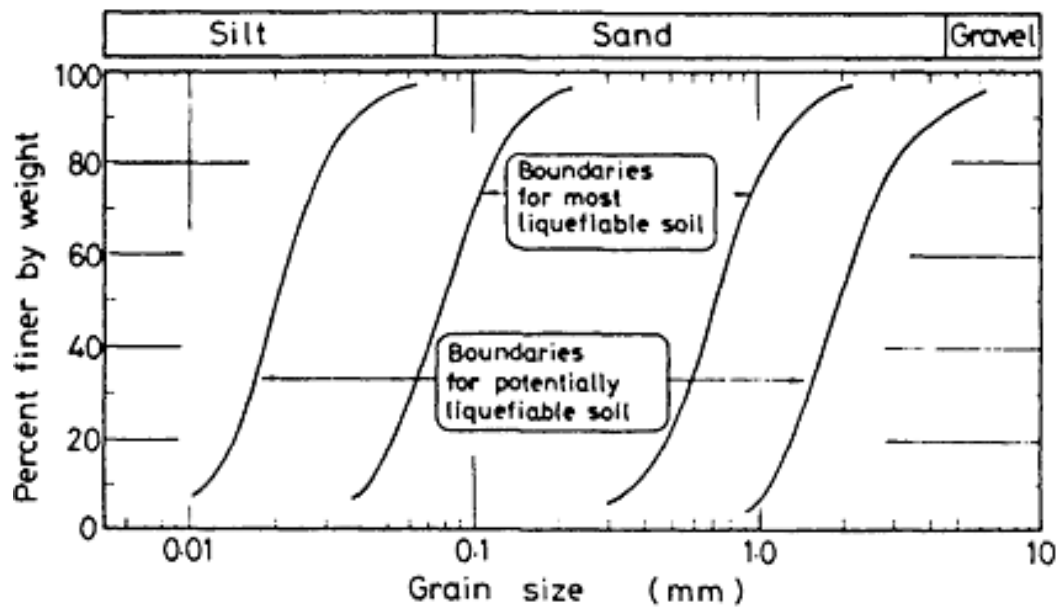


Figure 2.2. Grain size distribution of liquefaction soil (Tsuchida, 1970)

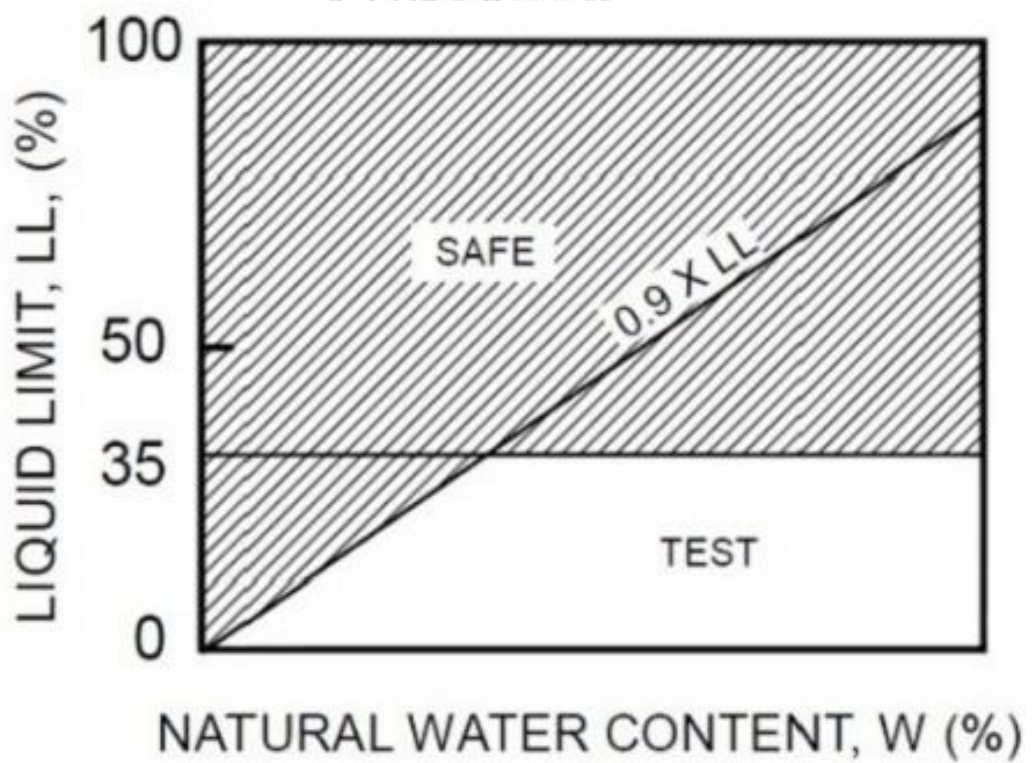


Figure 2.3. Modified Chinese Criteria (Seed et al., 2003)

Table 2. 1. Vulnerability criteria and silt loam soil against liquefaction according to Andrews and Martin (Seed et al., 2003)

Criteria	Liquid Limit ¹ < 32%	Liquid Limit ¹ ≥ 32%
Clay Concentration ² < 10 %	Vulnerable	Further investigation is needed (considering the non-clay granule plastic - example: Mica)
Clay Concentration ² ≥ 10 %	Further investigation is needed (considering the non-plastic clay grains - such as mine waste (tailings))	Not Vulnerable (safe)

1. Liquid limit is determined from Casagrande apparatus
2. Clay defined as the grains finer than 0.002 m

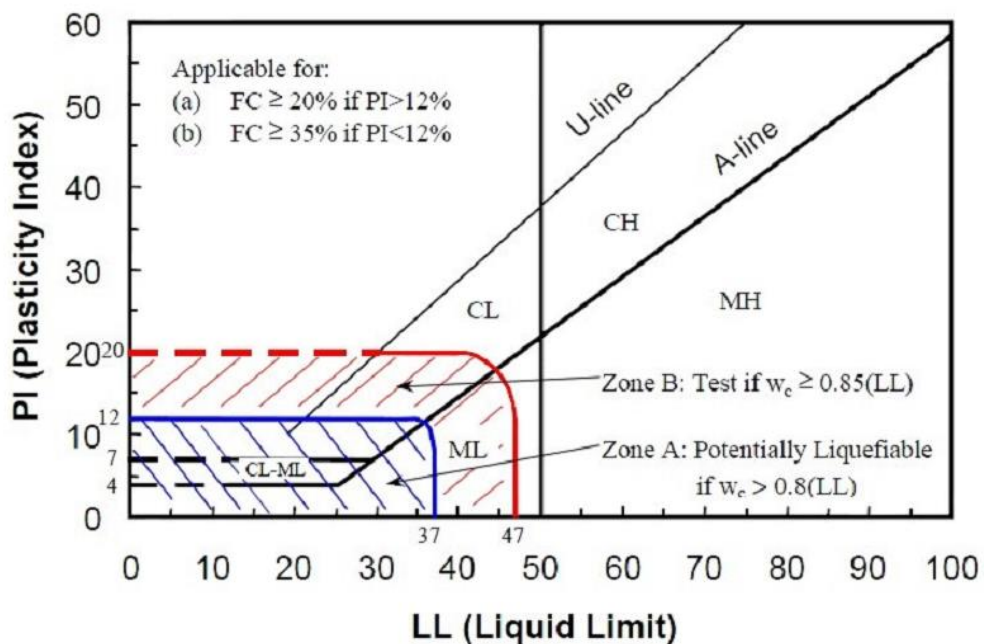


Figure 2.4. Recommendations graph for liquefaction criteria (Seed et al., 2003)

Bray et al. (2004) in Boulanger and Idriss (2004) conducted a test to compare the four criteria. The results from the studies are shown in Figure 2.5. In Figure 2.5a, the particle size distribution is not reaching the limits of potential liquefaction. The same with Modified Chinese Criteria (2.5b) and Andrews-Martin criteria (2.5c), some of liquefaction points are in the "not susceptible" zone, so that the three criteria are not

very accurate. In Figure 2.5d, all of liquefaction spots are in the A zone (vulnerable zones) of the criteria according to Seed et al. (2003); therefore, this criterion is accurate enough.

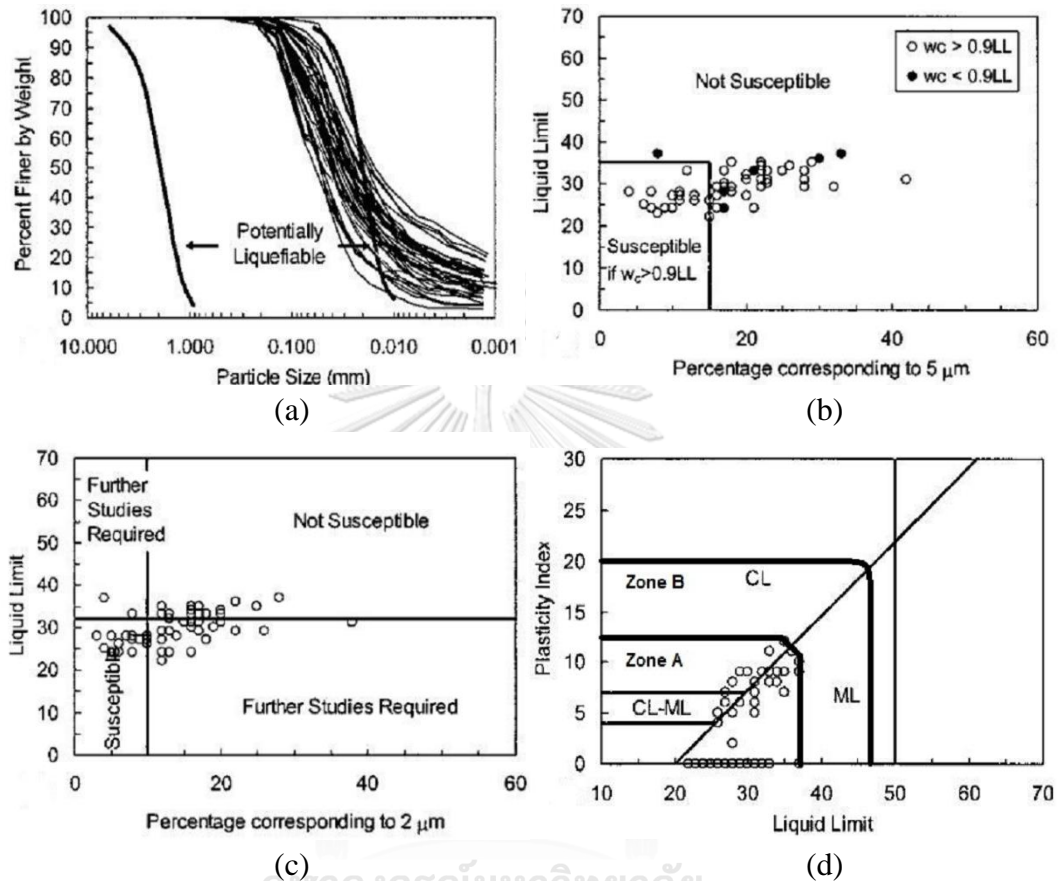


Figure 2.5. Comparison of laboratory test results from the test results of several criteria (a) Tsuchida (1970) (b) Modified Chinese Criteria, (c) Andrews and Martin (2000), (d) Seed et al. (2003)

2.1.3. Empirical approach of soil liquefaction potential

A. CSR (Cyclic Stress Ratio)

CSR (Cyclic Stress Ratio) reflects the cycles produced by an earthquake to trigger liquefaction. Idriss and Boulanger proposed the empirical formulation to determine CSR (Idriss and Boulanger, 2006). This empirical approach is a modification of Seed and Idriss equation. Moreover, this equation also considers overburden pressure in the calculation. The empirical approach is expressed as follows,

$$CSR = 0.65 \cdot r_d \cdot \frac{\sigma'_v}{\sigma'_v} \cdot \frac{a_{max}}{g} \cdot \frac{1}{MSF} \cdot \frac{1}{K_\sigma} \quad (2.2)$$

where CSR is the cyclic stress ratio (no dimension), r_d is depth reduction factor (no dimension), MSF is a magnitude scaling factor (no dimension), K_σ is an overburden correction factor (no dimension), a_{max} is maximum peak ground acceleration (in m/s^2), and g is the gravity acceleration (in m/s^2).

In Equation 2.2, there are many parameters (MSF , r_d , and K_σ) that should be calculated in determining CSR . These parameters are expressed as follows,

- Magnitude Scaling Factor (MSF) (Idriss, 1999)

$$MSF = 6.9 \cdot \exp\left(\frac{-M_w}{4}\right) - 0.058 \leq 1.8 \quad (2.3)$$

where M_w is defined as earthquake magnitude in moment magnitude scale

- Depth Reduction Factor (r_d) (Idriss and Boulanger, 2008),

$$r_d = \exp(\alpha(z) + \beta(z) \cdot M) \quad (2.4)$$

$$\alpha(z) = -1.012 - 1.126 \sin\left(\frac{z}{11.73} + 5.133\right) \quad (2.5)$$

$$\beta(z) = 0.106 + 0.118 \sin\left(\frac{z}{11.28} + 5.142\right) \quad (2.6)$$

where z is the depth of the analysed soil (in meters)

- K_σ (Idriss and Boulanger, 2008) is expressed as,

$$K_\sigma = 1 - C_\sigma \ln\left(\frac{\sigma'_{vc}}{P_a}\right) \leq 1.1 \quad (2.7)$$

$$C_\sigma = \frac{1}{18.9 - 2.55\sqrt{(N_1)_{60}}} \leq 0.3 \quad (2.8)$$

where P_a is atmospheric pressure (the same unit with σ'_{vc}), and σ'_{vc} is effective stress

B. CRR (Cyclic Resistance Ratio)

CRR (Cyclic Resistance Ratio) is a ratio reflecting the availability of soil resistance to retain from liquefaction. Idriss and Boulanger (2008) proposed the empirical formulation to determine CRR , which is expressed as follows,

$$CRR = \exp\left(\frac{(N_1)_{60cs}}{14.1} + \left(\frac{(N_1)_{60cs}}{126}\right)^2 - \left(\frac{(N_1)_{60cs}}{23.6}\right)^3 + \left(\frac{(N_1)_{60cs}}{25.4}\right)^4 - 2.8\right) \quad (2.9)$$

$(N_1)_{60cs}$ is corrected standard penetration normalized by clean sand effect (in blows/ft), which is expressed as follows,

$$(N_1)_{60cs} = (N_1)_{60} + \Delta(N_1)_{60} \quad (2.10)$$

$$\Delta(N_1)_{60} = \exp\left(1.63 + \frac{9.7}{FC + 0.01} + \left(\frac{15.7}{FC + 0.01}\right)^2\right) \quad (2.11)$$

Where FC is fines contents (in percentage)

For ease in determining the $\Delta(N_1)_{60}$, [Idriss and Boulanger \(2010\)](#) proposed the graph of relationship of fines content and $\Delta(N_1)_{60}$ as shown in Figure 2.6.

C. Factor of safety (FS)

Factor of safety of liquefaction (FS) is defined as the value of CRR and CRR in comparison, which is expressed in this equation below,

$$FS = \frac{CSR}{CRR} \quad (2.12)$$

Liquefaction potentially occurs, if $FS < 1$. Otherwise, liquefaction does not potentially occur, if $FS \geq 1$.

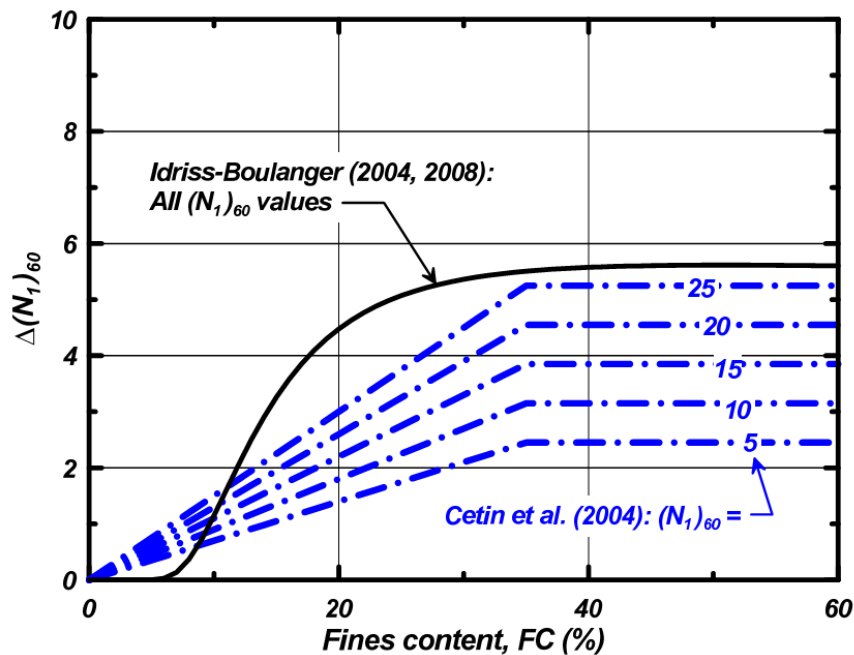


Figure 2.6. Variation of $\Delta(N_1)_{60}$ with fines content ([Idriss and Boulanger, 2010](#))

D. Probability of liquefaction

Many researchers published the empirical approaches of liquefaction probability. Some empirical approaches proposed in the last decade are elaborated as follows,

- [Cetin et al. \(2004\)](#)

[Cetin et al. \(2004\)](#) in their research had proposed the empirical approach of liquefaction probability (P_L). [Cetin et al. \(2004\)](#) considered many factors affecting liquefaction such as corrected SPT value ($(N_1)_{60}$), CSR , magnitude of the earthquake, effective stress, and fines content. The empirical approach proposed by [Cetin et al. \(2004\)](#) is expressed in this equation below,

$$P_L = \phi \left[\frac{\left((N_1)_{60} (1 + 0.004FC) - 13.32 \ln(CSR) - 29.53 \ln(M_w) \right) - 3.7 \ln \left(\frac{\sigma'_v}{P_a} \right) + 0.05FC + 16.85}{2.7} \right] \quad (2.13)$$

where $(N_1)_{60}$ in blows/ft, FC in percentage.

- [Hwang et al. \(2004\)](#)

[Hwang et al. \(2004\)](#) proposed the empirical approach of liquefaction based on practical reliability approach. [Hwang et al. \(2004\)](#) simplified the probability of liquefaction (P_L) by using FS as the main factor to determine probability of liquefaction. This approach proposed was calculated by using the normal distribution (ϕ) concept, which is expressed in this following equation,

$$P_L = 1 - \phi \left(-0.013 + \frac{\ln(FS)}{0.7758} \right) \quad (2.14)$$

- [Sonmez and Gokceoglu \(2005\)](#)

[Sonmez and Gokceoglu \(2005\)](#) introduced a simple equation to determine probability of liquefaction. This empirical approach is more applicable and depends on the value of FS . The empirical approach of liquefaction probability (P_L) is calculated by this equation,

$$P_L = \frac{1}{1 + \left(\frac{FS}{0.96} \right)^{4.5}} \quad (2.15)$$

- Juang et al. (2008) and Juang et al. (2012)

Juang et al. (2008) introduced the empirical approach to determine liquefaction probability (P_L). This approach is quite similar with Sonmez and Gokceoglu (2005) equation. Juang et al. (2012) updated the equation and it was published in 2008. The empirical approach proposed by Juang et al. (2008) is shown in Equation (2.16). The empirical approach proposed by Juang et al. (2012) is shown in Equation (2.17).

$$P_L = \frac{1}{1 + \left(\frac{FS}{1.05}\right)^{3.8}} \quad (2.16)$$

$$P_L = \frac{1}{1 + \exp(7.55(FS - 0.95))} \quad (2.17)$$

- Lai et al. (2006)

Lai et al. (2006) used multi-regression concept to define the probability of liquefaction (P_L). This proposed empirical approach is quite different from the other empirical approaches introduced by the other researchers. The empirical approach is shown in Equation (2.18),

$$P_L = \frac{1}{1 + 0.2(FS^3) + 0.8(FS^7)} \quad (2.18)$$

- Idriss and Boulanger (2010)

Idriss and Boulanger (2010) introduced the empirical approach based on normal distribution function. This equation is quite similar with Cetin et al. (2004) equation. Idriss and Boulanger (2010) included the normalized standard penetration test corrected by clean sand ($(N_1)_{60cs}$). The empirical approach is expressed in this following equation,

$$P_L = \phi \left[\frac{(N_1)_{60cs} + \left(\frac{(N_1)_{60cs}}{126}\right)^2 - \left(\frac{(N_1)_{60cs}}{23.6}\right)^3 + \left(\frac{(N_1)_{60cs}}{25.4}\right)^4 - 2.67 - \ln(CSR)}{0.13} \right] \quad (2.19)$$

where $(N_1)_{60cs}$ in blows/ft

E. Excess pore pressure

Liquefaction occurs because of the excess pore water pressure. Therefore, the analysis of liquefaction should also consider the excess pore water pressure ratio. [Yegian and Vitelli \(1981\)](#) proposed the formula to estimate excess pore water pressure ratio in liquefaction analysis, as expressed in this following equation,

$$r_u = \frac{2}{\pi} \arcsin\left(\frac{1}{FS}\right)^{\frac{1}{2\alpha\beta}} \quad (2.20)$$

where α is a constant which has a range of 0.1 to 0.25 (normally used 0.19), and β is also a constant, which has range of 0.5 to 0.1 (normally used 0.7) ([Seed and Booker, 1977](#)). It should be noted that FS used in Equation (2.20) is ≥ 1 , for $FS < 1$, liquefaction occurs, and excess pore water pressure ratio is equal to 1.

When the value of excess pore water pressure ratio is obtained, excess water pressure ratio can be estimated by using back analysis ([Gupta, 1977](#)) as follows,

$$r_u = \frac{\Delta u}{\sigma_v'} \quad (2.21)$$

where, Δu is excess pore water pressure (the same unit with σ_{vc}') and σ_v' is defined as vertical effective stress.

2.1.4. Liquefaction study in Thailand

Several researchers studied liquefaction in Thailand. Most of them used the empirical analysis approach combined with finite element simulation using FLIP program ([Iai et al., 1992b](#)) in the one-dimensional approach. These references are very important in the analysis of liquefaction potential.

[Pattararattanakul \(2003\)](#) studied liquefaction resistance of sands in the Northern Part of Thailand. In the analysis, [Pattararattanakul \(2003\)](#) used borehole data collected from Chiang Mai and Chiang Rai Provinces. Based on that study, Chiang Rai and Chiang Mai were underlain by loose to medium sand at shallow depths. $(N_1)_{60}$ of those sand layers varied in the range of 5 to 20 blows/ft. The method used in the analysis was by using the logistic regression based on the worldwide liquefaction database to perform the effective stress analysis. A simple tool correlating the liquefaction probability and the estimated pore water pressure using one-dimensional FLIP-PGA

were also used in the analysis. Based on the analysis, [Pattararattanakul \(2003\)](#) concluded that pore water pressure in sand deposits increases with the increase of P_L . According to the result, the probability of liquefaction of 30% well traced the deterministic criteria for clean sand based on curve proposed by [Seed et al. \(1985\)](#). The results also revealed that the maximum pore water pressure of sand layer was higher than clay layer. In the contrary, the amplification factor in sand sites is less than the clay sites.

[Ukritchon and Sangkhawilai \(2004\)](#) studied an analysis of liquefaction potential for Bangkok First Sand Layer. The method used in the analysis was based on standard penetration test (SPT) method. That study followed the latest recommendation of liquefaction resistance of soil from the 1996 and 1998 National Centre for Earthquake Engineering Research (NCEER) Workshop. In this study, the major parameters consisted of SPT value, PGA, and deep well pumping effect. The result of their study explained that at -2.0 m piezometric level, the case, that N of 25 blows/ft and PGA of 0.015g to 0.050g resulted in FS ranging of 3.3 to 11.9 for first sand layer at -32 m deep. Their study also revealed that the effect of deep well pumping potentially increased FS in the range of 3.7 to 12.2 due to the increase of effective stress.

[Teachavorasinskun et al. \(2009\)](#) studied liquefaction susceptibility in the Northern Provinces of Thailand, especially for two big provinces in the North of Thailand, i.e. Chiang Mai and Chiang Rai. In their study, the boring log data were collected to study the soil site condition. The method used in this research was similar with [Pattararattanakul \(2003\)](#) who used the concept of logistic regression using the probability concept combined with the analysis of finite element method to estimate the liquefaction potential based on effective stress and excess pore water pressure. The result of this study concluded that the liquefaction probability of 5%, there were some sites prone to partial liquefaction with the excess pore water pressure ratio (r_u) varied in the range of 0.1 to 0.4. Based on [Teachavorasinskun et al. \(2009\)](#) study, the phenomenon might cause the discernible damage to 2-3 stories buildings, which was generally rest on shallow foundation or short piles. [Teachavorasinskun et al. \(2009\)](#) suggested that the temporary effect should be compensated by providing a proper safety margin about 1.3, to handle the temporary increase of pore water pressure.

Pongvithayapanu and Teachavorasinskun (2010) analysed the liquefaction potential at Laem Chabang Port. That study focused on the backfill of materials, which were highly suspected to soil liquefaction phenomena from moderate to strong earthquakes. Laem Chabang Port was located near two major active faults in Thailand, which could trigger an earthquake with magnitude of 8 M_w . The method used in this study is simplified procedure analysis, in which the input parameters used were SPT-N value, peak ground acceleration (PGA), and soil density. The results of this study showed that some backfill soil layer, e.g. 6 to 10 m, with a low SPT value had a potential to be liquefied under strong earthquake activated by the nearest active fault. The results also revealed that PGA of 0.03 g and smaller would not cause liquefaction in the backfill. In this research, the analysis of liquefaction soil was also elaborated. Based on the result of liquefaction analysis, Laem Chabang Port was highly suspected to liquefy under some medium to strong earthquake at 8 to 9 m deep, with the value of FS resulted was low i.e. about 1.4. The assessment results also explained that PGA higher than 0.035g could cause the liquefaction phenomena around the port.

Soralump and Feungaugsom (2013) performed Probabilistic Analysis of Liquefaction Potential due to Tarlay Earthquake. This study was focused on the Mae Sai district (the closest district to the earthquake epicentre in the Northern Thailand). The method used in this analysis is the conventional liquefaction of cyclic stress combined with the calculation of liquefaction probability. The result of the study revealed that liquefaction potentially occurred at the depth of 3.5 to 11 m deep. The probability of liquefaction in Mae Sai was averaged to be 82.62%.

Tanapalungkorn and Teachavorasinskun (2015) studied the liquefaction susceptibility due to earthquake in Northern Part of Thailand. The method used in this study was the combination of cyclic stress approach with the estimation of excess pore water pressure using FLIP. The result of this study revealed that the liquefaction potentially occurred with PGA of 0.1 g to 0.2g, which was considered based on the map of earthquake zone for the research area. The excess pore water pressure ratio, which was potentially occurred in this area, was 0.5 to 0.9.

Referring to all previous studies, liquefaction potential in Northern Thailand has been an issue of earthquake research in Thailand since 2003. The method used by the previous studies is the combination of empirical analysis with simple finite element

model. However, the previous studies have not considered the finite element model to observe soil behaviour based on seismic ground response analysis yet. Therefore, this study also focuses on the simulation of the finite element model in liquefaction problem.

2.1.5. Subsoils and seismic characteristic of study area

Thailand is located in stable plate, which has been described as a low seismicity area (Ornthammarath et al., 2011). However, the Indo-Australian and Eurasian plates collision still causes frequently seismic activity, not only on along Sumatra-Andaman subduction zone, but also on widespread activity of intraplate where the faults seismic are dominant (Pailoplee et al., 2013). As a result, many hazardous earthquakes are continuously generated, including the latest event of Tarlay and Mae Lao earthquakes.

The subsoil in Northern Thailand is dominated by sandy soil on shallow depth. Soralump and Feungaugorn (2013) analysed boring data of Northern Thailand before liquefaction in 2011. The result of their investigation showed that the subsoil mostly consisted of sand layers with thin and medium stiff clay layers near the ground surface. The loose sand layers and the ground water were found in the shallow depth. The sand layers were liquefied and extruded out during the earthquake, as shown in Figure 2.7.

Tarlay Earthquake had epicentre in Tarlay, Myanmar. The damage of earthquake were found not only in Myanmar but also in Northern Thailand. Ruangrassamee et al. (2012) reported that the earthquake was triggered by the seismic activity of Nam Ma Fault. Location of Nam Ma and other surrounding active faults and epicentre is detailed in Chapter III.

Nam Ma Fault originates in Southern China, extends into north-western Laos, and propagates in north-eastern Myanmar. It continues to the southwest and terminates near the northern tip of the Mae Sai basin (The most destructive area caused by Tarlay Earthquake), which is developed as a pull apart basin between the movements of the Nam Ma, Phayao, and Mae Chan faults. The total length of Nam Ma Fault is approximately around 150 km. Based on the Thailand earthquake catalogue and its surrounding region since 1912, Nam Ma fault did not produce any earthquake greater than magnitude of 6 M_w for at least 100 years. Tarlay Earthquake was essentially filling

the gap of relatively short instrumental earthquake catalogue in this region. The first motion focal mechanism of this tremor was determined with an almost pure left lateral strike slip mechanism, confirming previous seismic information (Ruangrassamee et al., 2012).



Figure 2.7. A sand boiling phenomenon caused by 24th March 2011 Earthquake (Ruangrassamee et al., 2012)

2.1.6. Liquefaction mitigation efforts

The mitigation efforts are proposed to minimize the destructive effects of liquefaction. The efforts to reduce the liquefaction liquefaction are discussed as follows,

1. Drainage design

Drainage in the form of relief wells (gravel or rock) aims to control excess pore pressure. Installation of the drainage is expected to dissipate the high increase of pore water pressure. Drainage design developed for liquefaction potential soil is depicted in Figure 2.8.

2. Jet grouting

Jet grouting is an effort to improve the liquefaction potential soil by replacing liquefiable material with the mixture of cement and water. The replacement material is expected to increase the shear strength of the soil. The result of jet grouting as liquefaction mitigation effort can be seen in Figure 2.9.

3. Compaction

Loose sand is more vulnerable to undergo liquefaction than dense sand. The efforts that can be designed to minimize liquefaction potential is compaction. The layer of sand can be compacted using a roller to a shallow layer of sand, while the deep layer of sand can be compacted by the dynamics compaction method. Compaction is performed to increase the confining pressure. An example of the compaction method is shown in Figure 2.10.

4. Air injection

Soil improvement method using air injection is a new method. The concept of this method is to provide air pressure into the liquefaction potential soil by decreasing the degree of saturation. Research on air injection had been conducted by several researchers, including [Okamura and Teraoka \(2006\)](#). The results obtained from the research proved that the liquefaction susceptibility can be reduced using air injection method ([Yasuhara et al., 2008](#)). Scheme of ground improvement testing device with air injection can be seen in Figure 2.11.

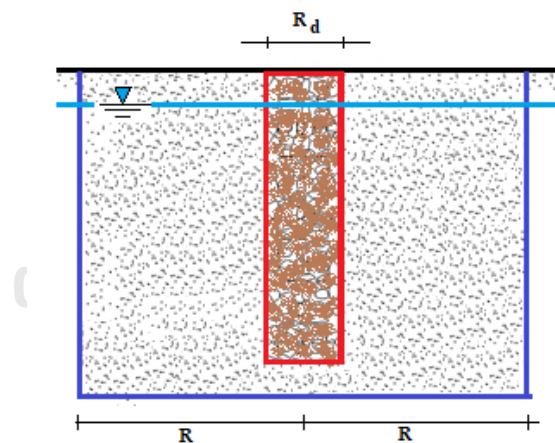


Figure 2.8. Drainage for liquefaction control (reproduced from [Seed and Booker \(1977\)](#))



Figure 2.9. Soil columns with jet grouting reinforcement (Yilmaz et al., 2008)



Figure 2.10. Dynamics compaction method (Kumar, 2001)

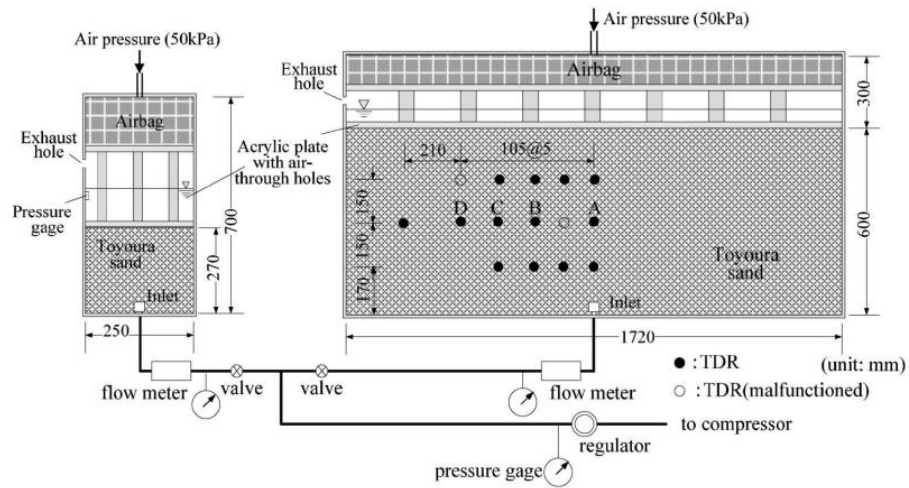


Figure 2.11. Air injection testing scheme (Yasuhara et al., 2008)

2.2. Numerical Modelling of Finite Element Liquefaction Program (FLIP)

2.2.1. Introduction

Analysis of liquefaction potential is very important in studying soil dynamics for sandy soils. Nowadays, the liquefaction study is not only limited in empirical and experimental analysis, but also in finite element analysis. Many sophisticated programs for liquefaction finite element analysis have been known in Geotechnical Earthquake Engineering. One of them is FLIP (Iai et al., 1992b).

In this sub-chapter, some important things related to FLIP are elaborated, particularly constitutive modelling of soil liquefaction, background of model, shear mechanism, and some studies of liquefaction using FLIP. Therefore, the detailed understanding of liquefaction in finite element analysis can be reached.

2.2.2. Constitutive modelling of soil liquefaction

Liquefaction model is derived from the observed undrained stress path during the built up of pore water pressure (Ishihara et al., 1975), correlation of excess pore water pressure and volume change tendency ((Martin et al. (1975) and Finn et al. (1977)), and the formulation of pore water pressure based on observed data as performed by Shibata et al. (1972), Ishibashi et al. (1977), and Sherif et al. (1978). Other techniques to derive liquefaction model are a plasticity theory in terms of volume change and related to pore water pressure built up as done by Mröz et al. (1978) and Zienkiewicz et al. (1978) and soil treatment as two phases medium (Liou et al. (1977) and Blazquez et al. (1981)).

Within the last decade, the model was developed based on the plasticity theory and the characteristic sand behaviour observed in laboratory test under monotonic and cyclic loading condition (Byrne et al., 2004), which is known as the UBCSAND Model. Another model developed was the PM4SAND model, which follows the basic framework of the stress-ratio in controlled conditions, critical state compatible, bounding surface plasticity model for sand, which were initially presented by Manzari and Dafalias (1997) and later extended by Dafalias and Manzari (2004). Modifications to the Dafalias-Manzari model were developed and implemented by Boulanger (2010) to improve its ability to approximate engineering design relationships. Now,

PM4SAND is used to estimate the stress-strain behaviours that are important for predicting liquefaction induced ground deformations during earthquakes.

Another liquefaction model is effective stress model proposed by [Iai et al. \(1992b\)](#). The model is developed from the plasticity theory concept, and the model is quite different from the conventional plasticity model type. In analysis, some steps should be conducted. The first step, the model is defined in strain space. The second step is the application of multiple shear mechanism for considering the effect of principal stress axes rotation. The dilatancy term is treated as an additional volumetric strain component due to creep and temperature as the third step. The soil behaviour under the plane strain condition is represented as the relationship between effective stress and effective strain defined in terms of vectors as follows,

$$\{\sigma'\}^T = \{\sigma'_x \ \sigma'_y \ \tau_{xy}\} \quad (2.22)$$

$$\{\varepsilon'\}^T = \{\varepsilon'_x \ \varepsilon'_y \ \varepsilon'_{xy}\} \quad (2.23)$$

Compressive stress and contractive strain are assumed as negative and the component of displacements (u) and (v) in x and y direction are notated as follows,

$$\varepsilon_x = \frac{\delta u}{\delta x} \quad (2.24a)$$

$$\varepsilon_y = \frac{\delta v}{\delta y} \quad (2.24b)$$

$$\gamma_{xy} = \frac{\delta u}{\delta x} + \frac{\delta v}{\delta y} \quad (2.24c)$$

the basic forms of the constitutive relations are derived as follows,

$$\{d\sigma'\} = [D]\{\{d\varepsilon\} - \{d\varepsilon_p\}\} \quad (2.25a)$$

$$[D] = K\{n^{(0)}\}\{n^{(0)}\}^T + \sum_{i=1}^I R_{L/U}^{(i)}\{n^{(i)}\}\{n^{(i)}\}^T \quad (2.25b)$$

in this relationship, $\{d\varepsilon\}$ in Equation 2.25a is the additional strain increment vector in determining the dilatancy and given from volumetric strain due to dilatancy $\{\varepsilon_p\}$ as follows,

$$\{d\varepsilon_p\}^T = \{d\varepsilon_p/2 \ d\varepsilon_p/20\} \quad (2.26)$$

in Equation 2.25b, the first term represents the volumetric mechanism with rebound modulus K and the direction vector is given by,

$$\{n^0\}^T = \{1 \ 1 \ 0\} \quad (2.27)$$

the second term in Equation 2.25b represents the multiple shear mechanism. Each mechanism $i = 1 \dots, I$, represents a virtual simple shear mechanism, with each simple shear plane oriented at an angle $\theta_i/2 + \pi/4$ relative to the x axis. A schematic mechanism is shown Figure 2.12. The tangential shear modulus R_{LU} represents the hyperbolic shear strain relationship with hysteresis characteristic. The direction vectors for the multiple shear strain mechanism in Equation 2.25b are given by,

$$\{n^i\}^T = \{\cos(\theta_i) \ -\cos(\theta_i) \ \sin(\theta_i)\} \quad (\text{for } i=1 \dots I) \quad (2.28a)$$

in which,

$$\theta_i = (i-1) \Delta\theta \quad (\text{for } i=1 \dots I) \quad (2.28b)$$

$$\Delta\theta = \pi / I \quad (2.28c)$$

the loading and unloading in shear mechanism are derived in virtual simple shear mechanism and notated as,

$$\{n^i\}^T \{d\varepsilon\} \quad (2.28d)$$

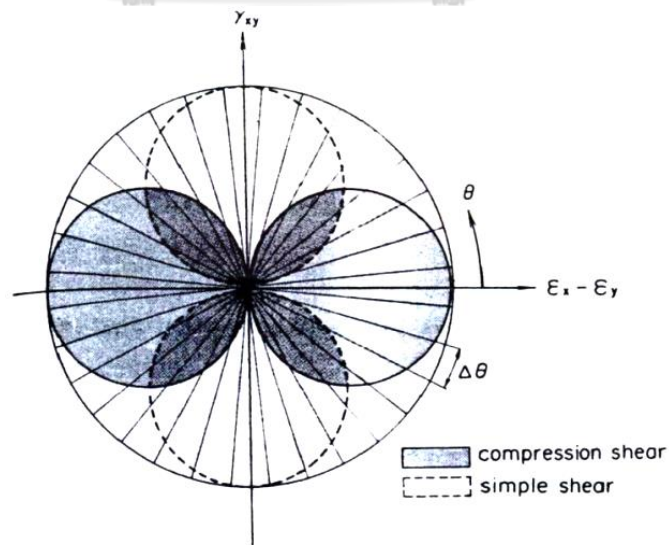


Figure 2.12. Systematic Mechanism of Shear Plane in FLIP (Iai, 1993)

2.2.3. Background of the model

The physical meaning of the strain space multiple mechanism model can be clearly obtained in the assembly mechanics on the sand particles (Iai et al., 1992b). In the mechanics of sand particles, the stress in sand as continuum is noted as a certain average in each contact forces between the sand particles. In this approach, the sand particle is assumed as spheres shape. Prior to obtain the value of representative volume, the contact forces in each element should be determined in each direction. In terms of defining the direction, a plane of an arbitrary direction should be considered. Moreover, the class of pairs of contact forces and contact normal must be found as well. Both are parallel to the plane. The average of contact forces related to the plan is the part of stress contribution of the virtual strain mechanism (Iai et al., 1992b).

The contact force in each plan is categorized based on the plane direction. To define this level of direction, the contact normal force of each direction is assumed at $\theta/2$ relative to the reference axis, which is approximately defined in the plane. The contact forces are divided into the normal and tangential component (Iai et al., 1992b). The interpretation of the schematic figure of contact normal tangential direction and contact force increment is presented in Figure 2.13.

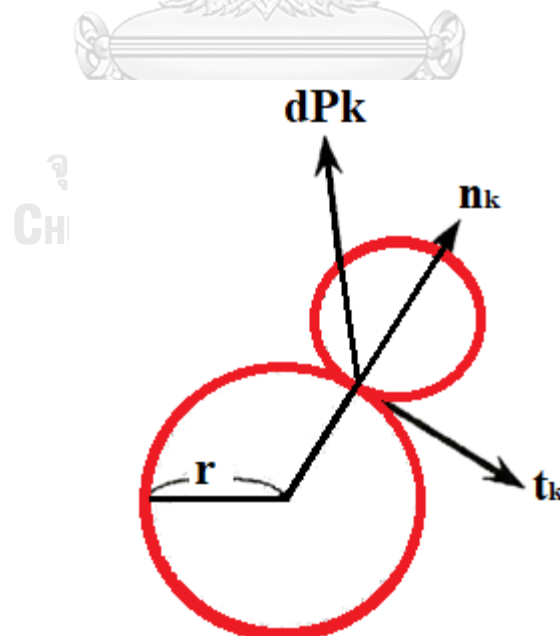


Figure 2.13. The schematic figure of contact normal n_k , tangential direction t_k and contact force increment dP_k (Iai et al., 1993)

In the identification of the basic level of partial stress contribution, a pair of those stress contributions related to the contact normal at the right angle is considered. Therefore, the pair of normal component is explained as the representation of volumetric and compression shear stress, whereas another pair of tangential component represents the simple shear stress distribution (Iai et al., 1992b).

The rotation of the reference axis with an angle $\pi/4$ results in the compression shear stress contribution relating to the contact normal at angle $\theta_i/2$ equal to the simple shear distribution with the contact normal at angle $\theta_i/2 + \pi/4$. The basic level of shear stress distribution is defined for the i to n^{th} mechanism of the virtual simple shear mechanism by the summation of the simple shear stress distribution from the normal component at angle $\theta_i/2$ and the tangential components at an angle $\theta_i/2 + \pi/4$.

The stress is composed of the stress distribution of the virtual plane strain mechanism. The virtual plane strain mechanisms are also consisted of the basic stress contribution of the virtual volumetric strains combined with the simple shear mechanism. All the contributions are resulted from the sand particle displacements related to the average strain for continuum. By the tensors representing the relevant quantities, the physical background of soil model can confirm through the manipulation series. For that, the detailed model should be presented to elaborate the model parameter meaning (Iai et al., 1993).

2.2.4. Shear mechanism

As mentioned in the previous part, each mechanism of virtual simple shear is assumed following the hyperbolic stress-strain relationship associated with hysteresis criteria, which is given by a rule that is Masing (1926) rule (Iai et al., 1992b). Based on this, the virtual tangent shear modulus is given for the initial loading by this equation,

$$R_L^I = \left[\frac{1}{\left(1 + \left|\gamma^i / \gamma_v\right|\right)^2} \right] \left(\frac{Q_v}{\gamma_v} \right) \Delta\theta \quad (2.29)$$

From the formulation above, Q_v is notated as the virtual shear strength and γ_v is notated as the virtual reference strain. The parameters Q_v and γ_v , are not directly measurable. However, they can be determined from shear strength τ_m and shear modulus of sand at the small strain level, G_m by using this formulation,

$$Q_v = \frac{\tau_m}{\sum_{i=1}^I \sin \theta_i \Delta \theta} \quad (2.30)$$

$$\gamma_v = \left(\frac{\tau_m}{G_m} \right) \left[\frac{\left(\sum_{i=1}^I \sin^2 \theta_i \Delta \theta \right)}{\left(\sum_{i=1}^I \sin \theta_i \Delta \theta \right)} \right] \quad (2.31)$$

The derivative of Equation 2.30 and 2.31 is similar as shown by [Towhata and Ishihara \(1985\)](#). For linking to the hysteresis, the Masing's rule is modified to simulate the realistic hysteresis loop instead of those given by the original Masing's rule. The approach to modify the hysteresis loop is like the concept proposed by [Ishihara et al. \(1985\)](#).

The parameters of friction angle ϕ'_f and elastic shear modulus G_{ma} measured at the reference confining pressure at σ'_{ma} are necessary to specify the hyperbolic relationship. These parameters have the function to determine the constant of hyperbolic relationship under the initial effective confining pressure, which is expressed as follows,

$$\tau_{mo} = \left(-\sigma'_{mo} \right) \sin \phi'_f \quad (2.32a)$$

$$G_{mo} = G_{ma} \left(\frac{\sigma'_{mo}}{\sigma'_{ma}} \right)^{0.5} \quad (2.32b)$$

$$\gamma_{mo} = \frac{\tau_{mo}}{G_{mo}} \quad (2.32c)$$

where, τ_{mo} is shear strength, G_{mo} is the elastic shear modulus, and γ_{mo} is the reference shear strain.

2.2.5. Volumetric mechanism

The volumetric (K) modulus and the volumetric strain under dilatancy in Equation (2.25b) should be firstly determined in defining the volumetric mechanism. The K modulus at the initial confining pressure (σ'_{mo}) can be expressed by this following equation,

$$K_0 = K_a \left(\frac{\sigma'_{mp}}{\sigma'_{mp}} \right) \quad (2.33)$$

Excess pore water pressure that is associated with the volumetric strain under the volumetric strain resulted from dilatancy ε_p is generated by step by step. The first step is defining the state variable (S), which is in the same term as σ'_m/σ'_{mo} under the undrained condition and total constant confining pressure. This state variable is expressed based on the stress ratio or $r = \tau/(-\sigma'_m)$ and the liquefaction parameter S_0 . Both parameters are based on cyclic mobility measured for simulating the stress path as presented in Figure 2.14. In detail, the relationship of both parameter is systematically expressed in these following equations,

$$S = S_0 \quad \text{for } r < r_3 \quad (2.34a)$$

$$S = S_2 + \sqrt{(S_0 - S_2)^2 + [(r - r_3)/m_1]^2} \quad \text{for } r > r_3 \quad (2.34b)$$

in which,

$$\tau = \sqrt{\tau_{xy}^2 + [(\sigma'_y - \sigma'_x)/2]^2} \quad (2.35a)$$

$$r_2 = m_2 S_0 \quad (2.35b)$$

$$r_3 = m_3 S_0 \quad (2.35c)$$

$$S_2 = S_0 - (r_2 - r_3)/m_1 \quad (2.35d)$$

$$m_1 = \sin \phi_f \quad (2.35e)$$

$$m_2 = \sin \phi_p \quad (\text{for the phase transformation angle}) \quad (2.35f)$$

$$r_3 = 0.67m_2 \quad (2.35g)$$

The liquefaction parameters in Equation (2.35) are the normalized plastic shear work (w) as the comparison of W_s/W_n , where W_s is the plastic shear work and W_n is the shear stress at the initial condition (τ_{mo}) multiplied by the half of shear strain at the initial condition. The description of this relationship is presented in Figure 2.15. The relationship of these formulations can be expressed as the following equations,

$$S_0 = 1 - 0.6(w/w_1)^p \quad (\text{if } w < w_1) \quad (2.36a)$$

$$S_0 = (0.4 - S_1)(w_1/w)^p + S_1 \quad (\text{if } w > w_1) \quad (2.36b)$$

The S_1 , w_1 , p_1 , and p_2 are the parameters, which characterize the sand cyclic mobility. In the previous equation, the additional parameter of c_1 is introduced to compute plastic shear work. This parameter can describe the explanation of the limit of threshold in the shear stress of strain amplitude. The function of this parameter is also important to generate the excess pore water pressure, as the variable in determining liquefaction together with the effective stress. These parameters are obtained from the back fitting to the test result from the undrained cyclic loading. When the effective stress analysis is performed, the state variable S , as expressed in Equation (2.34), then it is converted to the equivalent volumetric strain of plastic nature ε_p through the continuity condition. After the previous processes are completed, it is substituted to the Equation 2.25a to obtain the effective stress rate.

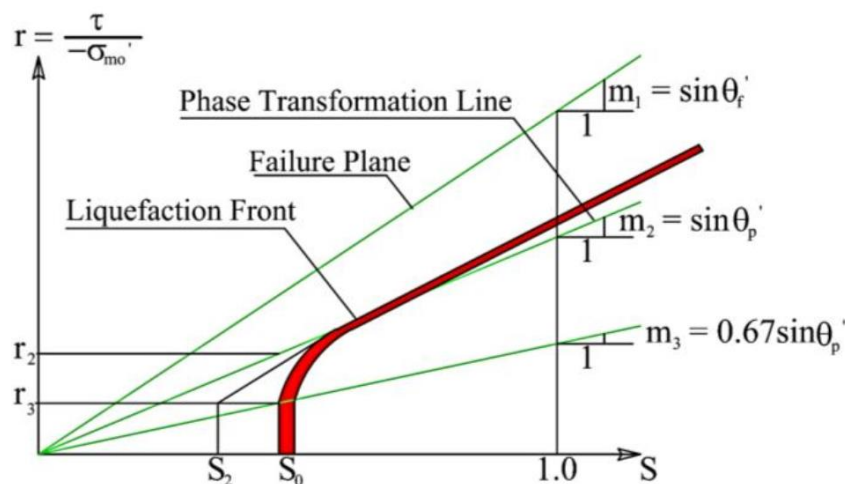


Figure 2.14. The Schematic figure of liquefaction front, state variable S and shear stress ratio r (reproduced from [Iai et al. \(1992b\)](#))

2.2.6. Liquefaction study using FLIP

Many researchers had conducted simulation of liquefaction phenomena using the Finite Element Liquefaction Program or FLIP. In this sub-chapter, some studies related to liquefaction based on FLIP simulation are presented.

[Wang and Iai \(2014\)](#) performed a study about the numerical study on seismic performances of geogrid reinforced soil retaining walls in the liquefiable backfill sand. In the study, FLIP was applied in simulation of seismic mechanism to reinforced retaining walls using the geogrid. The result of this study showed that the geogrid layers

could effectively decrease the excess pore water pressure and the geogrid could provide a liquefaction mitigation function for the reinforced soil retaining wall for saturated sandy soils.

Wang et al. (2013) studied the seismic performances of dyke in the liquefiable soil. In this study, Wang et al. (2013) performed centrifuge test combined with finite element modelling using FLIP 3D. A comparison of both experimental and numerical analyses showed that the result had a good agreement. The results showed that the vertical and the lateral displacements of soil at the top of the dyke central axis were larger than those at the bottom. The deeper layer under the dyke was easier to be liquefied than the shallow one. The excess pore water pressure in free field was larger than that under the dike at the same depth. The liquefiable soils in the free field and under dyke bottom presented different behaviours of shear dilatancy during shaking. The seismic performances of dyke on the liquefiable soils was a complex problem. Physical and numerical models under different shaking intensities only described the deformations and excess pore water pressure distribution ruled in the liquefiable soils.

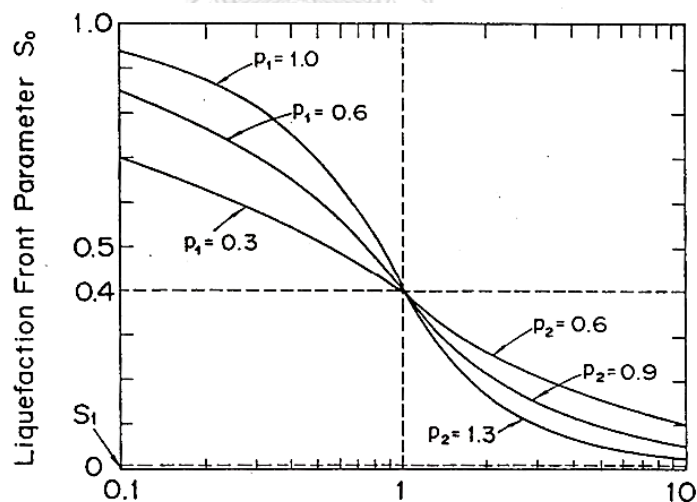


Figure 2.15. Relationship between normalized plastic shear work w and liquefaction front parameter S_0 (Iai et al., 1992b)

Ueda et al. (2012) studied the applicability of multi-springs model based on finite strain theory to the seismic behaviour of embankment on the liquefiable sand deposit. In that study, simplified large deformation and finite strain analyses were

performed to infinitesimal strain analysis under applied dynamic load to verify the applicability of an effective stress model. The results showed that the computed crest settlements and the excess pore water pressure of the embankment after shaking in the simplified large deformation and finite strain analyses gave close agreement with the experimental test (centrifuge test), while the infinitesimal strain analysis overestimated the experimental test result. Comparison of the two analytical methods indicated that the finite strain analyses had a higher accuracy than the simplified large deformation analysis for estimating the crest settlement of embankments. In the infinitesimal strain analysis, the deformed configuration, in most parts of the embankment sunk down into the liquefiable deposit, was widely different from the observed deformation. In the contrary, the simplified large deformation and finite strain analyses well simulated the observed deformed configuration.

[Tobita and Iai \(2007\)](#) conducted a study on failure mechanism of an embankment resting on the liquefiable ground. This study performed by comparing an experimental test resulted from the centrifuge experiment to simulation of finite element model using FLIP. Based on the result, an area of low excess pore pressure (non-liquefied area) was observed at the beginning of the shaking. The area of low excess pore pressure was larger when the amplitude of input acceleration was larger. The formation of the area was indicated also by the observed time history of excess pore water pressure during the experimental test. At the beginning of shaking, the excess pore water pressure under the embankment was consistently smaller than that of free field, and as shaking continued, both of records reached complete liquefaction. The deformation process recorded showed that initially, just after the liquefaction, sands under the overburden pressure were compressed vertically to form non-liquefied wedge. Then the wedge moved downward to push liquefied sands in front of it. Size of the wedge was larger as the inclination of the box, i.e. lateral force, became larger. This fact was consistent with the formation of the non-liquefied wedge in FLIP result. [Tobita and Iai \(2007\)](#) also concluded that the non-liquefied area in liquefied ground gave enormous influence on the deformation of peripheral ground.

[Sawada et al. \(2000\)](#) studied the liquefaction phenomena induced residual deformation of Quay walls collapsed due to 1995 Earthquake in Kobe (the Great Hanshin Earthquake), Japan. In their study, both of Showa-Ohashi Site and Uozaki

Hama Site were simulated by using FLIP. The result of this research show that the result of simulation was consistent with the observation of liquefaction induced residual deformation. [Sawada et al. \(2000\)](#) also stated that FLIP had the potential ability to simulate liquefaction induced residual strength deformation during earthquake.

2.3. Experimental Test of Soil Liquefaction

2.3.1. Shaking table test

One of the liquefaction potential experimental test is by using a shaking table. the shaking table test is a test of liquefaction potential that aims to find an increase in pore water pressure due to dynamic loads generated by the actuator. Analogy of liquefaction potential testing using shaking table is to model the physical condition of the soil during the horizontal dynamic loading (earthquake load). In the liquefaction test using a shaking table, there are some equipments supporting the test, such as pore pressure transducers, falling heads, and container. An example of the tools used in shaking table testing can be seen in Figure 2.8.

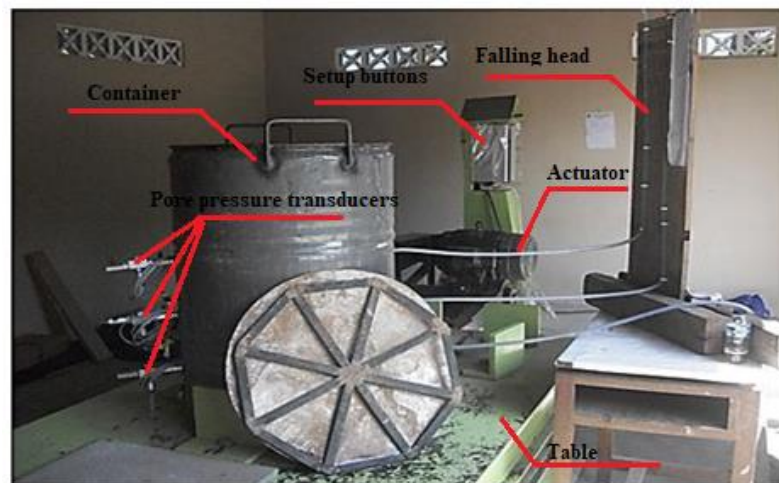


Figure 2.16. Shaking table equipment ([Mase, 2017](#))

According to [Tokimatsu \(1979\)](#), there are several advantages of shaking table tests of which are as follows:

1. Glass containers can be made of flexible glass or drums, so the process of stress phase during the testing can be viewed and read.
2. Homogeneous sand sample can be used in large numbers.

3. It can be equipped with the reading tools (pressure transducers), so that the distribution of pore water pressure can be observed and recorded precisely.
4. Determination of the sample thickness and height of shaking table test can be varied.

Gopalakrishna and Namdar (2009) studied the stability of embankment using a shaking table. The results show that the stress intensity plays a role in the stability of the embankment to the influence of the increase of pore water pressure. Scheme of the equipment used in the test can be seen in Figure 2.17.

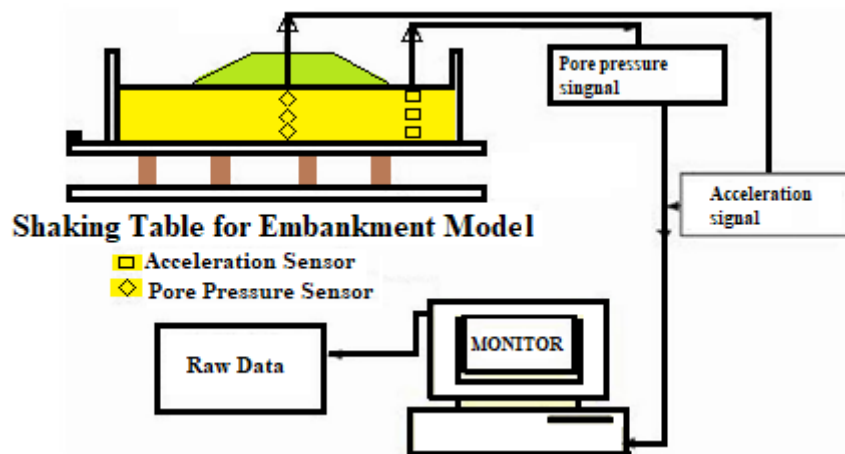


Figure 2.17. Modelling earth dam using a shaking table (reproduced from Gopalakrishna and Namdar (2009))

Özener et al. (2009) examined the potential for liquefaction of sand soil layer by using a shaking table test with a cylindrical container with a diameter of 24 cm and height of 60 cm. Results of these studies explained that the relative density contributes significantly to the occurrence of liquefaction. Effect of relative density to the volumetric strains can be seen in Figure 2.18.

Singh et al. (2008) examined the behaviour of Indian Solani Sand by using a mini shaking table (shown in Figure 2.19a). Results of the study explained that Solani Sand is vulnerable to undergo liquefaction due to dynamic loads. Singh et al. (2008) observed the excess pore water pressure as a parameter of the liquefaction occurrence. The increase of pore water pressure test results can be seen in Figure 2.19b.

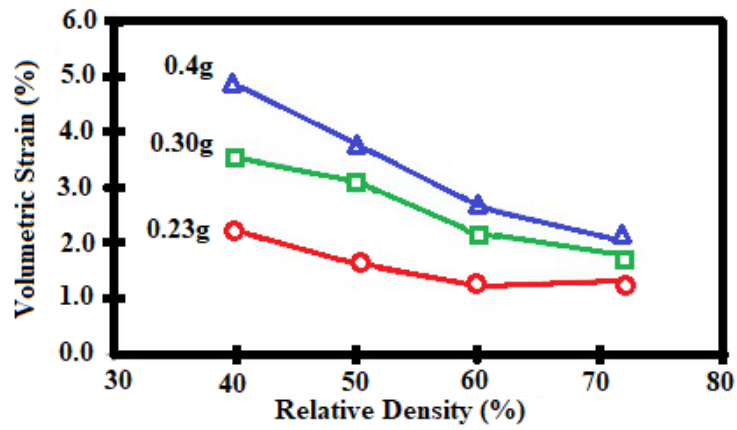
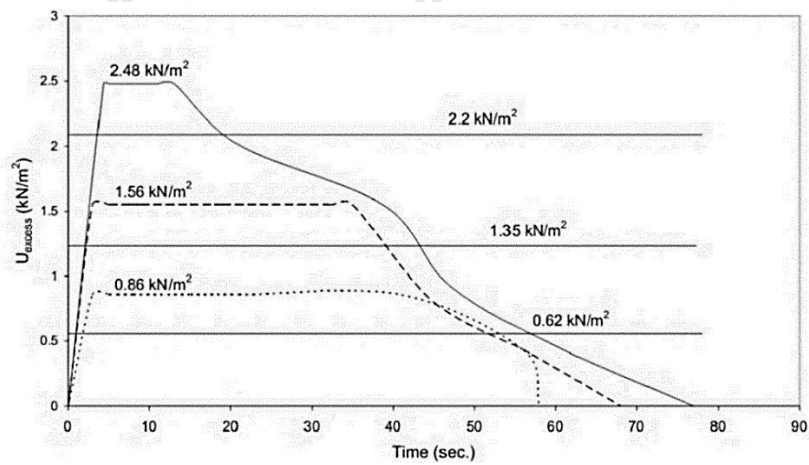


Figure 2.18. Effect of relative density to the volumetric strain (reproduced from

Özener et al. (2009))



(a)



(b)

Figure 2.19. The mini shaking table and the increase in pore water pressure (Singh et al., 2008)

Mase (2017) conducted a study on the liquefaction potential in the southern part of Yogyakarta Indonesia. The excess pore pressure ratio as the liquefaction parameter was used in the study. Mase (2017) modelled homogenous sand given dynamic load, i.e. maximum earthquake acceleration varied to be 0.3g to 0.4g, which are converted to 3 m/s^2 to 4 m/s^2 . Results showed that the given accelerations earthquake could cause liquefaction. Mase (2017) also stated that the applied dynamic load significantly influences the liquefaction stages, such as time to start liquefaction, time to start dissipation, and liquefaction duration.

Several studies have been presented previously were associated with liquefaction research by using a shaking table. Liquefaction potential study with a shaking table can be used to determine the parameters that can lead to liquefaction. Therefore, an experimental study of liquefaction by modelling the physical behaviour of liquefaction with a shaking table are more developed now.

2.3.2. Cyclic triaxial test

A. Overview of cyclic triaxial test procedure

To model the characteristic of dynamic properties of soil, the cyclic triaxial test can be used in the laboratory. Several researchers have investigated the dynamic properties of soil due to the cyclic loading. Ladd et al. (1989) stated that there are some factors should be concerned in cyclic triaxial test. Those factors include the relative density of soil, sample preparation, initial confining pressure, coefficient of lateral earth pressure, over consolidated ratio (OCR), the aging effect. Those factors should be carefully considered before testing.

In cyclic triaxial test, there are three popular methods to determine the dynamic properties of soil, i.e. cyclic shear stress controlled, cyclic shear strain controlled, and shear energy concept. The first two methods are very popular used by many researchers in the laboratory using either cyclic triaxial test or direct shear test. The detailed explanation of these methods is presented in the following,

1. Cyclic shear stress controlled test

This method emphasises in the cyclic stress, which according to Towhata (2008), the number of cycles is possible to trigger liquefaction depending on the applied of

cyclic shear ratio. In the testing, the earthquake loading which is irregular is modelled by simplification of the applied maximum shear stress as 0.65 times the maximum shear stress of the earthquake load. The application of this method to investigate the liquefaction resistance had been performed by Japanese Society of Soil Mechanics and Foundation Engineering (JSSMFE) in 1988, as presented in Figure 2.20. In Figure 2.20, it can be briefly estimated that the liquefaction resistance depends on the applied number of cycles in the testing. Therefore, Seed and Idriss (1982) suggested to alternate irregular time history of the earthquake loading by an equivalent stress at constant amplitude as shown in Table 2.2.

2. Cyclic shear strain controlled test

This method was firstly introduced by Ladd et al. (1989). The important thing that should be concerned in this method is the determination of threshold cyclic shear strain (γ) used in testing. The description of loading corresponding to cyclic shear strain is presented in Figure 2.21.

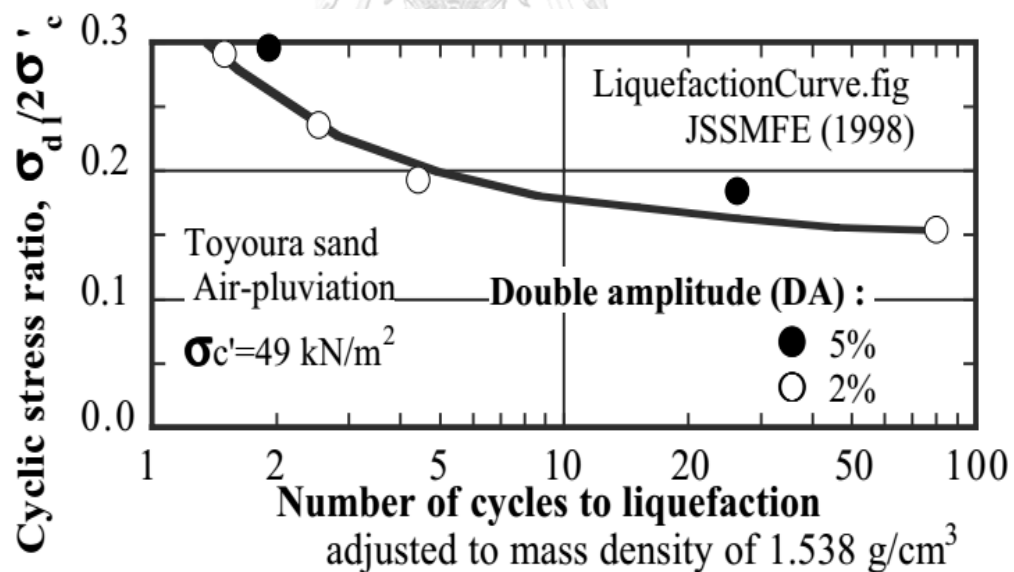


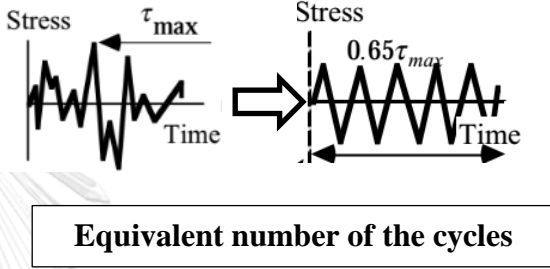
Figure 2.20. Liquefaction curve of loose Toyoura sand in large triaxial sample, relative density ($D_r = 65\%$) and sample diameter of 30 cm (Towhata, 2008)

Generally, in cyclic triaxial testing, the excess pore pressure raises significantly within first 10 cycles, whereas after 10 cycles there is no significant variation in excess pore pressure (Ladd et al. (1989), Hsu and Vucetic (2006), Unno et al. (2008)). Kazama

et al. (2000) detailed the procedure in cyclic triaxial testing in analysing the liquefaction resistance of Masado Sand during the Great Hanshin Earthquake in 1995. Based on the observation during earthquake, the maximum frequency of the earthquake is 1.2 Hz, with shear strain values are 2% for NS component and 1.5% for EW component. Furthermore, the observation is used as the information to set up the laboratory test. In the study, Kazama et al. (2000) used cyclic loading frequency of 0.1 Hz by applying the cyclic shear strain amplitude gradually from 0.65% to 1.8%.

Table 2.2. Equivalent number of cycles (Seed and Idriss, 1982)

Richter Scale of earthquake Magnitude	Equivalent number of stress cycles
8.5	26
7.5	15
6.75	10
6	5-6
5.25	2-3



Silver and Seed (1971) compiled the dynamic behaviour phenomena found on cyclic triaxial testing by using both previously elaborated methods. According to that study, Silver and Seed (1971) concluded that the result of cyclic strain controlled is not much influenced by sample preparation method. In general, the liquefaction parameter obtained from both test is r_u . The cyclic strain controlled method depicts the relationship between excess pore pressure and axial cyclic strain, whereas the cyclic stress controlled method depicts the relationship between excess pore pressure and cyclic stress ratio.

B. Influencing parameters in liquefaction test

Das and Ramana (2011) compiled the main factors influencing liquefaction in cyclic triaxial testing, such as relative density (D_r), confining pressure (σ_3), deviatoric stress (σ_d), and number of cycles, and over consolidated ratio (OCR). The internal factor such as soil grain size characteristic, particle shape, aging and cementation, depositional environmental, condition of drainage, preloading construction also have effect to

liquefaction. The effect of the main factors influencing liquefaction had been investigated by [Lee and Seed \(1960\)](#).

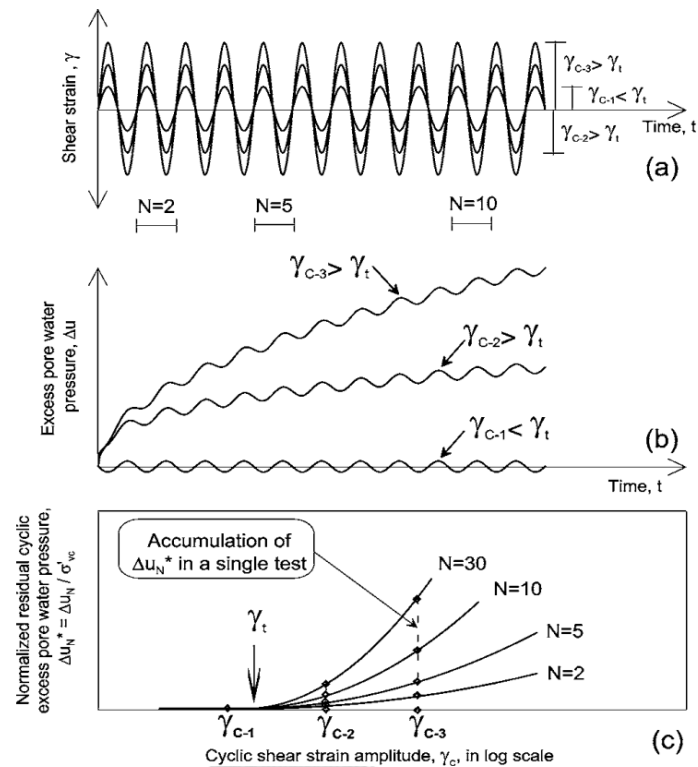


Figure 2.21. Sketch of typical results of three undrained cyclic simple shear strain-controlled test for the saturated sand with definition of cyclic threshold shear strain pore pressure ([Hsu and Vucetic, 2006](#))

The relative density (D_r) of soil liquefaction is believed as the main factor influencing the liquefaction potential. [Lee and Seed \(1960\)](#) had investigated the effect of this factor. In the study, [Lee and Seed \(1960\)](#) considered the double amplitude strain of 2% as the failure. In general, the increase of relative density tends to decrease the liquefaction potential. As shown in Figure 2.22, the increase of the relative density tends to increase the deviatoric stress to generate a failure.

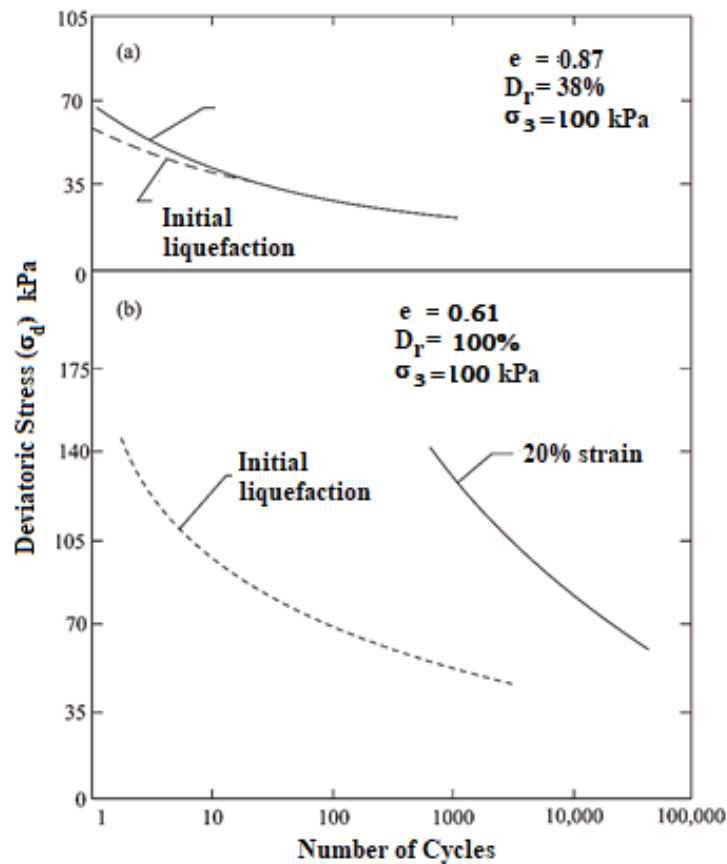


Figure 2.22. The effect of relative density on liquefaction for Sacramento River Sand (reproduced from [Lee and Seed \(1960\)](#))

Figure 2.23 presents the effect of confining pressure on liquefaction as investigated by [Lee and Seed \(1960\)](#). For the given value of deviatoric stress, the increase of confining pressure results in the increase of the number of cycles to generate liquefaction. This condition is valid for all relative densities. Therefore, the method to increase the confining pressure is very important to provide the high soil resistance against liquefaction.

The effect of deviatoric stress on liquefaction resistance is presented in Figure 2.24. In Figure 2.24, the relationship between confining pressure and deviatoric stress in 100 cyclic for initial liquefaction and 20% strain is normally linear. In general, sand with the same initial void ratio and confining pressure, the higher deviatoric stress inclined to trigger liquefaction in the lower cycles.

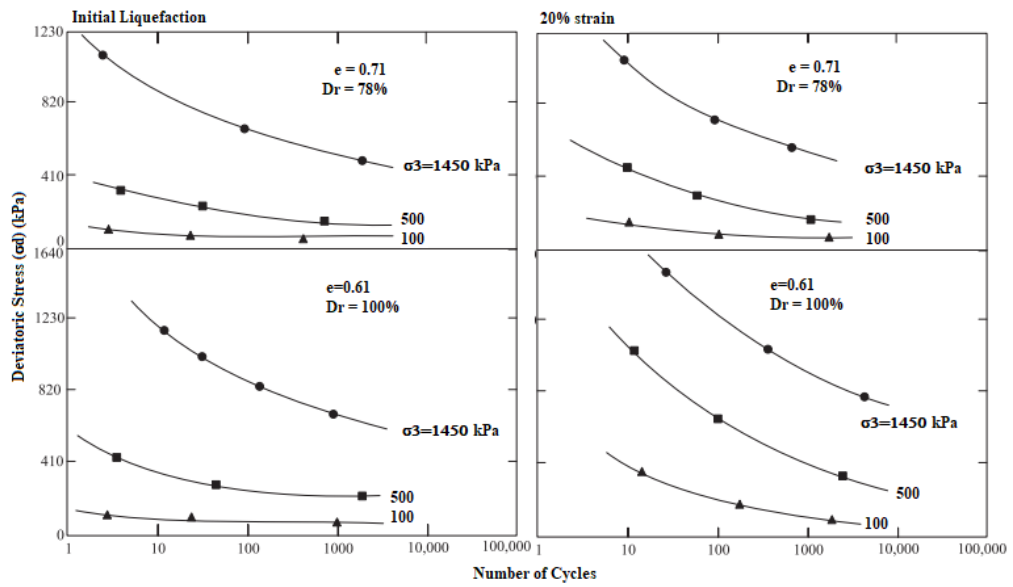


Figure 2.23. The effect of relative density on liquefaction for Sacramento River Sand (reproduced from Lee and Seed (1960))

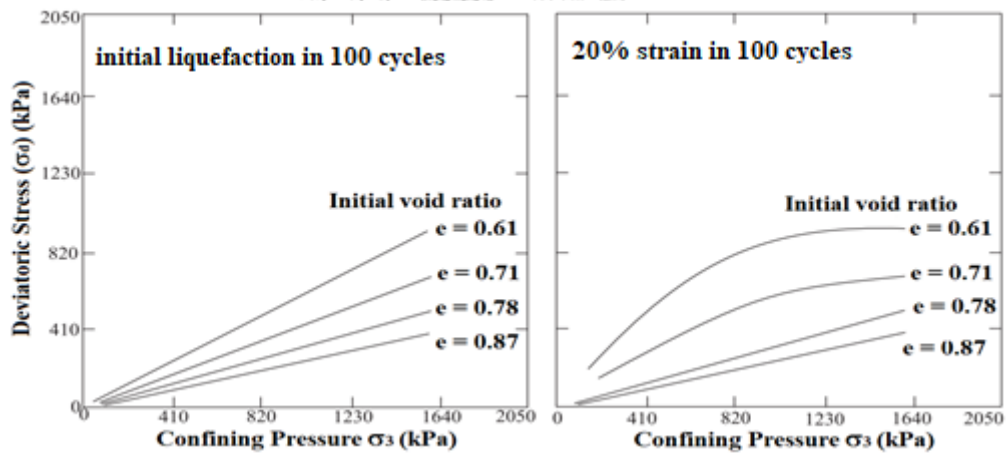


Figure 2.24. The effect of deviatoric stress on liquefaction resistance for Sacramento River Sand (reproduced from Lee and Seed (1960))

The effect of over consolidated ratio on liquefaction is presented in Figure 2.25. Over consolidated sand provides the higher soil resistance. In liquefaction aspect, the over consolidated sand tends to increase the cyclic stress ratio applied. It means that there is a need to increase the deviatoric stress to trigger liquefaction.

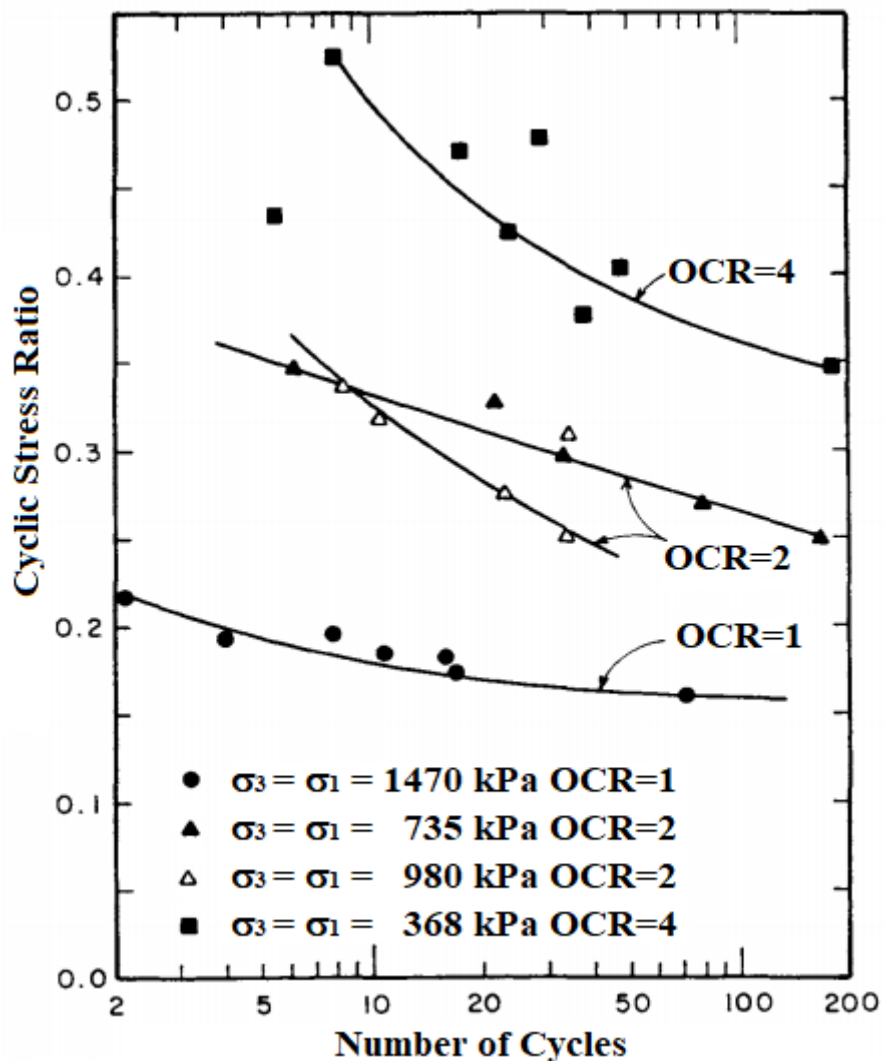


Figure 2.25. The effect of over consolidated ratio on liquefaction (reproduced from Campanella and Lim (1981))

2.3.3. Cyclic simple shear test

Cyclic simple shear test is one of the various test to investigate liquefaction resistance. In this test, the soil is consolidated by a vertical stress (σ_v). The lateral stress is noted as $K_0\sigma_v$. Afterwards, a cyclic loading of σ_h is applied. During the test, the excess pore water pressure and strain are observed corresponding to the number of cycles. The typical result of cyclic simple shear test is presented in Figure 2.26. In general, for an applied σ_v and a relative density, a lower σ_h tends to need the increase of the number of cycles to generate liquefaction. For a given relative density and number of cycles, a smaller σ_v requires a smaller of σ_h to generate liquefaction. For a given value of σ_v and

number of cycles of stress application, the higher σ_h is needed to generate liquefaction in the soil having high relative density.

In cyclic simple shear test, the effect of cyclic loading is very important. As shown in Figure 2.26, the variation of cyclic loading and relative density are significantly influence the number of cycles to generate initial liquefaction. For a relative density of 80%, the applied cyclic loading to generate initial liquefaction linearly increases with relative density, whereas at higher relative density, the trend is not linear. Another critical issue in the testing is over consolidated ratio. In cyclic simple shear testing, the value of σ_h is strongly dependent on the coefficient of lateral earth pressure at rest (K_0), which also depends on the over consolidated ratio. As shown in Figure 2.27, the number of cycles to generate liquefaction decrease with K_0 .

In the test, there is some uniformity, which causes the specimens to generate liquefaction is lower than that in the field. Considering this reason, [Seed and Peacock \(1971\)](#) investigated the ratio of cyclic loading in the laboratories and the fields, which showed that the field values of σ_h is higher than that found in the field.

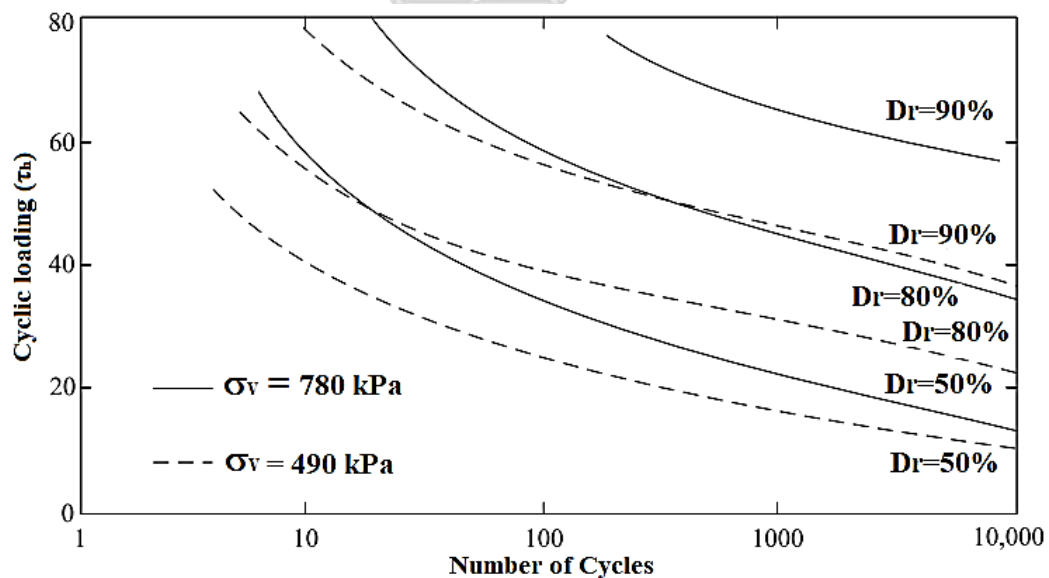


Figure 2.26. Initial liquefaction in cyclic simple shear on Monterey Sand (reproduced from [Peacock and Seed \(1968\)](#))

The main result of liquefaction test using cyclic simple shear test is the graph shows the relationship between r_u and the comparison of the number of applied cycles

with the number of cycles to generate liquefaction. The typical result of cyclic simple shear test is presented in Figure 2.27. As shown in Figure 2.27, the test result of sand in Chiang Rai Province in Northern Thailand is compared to various sand, such as investigated by [Seed et al. \(1976\)](#), [Lee and Albaisa \(1974\)](#), [Baziar et al. \(2011\)](#), and [El Hosri et al. \(1984\)](#). The trend of the compared results is similar each other, where the increase of the ratio of cycles (N/N_i) tends to result in the higher excess pore water pressure ratio.

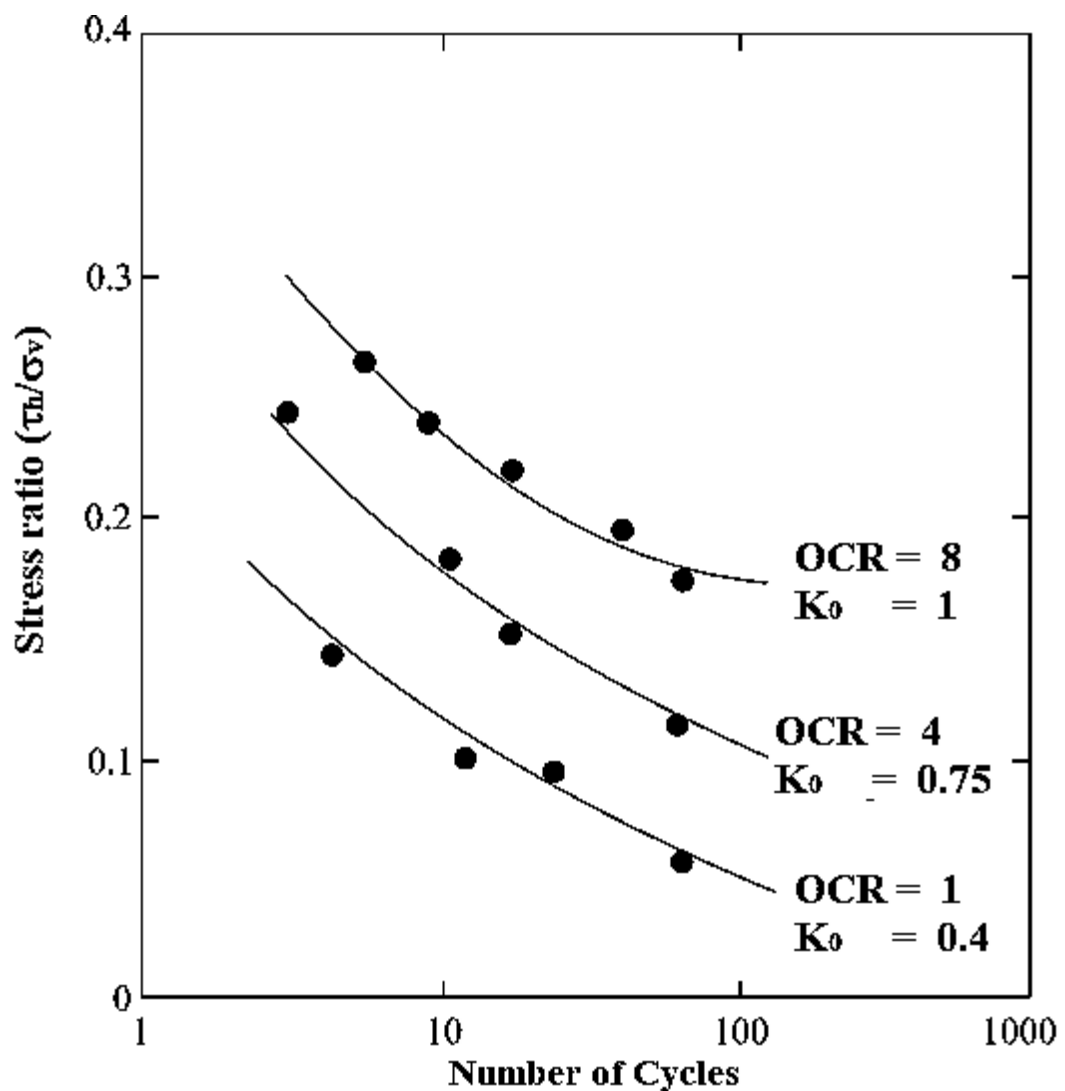


Figure 2.27. The effect of over consolidated ratio on liquefaction (reproduced from [Seed and Peacock \(1971\)](#))

2.4. Seismic Response Analysis and Ground Motion Prediction

2.4.1. Overview of one dimensional seismic response analysis

During its development, geotechnical engineering has continuously expanded the understanding of specific fields, such as earthquakes. Since the need of soil modelling during the earthquake is now becoming the concern for the engineers who focus on the geotechnical earthquake engineering, the development of soil models considering the dynamic load is intensively developed.

Many seismic response programs were developed in the last 50 years. One of the first computer program developed for simulating seismic response analysis was SHAKE (Schnable et al., 1972). This program was developed based on Kanai (1951), Roesset and Whitman (1969), and Housner et al. (1969). The assumption for cyclic soil behaviour used in SHAKE was the equivalent linear, (Seed and Idriss, 1970). Bardet et al. (2000) developed the computer program called EERA, which stands for Equivalent Linear Earthquake Response Analysis. This program was developed based on the concept in SHAKE program. Bardet and Tobita (2001) developed a Nonlinear Earthquake Response Analysis (NERA), which was developed based on material model developed by Iwan (1967) and Mroz (1967). The concept in NERA model had been also implemented by Joyner and Chen (1975), Prevost (1989), and Lee and Finn (1978). Elgamal et al. (2006) developed the computer program called Cyclic 1D, which was based on the framework of Prevost (1985). Cyclic 1D also expanded the liquefaction seismic response analysis, which was developed based on Parra (1996) and Yang (2000) nonlinear model. Recently, Hashash et al. (2015) developed DEEPSOILS computer program, which included equivalent linear and nonlinear model. The framework of equivalent linear model was developed based on Schnable et al. (1972) and Idriss and Sun (1992), whereas nonlinear model was developed based on Hashash and Park (2001).

In general, there are two cyclic behaviour of soil model in seismic response analysis i.e. equivalent linear and nonlinear model. Both models are now widely used in geotechnical earthquake engineering. The detail of the models was presented in Section 2.4.2 and 2.4.3.

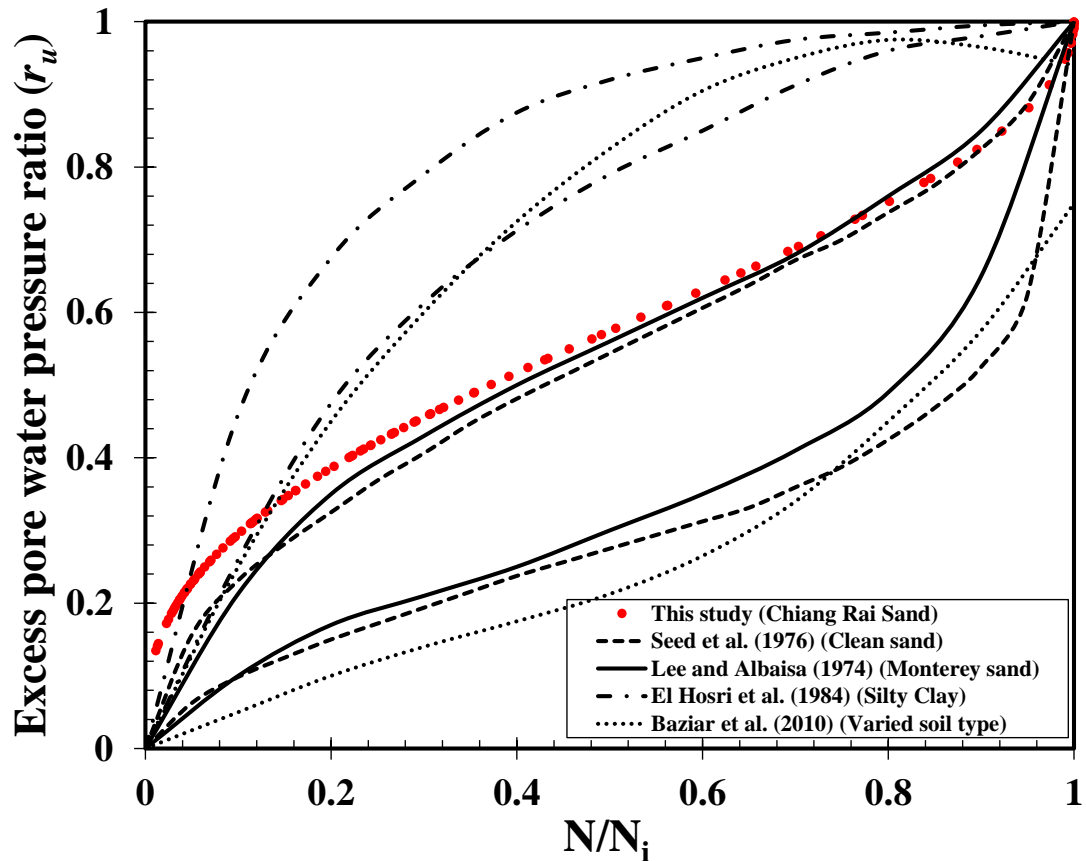


Figure 2.28. Rate of pore pressure build up cyclic simple shear test

2.4.2. Equivalent linear model

The implementation of equivalent linear is addressed to model the nonlinearity of soil, inelastic response of soil. In this model, the linear analysis is performed to the soil properties. The shear modulus of soil is considered as the secant modulus as shown in Figure 2.29a. The modulus secant of shear modulus is expressed in this following equation,

$$G_s = \frac{\tau}{\gamma} \quad (2.37)$$

where, τ and γ are the shear stress and shear strain amplitudes, respectively.

During the cycles, there is some dissipated energy, which is expressed by the following equation,

$$W_d = \int_{\tau} \tau d\gamma \quad (2.38)$$

The maximum energy stored in the soil is noted as,

$$W_s = \frac{1}{2} G \gamma^2 \quad (2.39)$$

by using Equation (2.38) and (2.39), the damping ratio (ξ) of the soil can be derived to be this following equation,

$$\xi = \frac{W_d}{4\pi W_s} \quad (2.40)$$

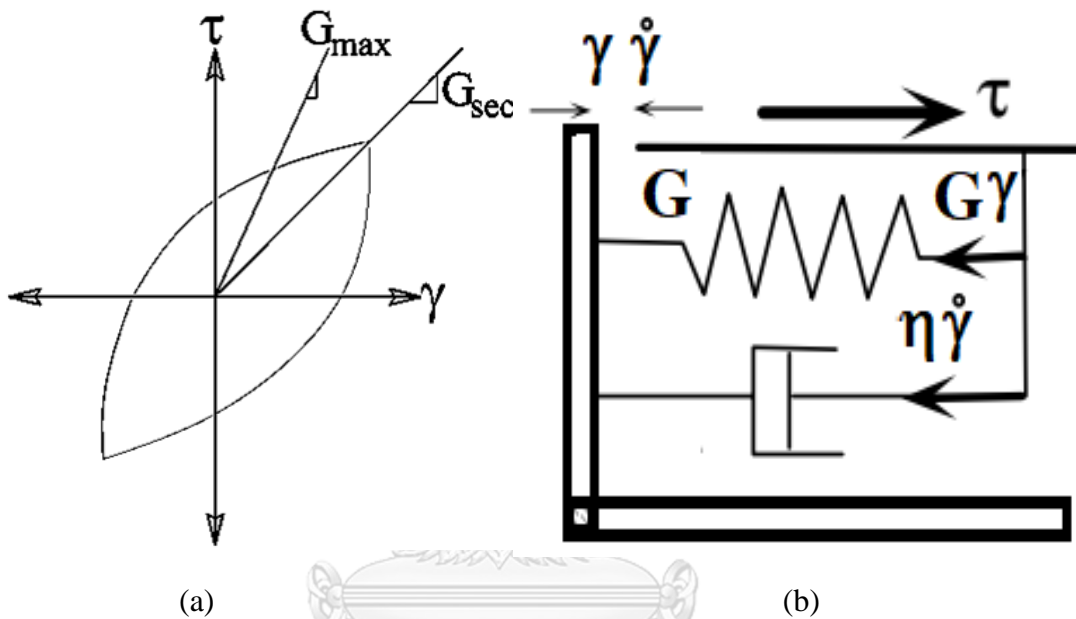


Figure 2.29. The assumption implemented in equivalent linear method (reproduced from Bardet and Tobita (2001) (a) estimating secant shear modulus and (b) Kelvin-Weight model

To account for soil nonlinearities, the Kelvin-Voigt model (Figure 2.29b) is employed in simulating the stress-strain response during the earthquake. In this model, the shear stress is depending on the shear strain (γ) and its rate ($\dot{\gamma}$), which is the first derivative of shear strain as expressed in this following equation,

$$\tau = G\gamma + \eta\dot{\gamma} \quad (2.41)$$

where, η is the viscosity.

For harmonic case under the circular frequency, Equation (2.41) becomes the following equation,

$$\tau(t) = \Sigma e^{i\omega t} = (G + i\omega\eta)\Gamma e^{i\omega t} = G^* \Gamma e^{i\omega t} = G^* \gamma(t) \quad (2.42)$$

where, G^* is the complex shear modulus, Σ is the amplitude of shear stress, and Γ is amplitude of shear strain.

Relating to damping ratio, Equation (2.40) can be expressed as,

$$\xi = \omega\eta / 2G \quad (2.43)$$

By transferring Equation (2.43) to Equation (2.42) the complex shear modulus can be derived as follows,

$$G^* = G + i\omega\eta = G(1 + 2i\xi) \quad (2.44)$$

In Equation (2.44), G is the shear modulus implemented in cyclic behaviour modelling, which in this case are secant shear modulus (G_{sec}) for equivalent linear model and tangent shear modulus (G_{tan}) for nonlinear model.

In seismic response analysis, the material behaviour is generally specified as shown in Figure 2.30. In Figure 30, the data of shear strain corresponding to shear modulus ratio (G/G_{max}) and Damping ratio are obtained from such examples as presented in [Seed and Idriss \(1970\)](#) for sandy soils and [Vucetic and Dobry \(1991\)](#) for clayey soils. The materials behaviours presented in Figure 30, are normally used as the input in seismic response analysis for both equivalent linear and nonlinear methods. The other references which also provided the assumption of the material behaviour of various soil types can be obtained in [Kramer \(1996\)](#), [Seed et al. \(1986\)](#) and [Hardin and Drnevich \(1972\)](#).

2.4.3. Nonlinear model

A. Iwan-Mroz (IM) model

Various nonlinear models had been developed in geotechnical engineering integrated in many computer programs. [Bardet and Tobita \(2001\)](#) implemented the nonlinear and hysteretic model in NERA program. The model was firstly proposed by [Iwan \(1967\)](#) and [Mroz \(1967\)](#), as shown in Figure 2.31a. The model was proposed to model nonlinear stress-strain using a series of several mechanical element with different stiffness (k_i) and sliding resistance (R_i). In what follows this model is referred as IM model. Before any force applied, the residual stress in all sliders are zero. During the

monotonic loading, when shear stress reaches R , the slider (i) yields. After that, slider i retains a positive residual stress equal to R_i . It should be noted that the sliders have the increase of resistance, i.e. $R_1 < R_2 < R_3 \dots < R_n$.

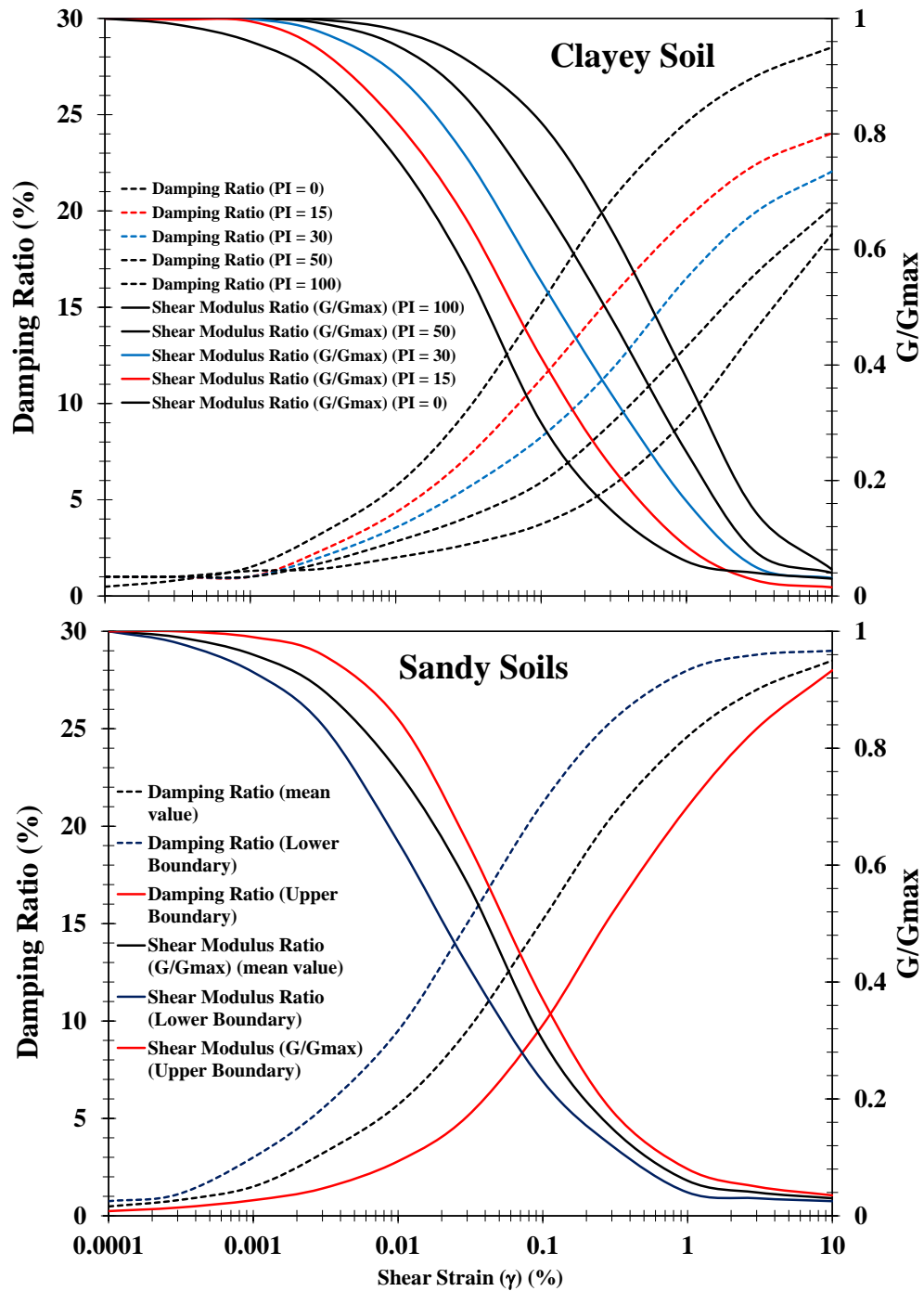


Figure 2.30. Variation of material behaviour for clayey soils (reproduced from (Vucetic and Dobry, 1991)) and sandy soils (reproduced from (Seed and Idriss, 1970))

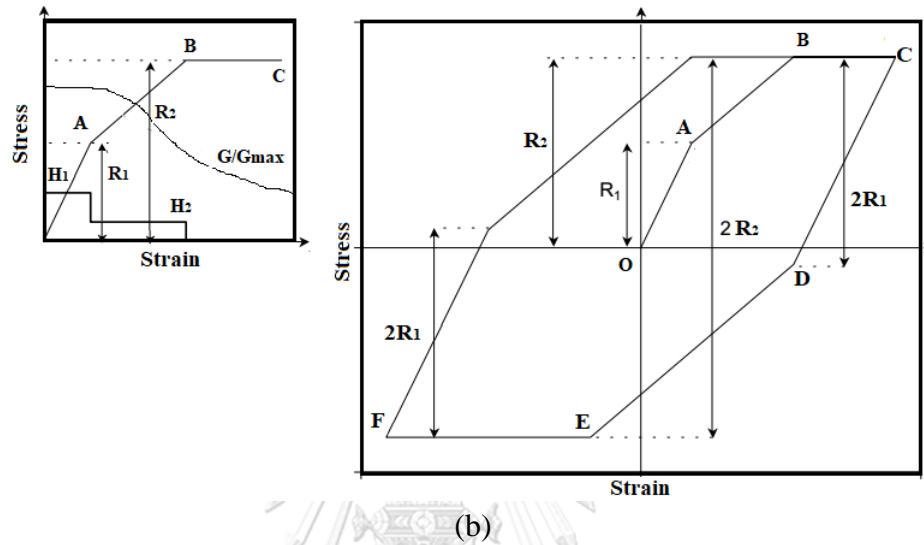
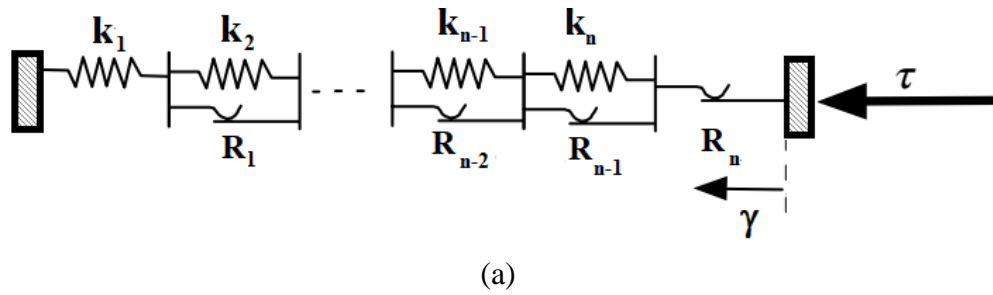


Figure 2.31. The illustration of nonlinear IM model applied in seismic response analysis (reproduced from [Bardet and Tobita \(2001\)](#)), (a) idealism of stress-strain in IM model (b) backbone curve and hysteresis loop generated during cyclic loading

As presented in Figure 2.31b, during the cyclic loading, the stress-strain curve generated by the IM model for two sliders is piecewise linear and the shear modulus of H is a tangential modulus varied in steps. Corresponding to this, the shear modulus of the backbone curve for the model can be derived as follows,

$$H_i = \frac{G_{i+1}\gamma_{i+1} - G_i\gamma_i}{\gamma_{i+1} - \gamma_i} \quad i = 2, \dots, n-1 \text{ and } H_n = 0 \quad (2.45a)$$

back stress α_i is initially assumed as zero, so that R_i becomes,

$$R_i = G_i\gamma_i \quad i = 1, \dots, n \quad (2.45b)$$

Equation (2.45a) and (2.45b) are combined to derive shear wave velocity modulus at each step corresponding to G - γ curve. If G/G_{max} is specified, then the derivation of both equations becomes,

$$H_i = G_{\max} \frac{G_{i+1}\gamma_{i+1} - G_i\gamma_i}{\gamma_{i+1} - \gamma_i} \quad i = 2, \dots, n-1 \text{ and } R_i = G_{\max} G_i' \gamma_i \quad i = 1, \dots, n \quad (2.45c)$$

where, $G_i' = G_i/G_{\max}$

The energy dissipated during cycles is determined based on the Masing similitude rule (Masing, 1926). As shown in Figure 2.32, the areas I_i and J_i corresponding to the unloading from $+\gamma_i$ to $-\gamma_i$ and the reloading from $-\gamma_i$ to $+\gamma_i$ are estimated as four times of the area A_i under the loading from 0 to γ_i . These areas can be calculated by,

$$A_i = \int_0^{\gamma_i} \tau d\gamma \quad (2.46a)$$

$$I_i = \int_{\gamma_i}^{-\gamma_i} (\tau_i - \tau) d\gamma = -4A_i \quad (2.46b)$$

$$J_i = \int_{-\gamma_i}^{\gamma_i} (\tau_i + \tau) d\gamma = 4A_i \quad (2.46c)$$

Using Equation (2.46), the dissipated energy (the areas of hysteresis loop) becomes,

$$W_{d_i} = \int_{\gamma_i}^{-\gamma_i} \tau d\gamma + \int_{-\gamma_i}^{\gamma_i} \tau d\gamma = -I_i + J_i - 4\tau_i\gamma_i = 8A_i - 4\tau_i\gamma_i \quad i = 1, \dots, n \quad (2.47)$$

Since the stress-strain curve is piecewise linear and generated by n discrete points $(\gamma_i, G_i\gamma_i)$, A_i becomes,

$$A_i = \frac{1}{2} \sum_{j=2}^i (G_j\gamma_j + G_{j-1}\gamma_{j-1})(\gamma_j - \gamma_{j-1}) \quad i = 2, \dots, n \quad (2.48)$$

by substituting Equation (2.48) to Equation (2.47), the dissipated energy becomes,

$$W_{d_i} = 8A_i - 4G_i\gamma_i^2 \quad i = 1, \dots, n \quad (2.49)$$

The maximum energy stored in the system is obtained based on this equation,

$$W_{s_i} = \frac{1}{2} G_i\gamma_i^2 \quad (2.50)$$

therefore, the critical damping ratio (ξ_i) at shear strain γ_i can be expressed,

$$\xi_i = \frac{W_{d_i}}{4\pi W_{s_i}} = \frac{2}{\pi} \left(\frac{2A_i}{G_i\gamma_i^2} - 1 \right) \quad i = 2, \dots, n \quad (2.51)$$

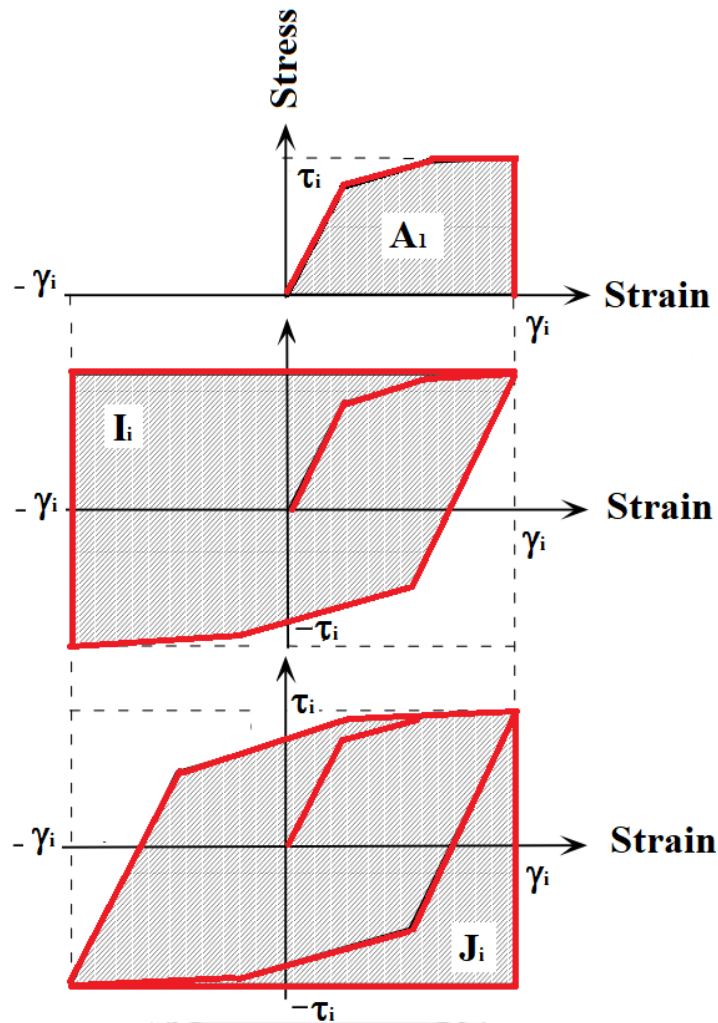


Figure 2.32. Areas A_i , I_i , and J_i calculated for hysteresis loop during the cyclic loading based on IM model (reproduced from Bardet and Tobita (2001))

During the loading, especially when the shear strain γ exceeds γ_n , the IM model assumes the shear stress is equal to shear strength R_n . Therefore, the secant modulus G and critical damping ratio becomes,

$$G = \frac{R_n}{\gamma} \quad (2.52)$$

$$\xi = \frac{2}{\pi} \left(\frac{2(A_n + R_n(\gamma - \gamma_n))}{R_n \gamma} - 1 \right) \quad (2.53)$$

whereas for very large strain, the secant modulus becomes zero and the damping ratio tends toward $2/\pi$.

In general, the ξ depends on the shape of G/G_{max} – strain curve. However, it is independent on G_{max} . The IM model calculated the hysteresis loop based on Masing similitude, where the material parameters are calculated point by point. The IM model can be assigned the same curves as used in equivalent linear model. However, it has the different damping ratio curves. In general, the damping ratio calculated based on IM model is none at small strain and the damping ratio inclines to decrease for some strain range due to the relative variation of A_i and W_s . Based on Equation (2.53), the first derivation of ξ can be expressed as follows,

$$\frac{d\xi}{d\gamma} = \frac{4 R_n \gamma_n - A_n}{\pi R_n \gamma^2} \quad \text{for } \gamma > \gamma_n \quad (2.54)$$

which is positive since $R_n \gamma_n$ is always larger than A_n . Therefore, the damping ratio tends toward re-increase for large strain, especially once the materials have failed at constant shear strength.

In case of rigid-perfectly plastic material, the IM model assumes that H_I is infinity and $n = 1$, which leads to the dissipated energy (W_d), the damping ratio (ξ), and the maximum strain energy (W_s) for cycles of strain amplitude (γ) expressed in these following equations,

$$W_d = 4\gamma R_1 \quad (2.55a)$$

$$\xi = \frac{W_d}{4\pi W_s} = \frac{2}{\pi} \quad (2.55b)$$

$$W_s = \frac{1}{2} \gamma R_1 \quad (2.55c)$$

In case of elastic-perfectly plastic material, the IM model assumed that $H_I = G_{max}$ and $R_I = \tau_{max}$. Therefore, G - γ strain and damping becomes,

$$\frac{G}{G_{max}} = \begin{cases} 1 & \text{when } \gamma < R_1 / H_1 \\ \frac{R}{H_1 \gamma} & \text{when } \gamma < R_1 / H_1 \end{cases} \quad (2.56a)$$

$$\xi = \begin{cases} 0 & \text{when } \gamma < R_1 / H_1 \\ \frac{2}{\pi} \left(1 - \frac{R_1}{H_1 \gamma} \right) & \text{when } \gamma < R_1 / H_1 \end{cases} \quad (2.56b)$$

B. Pressure dependent hyperbolic model

The pressure dependent hyperbolic model was firstly introduced by [Duncan and Chang \(1970\)](#) with numerous modification in other works, such as [Hardin and Drnevich \(1972\)](#), [Finn et al. \(1977\)](#), and [Matasovic \(1993\)](#). In DEEPSOILS program, this model was modified by [Hashash and Park \(2001\)](#) that extended the hyperbolic model proposed by [Matasovic \(1993\)](#). This model emphasized the hysteresis loop during cyclic loading having the backbone curve defined as the hyperbolic function as shown in Figure 2.33.

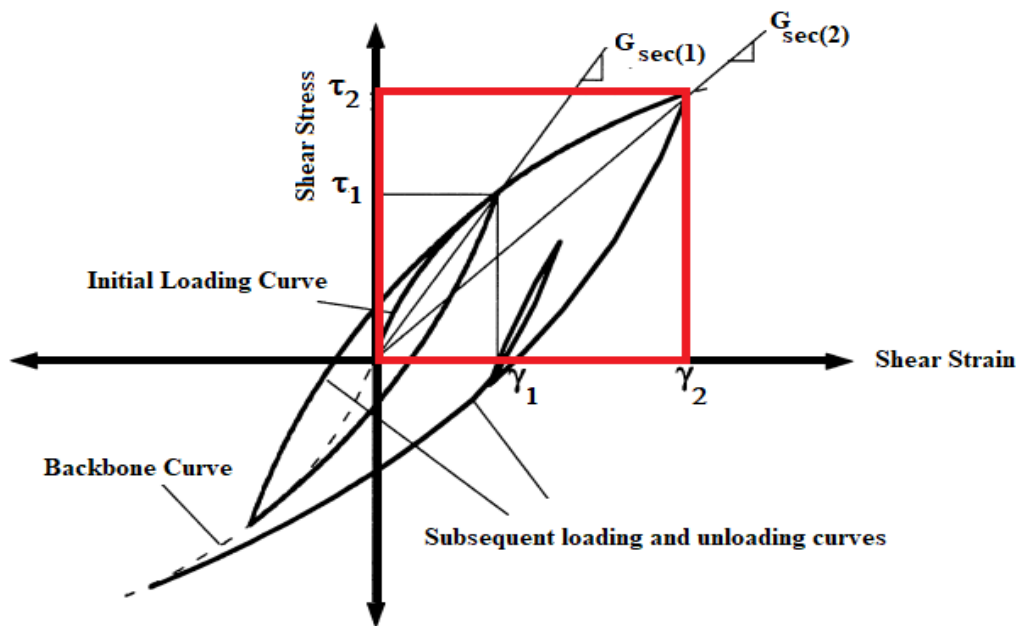


Figure 2.33. Hyperbolic, non-linear model with extended Masing's rule to define loading and unloading behaviour (reproduced from [Hashash and Park \(2001\)](#))

Nonlinear analysis is performed to analyse the important aspects such cyclic behaviour of soil. In nonlinear analysis, the motion equations and system equilibrium are defined in discrete time increments in time domain on lumped mass system, which is expressed as follows,

$$[M]\{\ddot{u}\} + [C]\{\dot{u}\} + [K]\{u\} = -[M][I]\{\ddot{u}_g\} \quad (2.57)$$

where, $[M]$ is mass matrix, $[C]$ is damping matrix, $[K]$ is stiffness matrix, $\{\ddot{u}\}$ = vector of nodal relative acceleration, $\{\dot{u}\}$ = vector of nodal relative velocity, and $\{u\}$ is

vector of nodal relative displacement, and $\{\ddot{u}_g\}$ is the acceleration at base of soil column and $[I]$ is the unit vector. All variables in Equation 2.57 are assembled with the increments of the soil layers.

In hyperbolic model proposed by [Matasovic \(1993\)](#), the backbone curve is expressed by the following equation,

$$\tau = \frac{G_{mo}\gamma}{1 + \beta \left(\frac{G_{mo}}{\tau_{mo}} \gamma \right)^s} = \frac{G_{mo}\gamma}{1 + \beta \left(\frac{\gamma}{\gamma_r} \right)^s} \quad (2.58)$$

where τ is shear stress, γ is shear strain, G_{mo} is initial shear modulus, τ_{mo} is the shear stress at approximately 1% shear strain, and γ_r is the constant value of referenced shear strain. The model was modified from the original one proposed by [Kondner \(1963\)](#), with the additional parameters β and s , which adjusted the shape of backbone curve to represent a wider range of measured soil behaviour.

To show that the reference strain is dependent on confining pressure, [Hardin and Drnevich \(1972\)](#) used laboratory test on clean dry sand by using a normalizing strain to capture modulus degradation with confining pressure. The use of γ_r proportional to $\sigma_o^{0.5}$ to reflect the confining pressure in hyperbolic model was proposed by [Shibata and Soelarno \(1975\)](#). However, [Matasovic \(1993\)](#) considered γ_r as a constant material property. [Hashash and Park \(2001\)](#) modified γ_r in the updated model, which can depict the effect of confining pressure on modulus degradation as expressed in the following equation,

$$\gamma_r = a \left(\frac{\sigma^i}{\sigma_{ref}} \right)^b \quad (2.59)$$

where a and b are curve fitting parameters and σ_{ref} is a reference confining pressure, i.e. 0.18 MPa.

In terms of damping ratio, [Matasovic \(1993\)](#) proposed a damping matrix equation, where the small strain viscous damping effects are assumed proportional only to stiffness of soil layers, which is expressed as follows,

$$[C] = \frac{2\xi}{\omega} [K] \quad (2.60)$$

where, ω is circular frequency and ξ is the critical damping ratio. $[C]$ is assumed as the independent parameter to strain level, so that the effect of hysteretic damping induced by nonlinear behaviour can be separated from viscous damping. ξ is determined from the curve of damping ratio at small strain.

A dependency of very small strain soil damping on confining pressure had been investigated by Laird and Stokoe (1993). Therefore, Hashash and Park (2001) proposed the dependency of zero strain equivalent for damping ratio on confining pressure, as expressed in the following equation,

$$\xi = \frac{c}{(\sigma')^d} \quad (2.61)$$

where c and d are material parameters and σ' is the vertical effective stress. Considering Equation (2.61), then Equation (2.60) is transformed to be the new formulation as expressed in the following equation,

$$[C] = \frac{2}{\omega} \begin{pmatrix} \xi_1 K_1 & -\xi_1 K_1 & \\ -\xi_1 K_1 & \xi_1 K_1 + \xi_2 K_2 & -\xi_2 K_2 \\ & -\xi_2 K_2 & \end{pmatrix} \quad (2.62)$$

The viscous damping is also considered in this model, which consist of any combination of mass and stiffness matrix as proposed by Clough and Penzien (1993) in the following equation,

$$[C] = [M] \sum_{b=0}^{N-1} a_b \left[[M]^{-1} [K] \right]^{b_c} \quad (2.63)$$

where, N is the number of modes incorporated. The viscous damping can be expressed as,

$$\xi_n = \frac{1}{4} \sum_{b=0}^{N-1} a_b (2\pi f_n)^{2b} \quad (2.64)$$

Park and Hashash (2004) included 4 models in their study and thus a_b parameters by,

$$\begin{bmatrix} \xi_m \\ \xi_n \\ \xi_o \\ \xi_p \end{bmatrix} = \frac{1}{4\pi} \begin{pmatrix} \frac{1}{f_m} & f_m & f_m^2 & f_m^5 \\ \frac{1}{f_n} & f_n & f_n^2 & f_n^5 \\ \frac{1}{f_o} & f_o & f_o^2 & f_o^5 \\ \frac{1}{f_p} & f_p & f_p^2 & f_p^5 \end{pmatrix} \begin{bmatrix} a_0 \\ a_1 \\ a_2 \\ a_3 \end{bmatrix} \quad (2.65)$$

where f_m to f_p are the selected frequencies and ξ_m to ξ_p are the damping ratios at these selected frequencies which may have the value of zero strain equivalent in Equation (2.61). [Park and Hashash \(2004\)](#) recommended the first two frequencies can be chosen in part to cover the range of frequencies where there was the significant energy in the input motion. The third and the fourth frequencies should be approximately 10 Hz to provide the best agreement of the results between a linear time-domain analysis and a linear frequency-domain analysis

C. Effective stress model

Effective stress model has been developed and implemented in many commercial programs, such as FLIP and CYCLIC 1D, which were proposed by [Iai et al. \(1992b\)](#) and [Elgamal et al. \(2006\)](#), respectively. The effective stress model implemented in FLIP has been elaborated in Section 2.2. In this section, the details of effective stress model proposed by [Elgamal et al. \(2006\)](#) is presented.

The cyclic stress-strain behaviour in saturated sandy soil is complex ([Pender et al., 2016](#)). However, there is any exception for loose sands at low confining pressure, which behave as contractive material marking generation of positive pore water pressure. To get the better understanding, [Ishihara et al. \(1975\)](#) introduced phase transformation (PT) to describe the behaviour of saturated sandy soil under dynamic load.

The general trend of cyclic effective stress path and shear-strain described by [Ishihara et al. \(1975\)](#) explanation is presented in Figure 2.34. Once the shear stress ratio has been reached, there is a transformation phase from contraction to dilation. This condition happens when the effective stress path achieves phase transformation line

(phase 1). The soil stiffness increments and effective stress path movement (phase 2) also happen. Once the reverse load is applied, the effective confining pressure reduction happens. Besides, soil will behave as contractive material (phase 3 to phase 4) and be followed by the accumulation of excess pore water pressure at phase 5. Furthermore, it may fail at phase 6. The reverse of compression to extension would reach the transformation line at phase 7. It would continuously result in shear strain and excess pore water pressure accumulations (phase 8). Like compression, it may fail at phase 9.

In 2006, a computer program called CYCLIC 1D was launched by [Elgamal et al. \(2006\)](#). This program was one of the most powerful program which can be used to analyse seismic response during wave propagation. This program also can be used to analyse liquefaction during earthquake. CYCLIC 1D employed the nonlinear model which called as effective stress model in the finite element framework. This program is operated in time-domain and allowing for linear ([Hughes, 1987](#)) and nonlinear studies. The incremental plasticity models are implemented to simulate the nonlinearity to allow for modelling permanent deformation and for generation of hysteresis damping. The finite element analysis code are defined within a coupled solid-fluid formulation for analysis of dry as well as saturated materials ([Chan \(1988\)](#) and [Zienkiewicz et al. \(1990\)](#)).

The liquefaction model in CYCLIC 1D is based on [Parra \(1996\)](#) and [Yang \(2000\)](#) studies. The model is developed within the framework of multi-yield surface which was originally proposed by [Prevost \(1985\)](#). The model emphasizes on the controlling the magnitude of cyclic permanent shear strain accumulation in various sand types ([Parra \(1996\)](#) and [Yang \(2000\)](#)). The cyclic mobility mechanism in terms of loading-unloading flow rules were devised to reproduce the observed strong dilation tendency, which also results the increase in cyclic shear stiffness and strength. In addition, the phases in Figure 2.34 are incorporated by developing the new flow rule in this model. The incorporated new flow rule may significantly change the characteristic of model response. The incorporated new flow rule may also reproduce cyclic mobility mechanisms. The incorporated flow rule also exercises more direct control over shear strain accumulation ([Elgamal et al., 2006](#)). In addition, a new kinematic hardening rule was developed into multi-yield surface. The stiffness is evaluated in each incremental step. In calculation, excess pore water pressure and pore water pressure dissipation are

modelled under cyclic loading (Elgamal et al., 2006). The description of multi-yield surface of effective stress model proposed by Elgamal et al. (2006) is shown in Figure 2.35.

Considering Figure 2.35, the interpretation of shear stress-shear strain relationship is drawn in Figure 2.36. Based on the figure, the number of yield surface can be divided to be many yield surfaces, where the outermost surface is noted as the envelope of failure surface. In the model, each yield surface has the different tangential shear modulus and is associated with a constant plastic modulus (Elgamal et al., 2003).

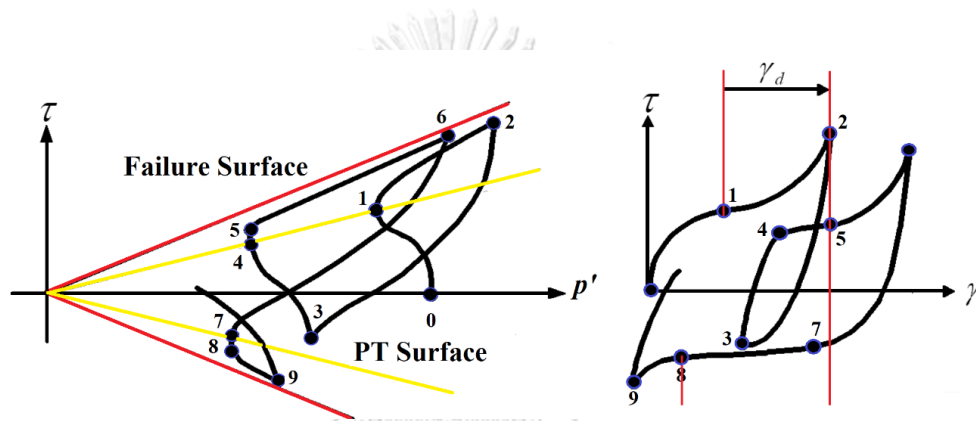


Figure 2.34. Schematic of constitutive model response showing shear stress, effective confinement, and shear-strain relationship (reproduced from Elgamal et al. (2006))

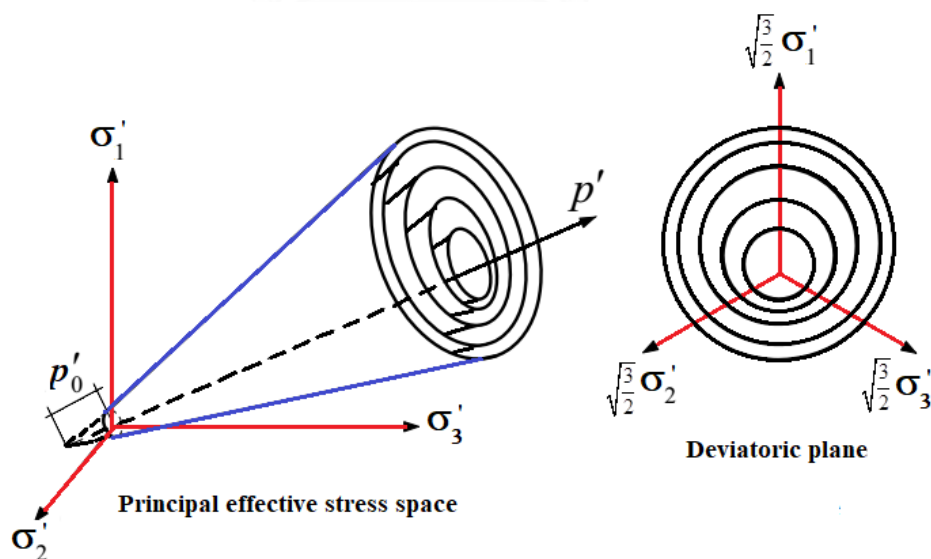


Figure 2.35. Multi-yield surfaces in principal stress space and deviatoric plane (reproduced from Parra (1996) and Yang (2000))

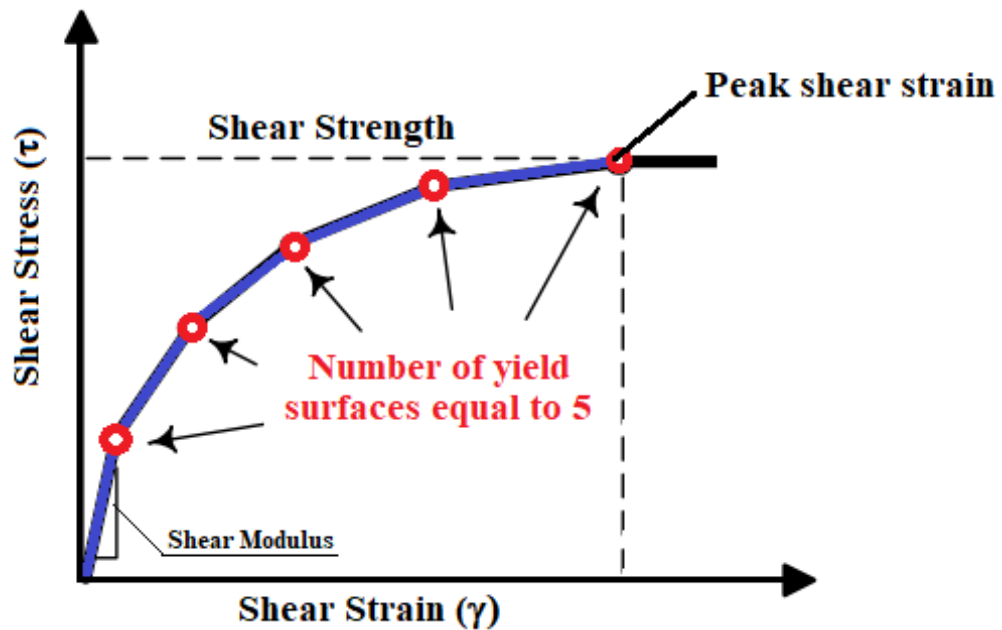


Figure 2.36. The backbone curves and yield surfaces (reproduced from [Elgamal et al. \(2006\)](#))

2.4.4. Computation method of one-dimensional seismic response analysis

One dimensional seismic response analysis analyses the wave propagation from bedrock to ground surface. The description of the geometry and the boundary condition of one-dimensional site response analysis is presented in Figure 2.37. In one-dimensional seismic response analysis, the shear wave is propagated vertically in one-dimensional layered system. The soil layers were assumed to be homogenous, infinite horizontal extension, and the input motion propagating from bedrock. In general, the governing equation of the system is expressed as,

$$\rho \frac{\partial^2 d}{\partial t^2} + \eta \frac{\partial d}{\partial t} = \frac{\partial \tau}{\partial z} \quad (2.66)$$

where ρ is the soil unit mass, d is the horizontal displacement, z is the depth, t is the time, τ is shear stress, and η is a mass-proportional damping coefficient. In the model, the boundary condition is limited at ground surface ($z = 0$) and at the bottom of soil ($z=H$), which is expressed as follows,

$$\tau = 0 \quad \text{for } z = 0 \quad (2.67a)$$

$$\tau = \tau_B \quad \text{for } z = H \quad (2.67b)$$

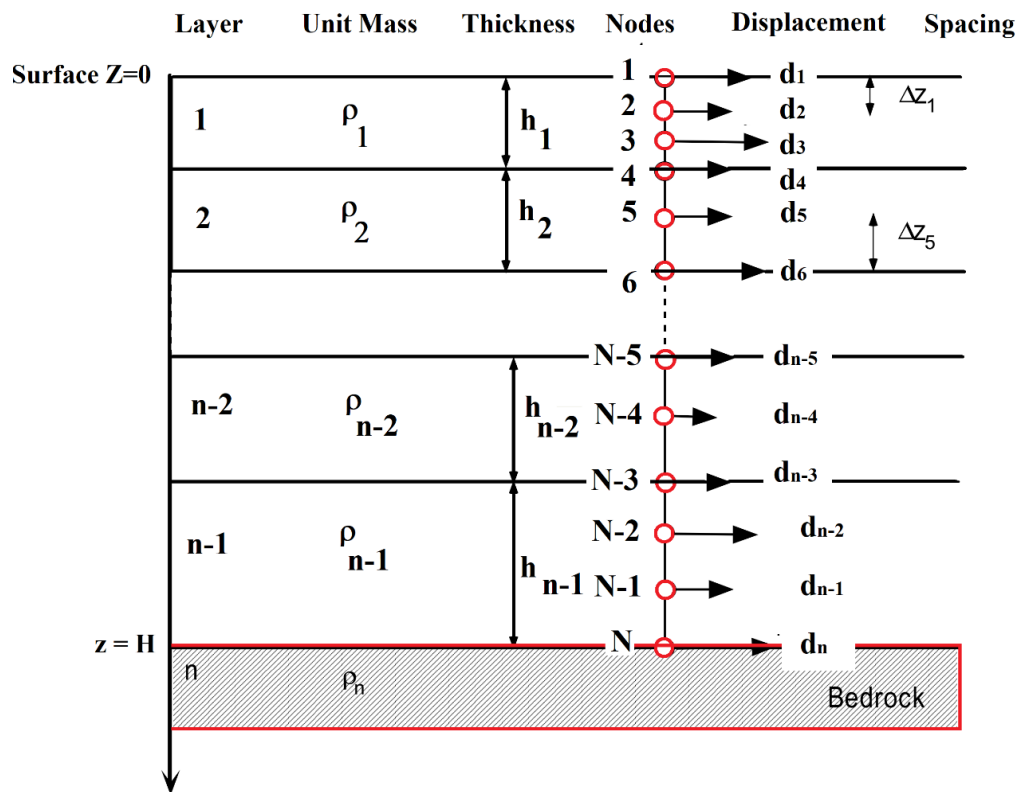


Figure 2.37. One dimensional layered soil deposit system and its spatial discretization (reproduced from Bardet and Tobita (2001))

The terminology of seismic response analysis is described in Figure 2.38. Based on the figure, there are three motions used in site response analysis. The first one is surface motion. The second and the third ones are bedrock and outcropped motions, respectively. During earthquake, the incoming motion propagated vertically and has amplitude d_I . At the bedrock, because of refracted wave, the propagated wave has the amplitude of $d_I + d_R$. At the outcropped rock, the propagated wave has amplitude $2d_I$, since there is no shear stress at the free surface. At the ground surface, the propagated wave has amplitude of d_I , which is determined by seismic response analysis.

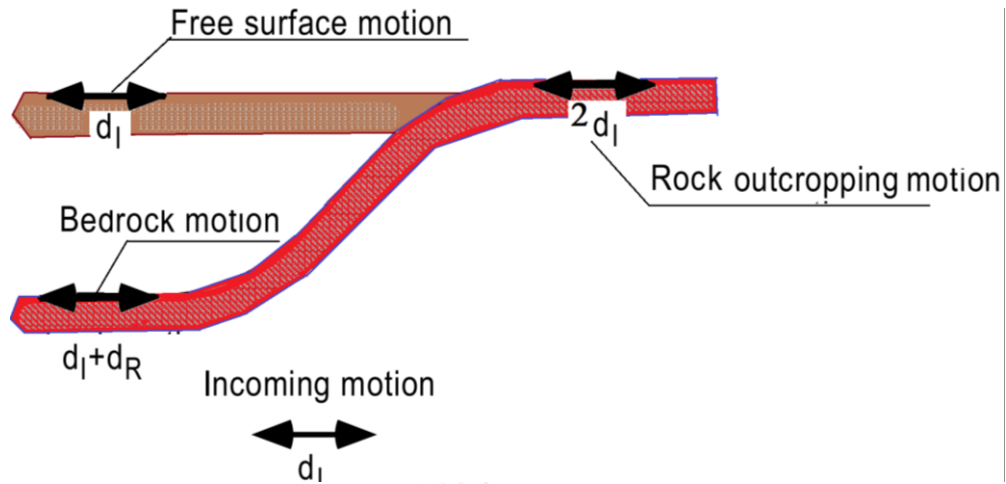


Figure 2.38. Terminology used in seismic response analysis and shear wave velocity at various location (reproduced from [Bardet and Tobita \(2001\)](#))

The shear stress at the bottom (τ_B) can be estimated using the velocity at depth of bedrock by using the particle displacement due to the incident wave in the bedrock ([Joyner and Chen, 1975](#)) as a function of z and time as follows,

$$d_I = d_I(z + v_s t) \quad (2.68a)$$

Due to the refracted wave, the displacement (d_R) can be calculated by,

$$d_R = d_R(z - v_s t) \quad (2.68b)$$

the shear stress at the bottom can be calculated by,

$$\tau_B = \mu \left(\frac{\partial d_I}{\partial z} + \frac{\partial d_R}{\partial z} \right) \quad (2.68c)$$

where, μ is the shear modulus at the bedrock. The first derivation of Equation (2.68a) and (2.68b) is expressed as follows,

$$\frac{\partial d_I}{\partial z} = \frac{v_I}{v_s} \quad (2.69a)$$

$$\frac{\partial d_R}{\partial z} = -\frac{v_R}{v_s} \quad (2.69b)$$

where, v_I and v_R are the velocity of incident mot and velocity of due to the refracted wave, respectively; therefore, the velocity at the bedrock (v_B) is expressed as,

$$v_B = v_I + v_R \quad (2.70)$$

Using Equation (2.68) to (2.70), the shear stress at the bedrock can be calculated by,

$$\tau_B = \frac{\mu}{v_s} (2v_1 - v_B) = \rho v_s (2v_1 - v_B) \quad (2.71)$$

where, ρ is mass density. For outcropped rock, where τ_B is 0, the velocity at the outcropped rock (v_R) is expressed as,

$$v_B = 2v_1 \quad (2.72)$$

In general, there are three conventional method used in one-dimensional seismic response analysis. The first one is Finite Difference Method. One program used this method in seismic response analysis is NERA. The second one is lumped mass system, which is implemented in DEEPSOILS Program. The last one is Finite Element Method, which is implemented in CYCLIC 1D and FLIP.

The detailed explanation of the computational analysis and model idealism are elaborated as follows,

- Finite difference method

As shown in 2.37, the column is divided into $m-1$ layer with various thickness and the soil parameters. First order derivative is approximated using a forward finite difference approximation as expressed in this following,

$$\frac{df(z_i)}{dz} = \lim_{\Delta z_i \rightarrow 0} \frac{f(z_i + 1) - f(z_i)}{\Delta z_i} \quad (2.73)$$

where, f represents the differential function, $\Delta z_i = z_{i+1} - z_i$. The strain in the layer below is expressed by,

$$\gamma_{i,n} = \frac{\partial d}{\partial z} = \frac{d_{i+1,n} - d_{i,n}}{\Delta z_i} \quad (2.74)$$

As shown in Figure 2.39, strain is constant between the nodes i and $i+1$, which implied that the stress is also between nodes i and $i+1$. The governing equation at nodes $i = 1, \dots, N$ at time t_n is expressed by,

$$\rho_i a_{i,n} + \eta_i v_{i,n} = F_{i,n} \quad (2.75)$$

where, ρ_i and η_i are the unit mass and viscosity between each node, respectively. F is the stress gradient at the node, which are expressed by,

$$F_{i,n} = \frac{\delta\tau}{\delta z} \approx 2 \frac{\tau_{i,n} - \tau_{i-1,n}}{\Delta z_i - \Delta z_{i-1}} \quad (2.76)$$

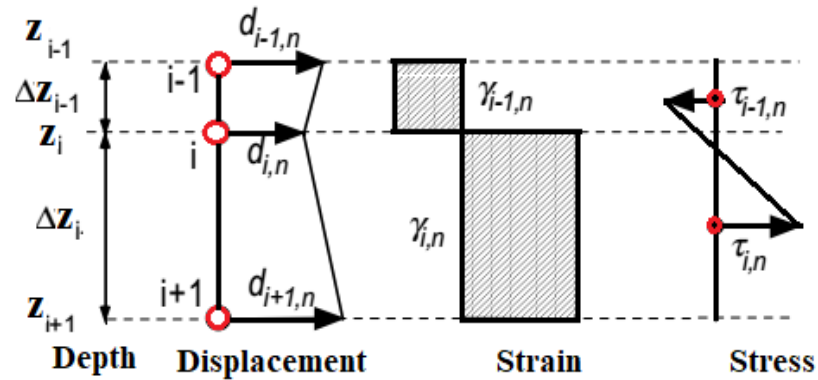


Figure 2.39. Definition of displacement, strain, and stress in finite difference formulation (reproduced from Bardet and Tobita (2001))

In Figure 2.40a, in Node 1, at fictitious node 0 and fictitious layer of Δz_i are introduced above node 1. The stress gradient at the surface is equal to zero. On this fictitious node, the stress $\tau_{0,n}$ should be equal to $-\tau_{1,n}$. Therefore, the average stress should be equal to zero at node 1, which is expressed by,

$$F_{i,n} = \frac{2\tau_{1,n}}{\Delta z_i} \quad (2.77a)$$

For the Node N (at the bottom), the stress should be equal to 0 (Figure 2.40b). a fictitious node $N+1$ and a fictitious layer of Δz_{N-1} are below Node N . This layer, the stress τ_N , is equal to $2\tau_{B,n} - \tau_{N-1,n}$, so that the average stress at Node N is equal to $\tau_{B,n}$. The stress gradient at this layer is calculated by,

$$F_{N,n} = \frac{\tau_{N,n} - \tau_{N-1,n}}{\Delta z_{N-1}} = 2 \frac{\tau_{B,n} - \tau_{N-1,n}}{\Delta z_{N-1}} \quad (2.77b)$$

To predict velocity, acceleration, and displacement time history in the selected node, the finite difference method can be used (Hughes, 1987). The example calculation to predict velocity is presented here.

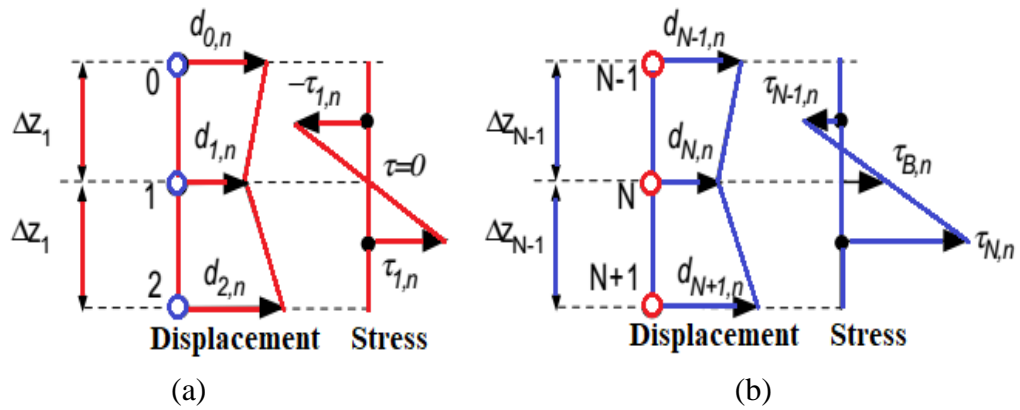


Figure 2.40. Definition of fictitious nodes 0 and N+1 at (a) ground surface and (b) at bottom of soil column (reproduced from Bardet and Tobita (2001))

Define the formulation of the predicted velocity by,

$$\tilde{v}_{i,n+1} = v_{i,n} + \frac{1}{2} a_{i,n} \Delta t \quad (2.78a)$$

where, $\tilde{v}_{i,n+1}$ is related to displacement and velocity corresponding to at times t_n and t_{n+1} by,

$$d_{i,n+1} = d_{i,n} + \Delta t \tilde{v}_{i,n+1} \quad (2.78b)$$

$$v_{i,n+1} = \tilde{v}_{i,n+1} + \frac{1}{2} a_{i,n+1} \Delta t \quad (2.78c)$$

Referring to Equation (2.78), the velocity and acceleration can be expressed as,

$$v_{i,n} = \frac{1}{2} (\tilde{v}_{i,n+1} + \tilde{v}_{i,n}) \quad (2.78d)$$

$$a_{i,n} = \frac{1}{\Delta t} (\tilde{v}_{i,n+1} - \tilde{v}_{i,n}) \quad (2.78e)$$

By substituting Equations (2.78d and e) to Equation (2.76) for i, \dots, N becomes,

$$\tilde{v}_{i,n} = \frac{1}{1 + \eta_i \frac{\Delta t}{2\rho_i}} (\tilde{v}_{i,n} (1 - \eta_i \frac{\Delta t}{2\rho_i}) + F_{i,n} \frac{\Delta t}{\rho_i}) \quad (2.78f)$$

Since viscosity is not considered; Equation (2.78) becomes,

$$\tilde{v}_{i,n+1} = \tilde{v}_{i,n} + F_{i,n} \frac{\Delta t}{\rho_i} \quad (2.78g)$$

At the bottom, Equation (2.71) becomes,

$$\tau_{B,n} = \rho_N v_s (2V_{I,n} - v_{N,n}) \quad (2.78h)$$

Using Equations (2.77a), (2.78d), (2.78e), and (2.78h), Equation (2.78g) becomes,

$$\tilde{v}_{N,n+1} = \frac{\tilde{v}_{N,n}(\Delta z_{N-1} - v_s \Delta t) + 4v_s v_{I,n} \Delta t - 2\tau_{N-1,n} \frac{\Delta t}{\rho_N}}{\Delta z_{N-1} + v_s \Delta t} \quad (2.78i)$$

For the bedrock, where v_s is assumed as the infinity (∞), Equation 2.78h becomes,

$$\tilde{v}_{N,n+1} = -\tilde{v}_{N,n} + 4v_{I,n} \quad (2.78j)$$

whereas at Node N , the velocity is expressed as,

$$\tilde{v}_{N,n} = \frac{1}{2}(\tilde{v}_{N,n+1} + \tilde{v}_{N,n}) = 2v_{I,n} \quad (2.78k)$$

which is the anticipated result for rigid bedrock. If the $\tilde{v}_{i,n+1}$ is obtained, by using Equations (2.78d) and (2.78e) $v_{i,n}$, $a_{i,n}$, and $d_{i,n+1}$ can be calculated.

In general, the steps in calculation process of seismic response analysis using finite difference method are listed in the following,

- ❖ Define the input material, which includes ρ_i : unit mass of soil layer i ρ_N : bedrock density and v_s : shear wave velocity at the bedrock
- ❖ Initialization

$$n=1, \tilde{v}_{i,n}=0, a_{i,n}=0, d_{i,n}=0, \tau_{i,0}=0, \gamma_{i,0}=0, i=1,\dots,N \text{ and } v_{i,0}=0, \\ a_{i,0}=0$$

- ❖ Calculate strain, strain increment, and stress ($i = 1,\dots,N-1$)

$$\gamma_{i,n} = \frac{d_{i+1,n} - d_{i,n}}{\Delta z_i}, \Delta\gamma_{i,n} = \gamma_{i,n} - \gamma_{i,n-1}, \text{ and } \tau_{i,n} = IM(\tau_{i,n-1}, \Delta\gamma_{i,n})$$

- ❖ Calculate input velocity from prescribed acceleration $a_{I,n}$

$$v_{I,n} = v_{I,n-1} + \frac{1}{2}(a_{I,n} + v_{I,n-1})\Delta t$$

- ❖ Calculate predicted velocity

$$\tilde{v}_{N,n+1} = \frac{\tilde{v}_{N,n} (\Delta z_{N-1} - v_s \Delta t) + 4v_s v_{I,n} \Delta t - 2\tau_{N-1,n} \frac{\Delta t}{\rho_N}}{\Delta z_{N-1} + v_s \Delta t} \quad \text{at Node } N \text{ (at the bottom)}$$

$$\tilde{v}_{i,n+1} = \tilde{v}_{i,n} + 2 \frac{\tau_{i,n} - \tau_{i-1,n}}{\Delta z_i + \Delta z_{i-1}} \frac{\Delta t}{\rho_i} \quad \text{at Node } i = 2, \dots, N-1$$

$$\tilde{v}_{i,n+1} = \tilde{v}_{i,n} + \frac{2\tau_{i,n}}{\Delta z_1} \frac{\Delta t}{\rho_1} \quad \text{at Node 1 at surface}$$

❖ Calculate displacement, velocity, and acceleration ($i = 1, \dots, N$)

$$d_{i,n+1} = d_{i,n} + \tilde{v}_{i,n+1} \Delta t$$

$$v_{i,n} = \frac{1}{2} (\tilde{v}_{i,n+1} + \tilde{v}_{i,n})$$

$$a_{i,n} = \frac{1}{\Delta t} (\tilde{v}_{i,n+1} - \tilde{v}_{i,n})$$

$N = n+1$ go to the second step

- Lumped mass system

For layered horizontally soils, the multi-degree of freedom can be employed to solve the problem of seismic response analysis. This method is normally used as lumped mass system. As shown in Figure 2.41, the layered soil system is described as multilayers, which have different layer properties, such as shear modulus, soil density, shear wave velocity, and layer thickness.

In the model, the specified parameter such as stiffness and viscous damping are also required in this analysis. The use of lumped mass system is addressed to solve the dynamic equation (Joyner and Chen, 1975) as shown in Equation (2.57). The stiffness matrix on each layer is calculated by,

$$k_i = \frac{G_i}{h_i} = \frac{\Delta \tau_i(\gamma_i)}{h_i \Delta \gamma_i} \quad (2.79)$$

where, k_i is the stiffness matrix. The stiffness matrix is updated each time increment to incorporate non-linearity of soil. It should be noted that for nonlinear analysis, shear modulus in Equation (2.79) should be the tangential modulus.

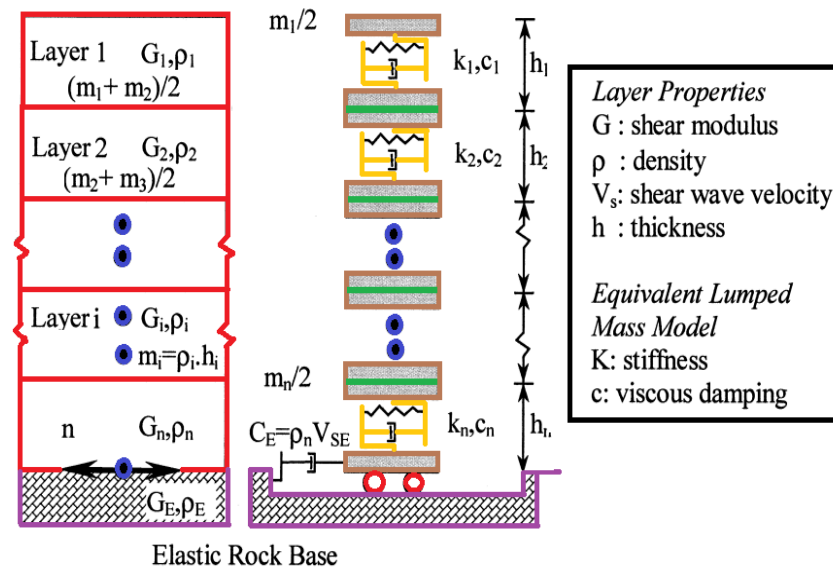


Figure 2.41. Illustration of lumped mass system (reproduced from Hashash and Park (2001))

In general, to perform one-dimensional seismic response analysis using lumped mass system method, the number of layers of soil (N) and the mass and the stiffness matrices (K) should be obtained. The mode shapes and frequencies are obtained from the characteristic value problem as,

$$[K]\{\phi^n\} = \omega_n^2 [M]\{\phi^n\} \quad (2.80)$$

where ϕ^n is the mode shape of i level during the n^{th} mode of vibration and ω_n is the circular frequency at the n^{th} mode of vibration.

Determine the relative displacement at level i as follows,

$$u_i(t) = \sum_{n=1}^N \phi_i^n X_n(t) \quad (2.81)$$

where $X_n(t)$ is the normal coordinate for the n^{th} node and $u(t)$ is the relative displacements at the i -th level at time t .

Determine the relative acceleration and the relative velocity

$$\dot{u}_i(t) = \sum_{n=1}^N \phi_i^n \dot{X}_n(t) \quad \text{for the relative velocity} \quad (2.82a)$$

$$\ddot{u}_i(t) = \sum_{n=1}^N \phi_i^n \ddot{X}_n(t) \quad \text{for the relative acceleration} \quad (2.82b)$$

Determine the total acceleration, velocity, and displacement at level i and time t can be given as follows,

$$\ddot{u} = \ddot{u}_i(t) + \ddot{u}_g \quad \text{for the total acceleration} \quad (2.83a)$$

$$\dot{u} = \dot{u}_i(t) + \dot{u}_g \quad \text{for the total velocity} \quad (2.83b)$$

$$u = u_i(t) + u_g \quad \text{for the total displacement} \quad (2.83c)$$

The shear strain and shear stress between level i and $i+1$ can be calculated by,

$$\text{Shear Strain } [u_i(t) - u_{i+1}(t)] / h_i \quad \text{for shear strain} \quad (2.84a)$$

$$\tau_i(t) = \gamma_i(t)G \quad \text{for shear stress} \quad (2.84b)$$

- Finite element method

Several computer programs such as FLIP and CYCLIC 1D employed finite element method in the ground response analysis. In general, there is no the difference on each program in implementing finite element method to simulate seismic response analysis. The steps to build a model in one dimensional analysis based on the recent study is reviewed.

[Mase et al. \(2016\)](#) illustrated the model of soil column subjected to the earthquake in Northern Thailand by using finite element method as shown in Figure 2.42. In the study, [Mase et al. \(2016\)](#) performed the analysis to derive mesh. The mesh derivation is obtained from the analysis of wave length. [Mase et al. \(2016\)](#) suggested the minimum size mesh of 0.5 m as the considered mesh size in simulation. This suggestion is also consistent with what was suggested by [Pender et al. \(2016\)](#) study.

The assumptions which were normally taken in the analysis are listed in the following,

- The drainage is assumed only on vertical direction.
- The input motion is applied at the bottom of soil column, where was assumed as engineering bedrock.
- There is no drainage path on both vertical and bottom sides, so the bedrock is assumed as impermeable layer.
- Soil column is assumed as fixed boundary.

- Vertical deformation is allowable.
- Horizontal displacements at both sides are the same.
- Lateral normal stress on both boundaries can be generated.
- Excess pore water pressure at the selected element can be estimated.
- The procedure in finite element simulation in seismic response analysis is the same with other simulations in many cases. Therefore, in its implementation, the difference in analytical procedure is depending on the soil model. Since the problems in soil dynamics are different from other fields (such as static slope stability analysis), the soil model is also different. In soil dynamics problem, equivalent linear model, nonlinear model, and effective stress model are used in the modelling.

2.5. Next Generation Attenuation Model

In 2008, PEER (Pacific Earthquake Engineering Research) Institute launched the Next Generation Attenuation Model for Western America (NGA-West). Several researchers had involved in the project, i.e. Dr. N.A. Abrahamson, Dr. W.J. Silva, Dr. G.M. Atkinson, Dr. D.M. Boore, Dr. K.W. Campbell, Dr. Y. Bozorgnia, Dr. B.S-J. Chiou, Dr. R.R. Youngs, and Dr. I.M. Idriss.

The NGA models are the next generation attenuation model developed for the earthquake event in Western America which is known as the tectonic active region in United States of America. Therefore, NGA-West models are suitable only for shallow crustal earthquake occurred at the active tectonic region. In the implementation, the NGA models are addressed to estimate peak ground acceleration for various sites. However, only four models which were destined to estimate ground motion at soil sites, i.e. [Abrahamson and Silva \(2008\)](#), [Boore and Atkinson \(2008\)](#), [Campbell and Bozorgnia \(2008\)](#), and [Chiou and Youngs \(2008\)](#) models. For rock sites, [Idriss \(2008\)](#) model is eligible to estimate ground motion. The list of models' parameters of each NGA is compiled in Table 2.3.

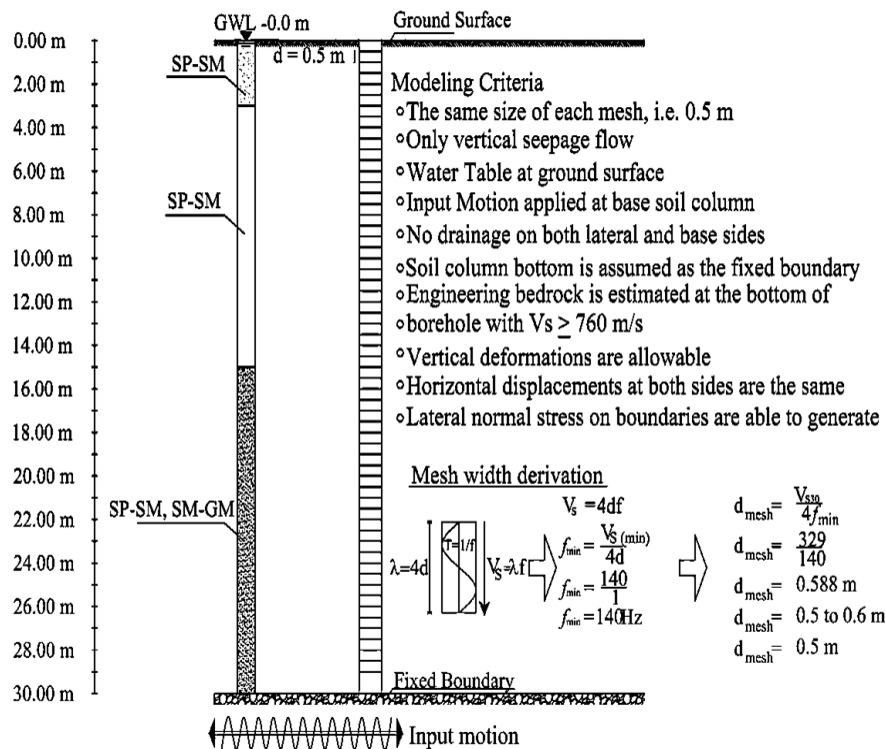


Figure 2.42. Soil column model subjected to earthquake in finite element method (modified from [Mase et al. \(2016\)](#))

In Table 2.3, there are specific parameters in terms of source mechanism, i.e. fault effect. The fault types considered in shallow crustal earthquake for active tectonic regions include the strike slip fault, reverse or normal fault for hanging wall site, and reverse or normal fault for foot-wall site. Prior to understand the concept of fault types, the understanding of primary geological structure should be achieved. The illustration of geology structure can be seen in Figure 2.43. Each layer has the dip, strike, rake as shown in Figure 2.43a. The information such as depth to rupture, the width and length of fault are needed in analysis of attenuation model using NGA. In addition, from the interpretation of geological structure, type of normal fault also can be specified, for example hanging wall or foot wall.

Table 2.3. Model applicability of NGA

NGA models	Symbols	Parameters	Unit	Model Ranges
Abrahamson and Silva (2008)	M_w	Moment magnitude	M_w	$3 \leq M_w \leq 8.5$
	R_{rupt}	Distance to Rupture	km	$0 \leq R_{rupt} \leq 300$
	V_{s30}	The average of first 30 m shear wave velocity	m/s	$180 \leq V_{s30} \leq 1000$
Boore and Atkinson (2008)	$M_w(SS)$	Moment magnitude for slip strike earthquake	M_w	$3 \leq M_w \leq 8.5$
	$M_w(RS)$	Moment magnitude for reverse strike earthquake	M_w	$3 \leq M_w \leq 8.5$
	$M_w(NM)$	Moment magnitude for normal fault earthquake	M_w	$3 \leq M_w \leq 7.0$
	R_{jb}	Distance to surface projection	km	$0 \leq R_{jb} \leq 400$
	V_{s30}	The average of first 30 m shear wave velocity	m/s	$150 \leq V_{s30} \leq 1500$
	$Z_{1.0}$	Depth to V_s of 1 km/sec	km	$0 \leq Z_{1.0} \leq 3$
Campbell and Bozorgnia (2008)	$M_w(SS)$	Moment magnitude for slip strike earthquake	M_w	$3 \leq M_w \leq 8.5$
	$M_w(RS)$	Moment magnitude for reverse strike earthquake	M_w	$3 \leq M_w \leq 8.5$
	$M_w(NM)$	Moment magnitude for normal fault earthquake	M_w	$3 \leq M_w \leq 7.5$
	R_{rup}	Distance to Rupture	km	$0 \leq R_{jb} \leq 300$
	V_{s30}	The average of first 30 m shear wave velocity	m/s	$150 \leq V_{s30} \leq 1500$
	$Z_{2.5}$	Depth to V_s of 2.5 km/sec	km	$0 \leq Z_{2.5} \leq 10$
	Z_{hyp}	Hypocentre depth from the earthquake	km	$0 \leq Z_{hyp} \leq 20$
	Z_{tor}	Depth to top of coseismic rupture	km	$0 \leq Z_{tor} \leq 20$
Chiou and Youngs (2008)	dip	Average dip of the rupture plane	$degree$	$15 \leq dip \leq 90$
	$M_w(SS)$	Moment magnitude for slip strike earthquake	M_w	$3 \leq M_w \leq 8.5$
	$M_w(RS)$	Moment magnitude for reverse strike earthquake	M_w	$3 \leq M_w \leq 8.5$
	$M_w(NM)$	Moment magnitude for normal fault earthquake	M_w	$3 \leq M_w \leq 8.0$
	R_{rup}	Distance to Rupture	km	$0 \leq R_{rupt} \leq 300$
	V_{s30}	The average of first 30 m shear wave velocity	m/s	$150 \leq V_{s30} \leq 1500$
	$Z_{1.0}$	Depth to V_s of 1 km/sec	km	$Z_{1.0} \leq 20$
Idriss (2008)	Z_{tor}	Depth to top of coseismic rupture	km	$0 \leq Z_{tor} \leq 10$
	M_w	Moment magnitude for slip strike earthquake	M_w	$M_w \geq 5.0$
	R_{rup}	Distance to Rupture	km	$R_{rup} \leq 150$
	V_{s30}	The average of first 30 m shear wave velocity	m/s	$V_{s30} \geq 450$

Figure 2.44 presents the detailed explanation of fault types to determine some distance to earthquake, such as R_{JB} (distance to coseismic rupture or Joyner-Boore distance), R_{rup} (distance to rupture), and R_X (distance from top rupture to the investigated site). In Figure 2.44a, the slip strike fault is presented, where the dip is almost perpendicular to the ground surface. Figure 2.44b and 2.44c, the inclined dip is presented. These figures are categorized as normal fault. In Figure 2.44b, the fault type is noted as hanging wall, otherwise the foot wall is presented in Figure 2.44c.

The implementation of NGA models in estimation of ground motion by considering the uncertainty in earthquake, such as magnitude, the site classification, source mechanism, and the distance to rupture had been performed in many areas. The data used in NGA models included many ground motion records that were collected from many regions, such as United States, Italy, Japan, New Zealand, Turkey, and Taiwan. Therefore, the use of NGA models to predict ground motion prediction in global locations can be acceptable.

2.6. Geophysical Survey

2.6.1. Ambient noise using microtremor

Many researchers ([Lachet et al. \(1996\)](#), [Bard \(2004\)](#), and [El-Hady et al. \(2012\)](#)) had performed the use of short-period microtremor for observation to the site effects. The assumption used in the microtremor observation is that the horizontal motion of microtremor consisted of spectral motion reflected the transfer function of the ground motion, which can estimate the predominant period (T_0) as well as the predominant frequency (f_0) from H/V ratio of sediments.

The empirical technique to estimate the H/V ratio of sites based on microtremor observation was introduced by [Nakamura \(1989\)](#). The method was derived based on spectral ratio comparison of the horizontal to vertical of the recorded ambient noise. The method was aimed to expect H/V ratio of sediment deposit during the recording of the ambient noise measurements. [Atakan \(2009\)](#) noted that the H/V ratio derived from the ambient noise measurement was consistent with the H/V ratio of the earthquake recorded on between the surface of the sediments and the surface of bedrock (the interface between bedrock and the sediment deposit). The technique of the approach

can depict the predominant frequency and resulted in the expected estimation of the site response of sediment soil deposits (Lachet and Bard, 1994).

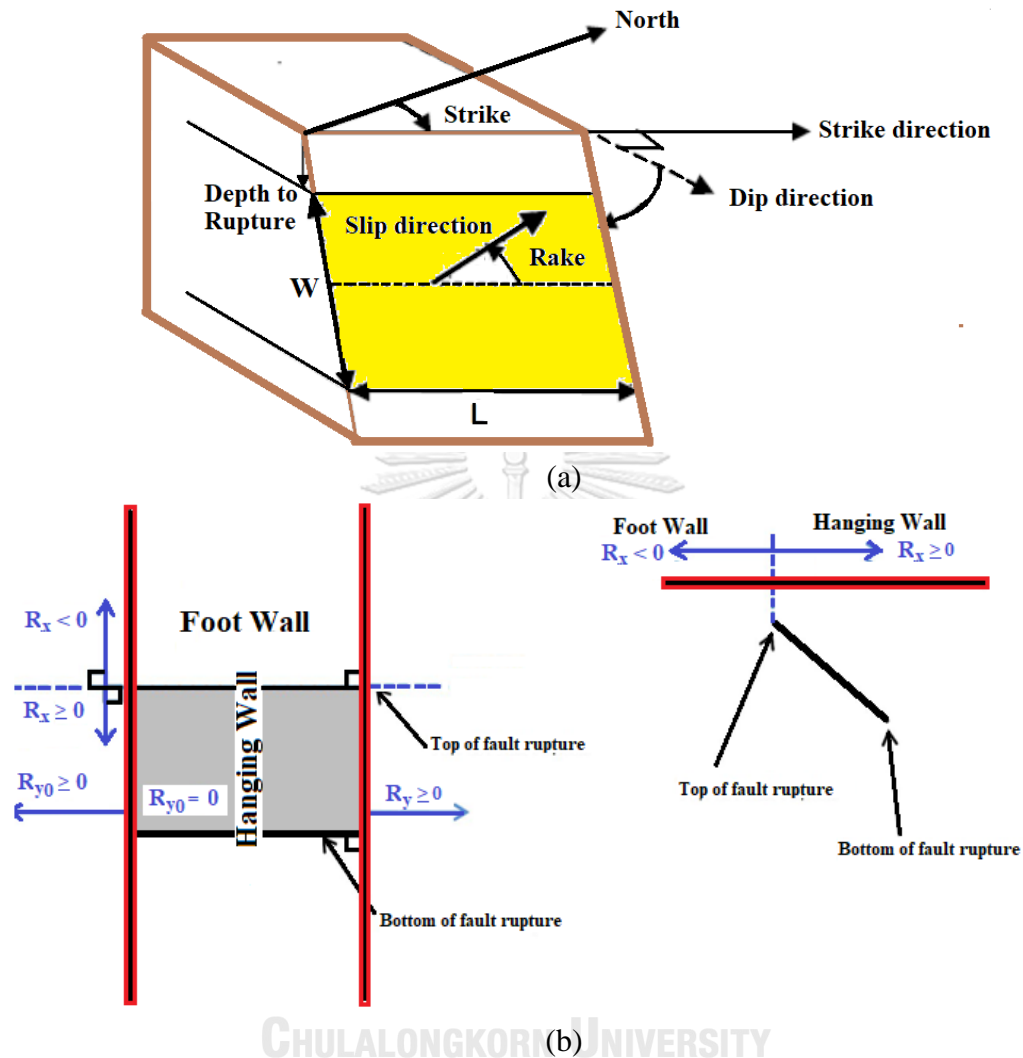


Figure 2.43. Description of geology structure (a) strike-rake-dip (b) foot wall and hanging wall (Courtesy Jenifer Donahue (with modification))

The estimation of H/V ratio of sites based on S waves comparison on horizontal and vertical direction is expressed in Equation (2.85) below,

$$H/V = \sqrt{\frac{H_{(EW)}^2 + H_{(NS)}^2}{2V^2}} \quad (2.85)$$

where, $H_{(EW)}$ and $H_{(NS)}$ are the horizontal spectral values in the EW and NS directions, respectively, and V is the vertical spectral value.

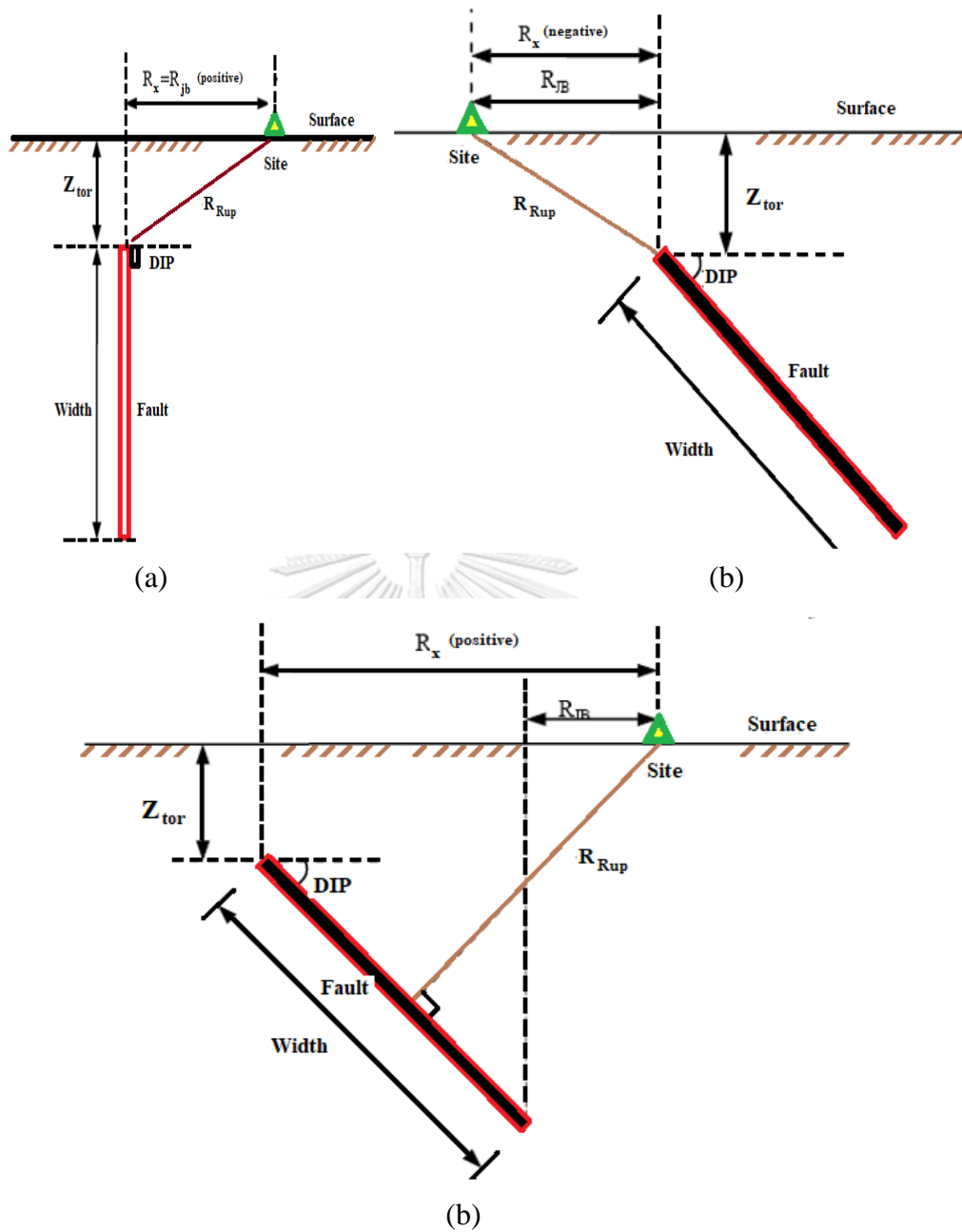


Figure 2.44. Fault types in active tectonic region (Courtesy Jenifer Donahue (with modification) (a) slip strike, (b) reverse strike for foot wall, (c) reverse strike for hanging wall

H/V ratio and f_0 are able to be used to determine the vulnerability of the site. This vulnerability index (Nakamura, 1997) is derived using Equation (2.86) below,

$$K_g = \frac{A^2}{f_0} \tag{2.86}$$

where K_g is the vulnerability index, A is the point of peak amplitude on the curve, and f_0 is the dominant frequency.

[Nakamura \(1997\)](#) also identified shear strain (γ) at the ground surface as a key parameter in K_g . The γ value range and its associated phenomena were compiled by [Ishihara \(1978\)](#), and are shown in Table 2.4. The value of γ is calculated as follows,

$$\gamma = \frac{K_g a}{\pi^2 V_b} \quad (2.87)$$

where γ is the shear strain of the dynamic soil properties, a is the acceleration of the seismic wave at the base rock, and V_b is the shear wave velocity at the base rock, which is assumed to be 600 m/s, following [Nakamura \(1997\)](#).

Table 2.4. Strain dependence of soil dynamic properties ([Ishihara, 1978](#))

Shear Strain (γ)	10^{-6}	10^{-5}	10^{-4}	10^{-3}	10^{-2}	10^{-1}
Phenomena	Wave Vibration		Crack Settlement		Landslide, Soil Compaction, Liquefaction	
Dynamic Properties	Elastic		Elastic-Plastic		Collapse Repeat-Effect, Speed-Effect of Loading	

Many studies had confirmed that the H/V ratio were much more stable than the raw noise spectra ([Lachet et al. \(1996\)](#), [Koçkar and Akgün \(2012\)](#)). The H/V ratio normally agree with the predominant frequency (f_0). The human noise and the environmental setting usually restricted the valuable measurement to provide the best description of soil site ([Lachet and Bard, 1994](#)). Therefore, the H/V ratio is possible to estimate the predominant frequency. However, it is not well enough to estimate the H/V ratio due to the constraint of velocity, Poisson's ratio, and receiver restriction during the measurement. In addition, due to the nature aspect and human noise, the H/V ratio is not totally clarified ([Bonnetfoy-Claudet et al., 2006](#)). [Raptakis et al. \(2005\)](#) mentioned that even though the limitation of H/V ratio reliability, there is a consensus that predominant frequency values obtained are still acceptable.

2.6.2. Spectral analysis surface wave (SASW)

The SASW Method is a relatively new in situ method to determine the local site condition in term of shear wave velocity (V_s) in a site. This method was firstly developed by Nazarian and Stokoe in 1984, during the measurement of elastic moduli of soil profile deposit and pavement systems (Lai, 2000). The technique used in this method was developed based on steady state vibration technique proposed by Jones (1958) using theoretically based-inversion. In 1960s, the method was developed by U.S Army Corps of Engineers to obtain the shear wave velocity profile of soil deposit using Rayleigh waves produced by ground surface harmonic vibration (Richart et al., 1970).

The shear wave velocity profile is generated from generating inversion of Rayleigh dispersion curve. Minimization of the error between the observed curve and the predicted one is the most common criteria to define shear wave velocity profile of the investigated site (Lai, 2000). Nowadays, this method has been widely used to in geotechnical engineering problem for site investigation. The measurement is sometimes paired with the other in situ site investigation method, such as SPT and CPT, which were developed to provide the empirical correlations as proposed by Sykora and Stokoe (1983) for SPT- V_s Correlation and Andrus et al. (2004) for CPT- V_s Correlation. The practice and low-cost consideration are becoming the reasons why this method is commonly used.

SASW testing is simply performed by measuring the surface dispersion curve at the site and interpreting it to obtain the shear wave velocity profile. A dynamic source was released to generate the energy to provide the surface wave, which were monitored by two or more receivers at known offset. Data from the forward and reversed back profiles are analytically averaged. The measurement result is the Rayleigh wave dispersion curve. The particle of spectral velocity is obtained from the spectral acceleration by the following equation,

$$V(r, \omega) = \frac{A(r, \omega)}{\omega} \quad (2.88)$$

where $V(r, \omega)$ is spectral velocity, $A(r, \omega)$ is spectral acceleration, and ω is circular frequency.

From the spectral velocity, two spectral quantities i.e. the auto-spectrum of velocity on each receiver (S_{rr}) and the cross power spectrum ($S_{r_1r_2}$) are obtained from the spectral velocity at the receivers $V(r, \omega)$, complex conjugate of spectral velocity recorded at two receivers ($\bar{V}(r, \omega)$), the spectral velocity at receiver 1 ($V(r_1, \omega)$) and the complex conjugate of spectral velocity at receiver 2 ($\bar{V}(r_2, \omega)$). Both components are expressed in these following equations,

$$S_{rr} = V(r, \omega) \cdot \bar{V}(r, \omega) \quad (2.89)$$

$$S_{r_1r_2} = V(r_1, \omega) \cdot \bar{V}(r_2, \omega) \quad (2.90)$$

The time delay between the receivers as a function of circular frequency is given by the angle of $S_{r_1r_2}(\omega)/\omega$. Therefore, the velocity of propagating Rayleigh wave ($V_R(r)$) can be computed based on this following equation,

$$V_R = \frac{\omega(r_2 - r_1)}{\arg[S_{r_1r_2}(\omega)]} \quad (2.91)$$

The above equation furthermore results in the dispersion curve of a pairs of receivers located at r_1 and r_2 . The verification of repeatability is performed for each hammer impact. The dispersion curves include the maximum, the minimum, and the average, which can be noted as the excellent repeatability if the difference among three curves is small in frequency. The quality of the results is assessed by the calculating the coherence function from data used in dispersion curve calculation. The coherence function describes how the relation of the measured acceleration $a(r_1, t)$ is associated with $a(r_2, t)$. The estimate coherence ($C_{r_1r_2}$) should lie between 0 and 1. The low coherence (close to zero) value describes the presence of noise attributing during the measurement or the near field effects. On the other hand, the high coherence (close to one) reflects that there is a strong exact linear relationship between $a(r_1, t)$ and $a(r_2, t)$ (Fernández et al., 2011). The coherence function is expressed in this following equation,

$$C_{r_1r_2}(\omega) = \sqrt{\frac{S_{r_1r_2}(\omega) \cdot \bar{S}_{r_1r_2}(\omega)}{S_{r_1r_1}(\omega) \cdot S_{r_2r_2}(\omega)}} \quad (2.92)$$

After the dispersion curve analysis, the analysis of soil profile is performed to obtain the site characterization. The analysis is performed by the iterative process initiated by a trial stratification with each layer having a given Rayleigh waves propagation velocities. The iteration process is continually performed until the theoretical dispersion curve is consistent with the experimental dispersion curve. During the process, the stratification will be changed due to the minimizing root mean square (RMS) error. In general, the iterations are needed to obtain the relevant V_s profile

2.6.3. Site classification

The well-known guideline to classify site characterization is NEHRP (Natural Earthquake Hazard Reduction Program), which is released by Building Seismic Safety Council (BSSC, 1997) for site characterization classification. The determination of site class based on NEHRP should be firstly performed by calculating the time-averaged shear wave velocity up to 30 m (V_{s30}), which is expressed in this following equation,

$$V_{s30} = \frac{30(\text{m})}{\sum_{i=1}^n \frac{di}{V_{si}}} \quad (2.93)$$

where di is the thickness of each layer, V_{si} is the shear wave velocity in each layer and n is the number of layers. Table 4 summarises the range of V_{s30} corresponding to the site class of NEHRP criteria.

For the total investigated depth less than 30 m, Boore (2004) proposed the equation to estimate V_{s30} as follows,

$$\log(V_{s30}) = a + b \cdot \log(V_{s(d)}) \quad (2.94)$$

where, a and b are the extrapolation (the detail is presented in Boore (2004)) and $V_{s(d)}$ is the time-averaged V_s up to d (depth less than 30 m).

The estimated value of V_{s30} is furthermore matched with the range of V_{s30} presented in Table 2.5. The effect of first 30 m shear wave velocity average to the ground motion was investigated by Anderson et al. (1996). Based on their study, for specific deeper soil deposit, the attenuation effect is possible to influence ground motion and so is the shear wave velocity. Both information of V_{s30} and ground motion prediction are considered in seismic hazard study.

Table 2.5. Site classification for seismic hazard analysis (BSSC, 1997)

NEHRP Site Class	General Description	Range of V_{s30} (m/s)
A	Hard Rock	$V_{s30} > 1500$
B	Rock	$760 \leq V_{s30} \leq 1500$
C	Very dense soil and soft rock	$360 \leq V_{s30} \leq 760$
D	Stiff Soil ($15 \leq N \leq 50$ or $50 \text{ kPa} \leq s_u \leq 100 \text{ kPa}$)	$180 \leq V_{s30} \leq 360$
E	Soil or any profile with more than 3 m soft clay defined as soil with $PI > 20$, $w \geq 40\%$, and $s_u < 25 \text{ kPa}$	$V_{s30} \leq 180$
F	Soils requiring site-specific evaluations	

Remarks: N = SPT (blows/ft), s_u = undrained shear strength, PI = Plasticity index, w = water content



CHAPTER III. EMPIRICAL ANALYSIS OF LIQUEFACTION POTENTIAL

3.1. Introduction

On March 24, 2011, a strong earthquake with a magnitude of 6.8 M_w located in Tarlay attacked Myanmar and Northern Thailand. The epicentre of this earthquake located about 33 km away from the northern border of Thailand. The measured acceleration of earthquake recorded in the Mae Sai Station (Chiang Rai Province) was 0.207g. This earthquake caused so many damages, i.e. loss of material, victim's death, buildings destruction, and temples collapse. This earthquake also triggered the other catastrophic damages, such as liquefaction. Chiang Rai Province was an area experienced the serious impact of damage caused by Tarlay Earthquake, especially liquefaction phenomena. A liquefaction phenomenon as sand boils and lateral spreads were signed massively in this province. According to general geological condition, Chiang Rai subsoil was dominated by sandy soil with very low ground water table. [Soralump and Feungaugsorn \(2013\)](#) investigated the grain size distribution of Chiang Rai to analyse liquefaction susceptibility of Chiang Rai sandy soil. Based on their analysis, the distribution of grain size was categorized as liquefiable soil or in another word, Chiang Rai was classified as the most vulnerable area to undergo liquefaction. Learning from the earthquake and liquefaction experiences in 2011, a liquefaction study was conducted to study the liquefaction phenomenon in Northern Thailand, particularly in Chiang Rai Province.

3.2. Study Area and Geological Characteristic

Site investigation was conducted in Chiang Rai Province. Several boring log data were investigated to study geological condition of Chiang Rai subsoils. In the investigated locations, SPT and SASW tests were performed. Layout of the investigated area is depicted in Figure 3.1. The boreholes coded BH were in Mae Sai (BH-1), Mae Chan (BH-2), Chiang Kong (BH-3), Muang (BH-4), Mae Lao (BH-5), Phan (BH-6), Wiang Pa Pao (BH-7). The additional investigated location (red rectangle) is focused

around BH-1, where liquefactions were found during Tarlay Earthquake. The investigated locations are noted as BH-A, BH-B, and BH-C. Examples of soil profile are shown in Figures 3.2 to 3.4., whereas the detailed investigation results are shown in Table 3.1.

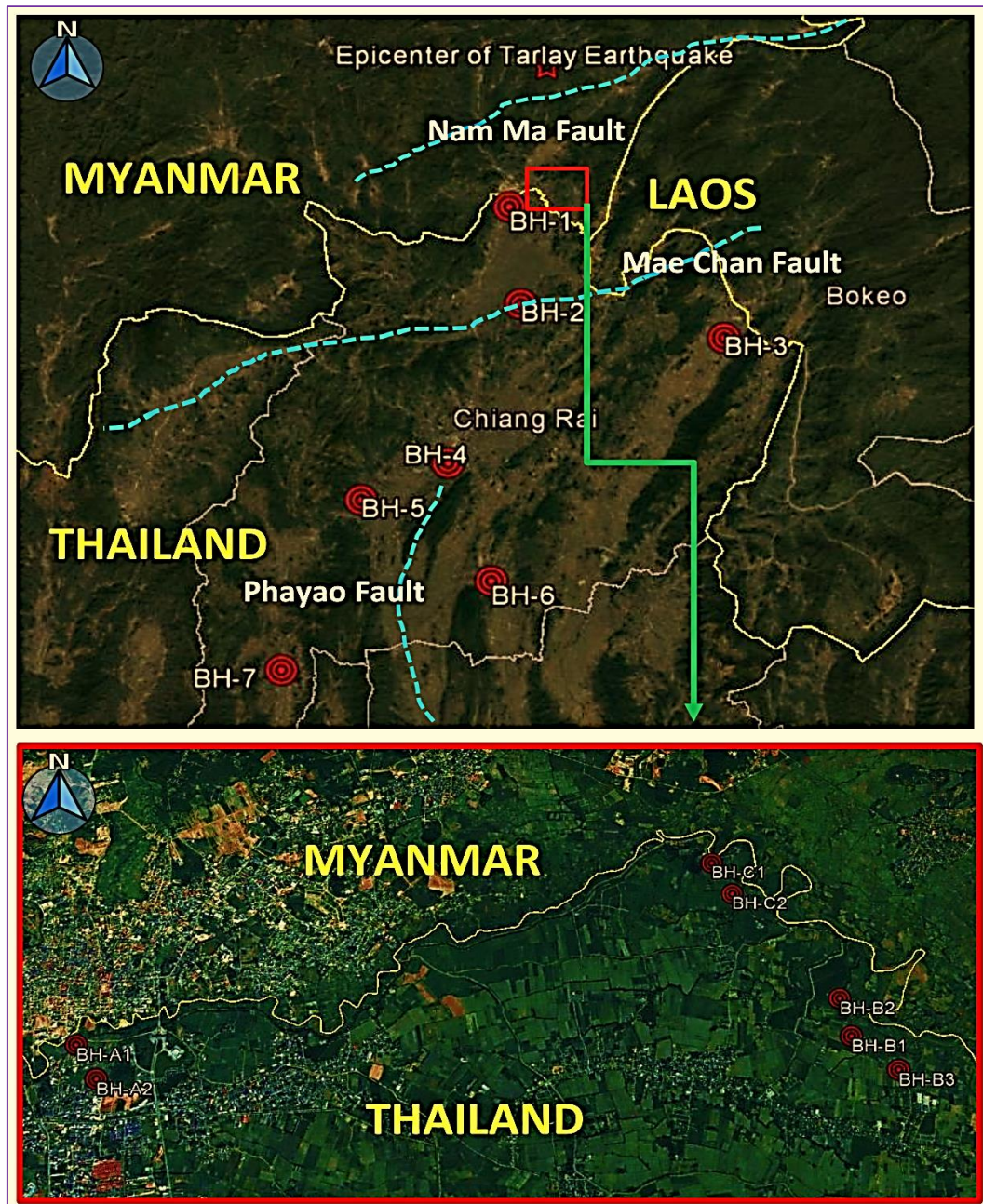


Figure 3.1. Study area of liquefaction empirical analysis

According to the geological characteristics, the subsoils in Chiang Rai are dominated by sandy soils. The sandy soils in Chiang Rai are classified as SP (poorly graded sand), SM (silty sand), and SC (clayey soil) with FC in the range of 5% to 45% and are found at average depths of 0 to 32 m. Even though sandy soil is dominant in this area, thin clay layers are also found in several investigated sites, particularly in BH-4, BH-7, BH-A, BH-B, and BH-C. The clay layers with quite large thickness are found on several investigated sites, especially in BH-2, BH-3, and BH-6. These soil is classified as CL (low plasticity clay) and CH (high plasticity clay) with FC up to 94%. The groundwater depth in this area is 1.0 to 3.16 m. The distribution of $(N_1)_{60}$ in this area ranges from 7 to 30 blows/ft, whereas V_{s30} ranges from 180 to 320 m/s. The value of V_{s30} is used to determine the site class of the investigation area based on the NEHRP criteria, where the site class of this area was categorized as Site Class D.

3.3. Research Methodology

This study is initiated by collecting site investigation data, such as SPT-Boring Log and Shear Wave Velocity Data (V_s). In addition, the information of Tarlay Earthquake ground motion is collected. Based on the information from Thai Meteorological Department, the maximum PGA recorded during the Tarlay Earthquake is 0.207g. After collecting the necessary information, the desk study of soil profile based on boring log data is performed. Furthermore, the preliminary analysis to the collected data is conducted to obtain some parameters in calculation.

The literature review to the liquefaction potential based on empirical approach is conducted. In this study, the method of [Idriss and Boulanger \(2006\)](#) is employed in the analysis. The literature review is also performed to the liquefaction study conducted by several researches focused on Northern Thailand, such as [Soralump and Feungaugorn \(2013\)](#), [Pattararattanakul \(2003\)](#), and [Tanapalungkorn and Teachavorasinskun \(2015\)](#).

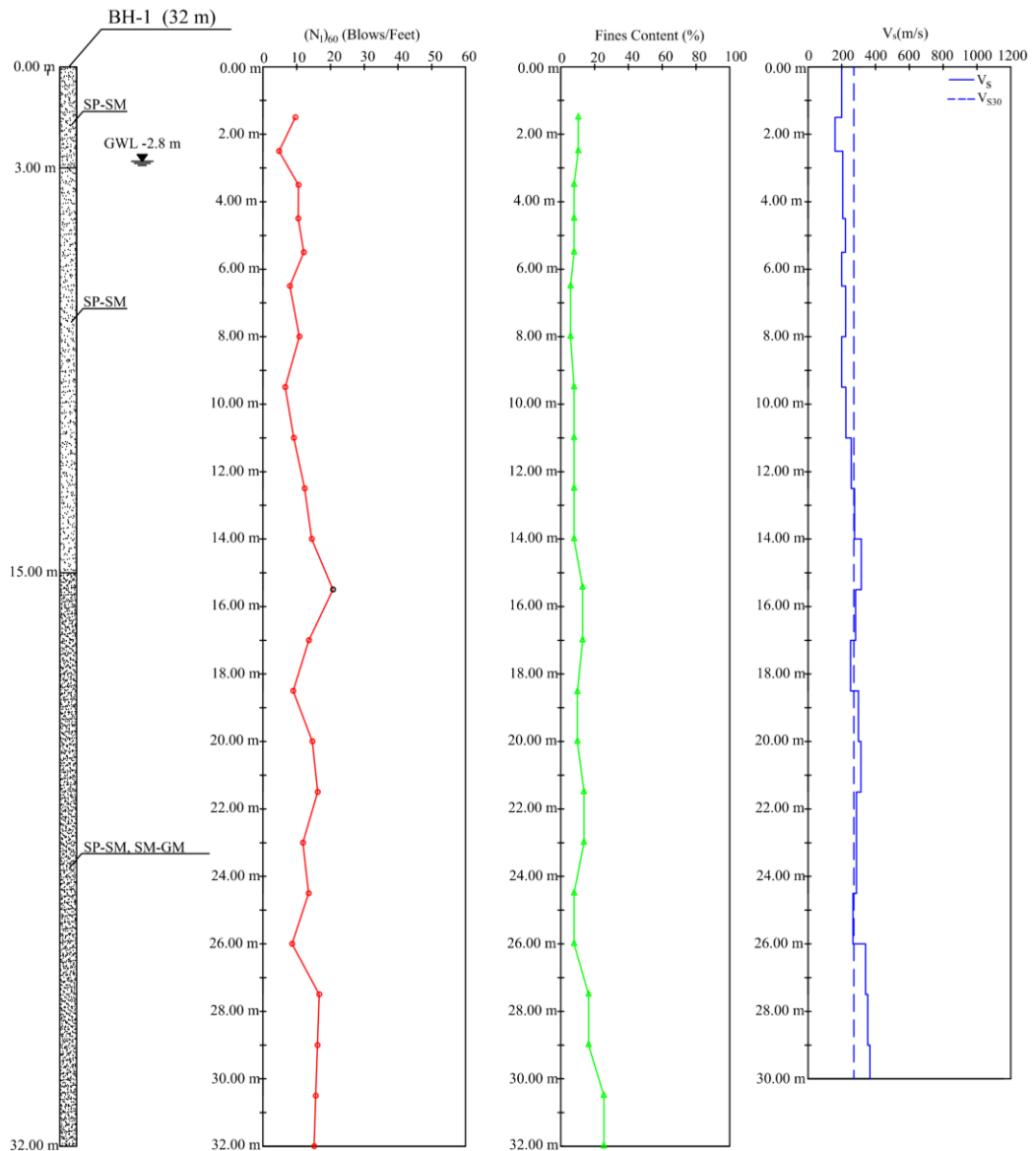


Figure 3.2. Site investigation results of BH-1

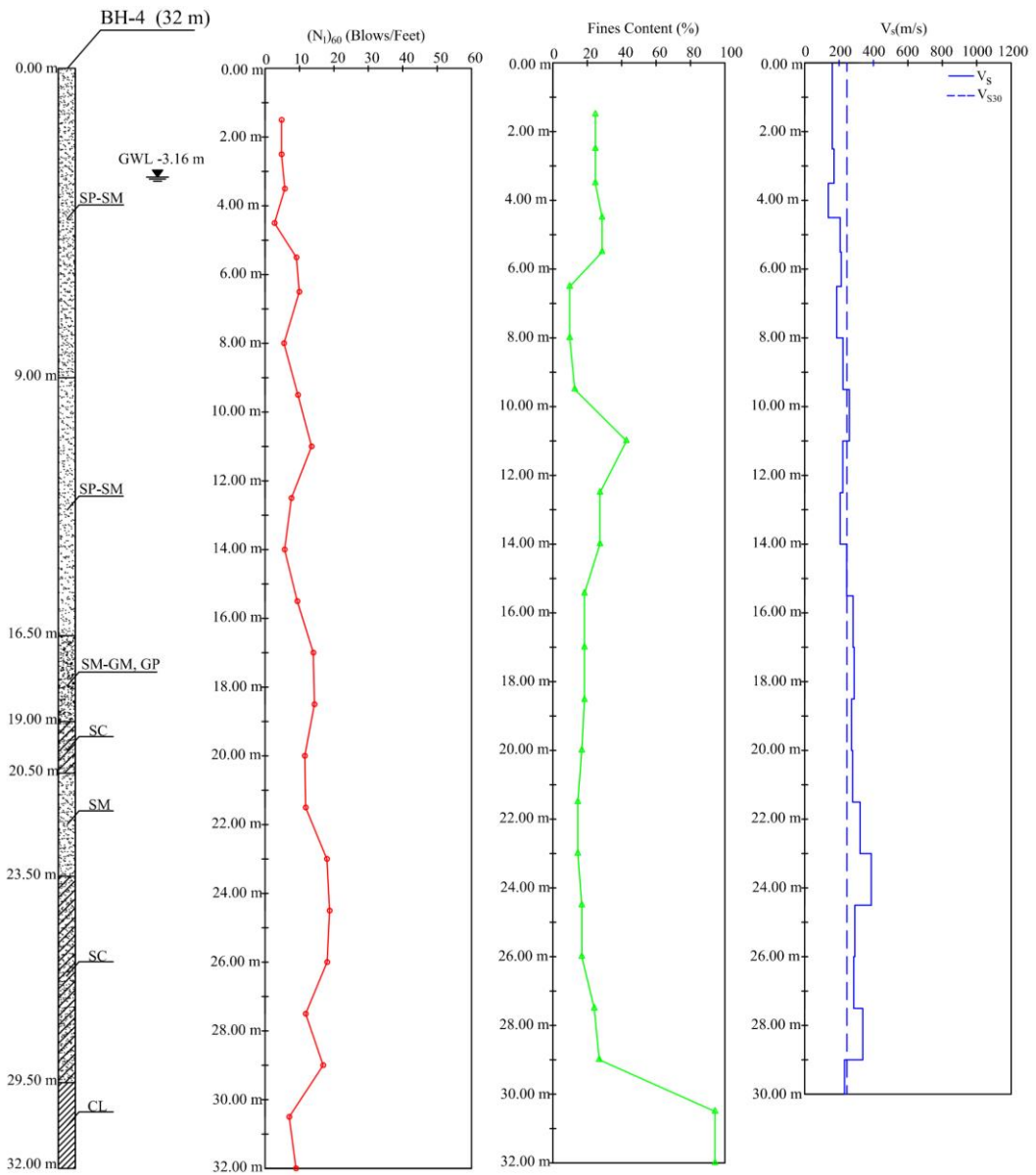


Figure 3.3. Site investigation results of BH-4

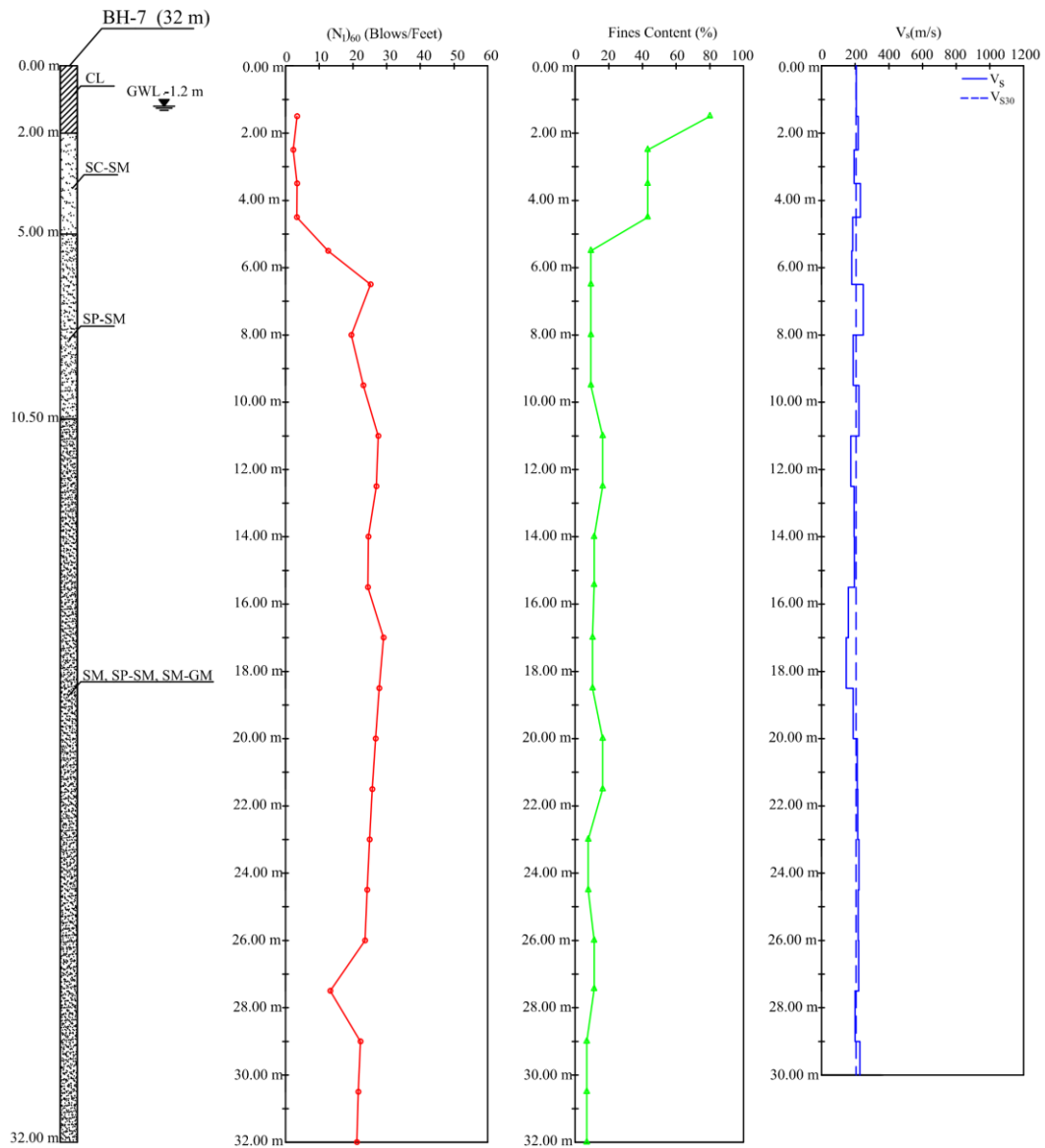


Figure 3.3. Site investigation results of BH-7

The third step is to perform the analysis of liquefaction potential. In this step, the *CRR-CSR* curve-SPT to distinguish liquefaction zone and no liquefaction zone is presented. In addition, the probability of liquefaction corresponding to *FS* is conducted. The comparison to the reviewed studies is also performed.

Table 3.1. Soil investigation data

Site Investigation	Soil Type	FC (%)	γ (kN/m ³)	Thickness (m)	(N ₁) _{60cs} (blow/ft)	Site Investigation	Soil Type	FC (%)	γ (kN/m ³)	Thickness (m)	(N ₁) _{60cs} (blow/ft)
BH-1	USCS					A2	USCS				
	SP,SM	6.9	17.77	3.00	7		SP	5	17.00	3.00	10
	SP,SM	8.6	18.32	12.00	11		CH	50	16.00	1.50	16
BH-2	SP-SM, SM-GM	9.0	22.31	17.00	17	SP	21	18.00	1.50	15	
	CL	82.0	16.36	7.00	15	SM	9	20.00	1.50	11	
	SM	12.0	20.98	6.00	13	SM	10	21.00	1.50	22	
	CH	78.0	21.33	9.00	10	SC	12	21.00	3.00	26	
BH-3	SC	27.5	21.61	10.00	18	SC-GC	17	22.00	2.00	30	
	CL	92.0	16.36	11.50	14	CL	60	19.00	2.50	22	
	CL	71.0	21.33	4.50	9	CL	51	20.00	0.50	22	
BH-4	GP-GM	9.0	22.13	4.00	33	SP	5	17.00	2.50	8	
	SM	21.0	18.32	9.00	11	SM	4	18.00	3.00	10	
	SP-SM	26.0	18.00	7.50	14	SP	11	17.00	1.50	13	
BH-5	SM,GM, GP	19.0	19.05	2.50	23	SM	17	20.00	6.00	21	
	SC	18.0	20.37	1.50	19	SC	35	20.00	1.50	24	
	SM	16.0	20.98	3.00	24	SM	18	20.00	10.00	25	
	SC	21.0	21.61	6.00	26	CL	80	20.00	2.00	26	
BH-6	CL	94.0	21.43	2.50	13	SM	12	20.00	6.50	18	
	SC-GC	25.0	20.00	4.00	14	SC	19	20.00	1.50	21	
	CL	54.0	21.00	2.00	23	SM	22	20.00	11.50	26	
	SC	30.0	20.00	8.50	19	CL	60	19.00	1.00	26	
BH-7	CL	63.0	19.00	16.50	15	SP	13	17.00	6.00	14	
	SC	33.0	19.00	1.00	29	SM	18	18.00	11.50	28	
	CL	68.0	20.80	3.00	22	CL	60	20.00	2.00	23	
	SM	23.0	20.02	4.00	16	SP	10	17.00	5.00	6	
BH-8	CH	85.0	20.40	10.50	14	CL	60	16.00	1.50	11	
	SC	45.0	21.10	3.00	17	SP-SM	12	19.00	2.50	14	
	CH	87.0	20.60	9.00	18	SM	15	20.00	5.00	28	
	CL	56.0	20.70	1.50	23	CL	60	20.00	1.50	21	
BH-9	SC	36.0	19.60	1.00	11	SP	5	17.00	4.00	11	
	CL	80.0	16.36	2.00	9	CH	60	19.00	1.50	30	
	SP-SM	42.0	17.63	3.00	9	SP	15	20.00	5.00	25	
	SC-SM	8.0	20.38	5.50	16	SC-GC	15	22.00	1.50	25	
A1	SM-GM	11.1	20.17	21.50	22	SM	18	20.00	5.00	27	
	CL	10	17.00	3	14						
	SP	19	18.00	1.5	12						
	SM	5	20.00	1.5	13						
	SC	8	21.00	3	21						
	SC	10	21.00	1.5	24						
A2	SC	12	21.00	1.5	27						
	SC	15	22.00	2	29						

In general, this study is destined as the preliminary evaluation of soil liquefaction during the Tarlay Earthquake to understand the vulnerability of subsoils to liquefaction. The study is also addressed as the milestone to step out the further study, especially related to local site condition and site response analysis.

3.4. Result and Discussions

The examples of factor safety against liquefaction-depth (BH-1, BH-4, and BH-7) are presented in Figure 3.4. In general, the sandy soils at the shallow depths are unsafe from liquefaction. It is confirmed by *FS* value less than 1. At the deeper depths, the sandy layers seem to be safe from liquefaction, where *FS* is larger than 1. Overall, the results confirm the previous studies performed by [Mase et al. \(2015\)](#), [Tanapalungkorn and Teachavorasinskun \(2015\)](#), [Soralump and Feungaugorn \(2013\)](#), [Teachavorasinskun et al. \(2009\)](#), and [Pattararattanukul \(2003\)](#).

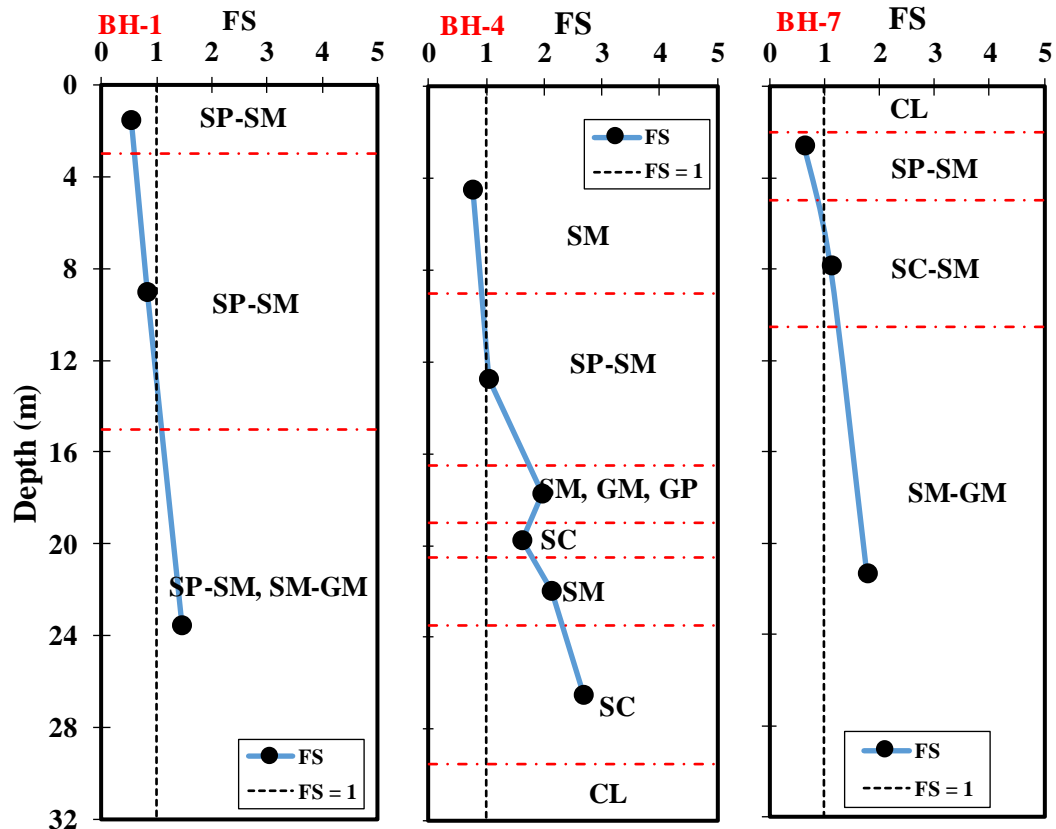
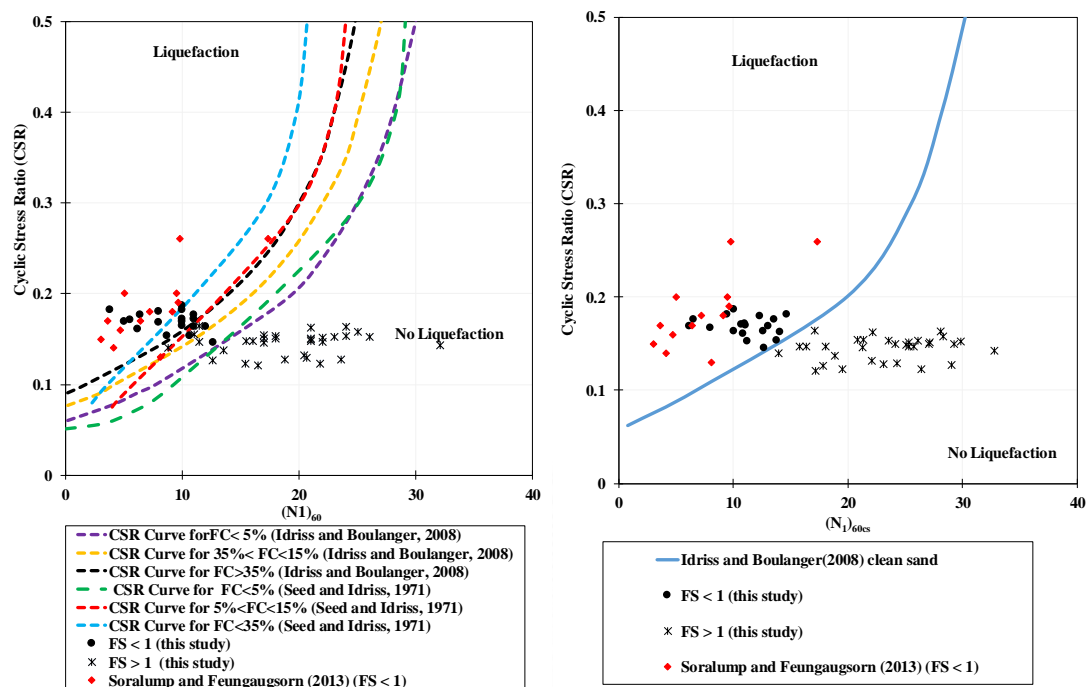


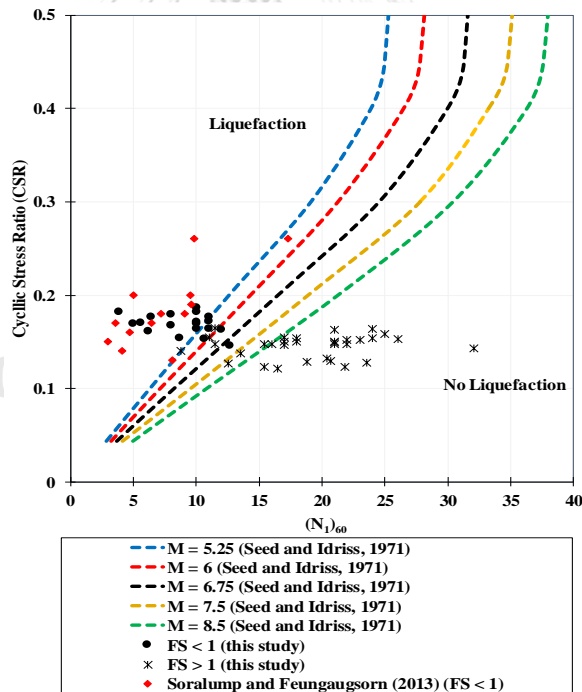
Figure 3.4. Examples of FS-depth on the investigated sites

Figure 3.5 presents the plotted $CSR-(N_1)_{60}$ or $(N_1)_{60cs}$ corresponding to various earthquake magnitudes and percentage of fines contents graphs from Idriss and Boulanger (2008) and Seed and Idriss (1971). In Figure 3.5a, the liquefaction points are generally categorized as sand with $FC \leq 5\%$. However, the sand with FC more than 5% seems to be unsafe from liquefaction as well, especially for sandy soils with $(N_1)_{60} \leq 10$ blows/ft. In Figure 3.5b, based on the criteria of clean sand curve for CSR from Idriss and Boulanger (2008), it can be seen that the liquefied points are generally having $(N_1)_{60} \leq 15$ blows/ft.

In Figure 3.5c, the liquefaction points are generally liquefied due to the $6.7 M_w$ earthquake. This result is consistent with the analysis of liquefaction potential during the Tarlay Earthquake, which had magnitude of $6.8 M_w$. The minimum criteria of earthquake magnitude to trigger liquefaction, i.e. $5.25 M_w$ tends to liquefy the soil layers having $(N_1)_{60}$ less than 11 blows/ft, whereas the $6.8 M_w$ is possible to generate liquefaction for $(N_1)_{60}$ less than 15 blows/ft, which are generally considered as loose sand. The results are also generally consistent with the previous studies.



(a) (b)



(c)

Figure 3.5. CSR versus $(N_1)_{60}$ or $(N_1)_{60cs}$ (a) based on FC , (b) clean sand criteria, (c) based on magnitude

The interpretation of probability of liquefaction versus factor of safety against liquefaction is shown in Figure 3.6. In general, the results showed that at critical condition, i.e. FS of 1, the probability of liquefaction is about 48%. The results also show the similar tendency as performed by previous studies (Soralump and Feungaugsorn (2013) and Pattararattakul (2003)). Overall, liquefaction (FS less than 1) can happen with the minimum liquefaction probability about 0.48.

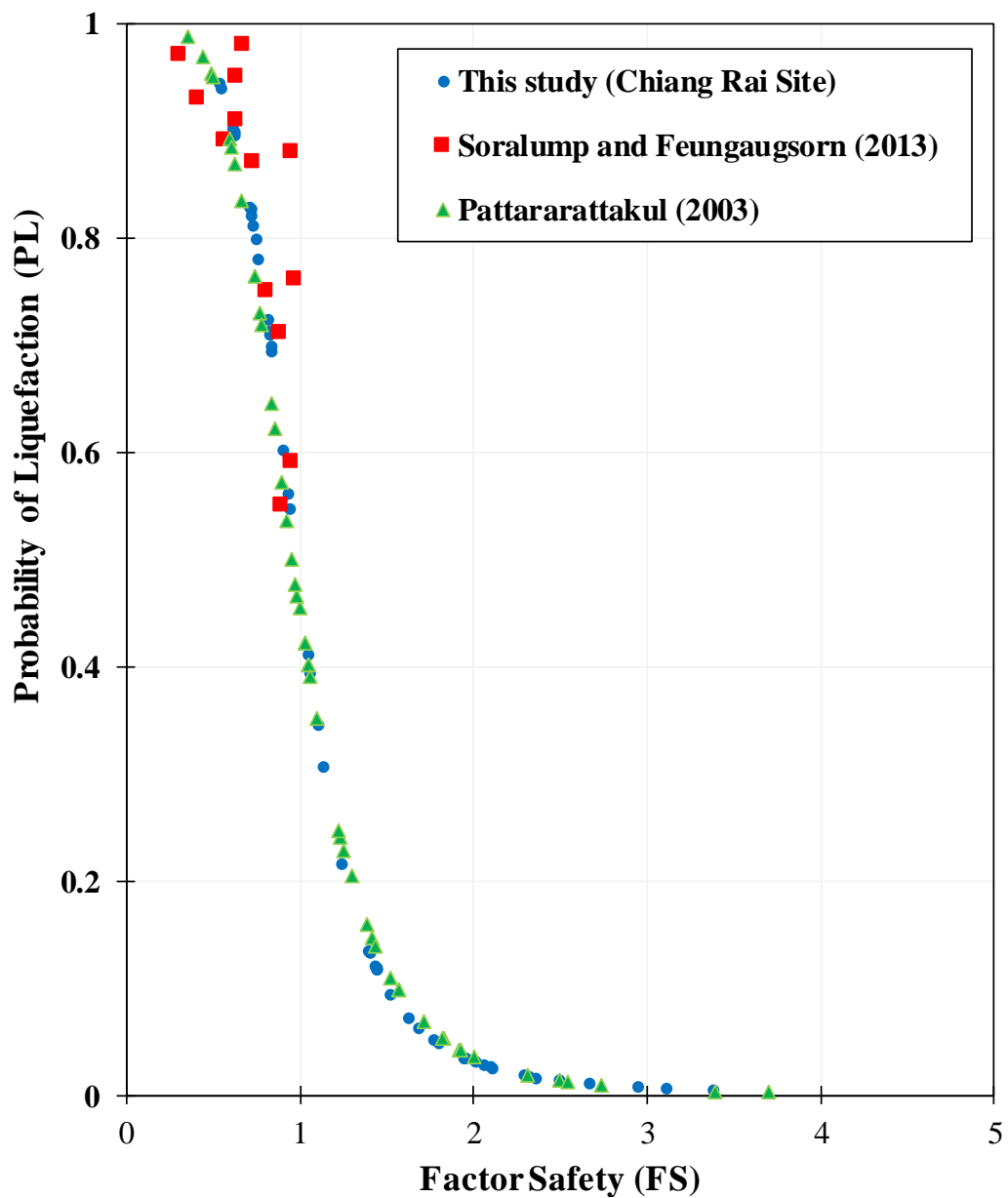


Figure 3.6. Probability of liquefaction versus FS

3.5. Concluding remarks

This chapter presented the empirical analysis of soil liquefaction in Chiang Rai Province. Several concluding remarks can be drawn as follows,

1. The earthquake magnitude of 6.8 M_w with maximum PGA of 0.207g was possible to trigger liquefaction in the Northern Thailand.
2. Generally, liquefaction can occur at shallow depth, where $(N_1)_{60}$ less than 15 blows/ft.
3. The probability of 0.48 can be noted as the threshold of liquefaction condition in the study area.
4. The further study can be focused on the site response analysis for the sites dominated by sandy soils. The detail of site response analysis is presented in Chapter IV.
5. The detail local site investigation to the liquefied sites in Northern Thailand could be performed to investigate the subsoils condition in detail. The local site investigation to the liquefied locations is presented in Chapter V.

CHAPTER IV. SITE RESPONSE ANALYSIS

4.1. Introduction

Northern Thailand has experienced many earthquakes in the past; however, most of them did not cause extensive damage since they were low in magnitude and their epicentres located primarily in neighbouring countries (i.e., Myanmar and Laos). Nevertheless, on March 24, 2011, the Tarlay Earthquake triggered by the Nam Ma Fault (Figure 4.1) struck Myanmar-Northern Thailand. Thai Meteorological Department or [TMD \(2015\)](#) noted that the measured acceleration recorded at the Mae Sai station of Chiang Rai Province was 0.207g. Figure 4.2 presents the acceleration caused by Tarlay earthquake recorded at the Mae Sai station.

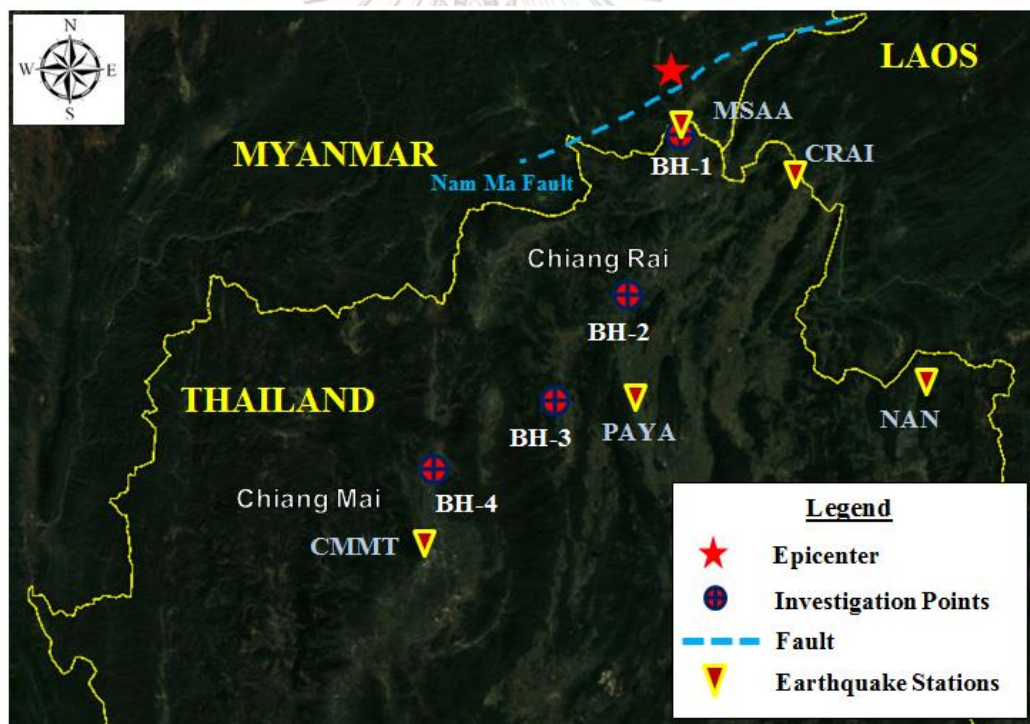


Figure 4.1. Locations of Nam Ma Fault, epicentre of Tarlay Earthquake in 2011, site investigations, and surrounding seismic stations [TMD \(2015\)](#).

[Ruangrassamee et al. \(2012\)](#) and [Soralump and Feungaugorn \(2013\)](#) reported that the earthquake caused considerable damage (e.g., loss of life, loss of property, and temple collapse) in Northern Thailand. The epicentre of the earthquake was about 33

km from the Mae Sai District station in Chiang Rai Province (Ornthammarath, 2013), and the earthquake caused the most damage in that district. Other districts in Chiang Rai Province, such as Mueang and Wiang Pa Pao, also experienced the damage. In Chiang Mai, ground shaking was also felt by the people, although it was not as intensive as in Chiang Rai. Even though the central city of Chiang Mai lies far from the epicentre (about 235 km away), Chiang Mai could experience severe damage if a stronger earthquake is to hit this area in the future. Thus, because Chiang Mai is the largest city in Northern Thailand where socio-economic aspects are centered. It is critical to consider the potential impacts of future earthquakes in this region.

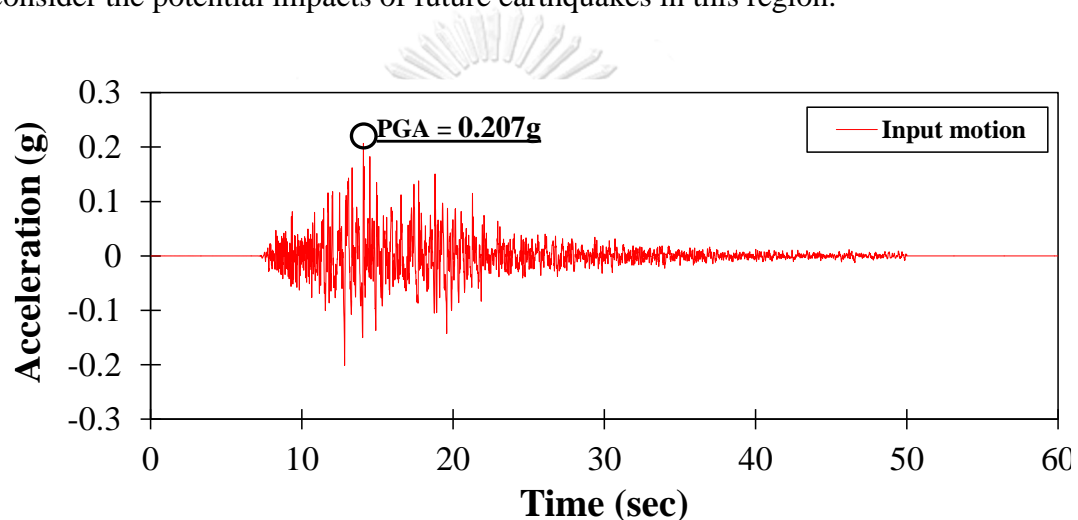


Figure 4.2. Acceleration record at Mae Sai station due to Tarlay earthquake on March 24, 2011 (TMD, 2015).

With the goal of learning from Tarlay Earthquake, this chapter presents an analysis of seismic ground response in Northern Thailand. The objective is to observe the seismic response in Chiang Rai and Chiang Mai to Tarlay Earthquake based on wave propagation analysis and attenuation model analysis. The recorded spectral acceleration at each site was also compared with the spectral acceleration design of Thai Design Seismic or TDS (2009) for those areas. The results describe the ground response in Northern Thailand to Tarlay Earthquake and are expected to be applicable to other research related to ground-shaking phenomena in Northern Thailand related to Tarlay Earthquake (e.g., liquefaction).

4.2. Study Area and Geologic Characteristic

Based on the empirical analysis of liquefaction, the seismic ground response analysis due to Tarlay Earthquake is performed. In this study, only sites dominated by sandy soils are picked up in the analysis. The study area is shown in Figure 4.1. The standard penetration test (SPT) and shear wave velocity (V_s) test were conducted at three sites in Chiang Rai (BH-1, BH-2, BH-3 or BH-1, BH-3, and BH-7 in Chapter III) and one site in Chiang Mai (BH-4). The results of soil investigation test conducted in the study area are presented in Figure 4.3. In Chiang Rai, sites BH-1, BH-2, and BH-3 were in Mae Sai, Mueang, and Wiang Pa Pao districts, respectively. In Chiang Mai, site BH-4 is in the Mae Taeng district. The reason why those areas are selected, because Chiang Rai and Chiang Mai is that the trading gate and the economic centre of Northern Thailand, respectively. This area is also considered as the centre of social-economy aspect in Golden Triangle, which is encompassing Laos, Myanmar, and Thailand.

Generally, the subsoil conditions in Chiang Rai and Chiang Mai are dominated by granular materials. SP (poorly graded sand), SC (clayey sand), and SM (silty sand) dominantly exist in the first 15 m deep, with FC (fines content) in the range of 5 to 40%. These soil layers are followed by GC-SC (clayey gravel to clayey sand), GM (silty gravel), and GP (poorly graded gravel) until 30-32 m depth, with FC in the range of 10-30%. Even though granular material is dominant in this area, thin layers of clay are also found in several areas, particularly in BH-3 (depth = 0 to 2 m) and BH-2 (depth = 29.5 to 32 m). This soil is classified as CL (low plasticity clay) with FC up to 90%. The groundwater depth in this area ranges from 1.2 to 3.16 m deep. The distribution of $(N_1)_{60}$ in this area ranges from 3 to 30 blows/ft, whereas V_{s30} ranges from 245 to 290 m/s. The value of V_{s30} is used to determine the site class of the investigation area based on the criteria of National Earthquake Hazards Reduction Program (NEHRP) in [BSSC \(1997\)](#); the site class of this area is categorized as stiff soil (Site Class D).

4.3. Attenuation Model

Several researchers studied earthquakes in Thailand using the attenuation models summarized in Table 4.1. [Chintanapakdee et al. \(2008\)](#) studied the attenuation models for shallow crustal and subduction earthquakes in Thailand; they compared the

PGAs estimated by attenuation models to the ground motion recorded between July 2006 and July 2007. [Soralump and Feungaorsorn \(2013\)](#) studied liquefaction in Northern Thailand due to Tarlay Earthquake. They matched the PGAs estimated by an attenuation model to the PGA of 0.206 g recorded at the Mae Sai station. [Lukkunaprasit et al. \(2016\)](#) studied the performances of structures during the Mae Lao earthquake on May 5, 2014. Same as [Soralump and Feungaorsorn \(2013\)](#), they plotted and matched the PGAs recorded at some stations in Thailand during the May 5, 2014 earthquake (Mae Lao Earthquake). Among these previous works, [Idriss \(1993\)](#) model was identified as the most suitable attenuation model for Thailand, particularly for shallow crustal earthquake or fault earthquakes in Northern Thailand.

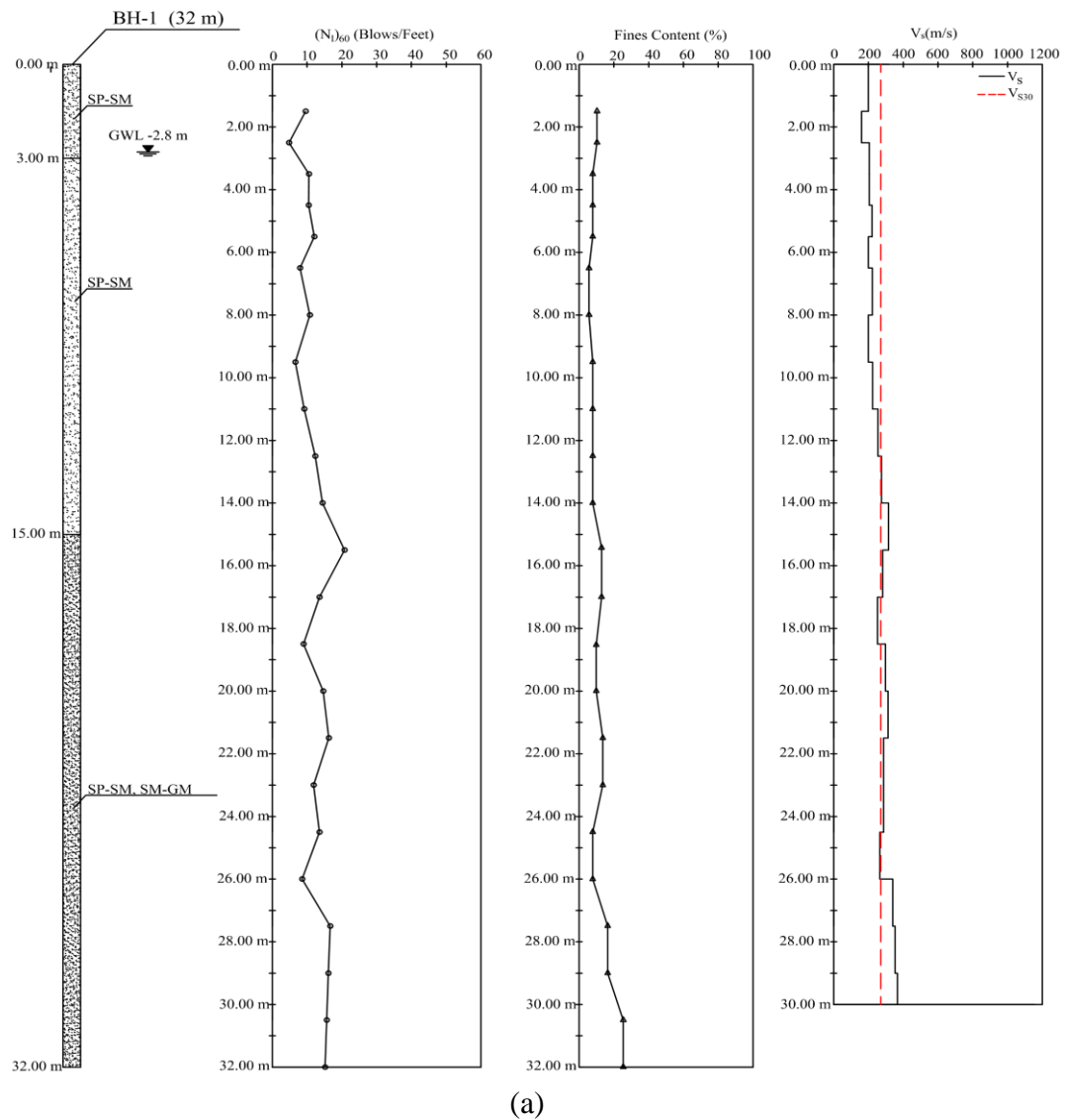
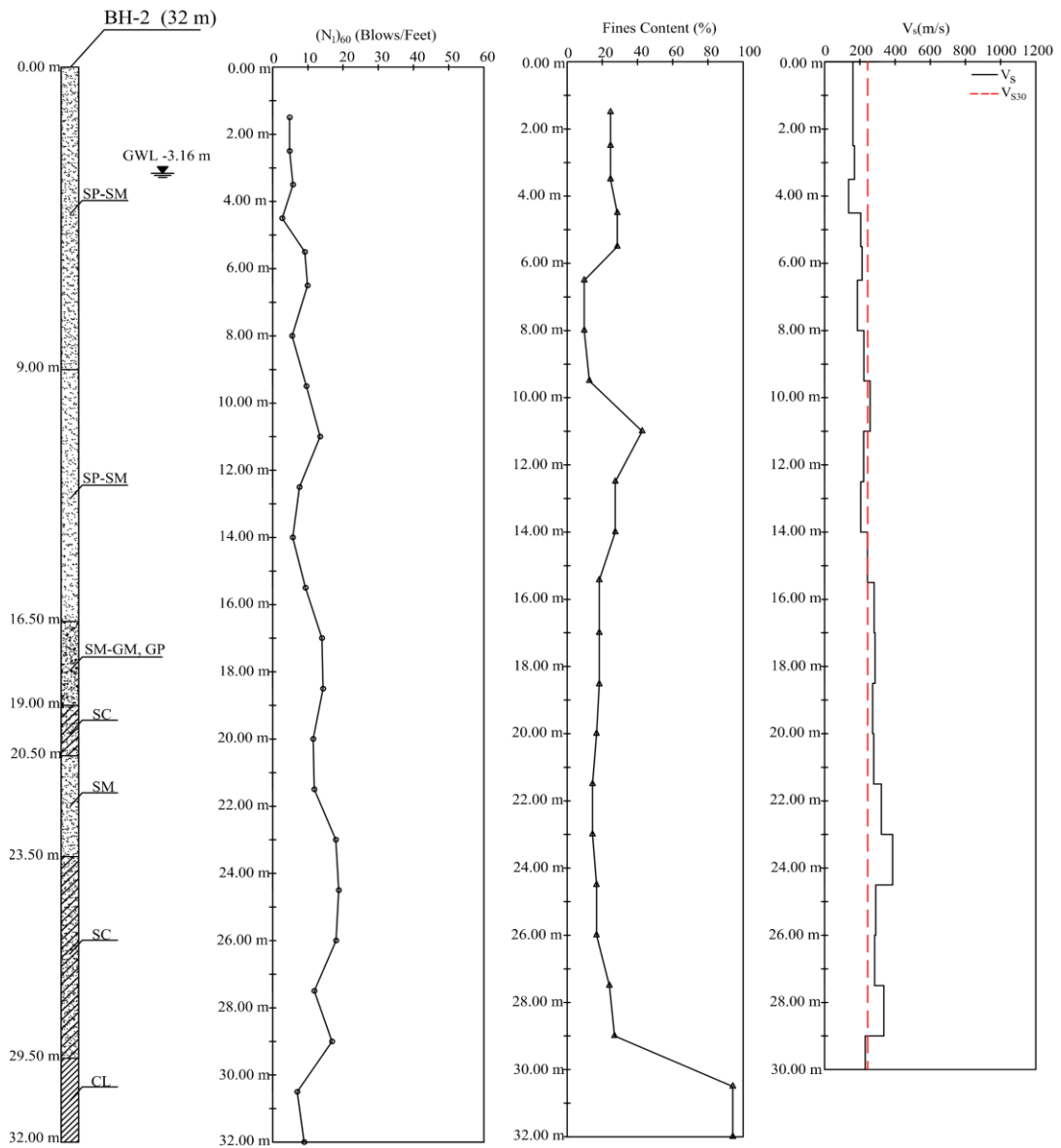
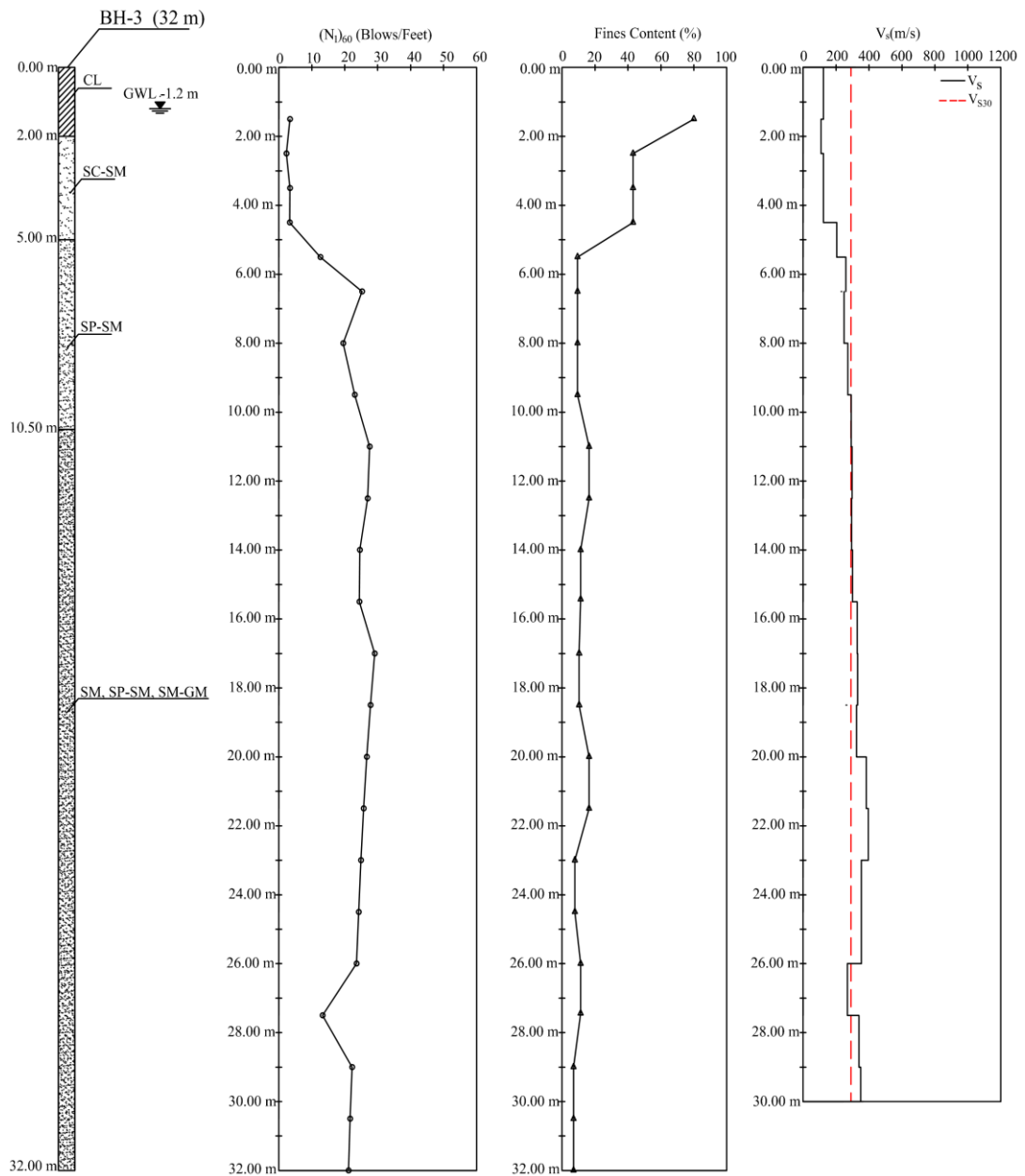


Figure 4.3. Continued



(b)

Figure 4.3. Continued



(c)

Figure 4.3. Continued

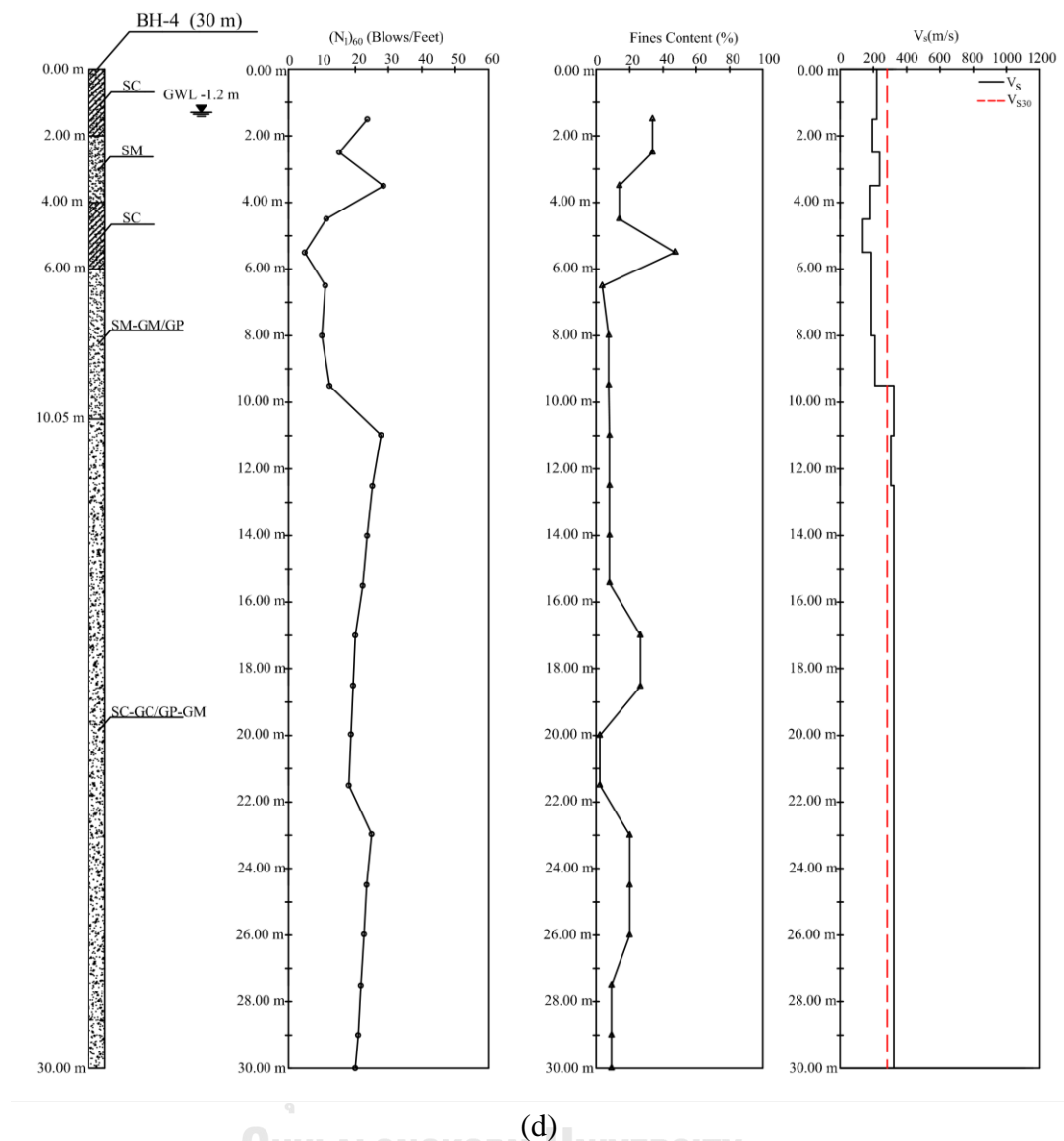


Figure 4.3. Site investigation results at study area, (a) BH-1, (b) BH-2, (c) BH-3, and (d) BH-4

Four Next Generation Attenuation (NGA) Models are employed to determine the most suitable attenuation model for Tarlay Earthquake. However, Idriss (2008) model is not considered in this analysis since this NGA model is only suitable for rock sites, whereas based on NEHRP criteria, the location of seismic stations are categorised as soil sites. Ground motions recorded at many stations around Thailand are plotted and matched to the PGAs attenuation model graphs. Furthermore, the closest attenuation model to the plotted ground motion points are considered as the most suitable attenuation model. The PGAs and earthquake ground motions recorded at each station

during Tarlay Earthquake were collected from Thai Meteorological Department. The location of seismic stations and the recorded data are presented and plotted in Figure 4.4, and Table 2, respectively.

4.4. Research Methodology

SPT, shear wave velocity test, and Tarlay Earthquake event data (ground motion and earthquake information) are collected. In this study, SPT and shear wave velocity data (Figure 4.1) are obtained from site investigation, whereas the earthquake event data are obtained from the TMD. Afterwards, the preliminary understanding of the soil condition particularly related to physical properties, soil profile, $(N_1)_{60}$ and V_{s30} is conducted to reach the general description of soil site. Parameters such as shear modulus (G), modulus reduction (G/G_{max}), damping ratio, and initial damping are determined based on the collected data. Furthermore, the obtained earthquake data are sorted based on the distance from the epicentre, and the sorted data are used to determine the maximum PGA of recorded ground motion.

The data are analysed in three analyses: (1) PGA based attenuation model analysis; (2) seismic ground response analysis (ground motion wave propagation); and (3) spectral acceleration design comparison analysis (design seismic code). Generally, this chapter focuses on the effect of ground motion propagation on seismic response based on the maximum PGA.

In the first analysis, we determine the most suitable attenuation model for the obtained earthquake event data by plotting the PGA values of the earthquake event alongside data from different attenuation models. PGAs resulted in this analysis are also presented to confirm the distance effect to the energy (maximum acceleration) received by the considered sites. The site that is far from the epicentre, receives lower energy or lower PGA compared to the site that is close to the epicentre.

Seismic ground response analysis is conducted using one-dimensional wave propagation according to the equivalent linear (Schnable et al., 1972) and the non-linear approach (Hashash et al., 2015). Ground motion used in this study (Figure 4.2) is the one recorded at the closest station to epicentre (i.e., BH-1, Mae Sai station). For other sites (BH-2, BH-3, and BH-4), which there are no ground motion records, the scaled

ground motions of maximum recorded ground motion (Figure 4.2) are used in the analysis. The scaling factor of ground motion is based on the maximum ground motion prediction obtained from the most suitable attenuation model.

Furthermore, those waves are applied at the bottom of each borehole to observe the site response to propagated ground motion. The engineering bedrock of the site is assumed to be located at the bottom of each borehole as no information on bedrock location in the study area is available. Therefore, the shear wave velocity of 760 m/s (Miller et al., 1999) is used as the shear wave velocity of the layer below the investigated depth. The results obtained from this analysis are the PGAs of seismic ground response and the spectral acceleration of ground response.

The spectral accelerations at the ground surface determined by both approaches are then compared with the design spectral accelerations for the study region reported by TDS (2009). For the seismic design code of Thailand, the design spectral acceleration corresponds to the return period of 2,475 years with a 2% probability of exceedance in 50 years and a return period of 475 years with a 10% probability of exceedance in 50 years. The comparison of site spectral response acceleration and design spectra acceleration give the seismic vulnerability to the building period. The PGAs produced using the two approaches are compared to determine the limitations of spectral analysis and identify the better method for estimating spectral response in the study area.

4.5. Result and Discussions

4.5.1. Attenuation model analysis of Tarlay Earthquake

The NGA models (Table 4.1) are studied to determine the most suitable attenuation for the studied earthquake. During Tarlay Earthquake, at least 33 seismic stations in 1,500 km radius (Table 4.2) had recorded the ground motions of the earthquake. In Figure 4.1, several stations surrounding within 250 km of epicentre radius is presented. Those stations include MSA in Mae Sai District at the border of Thailand-Myanmar, CRAI in Chiang Rai Province, PAYA in Phayao Province, NAN in Nan Province, and CMMT in Chiang Mai Province. During the earthquake, the maximum peak ground acceleration (PGA) of 0.207g (Figure 4.2) was recorded at

MSSA station, which was the closest station to the epicentre. It is noted that BH-1 site is close to MSSA station. In general, the locations of seismic station are classified as Site Classes C and D. Therefore, in the attenuation model analysis, only the NGA models for soil sites are employed in this study.

The PGAs recorded in Thailand due to Tarlay Earthquake are plotted against the PGAs of the different attenuation models corresponding to strong motion parameters (maximum PHA, spectral acceleration (SA) at 0.2s, and spectral acceleration at 1s. These comparisons are shown in Figure 4.5.

The results indicate that the NGA models of [Abrahamson and Silva \(2008\)](#) and [Boore and Atkinson \(2008\)](#) are the closest fit (R^2) to the recorded ground motions and are probably the most suitable attenuation model for Tarlay Earthquake. In addition, to estimate the more accurate performance of Ground Motion Prediction Estimation (GMPE) relative to data, the residual analysis is performed to understand the characteristic of Tarlay Earthquake ground motion. The residual analysis for each data point comparing to the estimated GMPEs is defined as,

$$R_i = \ln(PGA_i)_{rec} - \ln(PGA_i)_{GMPE} \quad (4.1)$$

$$R_i = \ln(SA_i)_{rec} - \ln(SA_i)_{GMPE} \quad (4.2)$$

where $(PGA_i)_{rec}$ and $(SA_i)_{rec}$ are values of peak ground acceleration and spectral acceleration from each station, respectively. $(PGA)_{GMPE}$ and $(SA)_{GMPE}$ are the median value of peak ground acceleration and spectral acceleration obtained from ground motion predictions. The evaluated strong motion parameters are PGA and SA at 0.2 and 1.0 s for [Abrahamson and Silva \(2008\)](#) and [Boore and Atkinson \(2008\)](#) models are shown in Figure 4.6, whereas the evaluated residual analysis of strong motion parameters are shown in Figure 4.7.

Some principal trends can be illustrated by Figures 4.5, 4.6, and 4.7 as follows:

- Figure 4.5: the PHA (peak horizontal acceleration) (Figure 4.5a) shows no significant difference over 0 to 200 km. Both models show the accurate prediction to the ground motion, especially in the distance between 200 to 600 km. For the recorded ground motion of Mae Sai Station (MSSA), [Boore and Atkinson \(2008\)](#) model predicts more accurate than [Abrahamson and Silva \(2008\)](#) model. For SA

(spectral acceleration) at 0.2s (Figure 4.5b), both models show accurate prediction in the distance over 1,000 km. For SA at 1s (Figure 4.5c), [Boore and Atkinson \(2008\)](#) shows a more accurate prediction than [Abrahamson and Silva \(2008\)](#) model.

Table 4.1. Attenuation models used for earthquake studies in Thailand

Attenuation Model	Researchers who used the attenuation models			
	Chintanapakdee et al. (2008)	Soralump and Feungaugorn (2013)	Lukkunaprasit et al. (2016)	This Study
McGuire (1977)	-	-	-	-
Sabetta and Pugliese (1987)	√	-	-	-
Crouse (1991)	√	√	-	-
Idriss (1993)	√	√	√	-
Boore et al. (1997)	√	√	√	-
Spudich et al. (1997)	√	-	-	-
Abrahamson and Silva (1997)	√	-	-	-
Youngs et al. (1997)	-	√	-	-
Sadigh et al. (1997)	√	√	√	-
Toro (2002)	-	-	√	-
(Ambraseys et al., 2005)	√	-	-	-
Abrahamson and Silva (2008)	-	-	-	√
Boore and Atkinson (2008)	-	-	-	√
Campbell and Bozorgnia (2008)	-	-	-	√
(Chiou and Youngs, 2008)	-	-	-	√

- Figures 4.6: the PHA (Figure 4.6a) presents that the recorded ground motions are within the \pm one standard deviation of the ground motion predictions. [Abrahamson and Silva \(2008\)](#) accurately predicts the ground motion for the distance up to 1,000 km, whereas [Boore and Atkinson \(2008\)](#) well predicts the ground motion up to 500 km. For SA at 0.2s (Figure 4.6b), the recorded values are within the \pm one standard deviation of the spectral acceleration 0.2s prediction. [Boore and Atkinson \(2008\)](#) predicts more accurately for the distance up to 500 km, whereas [Abrahamson and Silva \(2008\)](#) predicts more accurately for the distance 400 to 1,000 km. For SA at 1s (Figure 4.6c), [Boore and Atkinson \(2008\)](#) model shows a more accurate prediction than [Abrahamson and Silva \(2008\)](#) model. At Mae Sai station, the recorded ground motion is underestimated by both [Boore and Atkinson \(2008\)](#); and [Abrahamson and Silva \(2008\)](#) models. However, they are inside positive standard

deviation. [Boore and Atkinson \(2008\)](#) also well predicts the ground motion values for the observed radius less than 250 km in the study area.

- Figure 4.7: in term of PGA residuals (Figure 4.7a), there is no significant bias over the applicable distance range from 0 to 200 km. The large positive residuals at larger distance show the underestimation of ground motion prediction comparing to the recorded ground motions. In this case, [Boore and Atkinson \(2008\)](#) residuals are larger than [Abrahamson and Silva \(2008\)](#) residuals. For SA at 0.2s (Figure 4.7b), [Boore and Atkinson \(2008\)](#) model presents a better prediction than [Abrahamson and Silva \(2008\)](#). The large negative residuals show the overestimation of ground motion, which in this case is resulted from [Abrahamson and Silva \(2008\)](#) model, especially for the distance less than 600 km. Meanwhile, the underestimation of SA 0.2s values made by [Boore and Atkinson \(2008\)](#) model are observed in the distance more than 1200 km. For SA at 1s residual (Figure 4.7c), [Abrahamson and Silva \(2008\)](#) model respectively shows the similar trend of negative value. However, [Boore and Atkinson \(2008\)](#) model shows the lower overestimation of SA at 1s than [Abrahamson and Silva \(2008\)](#) model.

Considering the prediction analysed by both models, [Boore and Atkinson \(2008\)](#) model can be assumed the suitable NGA model for the study area during the Tarlay Earthquake.

4.5.2. PGA of suitable attenuation model

The PGA of the most suitable attenuation model (i.e., [Boore and Atkinson \(2008\)](#) model) was calculated for each borehole. In addition, the recorded ground motions of the earthquake stations surrounding the study area (MSAA, CRAI, PAYA, NAN, and CMMT) as shown in Figure 4.1 are compared to the predicted ground motions obtained from [Boore and Atkinson \(2008\)](#) model.

Figure 4.8 presents the comparison of the predicted ground motion to the recorded ground motion during the Tarlay Earthquake. In attenuation analysis, the distance from the earthquake source is an important determinant of the PGA. In Figure 4.8, BH-1 was the closest site to the Tarlay Earthquake source and located at Mae Sai Station (MSAA), whereas BH-4 was the farthest one. The recorded ground motions obtained from the surrounding stations also deal with the predicted ground motions of

the [Boore and Atkinson \(2008\)](#) model. The plotted value also shows that [Boore and Atkinson \(2008\)](#) underestimated the recorded PGA at Mae Sai Station as mentioned earlier. In addition, Figure 4.8 suggests that BH-1 might have sustained severe damage due to the Tarlay Earthquake, whereas severe damage would have been unlikely at the other sites. Based on [Kramer \(1996\)](#), who reported that liquefaction is possible when PGA reaches 0.1g, liquefaction may have occurred at site BH-1. This prediction has been confirmed by several liquefaction evidences during the Tarlay Earthquake in Mae Sai (BH-1) as reported by [Ruangrassamee et al. \(2012\)](#) and [Soralump and Feungausorn \(2013\)](#).

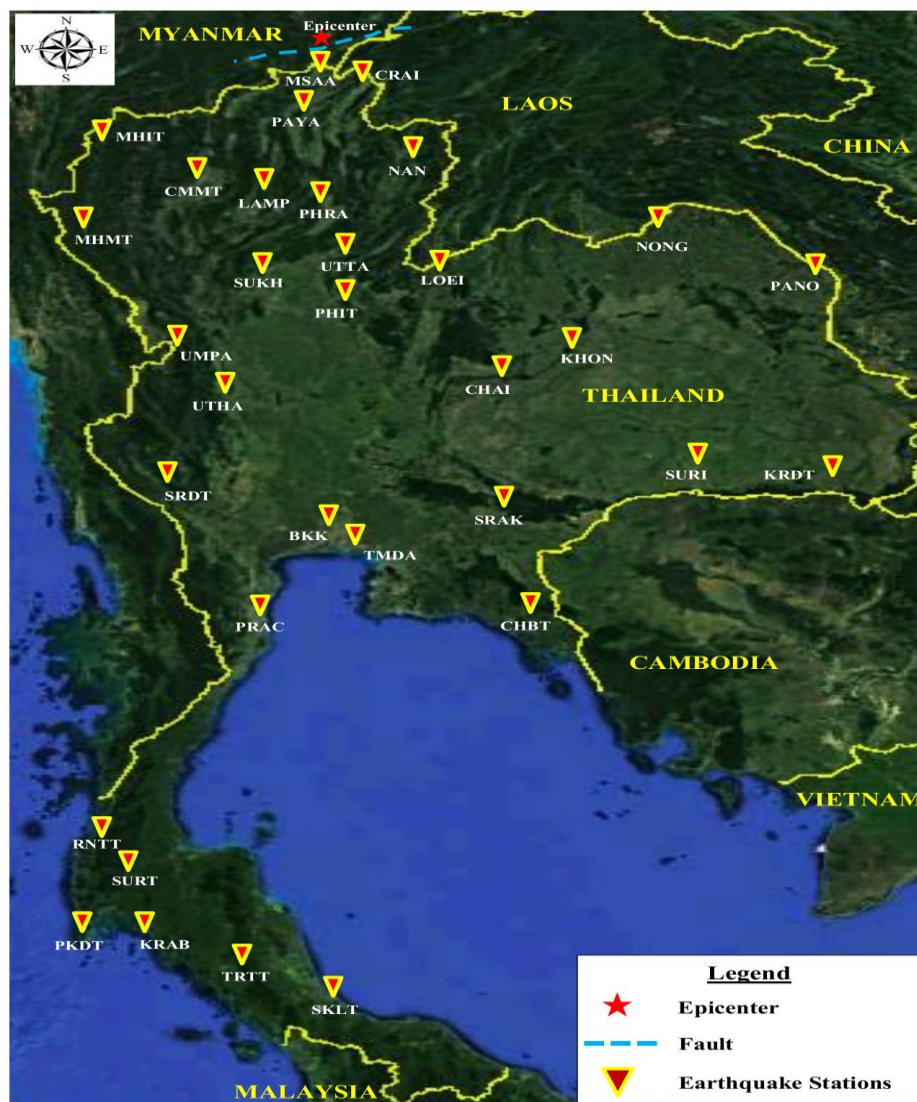


Figure 4.4. Location of earthquake stations recording the ground motion of Tarlay Earthquake (TMD, 2015).

Table 4.2. The 6.8 M_w Tarlay earthquake event data on March 24, 2011 (TMD, 2015)

No	Recording Stations	Station Code	NEHRP Class	PGA _h (g)	PGA _v (g)	PGV (cm/s)	PGD (cm)	R _{jb} (km)
1	Bangkok	BKK	D	0.00111	0.00042	0.82010	1.32555	770
2	Chaiyaphum	CHAI	D	0.00071	0.00046	0.65872	1.58909	574
3	Chantaburi	CHBT	D	0.00057	0.00015	0.68559	1.51420	913
4	Chiang Mai	CMMT	D	0.00232	0.00306	0.49803	0.91582	229
5	Chiang Rai	CRAI	C	0.09006	0.02997	3.32170	7.16235	72
6	Khon Kaen	KHON	D	0.00119	0.00068	0.86753	1.65686	573
7	Krab	KRAB	C	0.00008	0.00008	0.06635	0.12081	1377
8	Nakhon Ratchasima	KRDT	D	0.00045	0.00382	0.29868	0.63673	855
9	Lampang	LAMP	D	0.00358	0.00091	1.13970	1.39572	238
10	Loei	LOEI	D	0.00151	0.00098	0.85332	1.39309	379
11	Maehongson	MHIT	C	0.00747	0.00340	1.14675	0.98031	251
12	Maesariang	MHMT	C	0.00470	0.00425	0.27195	0.21585	347
13	Mae Sai	MSAA	D	0.20684	0.11436	13.99598	5.88315	30
14	Nan	NAN	C	0.00251	0.00152	0.22921	0.06075	189
15	Nong Khai	NONG	D	0.00135	0.00103	1.28536	1.81409	449
16	Nakhon Phanom	PANO	D	0.00054	0.00059	0.61215	1.13334	634
17	Phayao	PAYA	D	0.01349	0.00990	2.54984	3.04895	146
18	Phitsanulok	PHIT	D	0.00137	0.00123	1.12227	2.21605	387
19	Phrae	PHRA	D	0.08427	0.08619	2.83685	5.07473	243
20	Phuket	PKDT	C	0.00016	0.00011	0.21786	0.41154	1423
21	Prachuap	PRAC	C	0.00024	0.00013	0.32798	0.72768	907
22	Ranong	RNTT	C	0.00007	0.00004	0.08237	0.19477	1257
23	Songkhla	SKLT	D	0.00343	0.00093	0.15385	0.35297	1496
24	Sa Kaeo	SRAK	D	0.00051	0.00039	0.08890	0.03770	771
25	Kanchanaburi	SRDT	C	0.01496	0.00919	0.63491	1.63733	700
26	Sukhothai	SUKH	D	0.00119	0.00084	0.75282	1.33225	354
27	Surin	SURI	D	0.00041	0.00023	0.49506	1.18571	762
28	Suratthani	SURT	C	0.00060	0.00096	0.03943	0.07493	1298
29	Bang Na	TMDA	D	0.00028	0.00018	0.49033	1.96422	779
30	Trang	TRTT	C	0.00008	0.00006	0.13263	0.34627	1419
31	Tak	UMPA	C	0.00068	0.00056	0.35385	0.62900	505
32	Uthaithani	UTHA	C	0.00011	0.00008	0.02051	0.00618	567
33	Uttaradit	UTTA	C	0.00133	0.00073	1.12616	2.13665	330

4.5.3. Spectral acceleration of seismic response analysis

One-dimensional equivalent linear and non-linear approaches are used to analyse the site response analysis of the investigated area. Only BH-1 located at Mae Sai station has the ground motion records during the Tarlay Earthquake, whereas the other sites (BH-2, BH-3, BH-4) have no records of the ground motion (because no stations in those areas). Therefore, the scaled ground motion from the maximum ground motion of 0.207g were analysed in this study. The ground motions at BH-2, BH-3, and

BH-4 are scaled down based on the prediction of peak ground acceleration from the [Boore and Atkinson \(2008\)](#) model.

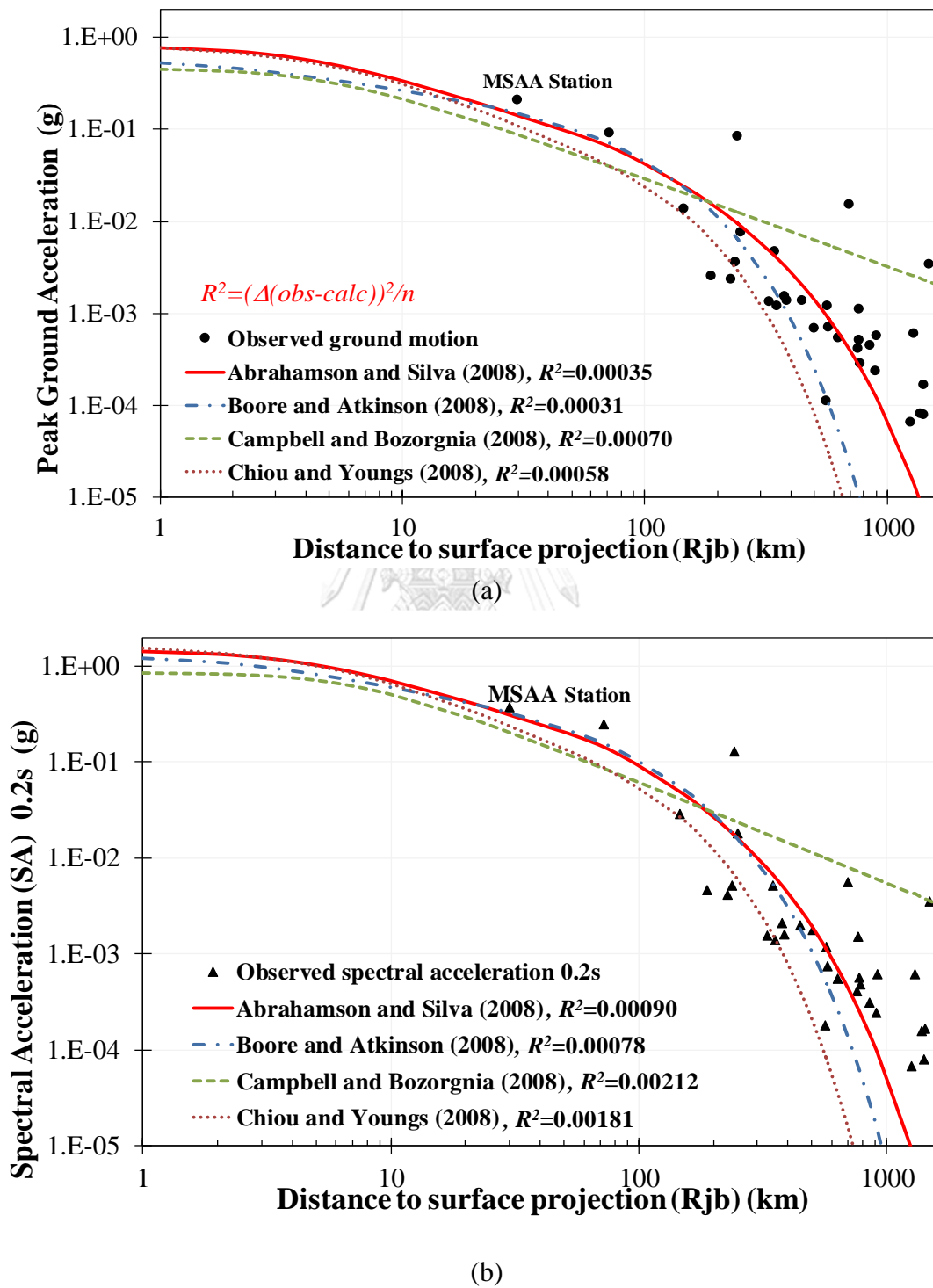
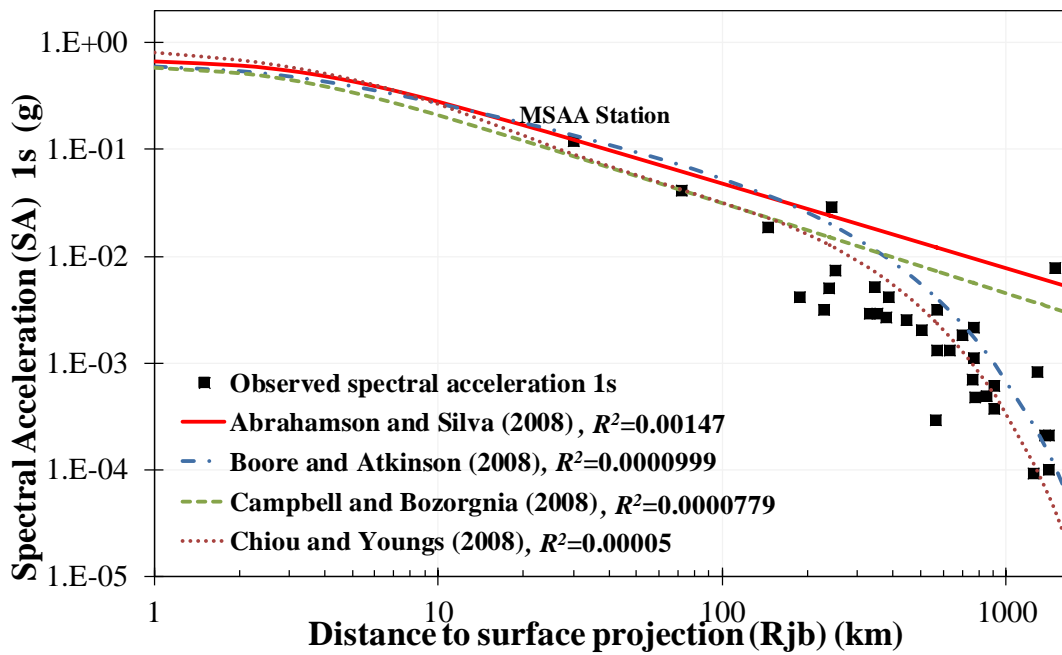
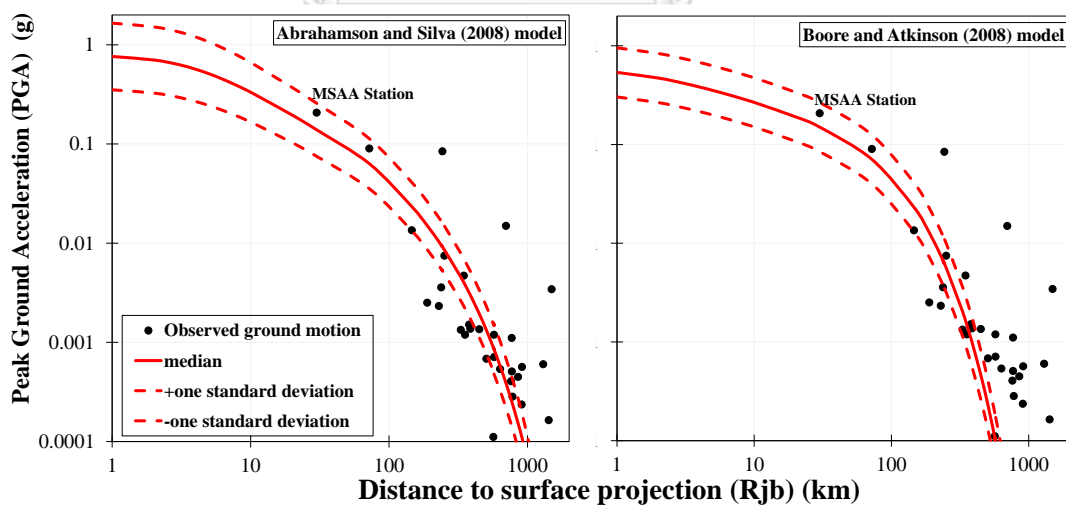


Figure 4.5. (continued)



(c)

Figure 4.5. NGA attenuation model analysis (medians) to the ground motion recorded during Tarlay Earthquake, (a) peak ground acceleration, (b) spectral acceleration at 0.2s, and (c) spectral acceleration at 1s.



(a)

Figure 4.6. (continued)

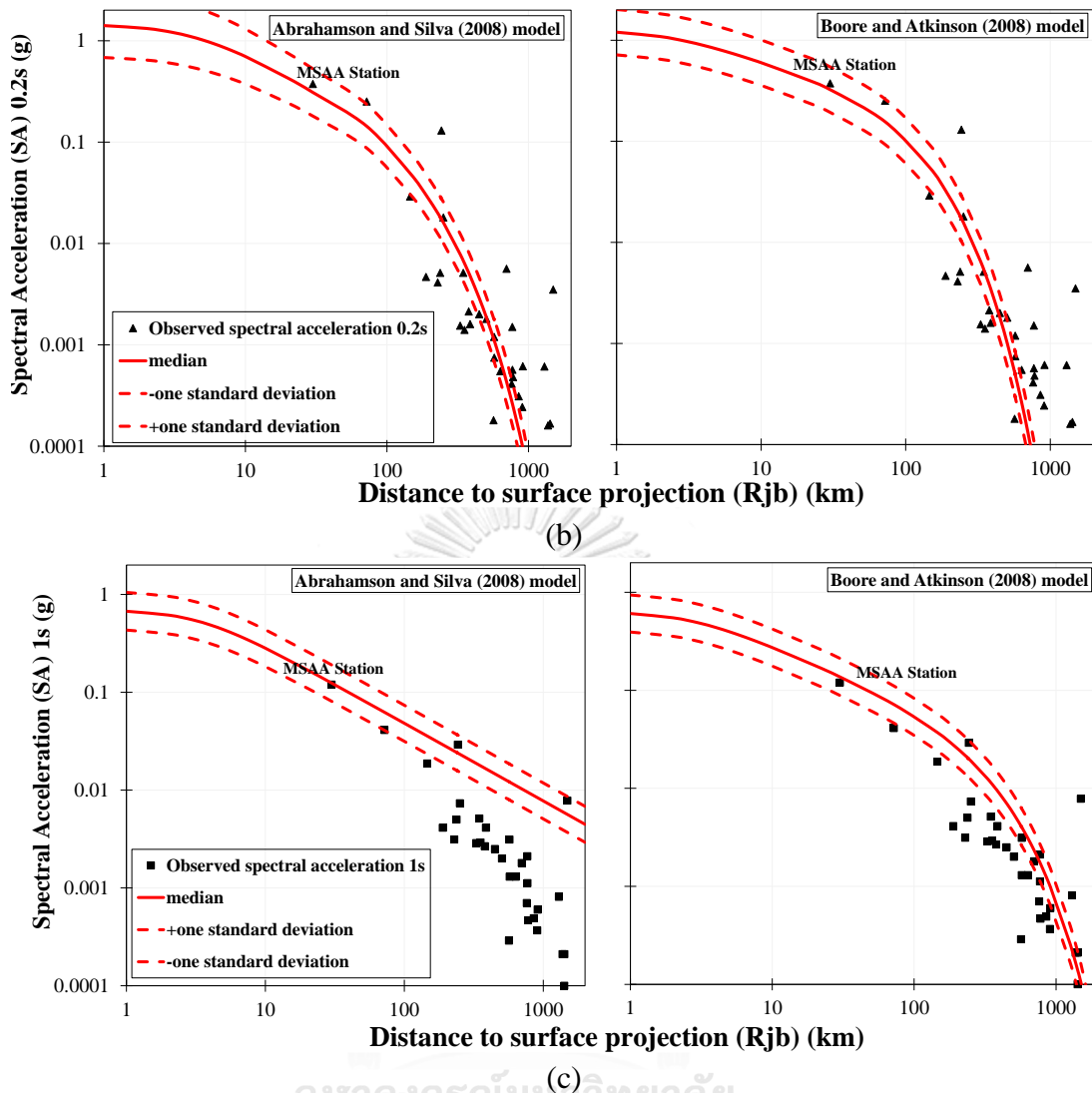


Figure 4.6. Comparison of Abrahamson and Silva (2008) and Boore and Atkinson (2008) models analysis to the ground motion recorded during Tarlay Earthquake for (a) peak ground acceleration (PGA), (b) spectral acceleration (SA) at 0.2s, and (c) SA at 1s

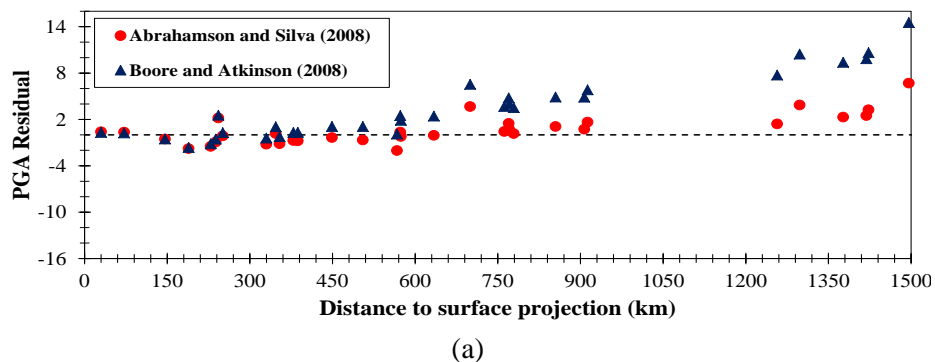


Figure 4.7. (continued)

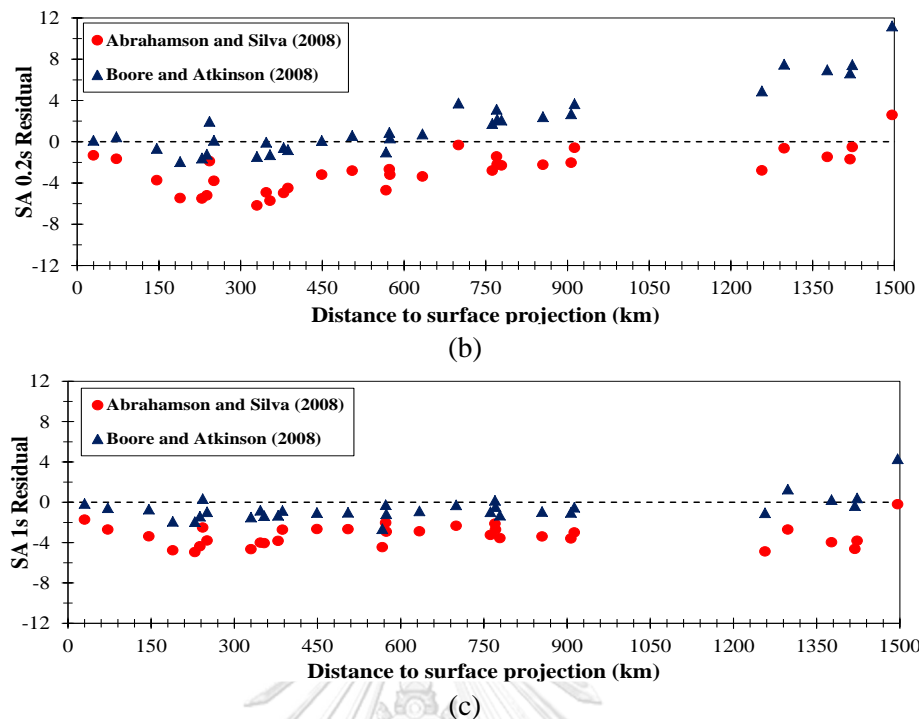


Figure 4.7. Residual of ground motion parameters from recorded ground motions relative to predictions for (a) peak ground acceleration (PGA), (b) spectral acceleration (SA) at 0.2s, and (c) SA at 1s

Furthermore, the spectral accelerations at ground surface on the study sites are compared to the local design values (with 5% damping) of [TDS \(2009\)](#). The comparison results for both the equivalent linear approach and non-linear approach are shown in Figure 4.9. The spectral accelerations experienced by the different study sites based on both approaches decrease in the following order: BH-1 > BH-2 > BH-3 > BH-4, which is the influence of the distance. In general, the trends of spectral acceleration obtained from both equivalent linear and non-linear approaches are in a good agreement. For BH-1 and BH-2, the trends of spectral acceleration curve are almost similar. The spectral acceleration curves of BH-3 and BH-4 also shows the similarity each other. It may be caused by the similar soil type and geological condition in those sites, which influence of the non-linear parameters in seismic response analysis.

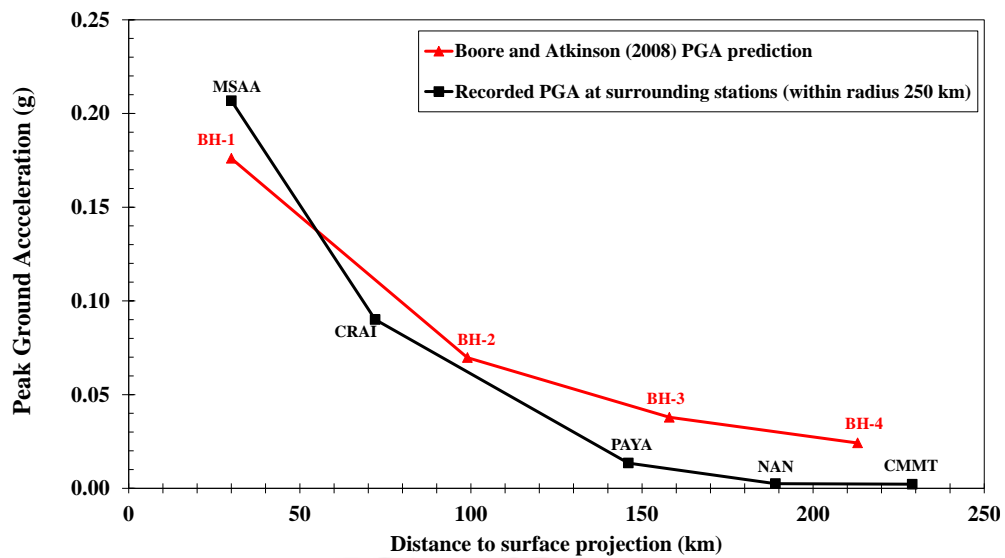


Figure 4.8. Comparison between PGA of the Boore and Atkinson (2008) model and maximum recorded ground motion at surrounding stations

In terms of spectral acceleration curve tendency, at the long-period ($T \geq 1$ s), the estimations from both methods show the good agreement, which both spectral accelerations slightly drop at the same value of spectral acceleration. At the beginning period, the spectral of acceleration of equivalent linear approach is higher than non-linear approach. This means that peak ground acceleration of equivalent linear approach is higher than non-linear approach (detailed in Section 4.5.4). Generally, the peak spectral acceleration of each site occurs in a period range of 0.1 to 0.6s. For BH-1 and BH-2, the peak spectral accelerations occur at the period of 0.6s, whereas for BH-3, the peak spectral acceleration occurs at the period of 0.18 s and BH-4 at the period of 0.14s. Compared with the spectral acceleration of input motions, which reaches the peak values at the period of 0.13s, the spectral acceleration resulted by both equivalent linear and non-linear methods shows those sites undergoing the higher spectral response at period, which is larger than the peak spectral acceleration of input motion.

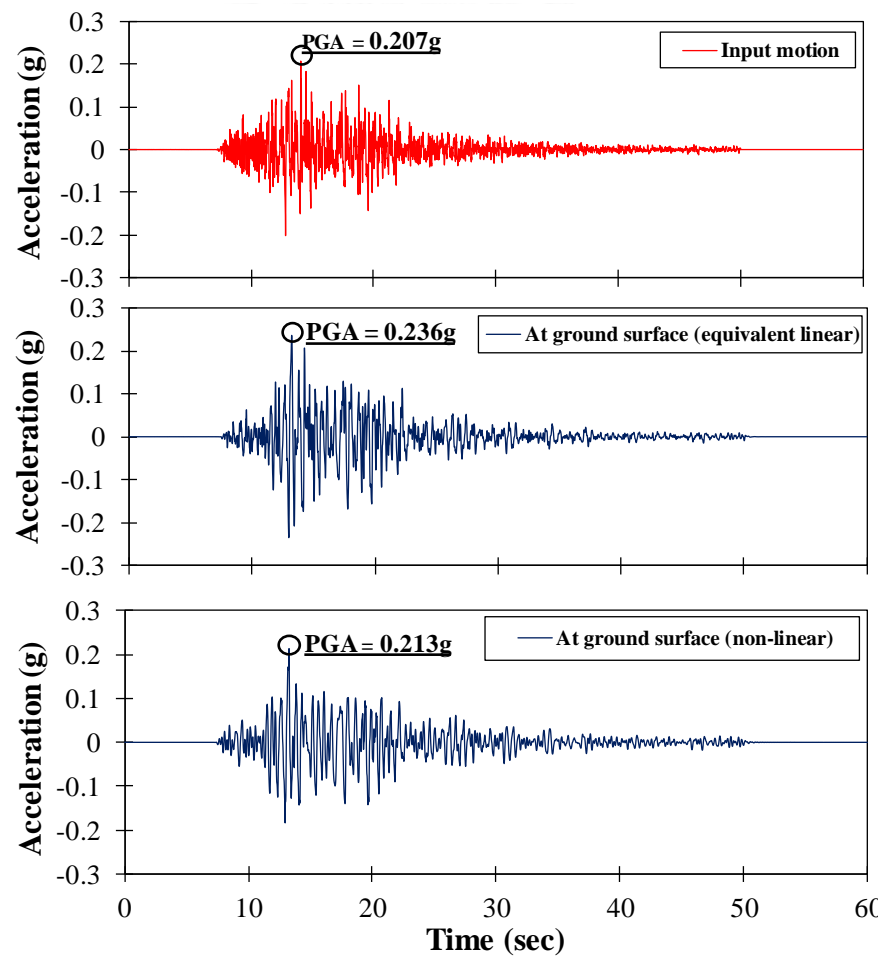
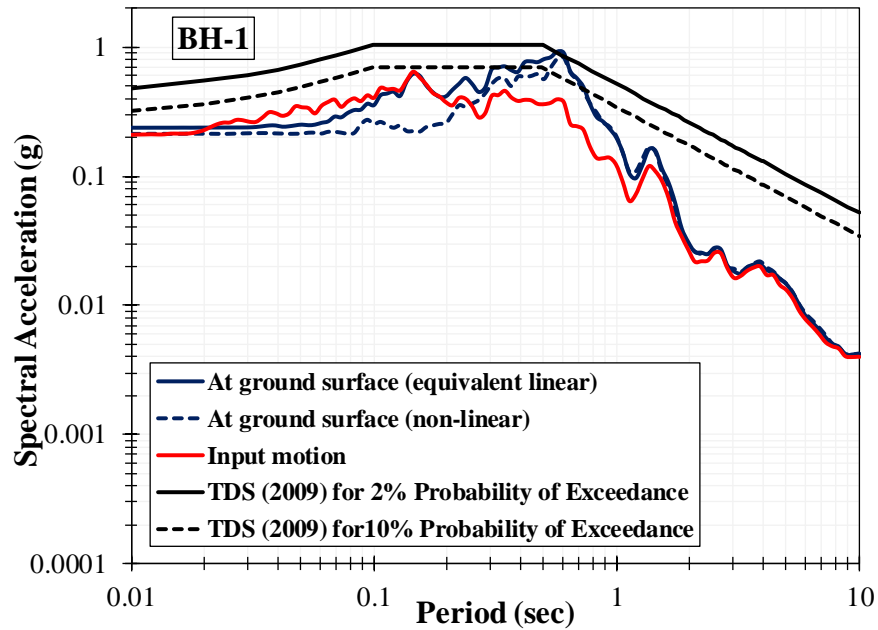
The comparison between spectral acceleration values and seismic response analysis spectral acceleration values shows that the local design values are not exceeded by the maximum spectral acceleration obtained from the analyses at each site for a long-period stage of spectral acceleration (period at 1s). However, the seismic design code of Thailand should be carefully concerned for a period (T) of 0.6 s, particularly for site

BH-1. This peak period reflects the low to medium-rise building natural period (simply predicted by $T_n = 0.1n$), which is also as the major building in this area (i.e. the 1 to 6 stories building). Therefore, the study result suggests that the local seismic design values shall be considered for anticipating the more severe damage if the stronger earthquake happens in the future.

4.5.4. PGA of seismic response analysis

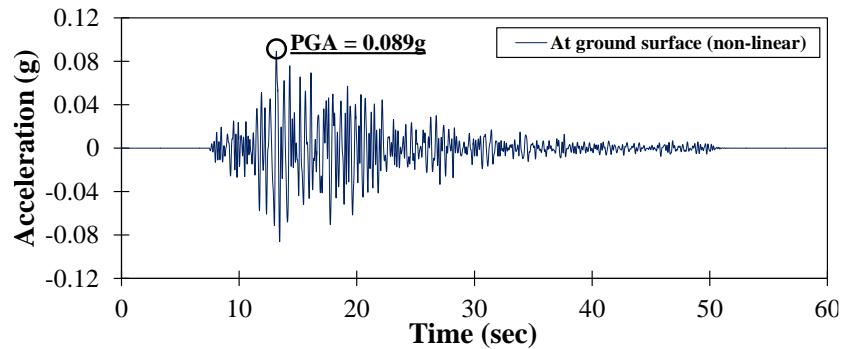
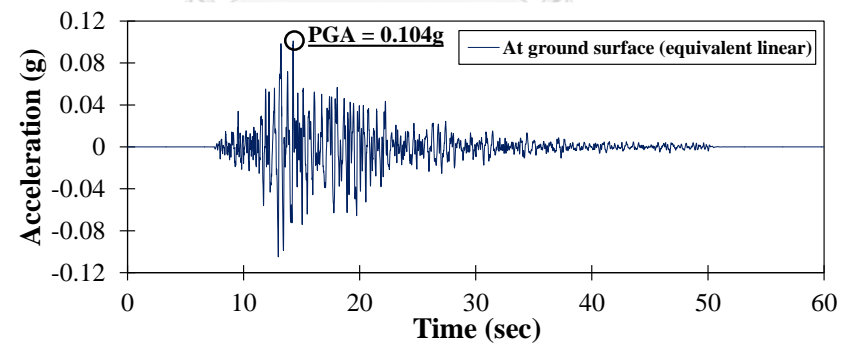
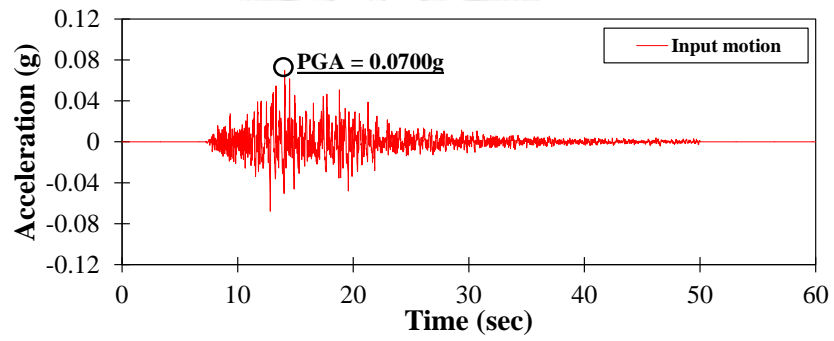
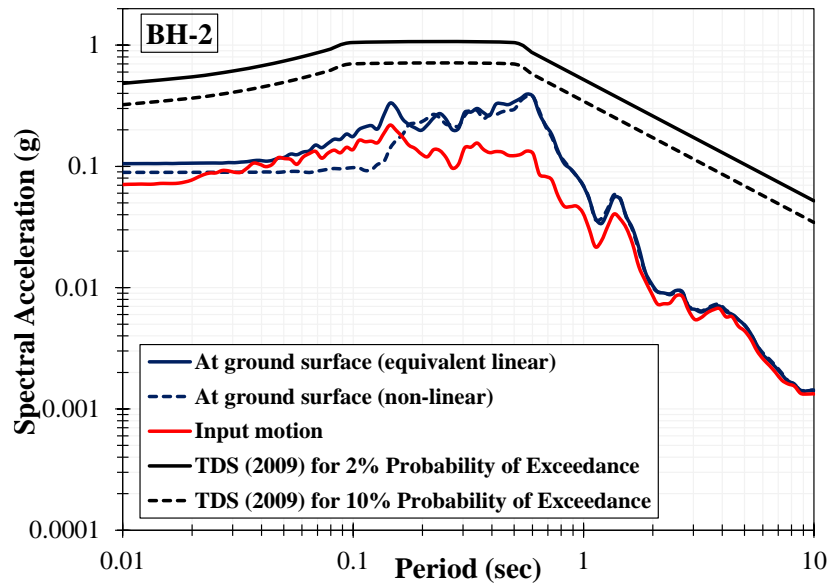
The PGAs of seismic response analysis at ground surface for the investigated locations are presented in Figure 4.9. Figure 4.9 suggests that the PGAs produced by the equivalent linear approach are more conservative than those obtained using the non-linear approach. In general, the equivalent linear approach overestimates acceleration (Finn et al., 1978) due to the assumption of linearity, especially for the estimation of shear strain. The overestimation occurs when the stress–strain curve is in a perfectly plastic state in equivalent linear approach. As a result, the overestimation of the propagated wave also happens in the weakest layer, in which the shear-strength of that controls the maximum acceleration at the ground surface. The difference also results in the higher maximum acceleration of equivalent linear approach analysis (Yoshida, 2015). This overestimation also affects the amplification factor ($PGA_{surface}/PGA_{input}$) of sites, which is shown in Figures 4.10 and 4.11. Since the estimations of peak ground acceleration at ground surface obtained from equivalent linear approach are higher than non-linear approach (Figure 4.10), so the amplification factor for sites are also higher. Figure 4.11 suggests that the amplification factor resulted by equivalent linear approach is about 2 times of non-linear approach.

Overall, the PGAs at ground surface obtained are higher than the input motion, which confirms that input motions amplify. However, the concern is also addressed to Chiang Mai area (BH-4), which has the highest amplification factor among the other sites. As we know, Chiang Mai is the centre of economic-social in Northern Thailand and has many high-rise buildings, which are possible to undergo serious impact of seismic propagation caused by earthquake. The subsoil conditions of the investigated area are dominated by sandy soil with low ground water level. This condition is very vulnerable to undergo liquefaction caused by earthquake.



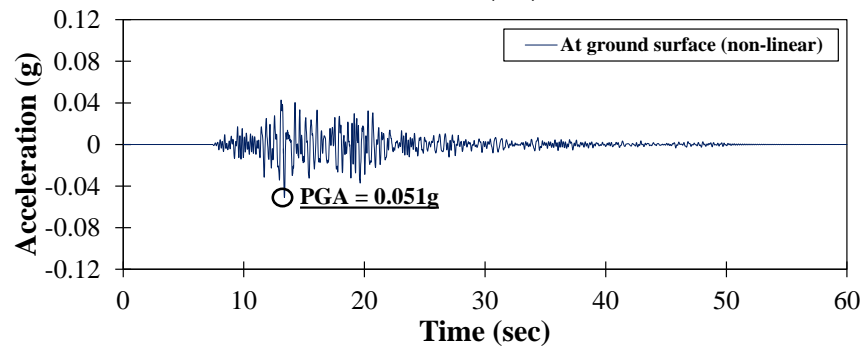
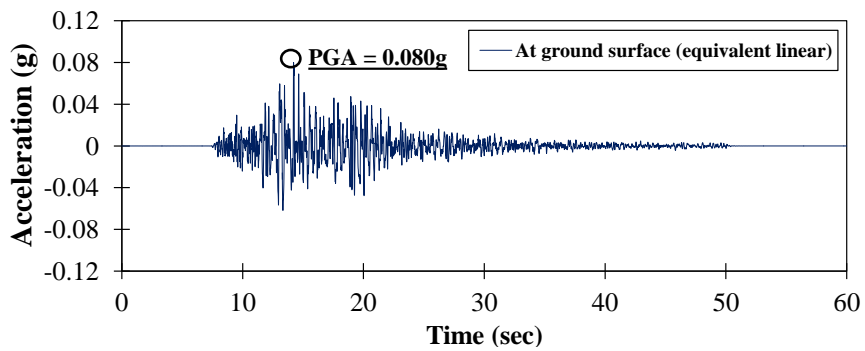
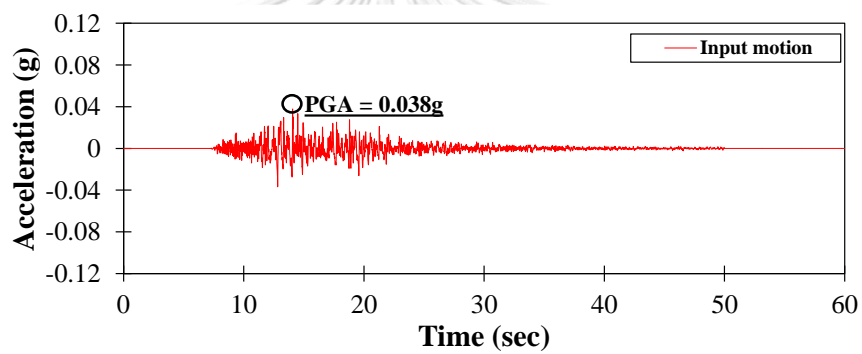
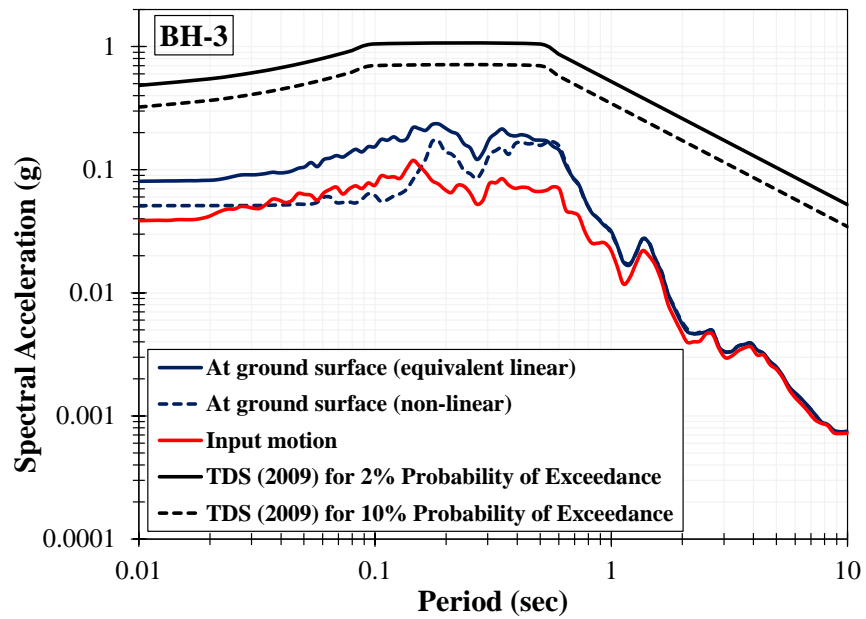
(a)

Figure 4.9. (continued)



(b)

Figure 4.9. (continued)



(c)

Figure 4.9. (continued)

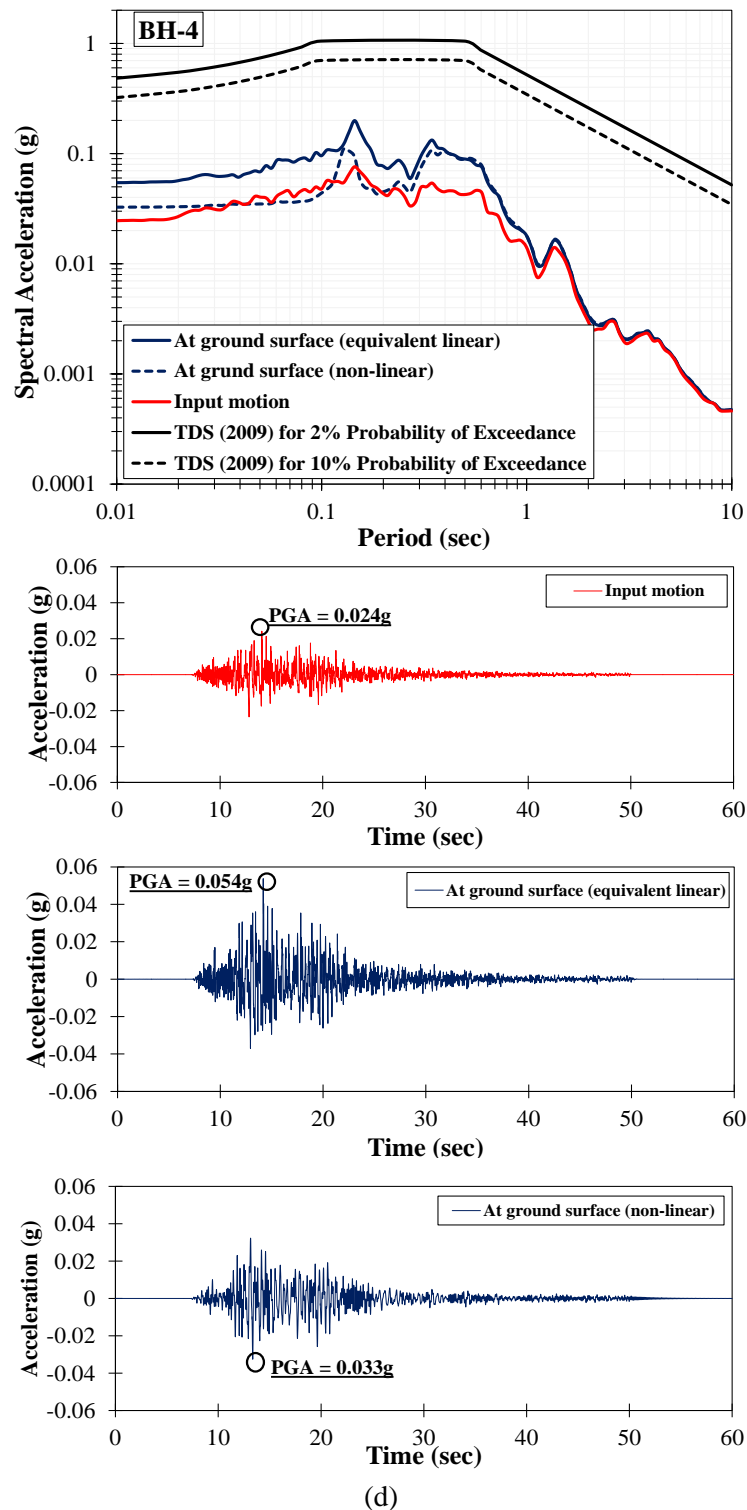


Figure 4.9. Comparison of ground surface spectral acceleration of seismic response analysis and spectral acceleration of input motion and local design spectral acceleration (TDS, 2009), and ground surface acceleration of both equivalent linear and non-linear approach on study area, (a) BH-1, (b) BH-2, (c) BH-3), and (d) BH-4.

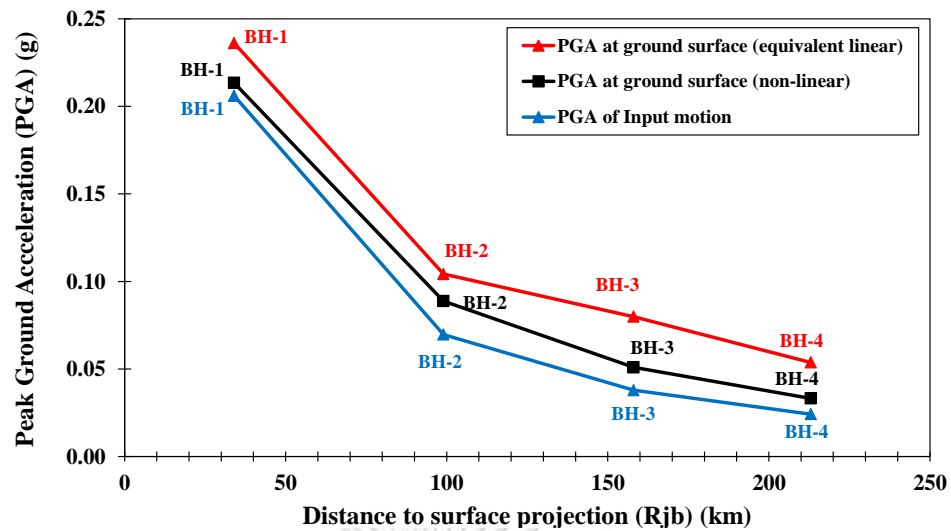


Figure 4.10. Comparison of PGA of seismic response analysis obtained from both equivalent linear and non-linear approaches the on the study area.

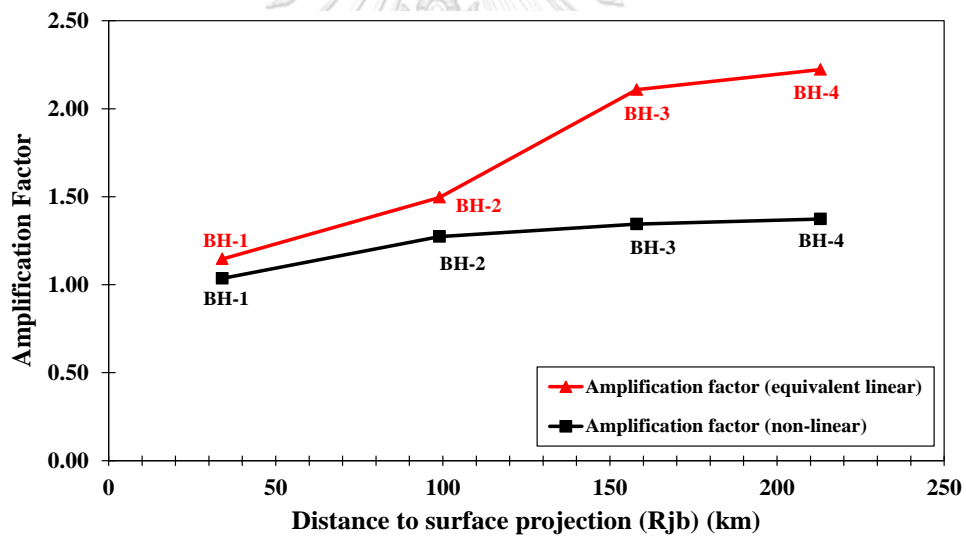


Figure 4.11. Comparison of amplification factor of seismic response analysis obtained from both equivalent linear and non-linear approaches on the study area.

4.6. Concluding remarks

This study focuses on seismic ground response analysis due to the strong earthquake in Northern Thailand. Several concluding remarks are drawn as follows,

1. The study area found to be dominated by sandy soil and classified as stiff soil (Site Class D) based on NEHRP.

2. In general, the closer distance to epicentre tends to undergo more potential impact of earthquake shaking. Corresponding to seismic response analysis result, the BH-1 is the most vulnerable area due to Tarlay earthquake. This was shown by spectral acceleration at the ground surface, which slightly exceeds the local design value recommended by TDS. In BH-1, the acceleration of more than 0.1g at ground surface due to seismic wave propagation confirms that this site possibly underwent the liquefaction during Tarlay earthquake as reported by [Ruangrassamee et al. \(2012\)](#) and [Soralump and Feungaugsorn \(2013\)](#).
3. [Boore and Atkinson \(2008\)](#) model was found to be the most suitable attenuation model for Northern Thailand during Tarlay Earthquake. The model exhibits the accurate prediction on the observed strong motion parameters including peak ground acceleration, spectral acceleration at 0.2s, and spectral acceleration at 1s. The model was also used in some cases of ground motion prediction analysis, such as [Stafford et al. \(2008\)](#) for earthquake events in Euro-Mediterranean region, [Joshi et al. \(2012\)](#) for Himalayan earthquake events in India, [Adnan et al. \(2012\)](#) for seismic hazard assessment based on earthquake events in Malaysia, and [Frankel et al. \(2011\)](#) for seismic hazard assessment based on earthquake events in Haiti.
4. The spectral acceleration obtained using the equivalent linear approach is generally more conservative than that given by the non-linear approach. In general, the spectral acceleration of $0.2s \leq T \leq 0.6s$ for low to medium-rise building is critically considered. Comparisons of the spectral accelerations obtained from the analyses to a seismic design code of Thailand indicated that some awareness should be considered for this area to ensure that the sufficient design values are required against the stronger earthquakes in the future.
5. The amplification factor analysis shows that Chiang Mai site (BH-4) was predicted to undergo the high acceleration amplification during Tarlay Earthquake. Therefore, the amplification factor in Chiang Mai shall be carefully considered, as most of high-rise buildings exists in this city.
6. The granular materials with low ground water level of the investigated areas is very vulnerable to undergo liquefaction. The study of soil liquefaction during strong earthquakes shall be conducted (detailed in Chapter VI).

CHAPTER V. LOCAL SITE INVESTIGATION TO THE LIQUEFIED LOCATIONS DURING THE MAE LAO AND TARLAY EARTHQUAKES

5.1. Local Site Investigation in Mae Lao

5.1.1. Introduction

Thailand is in South-East Asian Region, which has known as the boundary of the Indo-Australian and Eurasian Plates. This zone was comprised by the convergent margin, including Myanmar oblique subduction zone, Andaman thrust, and Sunda arch to the northwest, west, and south (Ornthammarath and Warnitchai, 2016). McCaffrey (1996) explained that the activity of Australian movement to Southeast Asia, which has convergence rate of 65-70 mm/year, is possible to produce large earthquake event in the region, especially at the boundary of two plates. One of past event in Southeast Asia, which was triggered by the subduction activity of both plates is Sumatra Megathrust Earthquake (Ammon et al., 2005). Ornthammarath and Warnitchai (2016) reported that due to India drove into the Eurasia south margin, the clockwise rotation of about 25° occurred. This activity extruded the Indochina to southeast direction by approximately 800 km along the Red River and Three Pagoda Faults during the first 20-30 million years. In Northern Thailand, the extended crust, which has dominated by rift basins and isolated plains has underwent the earthquake with magnitude higher than 5 since 1970. The seismic activity in this zone is generally dominated by normal and strike-slip faulting along the east-west to northeast direction (Fenton et al., 2003).

Over the five-year period from 2011 to 2016, at least two major earthquakes occurred in the northern part of Thailand i.e. Tarlay Earthquake with a magnitude of 6.8 M_w and Mae Lao Earthquake with a magnitude of 6.1 M_w (Figure 5.1). These earthquakes caused building collapse, ground liquefaction, and subsidence (Ruangrassamee et al. (2012); Soralump and Feungaugorsorn (2013); Soralump et al. (2014); Lukkunaprasit et al. (2016)). Chiang Rai Province was the most heavily impacted area due to both earthquakes.

General geological conditions in the Chiang Rai area and particularly liquefaction during the earthquakes have been briefly discussed in several studies. [Soralump and Feungaosorn \(2013\)](#) reported that the subsoil in Mae Sai (the northernmost district of Chiang Rai Province) comprises sand layers and thin medium-stiff clay layers near the ground surface, with a shallow water table. It was suggested that the sand layers were liquefied and extruded during Tarlay Earthquake ([Soralump and Feungaosorn, 2013](#)). The grain size distribution of this area matched with the graph of [Iwasaki \(1986\)](#) for the vulnerable soils to liquefaction. At the Mae Lao site, [Soralump et al. \(2014\)](#) reported evidence of liquefaction in quaternary deposits (Qa) dominated by gravel, sand, silt, and clay.

Field measurements using microtremor and SASW (Spectral Analysis of Surface Waves) are commonly used to investigate local site condition. [Nakamura \(1989\)](#) proposed a method for studying local site effects based on comparison of horizontal and vertical spectrum from ambient noise measurement. This can be used to identify horizontal to vertical spectral ratio (H/V ratio) and predominant frequency of the site (f_0) at a relatively low cost ([El-Hady et al., 2012](#)). SASW is widely used to interpret the shear wave velocity (V_s) of site class. Site classification groups appear in several international codes, such as National Earthquake Hazard Reduction Program ([BSSC, 1997](#)) has adopted shear wave velocity as the basis of site classification.

Several local researchers have studied the local site classification in Northern Thailand. For examples, [Poovarodom and Pitakwong \(2010\)](#) studied the local site classification of Mae Sai Basin (the most impacted area during Tarlay Earthquake) by using microtremor measurement, concluded that the area was classified as Site Class D, with V_{s30} around 335 m/s. [Thitimakorn and Channoo \(2012\)](#) investigated the site class of Chiang Rai Province using MASW (Multichannel Analysis of Surface Waves), showed that the Chiang Rai site class in mountainous area was classified as site class type C with V_{s30} around 418 m/s, whereas the northern and the eastern parts (basin area) of Chiang Rai were classified as site class type D with V_{s30} around of 338 m/s. Based on these previous studies, Site Class D can be assumed to be the dominant site class in Northern Thailand, especially for two areas that underwent the impact during the strong earthquakes in Northern Thailand (Tarlay and Mae Lao Earthquakes).



Figure 5.1. Focused areas of local site investigation.

Following the earthquake events in the Northern Thailand, surveys are conducted to investigate the subsoil. However, no investigation has yet been carried out using ambient noise (microtremors) combined with SASW measurement. In general, the previous studies were focused on the capital cities in Northern Thailand only, where the social-economy aspects are addressed there. The necessary to study the site characterization of the liquefiable spots during the recent earthquake has not yet been performed. Therefore, the importance to understand the site characterization of those liquefied points found in Mae Lao during the earthquake is the goal of this chapter. In the current study, both microtremor and SASW measurements were conducted in locations that had undergone liquefaction and ground failure during the Mae Lao earthquake. This chapter presents the local site investigation of the liquefied sites found during Mae Lao earthquake. The soil profile corresponding to shear wave velocity on each site is presented. In addition, the site class of those locations is analysed.

Furthermore, the estimation of possibly extruded layer at shallow depth during soil liquefaction in this area is presented in this chapter. In general, the results could bring a recommendation to understand site specific response of the impacted locations, especially the soil behaviour under the Mae Lao Earthquake shaking.

5.1.2. Study area

The research area and its topographic conditions are shown in Figure 5.1. The locations centred on Mae Lao (the yellow rectangle). Site studies were conducted using microtremor measurements and SASW as shown in Figure 5.2. Sites are coded as ML-1 to ML-5. ML-1 was located at Nam Lorm Temple, ML-2 was located at Ban Nong Kao Hong School, ML-3 was located at Dong Mada road, ML-4 was located at San Ton Muang Temple, and ML-5 was located at Pa Kom Temple. These locations were selected after discussions with local citizens who had witnessed liquefaction in the area during the earthquake. The coordinates of the investigated locations are summarised in Table 5.1.

Mae Lao is located at the middle of Chiang Rai Province. This district suffered minor damage in Tarlay Earthquake, as it was some distance from the epicentre. However, its location is close to two active faults: the Mae Chan and Phayao Faults. In May 2014, the 6.1 M_w Mae Lao Earthquake, with an epicentre 10 km from Mae Lao, occurred in the area, results in liquefaction, as reported by [Soralump et al. \(2014\)](#) and [Lukkunaprasit et al. \(2016\)](#). According to Thai Meteorological Agency (TMD, 2015), Mae Lao Earthquake was triggered by Phayao Fault and recorded as the second largest earthquake in Thailand after the 6.3 M_w Nan Earthquake (in Nan Province) in 1935. [\(Ornthammarath and Warnitchai, 2016\)](#) reported that the MMI (Modified Mercalli Intensity) level VIII was resulted during the earthquake and resulted in the extensive damage up to 50 km epicentre distance. In seismic hazard interpretation, Mae Lao is categorized as the area having the high seismic hazard zone due to the small to moderate earthquakes frequently occurred in this area triggered by the activity of Phayao Fault [\(Ornthammarath and Warnitchai, 2016\)](#). The estimated peak ground accelerations of seismic hazard studies in this area range from 0.15g to 0.3g for return period of 475 and 2475 years, respectively [\(Ornthammarath et al., 2011\)](#).

Table 5.1. Location of investigated location and earthquake epicentres (TMD, 2015)

Sites	Location	Latitude (°)	Longitude (°)
ML-1	Nam Lorm Temple Ban Nong Kao Hong	19.752	99.697
ML-2	School	19.754	99.692
ML-3	Dong Mada Road	19.764	99.720
ML-4	San Ton Muang Temple	19.800	99.704
ML-5	Pa Kom Temple	19.807	99.677
Epicentres	Location	Latitude (°)	Longitude (°)
Tarlay Earthquake	Tarlay, Myanmar	20.705	99.949
Mae Lao Earthquake	Chiang Rai, Thailand	19.737	99.699

Several earthquake stations (Figure 5.3) recorded the ground motion of the earthquake, as compiled in Table 5.2. In Table 5.2, the ground motion parameters including the maximum peak ground acceleration on vertical and horizontal directions (PGA_v and PGA_h), the peak ground velocity (PGV), the effective duration (D_{5-95}) and the distance to surface projection (R_{jb}) are presented. Table 5.2 also presents the site class of seismic stations recorded the ground motion of the Mae Lao Earthquake. The maximum horizontal acceleration (PGA_h) of 0.3g was recorded at MSAC station (Mae Suai Station), which was also reported by [Ornthammarath and Warnitchai \(2016\)](#). The location of MSAC station is only at 10 km to the southwest direction of the earthquake epicentre.

The location of study area is within 8 km of the epicentre radius, which means the acceleration would be higher than the maximum one recorded at MSAC station. The ground motion prediction (GMP) corresponding to site class using the NGA attenuation models is shown in Figure 5.4. The NGA models used in the analysis include [Abrahamson and Silva \(2008\)](#) (AS08), [Boore and Atkinson \(2008\)](#) (BA08), [Campbell and Bozorgnia \(2008\)](#) (CB08), [Chiou-Youngs \(CY08\)](#), and [Idriss \(2008\)](#) (I08). It should be noted that I08 model is only destined to predict ground motion at rock site. In Figure 5.4, the ground motion prediction analysis is performed corresponding to Site Class in Table 5.2, in which only three site classes are observed in this area. They are Rock Site ($V_{s30} = 760$ m/s), Very Dense Soil ($V_{s30} = 360$ m/s), and Stiff Soil ($V_{s30} = 300$ m/s), which according to NEHRP site class are Site Class B, C, and D, respectively. In attenuation analysis, the V_{s30} at each seismic station was

employed. The results of the attenuation models (as shown with black rectangular in Figure 5.4) provided the PGA ranges from 0.2 to 0.4g for all site classes. According to (Kramer, 1996), the minimum PGA_h of 0.1g could trigger liquefaction in sandy soils. Therefore, in the study area, liquefaction could be found during the earthquake.

Table 5.2. Observed ground motion within 200 km from the 6.1 Mae Lao Earthquake (TMD, 2015)

Stations	Location		NEHRP Class	V_{s30} (m/s)	R_{jb} (km)	Source to Site Azimuth (deg)	Ground Motion Parameters			
	Lat (N)	Long (S)					PGA_h (g)	PGV (m/s)	PGA_v (g)	D_{5-95} (s)
MSAC	19.679	99.536	B	760	14	234	0.3	21.6	0.21	4.5
MACR	19.675	99.928	D	300	25	116	0.13	2.8	0.09	13.5
MEAJ	20.146	99.852	D	300	38	20	0.04	2.5	0.02	19.5
PAYA	19.36	99.869	C	360	48	160	0.06	3.5	0.03	5.5
POPY	19.17	100.283	D	300	85	135	0.03	2.4	0.01	31
CDCM	19.409	98.982	C	360	85	244	0.03	2.7	0.01	10.5
NGLP	18.785	99.938	D	300	112	164	0.02	2.7	0.008	28
CHTO	18.808	98.96	B	760	129	217	0.01	0.2	0.01	9.7
LAMP	18.517	99.632	B	760	132	183	0.005	0.35	0.003	13
NAN	19.303	100.89	D	300	136	111	0.01	0.9	0.005	36
SMCM	18.853	98.739	C	360	139	225	0.04	1.6	0.02	15
PHRA	18.493	100.225	C	360	145	158	0.005	0.7	0.003	24
LUMP	18.566	99.038	D	300	150	208	0.02	1.6	0.01	50
PHEA	18.127	100.165	C	360	185	164	0.01	1.5	0.002	80
MJCM	18.501	98.373	C	360	194	225	0.02	2.7	0.01	25

Mae Lao has complex geological formation. The mountainous area of Mae Lao is dominated by sandstone (CP), silt, and clay with a lateritic layer (Qt), with volcanic basic rocks (SD) along the northern–western part. The basin area at the middle part of Mae Lao is dominated by clay and silt sediment (Qff), alluvial deposits (Qa), and a minor component of partly metamorphosed stone (P2). According to Thai Department of Mineral Resources (TDMR, 2016), in the eastern mountainous area, the geological morphology is characterized by siltstone (Tr), valley plain (Qfv), and high terrain (Qt) deposits. In the geology map, the liquefaction spots were generally found on Qa formation. The formation was dominated by alluvial deposits composed of gravel, sand, silt, and clay. An investigation after Mae Lao earthquake reported that liquefaction phenomena were found mainly in the basin area of Mae Lao. Soralump et al. (2014) identified the quaternary deposits, including clean sand and silty sand, as potentially

liquefiable soil. The result seemed to be consistent with the vulnerable geological formation to liquefaction in the map.

The site investigation including SPT and seismic downhole tests in Mae Lao was performed at BH and the results are shown in Figure 5.5. In general, the subsoil in Mae Lao is dominated by two types of soils, i.e. sandy and clayey soils. Sandy soils are normally found on shallow depth, which was predicted as the liquefied layer during the Mae Lao Earthquake. The top sand layer classified as SC-GC based on USCS (Unified Soil Classification System) is found at the first 4 m depth. This layer has the $(N_1)_{60}$ average of 6 blows/ft, with fines content (FC) of 20%. Other sand layers are also found from 6 to 14.5 m and 31 to 32 m. These sand layers are classified as SC, with FC of 30 to 40%. The average $(N_1)_{60}$ value for these sand layers ranges from 12 to 19 blows/ft. The clay layers are found on depth of 4 to 6 m and 14.5 to 31 m. These clay layers are categorized as low plasticity clay (CL). These clay layers have the $(N_1)_{60}$ average of 11 to 16 blows/ft, with FC of 50 to 65%. The V_{s30} from seismic downhole tests of BH is 310 m/s. Based on National Earthquake Hazard Reduction Program or NEHRP, the site can be classified as Site Class D. In addition, the ground water table of the site is found at 1 m depth below ground surface.

5.1.3. Analysis procedures

The ambient noise measurement was performed by field equipment of a DATAMARK JU410 with 24-bit digital acquisition unit A/D type measuring instrument manufactured by Hakusan Co. Ltd. The equipment consisted of 3 accelerometers (tri-direction accelerometer) component, i.e. (NS, EW, and UD (vertical)), which was originally developed for temporal observation of strong and weak motions (Koçkar and Akgün, 2012). The accelerometers are developed to record the strong and weak motions; therefore, the sensitivity tends to be low compared with the seismometer sensors (Bard (2004) and Koçkar and Akgün (2012)). During the measurement, the electric noise is very small, and it can be ignored. The digitizers of JU410 were sensitive enough to detect the ambient vibration level for spectral ratio microtremor testing compared with the other accelerometer sensors. Before measurement, the digitizers were let to warm up for five minutes to avoid the problem

of the low frequency range and for the reliable quality of a digitized waveform (Koçkar and Akgün, 2012).

The ambient noise record is processed to determine the H/V ratio, which is then further analysed to generate V_s profile using the HV-Inv computer program developed by García-Jerez et al. (2016). The HV-Inv is a computer code for the ambient noise analysis including the inversion analysis. The inversion of H/V spectral ratios of ambient noise (HVS RN) is computed based on Monte Carlo sampling simulated annealing.

The model consists of five parameters of each layer including thickness, pressure wave velocity (V_p), shear wave velocity (V_s), soil density (ρ), and Poisson's ratio (ν) (García-Jerez et al., 2016). The elastic half space assumption is adopted for the bottom layer. In Monte Carlo simulation, each parameter is ranged from a minimum to a maximum value defined by the a-priori knowledge of the soil structure and/or the physical properties of the materials (Wathelet, 2008). The values of soil density, thickness, and Poisson's ratio and V_s profile are based on the information in Figure 5.5. The shear wave velocity (V_s) can be derived from the elastic theory, which is related to the Poisson ratio and elastic modulus (Salençon, 2012). To predict pressure wave velocity (V_p), the ratios of V_p/V_s can be used (Tatham, 1982). Wathelet (2008) also suggested that V_p and V_s are the compatible variable with Poisson's ratio or in another word, V_p , V_s , and Poisson's ratio are interdependent (García-Jerez et al., 2016). The Monte Carlo search is initiated with the starting guess model, whose parameters are randomly within the ranges as listed in Table 5.3. The velocity profiles and other geotechnical parameters are repeatedly calculated until the estimated H/V curve matched with measured H/V curve.

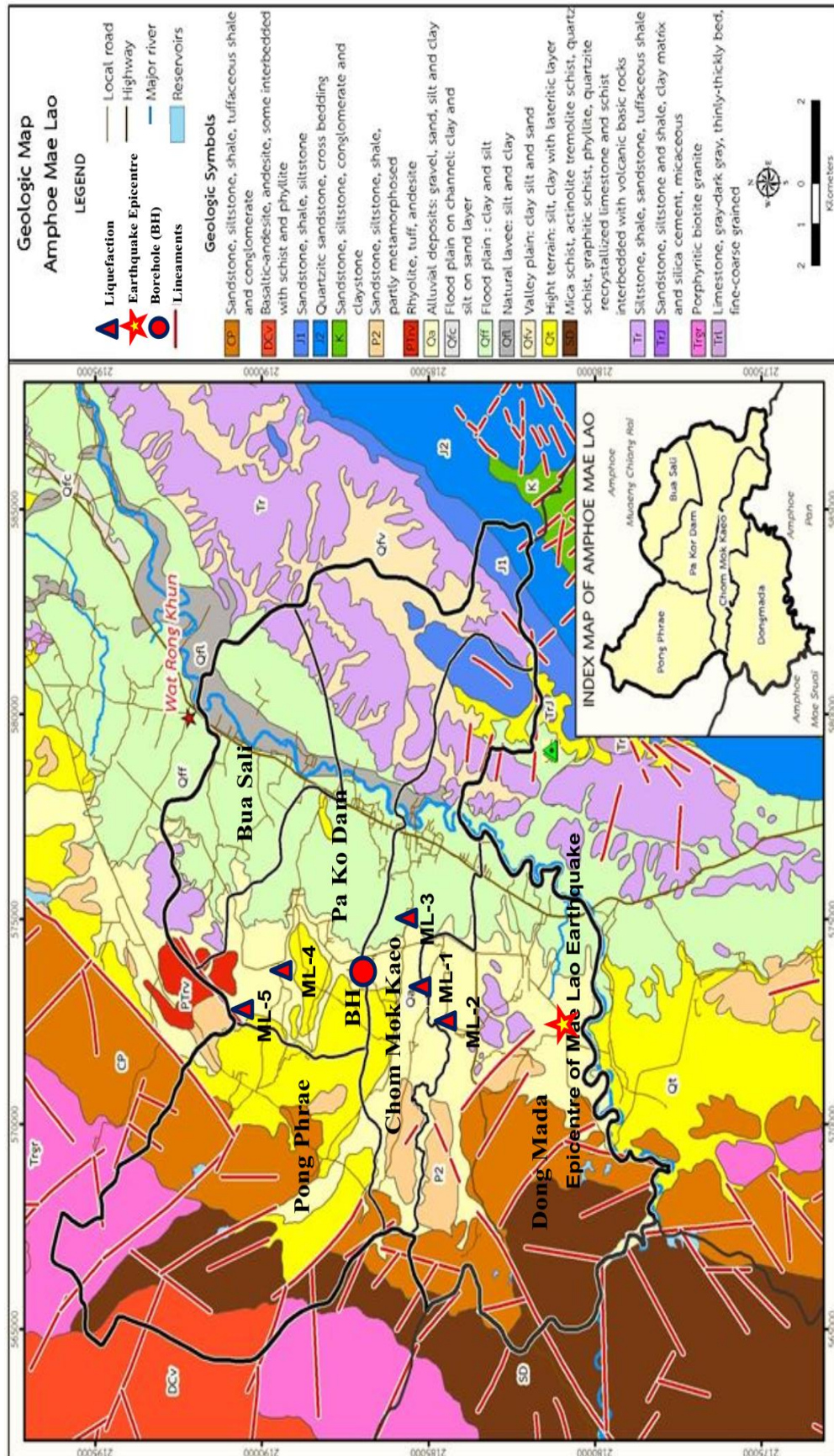


Figure 5.2. Geological setting of study area (TDMR, 2016).

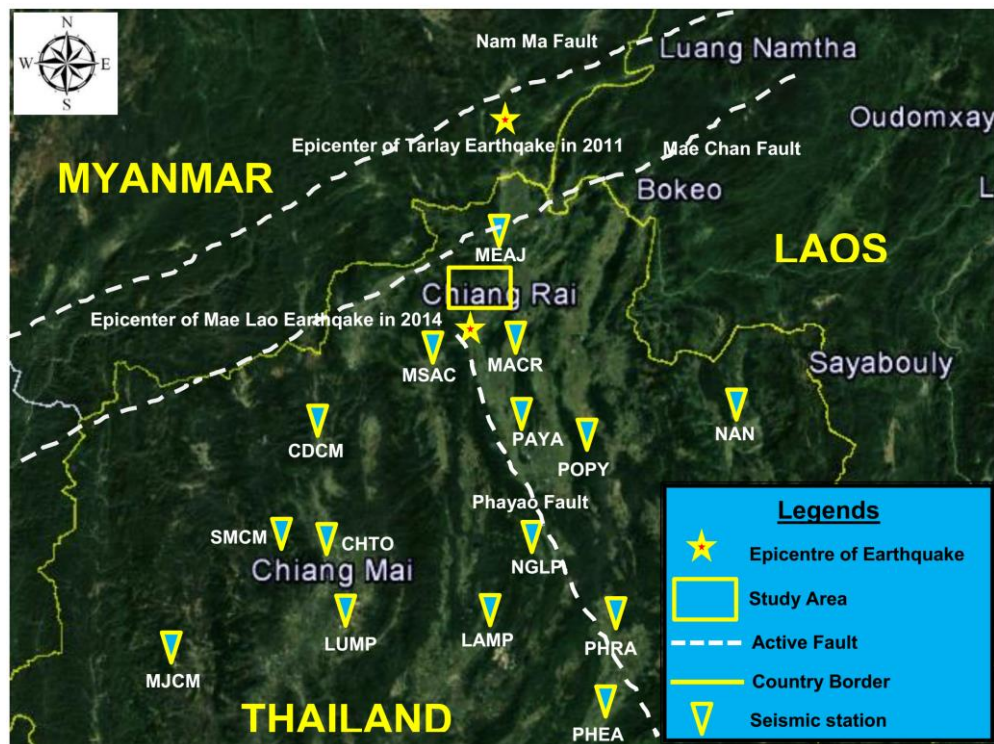


Figure 5.3. Location of seismic stations recorded Mae Lao earthquake ground motion.

5.1.4. Result and discussions for the local site investigation in Mae Lao

A. Measurement result

1. Ambient noise measurement

Microtremor tests were performed at five sites undergone liquefaction during Mae Lao Earthquake, as shown in Figure 5.2. During the tests, the weather was generally calm with no rain and wind. The measurement was performed based on [SESAME \(2004\)](#) to ensure reliable experimental conditions, especially related to recording duration, measurement spacing, and equipment. The minimum suggested signal duration is 1,000 s with a sampling frequency of 100 Hz as suggested in TremorDataView ([Naito et al., 2013](#)). The tests were performed for 30 mins.

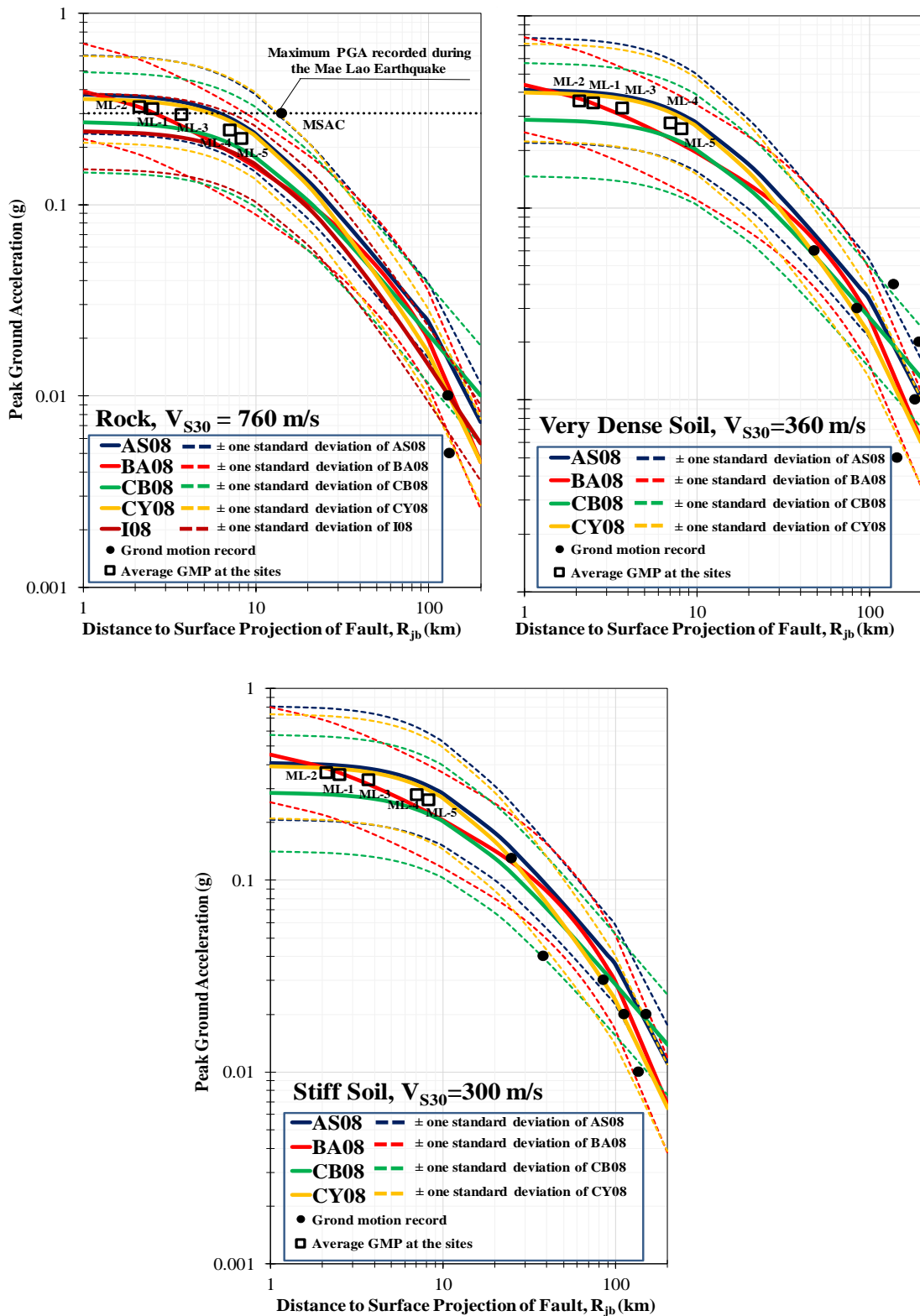


Figure 5.4. Comparison of recorded ground motion and ground motion prediction during Mae Lao Earthquake to median and median \pm one standard deviation from NGA models.

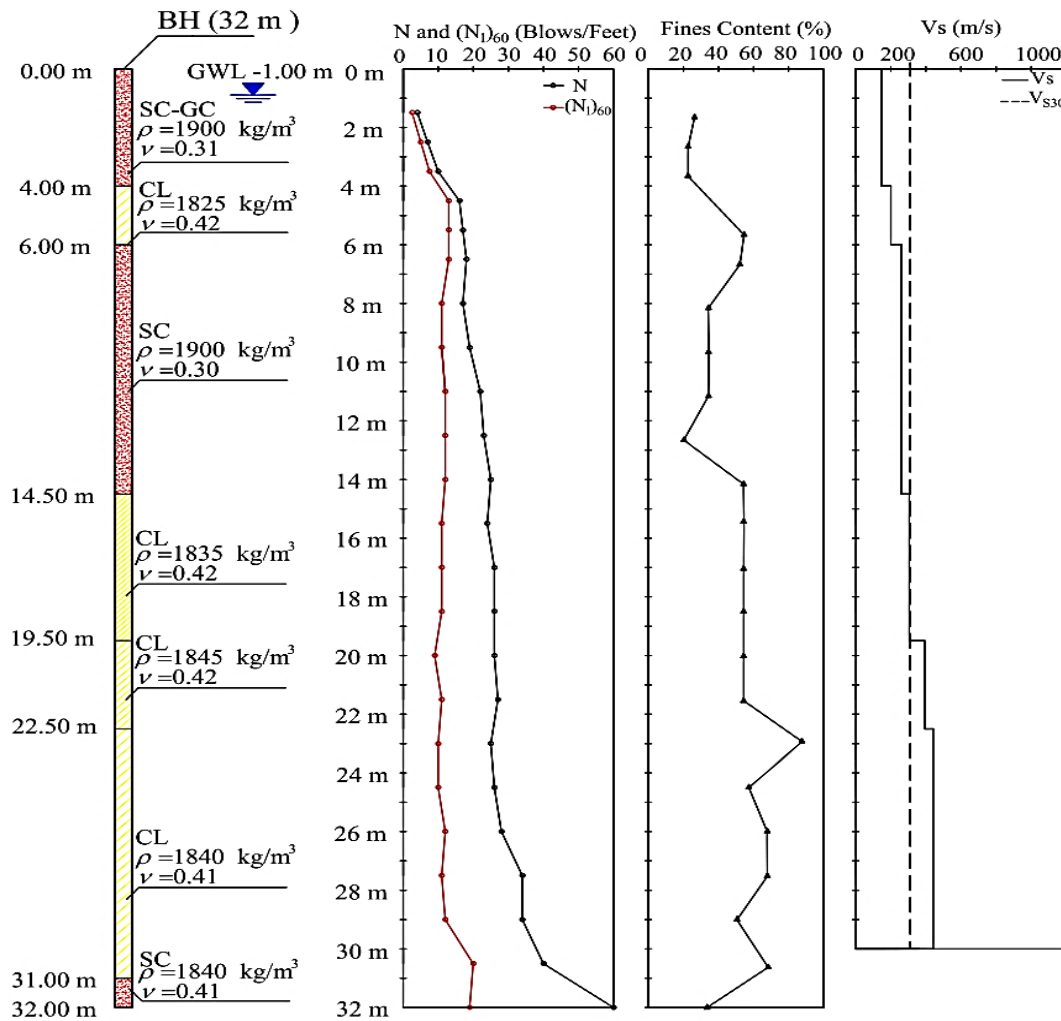


Figure 5.5. Soil boring log data and downhole seismic test at BH.

Table 5.3. Initial model for *H/V* inversion

Layer	Soil Type USCS	Thickness (m)	V_s (m/s)	V_p (m/s)	Density ρ (kg/m ³)	Poison Ratio ν
Layer 1	SC-GC	1.0 - 20.0	120 - 200	200 - 300	1800 - 2000	0.200 - 0.400
Layer 2	CL	1.0 - 20.0	130 - 250	300 - 400	1800 - 2000	0.400 - 0.495
Layer 3	SC	1.0 - 20.0	150 - 300	350 - 500	1800 - 2000	0.200 - 0.400
Layer 4	CL	1.0 - 20.0	200 - 350	400 - 600	1800 - 2000	0.400 - 0.495
Layer 5	CL	1.0 - 20.0	250 - 450	450 - 700	1800 - 2000	0.400 - 0.495
Layer 6	CL	1.0 - 20.0	300 - 550	600 - 1000	1800 - 2000	0.400 - 0.495
Layer 7	SC	1.0 - 20.0	350 - 600	700 - 2000	1800 - 2000	0.200 - 0.400
Half Space	Rock	1.0 - 20.0	450 - 760	1000 - 2200	2000 - 2200	0.100 - 0.300

Figure 5.6 presents the interpretation of *H/V* ratio corresponding to frequency for the investigated locations. The results have fulfilled the criteria defined by [SESAME \(2004\)](#) for reliable curve and clear peak. In general, the peak

H/V ratio (A) in the study area ranges from 2.1 to 4.7 with f_0 of 2.0 to 6.3 Hz. ML-1 shows f_0 of 6.298 Hz and A of 3.187. This indicates that the sediment thickness was thin to medium enough with the relatively medium impedance contrast between bedrock and the sediment. This predicts roughly that the subsoil may be dominated by the medium-stiff soils. ML-2 has A of 2.152 at predominant frequency of 4.199 Hz. In this site, the thickness of the sediment is probably medium. Compare with ML-1, the impedance contrast between bedrock and sediment in ML-2 is relatively higher, since A is larger and possibly dominated by medium-loose or soft materials. In ML-3, A of 3.251 was measured at f_0 of 2.979. It reflects the relatively higher impedance contrast between bedrock and sediment and the thicker sediment thickness than the previous elaborated sites. ML-4 and ML-5 have A of 3.855 and 4.725; f_0 of 2.051 and 4.192, respectively. The values of both sites are relatively higher than the other sites. However, the existence of the lower f_0 at ML-4 indicates that the sediment thickness is relatively thicker than ML-5. In ML-4, the subsoil is possibly dominated by medium to soft of loose material with the thicker thickness than ML-5.

From the H/V ratio and frequency interpretation, the inversion analysis was performed and interpreted in Figure 5.7. In general, each H/V curve resulted from inversion analysis is in a quite good agreement with the measured H/V curve. From the inversion analysis, V_s profile is furthermore generated. V_s profile up to 30 m deep on each investigated site was derived in Figure 5.8. In general, V_s profile increases with depth on each investigated point and consists of 5 to 7 soil layers. Overall, the investigated sites have V_{s30} ranging from 254 m/s to 336 m/s, which based on NEHRP criteria are categorized as Site Class D.

2. SASW measurement

The SASW testing was conducted using a sledge hammer (Figure 5.9a) and a 100 kg drop weight (Figure 5.9b) as seismic sources. The two receivers were 4.5 Hz geophones model 11D manufactured by Geospace Technologies (Figure 5.9c). The spacing was ranged from 0.5 up to 30 m.

The dispersion curves of the measurement on each site are presented in Figure 5.10. In general, the experimental dispersion curves of phase velocity

(shown by dot symbol) and theoretical dispersion curves of phase velocity (shown by circle symbol) are consistent each other, with RMS Error of 38 to 77 m/s. From the dispersion curve analysis, shear wave velocity profile on each site is derived, which is shown in Figure 5.8. In general, the V_s profile on each measurement had not reached the necessary depth, i.e. 30 m (only 7 to 27 m). This is because the biggest active source used in this study, i.e. 100 kg drop weight was not strong enough to result in the wave to propagate through the deeper layer. Therefore, the extrapolation of V_s profile up to 30 m deep (using Boore (2004) method) should be performed to reach the further explanation of site class. Similar with H/V inversion, V_s profile determined from SASW on the study sites generally increases with depth. The V_s values of 7 layers are summarized in Table 5. The V_{s30} on each site ranges from 244 to 341 m/s, which is categorised as Site Class D according to NEHRP.

B. Comparison of shear wave velocity

Table 5.4 presents the comparison of shear wave velocity from microtremor and SASW measurements. In general, the shear wave velocities measured from both measurements are consistent with each other. However, the shear wave velocity calculated from H/V inversion method tends to be closer to the shear wave velocity from seismic downhole measurement at BH location.

V_{s30} comparison of both H/V inversion and SASW measurement is presented in Figure 5.11. Corresponding to both results of shear wave velocity profile, the measurements are consistent to reveal that the study area is classified as Site Class D. According to NEHRP, the site class with the low V_{s30} could undergo more earthquake shaking due to wave amplification than site class with the higher V_{s30} . In the study area, the effect of earthquake shaking is larger. It was influenced by the short distance to the earthquake rupture propagating the site having relatively low V_{s30} . The conjecture was confirmed by the massive damage found on both structural buildings and ground. It can be concluded that the study area is under the high-risk of seismic hazard.

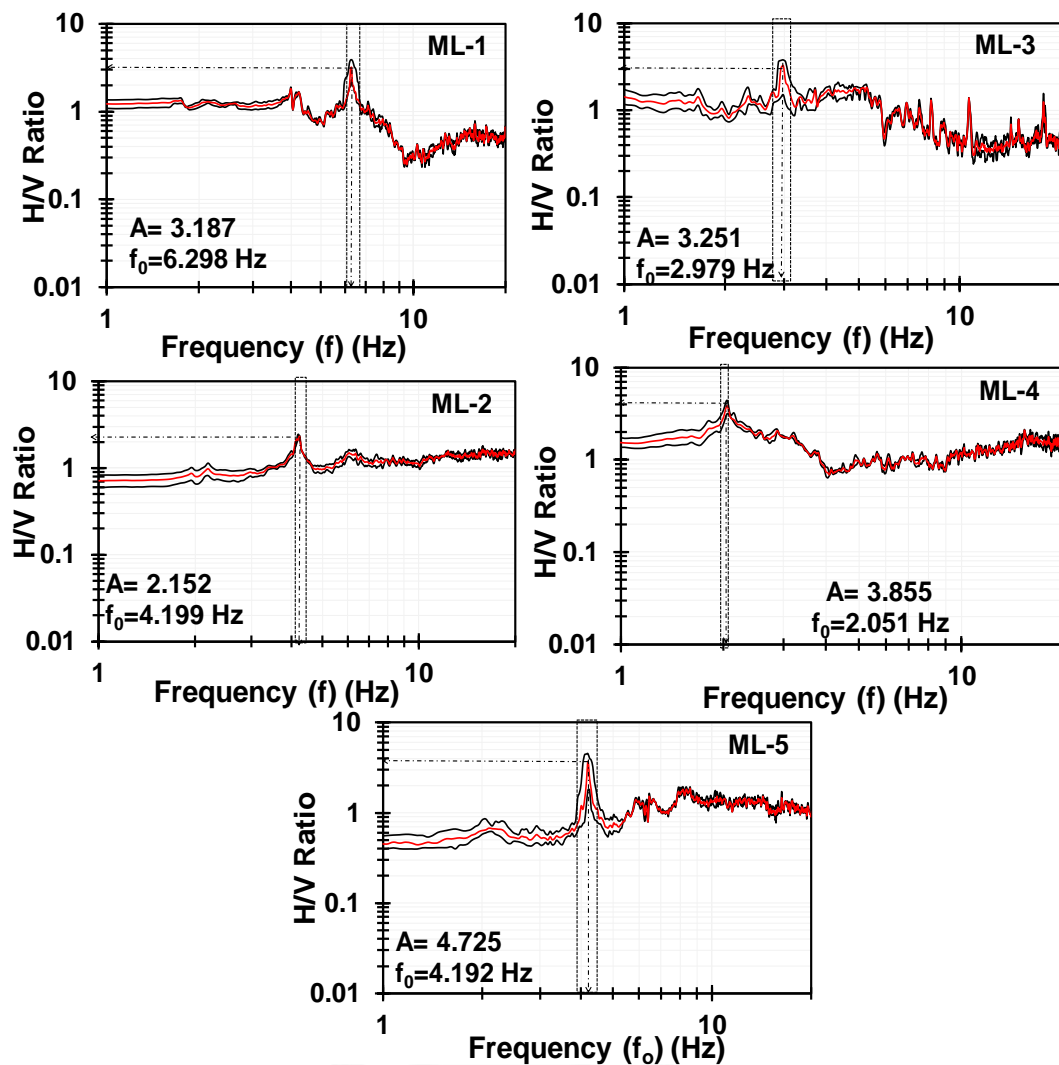


Figure 5.6. Interpretation of amplitude versus frequency for the investigated locations.

Table 5.4. Comparison of shear wave velocities measured from seismic downhole, SASW and microtremor tests

Sites	Layer	Soil Type	V _s (m/s)		
			Seismic Downhole	SASW	H/V inversion
Mae Lao	1	SC-GC	147	110 - 160	130 - 160
	2	CL	200	125 - 170	140 - 180
	3	SC	260	175 - 230	182 - 235
	4	CL	305	180 - 315	200 - 315
	5	CL	394	220 - 320	255 - 390
	6	CL	442	260 - 390	300 - 412
	7	SC	500	385 - 495	430 - 512

The values of V_{s30} obtained from both measurements is compared each other. In general, V_{s30} resulted from the inversion of H/V is slightly higher than V_{s30} resulted from the SASW measurement. This may be caused by the extended of V_s on the last layer, which has not reached 30 m deep. The extended V_s profile seems to influence V_{s30} of the soil sites to be low conservative than the V_{s30} of H/V inversion result. However, both results of V_{s30} from H/V inversion and SASW measurements show the consistency of site class on the study area. The results also deal with the [Poovarodom and Pitakwong \(2010\)](#) and [Thitimakorn and Channoo \(2012\)](#) studies which stated Mae Sai Basin and Chiang Rai were in majority classified as Site Class D. [Ornthammarath and Warnitchai \(2016\)](#) in their study also reported the site class of seismic stations spread in Northern Thailand (including the study area) was generally classified as Site Class D.

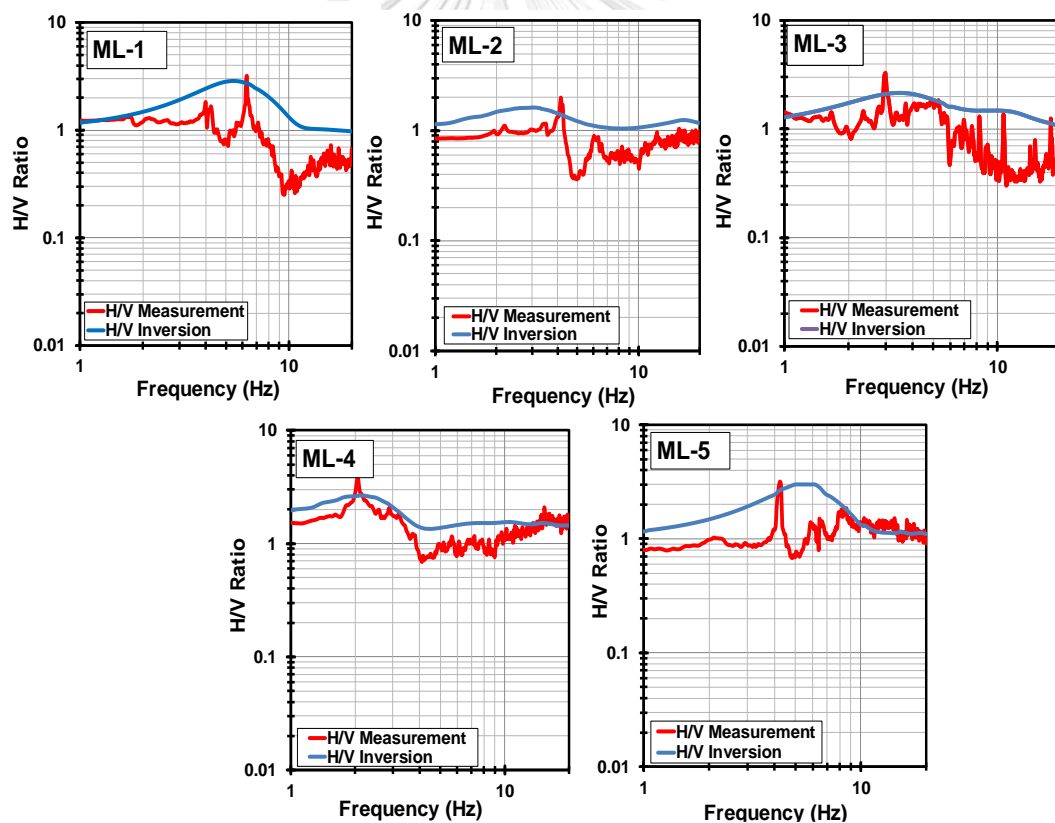


Figure 5.7. Comparison of measured H/V and inversed H/V .

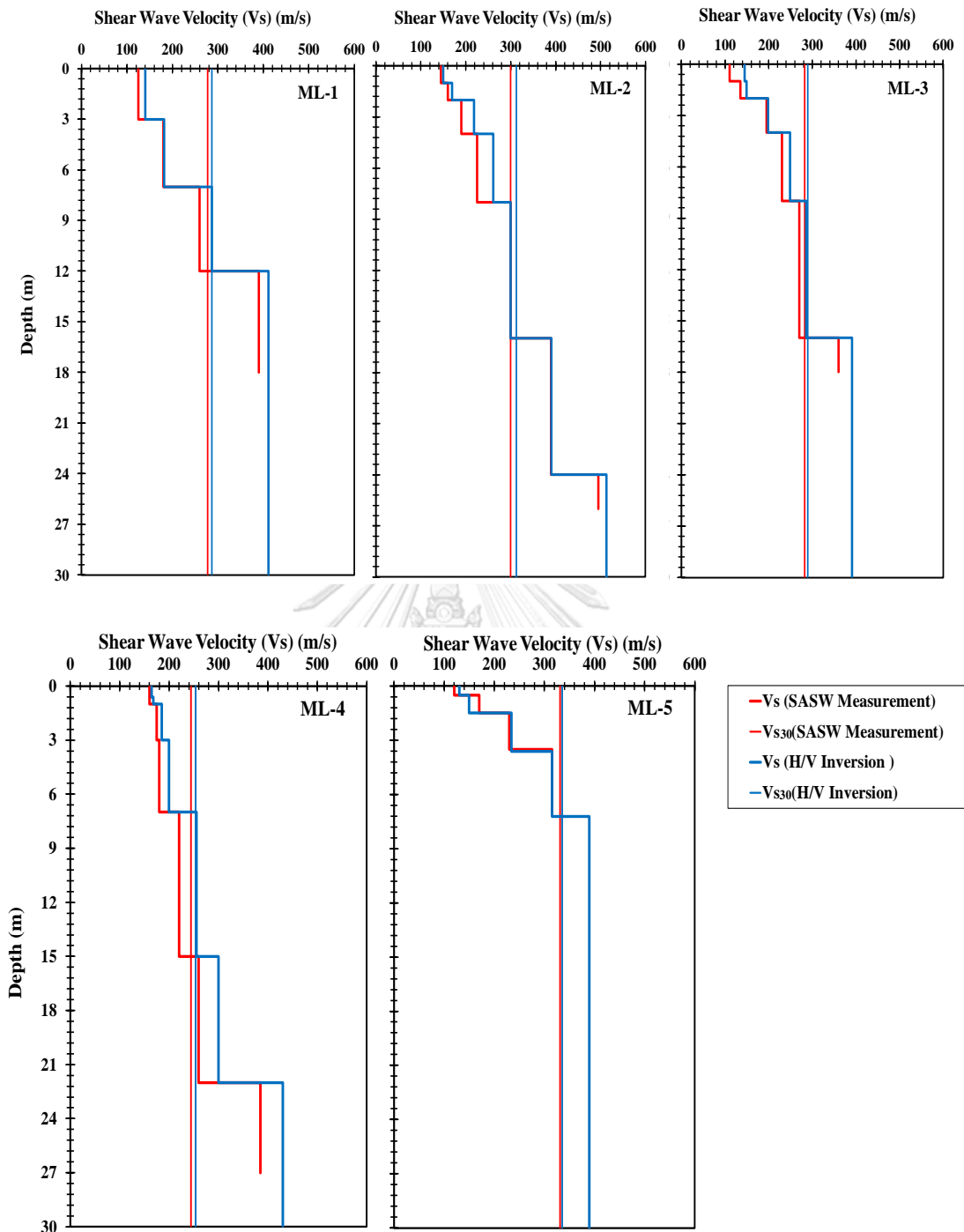


Figure 5.8. Comparison of V_s from both geophysical surveys in the study area.

C. Suspected liquefiable layer

Linking to geological condition of the study area, the study area has dominated by Qa formation, where gravel, sand, silt, and clay are dominant. The subsoil conditions of Mae Lao presented in Figure 5.5 could exhibit the liquefaction potential. It is because

the Mae Lao subsoil contains a 4-m depth of sandy soil with low resistance at the top surface as well as the water table is located near ground surface. Moreover, the thick underneath soft clay can stimulate the earthquake amplification. All these conditions seem to be very ideal for the soil to undergo liquefaction (Kramer, 1996).

Corresponding to geological condition and subsoil in the study area, at shallow depth, the sandy soil was predicted to extrude out during Mae Lao earthquake. Regarding to the result, the $V_s \leq 180$ m/s exists at shallow depth of 0 to 3 m in the study area. These layers were believed undergoing liquefaction as reported by Soralump et al. (2014). According to Stokoe et al. (1988), the sandy layer with $V_s \leq 180$ m/s is vulnerable to undergo liquefaction. Andrus et al. (2004) suggested that stress corrected $V_s (V_{s1})$ less than 215 m/s could be vulnerable to undergo liquefaction. In this study, the V_{s1} of the sites ranges from 156 to 213 m/s, which confirms that the values are in the vulnerable range to liquefaction. Based on this finding, it can be predicted that the first 3 m deep of the sites were possibly to undergo liquefaction during the earthquake.



Figure 5.9. Equipment used for SASW measurement (a) a sledge hammer, (b) a drop weight, and (c) two geophone receivers.

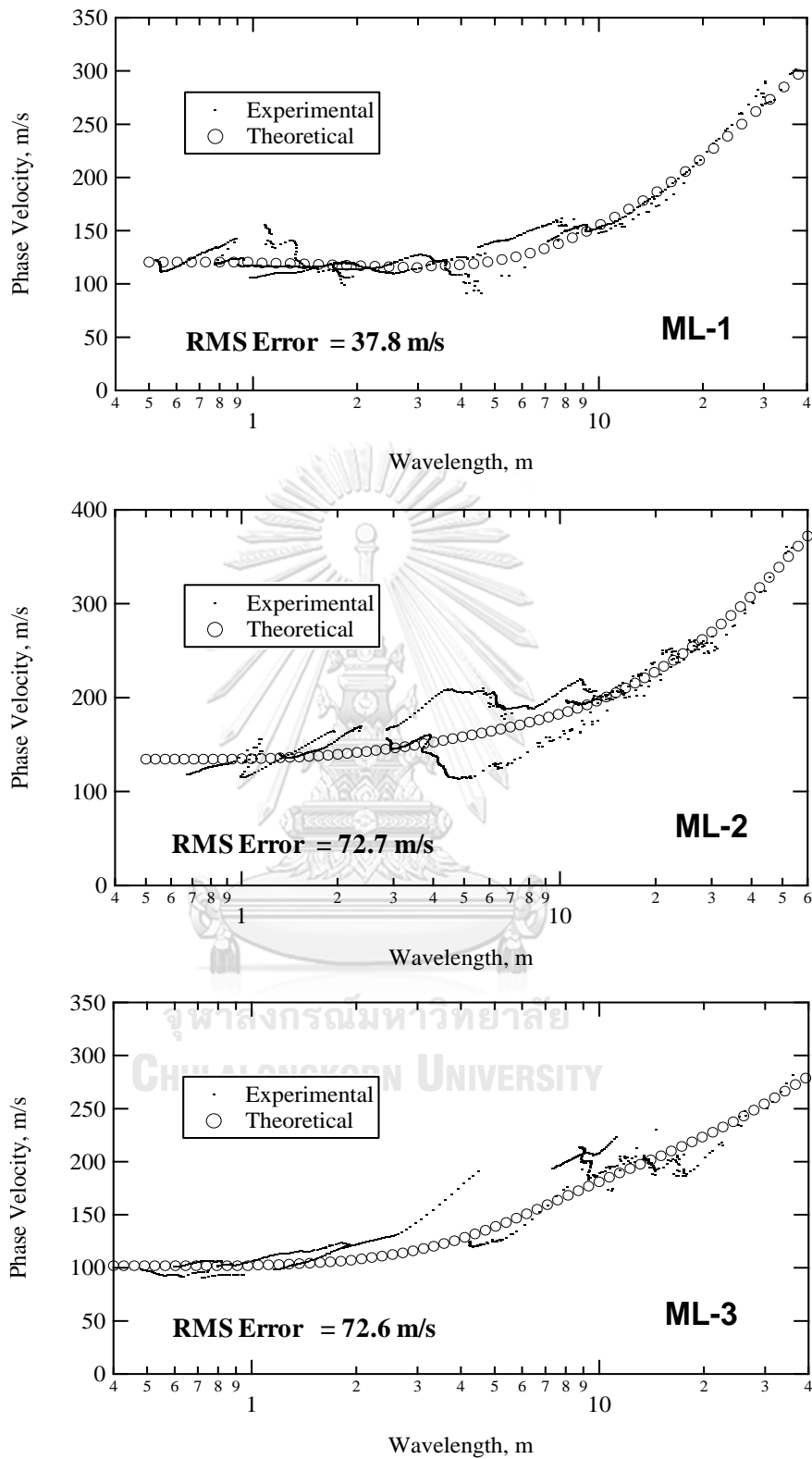


Figure 5.10. (continued)

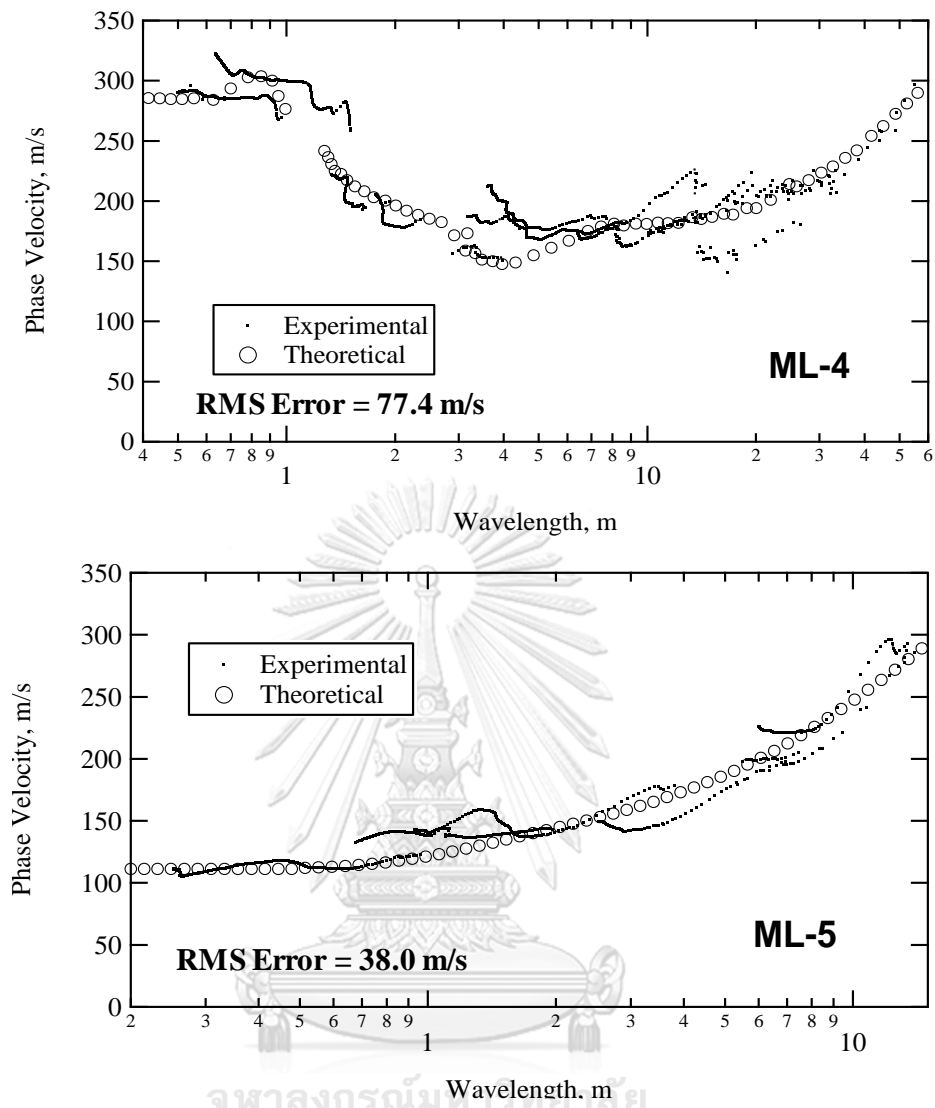


Figure 5.10. The dispersion curves of phase velocity in the measurement of SASW in the study area.

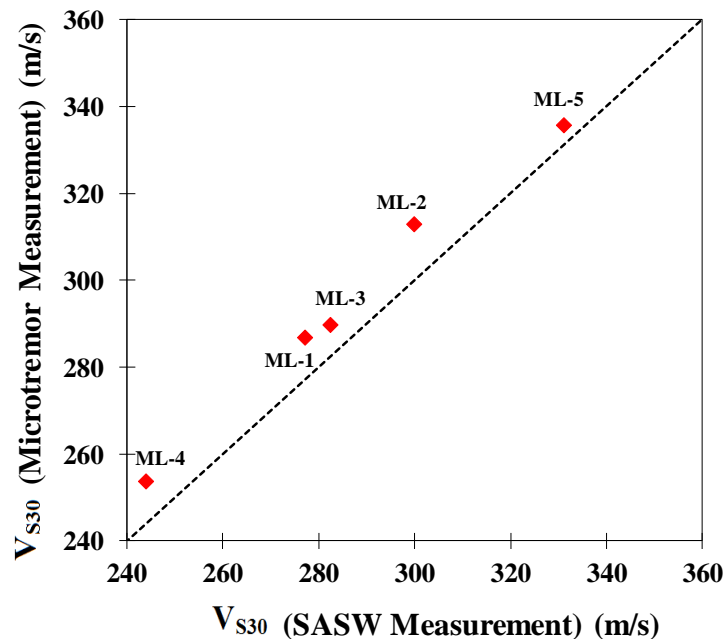


Figure 5.11. Comparison of V_{s30} of both measurements in the study area.

5.2. Local Site Investigation in Mae Sai

5.2.1. Introduction

Since developed as the trade and tourist zone in 1980s, Chiang Rai Province has transformed to be a high economy area in the Northern Thailand. However, earthquakes with low to medium magnitude frequently threat this area. On March 24, 2011, the Tarlay Earthquake hit Chiang Rai (Figure 5.12) and resulted in heavy damages Mae Sai district-the northernmost part of Thailand where the northern trade gate of Thailand-Myanmar exists. The earthquake impacts had influenced social-economy activities in the border of Myanmar, Laos, and Thailand commonly known as Golden triangle area. Moreover, liquefaction was observed in many locations in Mae Sai district. This was noted as the first earthquake induced liquefaction in Thailand during the modern era (Soralump and Feungaosorn, 2013).

Several Thai researchers (Ruagrassamee et al. (2012); Soralump and Feungaosorn (2013); Mase et al. (2015); Tanapalungkorn and Teachavorasinskun (2015)) had studied the earthquake impacts of Tarlay Earthquake in Northern Thailand, especially liquefaction. In general, they focused on reporting the impact of earthquake and analyses of the liquefaction potential by conventional methods (Seed and Idriss

(1971); Youd and Idriss (2001); Idriss and Boulanger (2006)). The basic information had been achieved from previous studies, i.e. the rough estimation of liquefaction susceptibility in this area. However, the detail description of local site related to the earthquake has not still achieved in previous studies.

Some studies related to seismic hazard and local site effect in Northern Thailand had been performed by some researchers. Poovarodom and Pitakwong (2010) performed a study of site classification in Mae Sai Basin and reached the conclusion that the area was generally classified as Site Class D. Ruangrassamee et al. (2012) reported that liquefaction damage was found in many locations in Mae Sai Basin. The study also reported that loose to medium sand with $(N_1)_{60}$ of 5 to 20 blows/ft was liquefied during Tarlay Earthquake. However, there is no detail explanation to the soil site of these liquefiable layers in specific.

The objective of this study is to present the results of the local site observation using microtremor. The interpretation of frequency (f_0), amplification ratio (horizontal to vertical spectral ratio, H/V), and its inversion to obtain the shear wave velocity (V_s) profile are performed. Besides, this study presents the site class of the liquefiable sites based on the widely used standard for seismic hazard study. A brief analysis of suspected liquefiable layer is also described in this study. In general, the results from this study could help better understanding of local site condition on liquefaction spots and make preparedness plan for recurrence earthquake impacts at the border of Thailand-Myanmar in the future.

5.2.2. Study area

Figure 5.13 presents the geology map plotted by the site locations investigated in this study. In general, geologic condition of the Mae Sai basin is dominated by Fluvial deposit (Qff), which was formed in quaternary age. This formation is dominated by sand, gravel, silt, and clay materials. Some parts including sandstone, limestone, shale, and chert (CPk) dominate the geological formation in high terrain of Mae Sai. These formations were formed during the Permian to Carboniferous ages. In mountainous area, the basic igneous rock (PTrv) and granite formed during cretaceous to carboniferous ages exist in this area (TDMR, 2016).



Figure 5.12. Research area and epicentre of the 6.8 M_w Tarlay Earthquake rupture hit the border of Thailand-Myanmar.

Figure 5.14 shows the site investigation results at BH as shown in Figure 5.13. The subsoil in MS-2 is dominated by sandy soils, which based on USCS (Unified Soil Classification System) were categorized as SP-SM, SM, and SC, and SM-GM, GP. SP-SM layers were found at 0 to 9 m depth with the average of $(N_1)_{60}$ about 6 blows/ft, with fines content (FC) of 15 %. SM layers were found at 9 to 16.5 m and 20.5 to 23.5 m depth. These layers had the average of $(N_1)_{60}$ about 10 blows/ft with FC of 15 %. SC layers which had the average of $(N_1)_{60}$ around 15 blows/ft and FC of 20%, were found on 19 to 20.5 and 23.5 to 30 m depth. The thin mixed sandy and gravelly soils, i.e. SM-GM, GP was found at 16.5 to 19 m depth. This layer had the average of $(N_1)_{60}$ around 17 blows/ft, with FC about 20 %. Moreover, the ground water was found on approximately 1.2 m below ground surface. The average of shear wave velocity up to 30 m (V_{s30}) at BH was about 200 m/s, which based on National Earthquake Hazard Reduction Program is categorised as Class D. During Tarlay Earthquake, the sand layers with the low soil resistance deposit were suspected to be the susceptible

geological formation to undergo the earthquake shaking impact and resulted in liquefaction, as reported by [Soralump and Feungaugson \(2013\)](#).

Four microtremor measurements (as listed in Table 5.5) in the basin area of Mae Sai were conducted on the liquefied points found during Tarlay Earthquake, which are noted as MS-1 to MS-3 (Figure 2). MS-1 was located at the paddy field area in Mae Sai sub-district, MS-2 was located near the reservoir of Child Development Centre, and MS-3 was located at the fruits farming area in Ko Chang sub-district. Another site, MS-4, which was located at the seismic station of Mae Sai (MSAA) was also studied. The measurement results are then processed to perform some analyses, including interpretation of H/V ratio and predominant frequency (f_0), the resonance prediction corresponding to actual earthquake, the description of vulnerability aspect, and the inversion of H/V ratio to generate V_s profile.

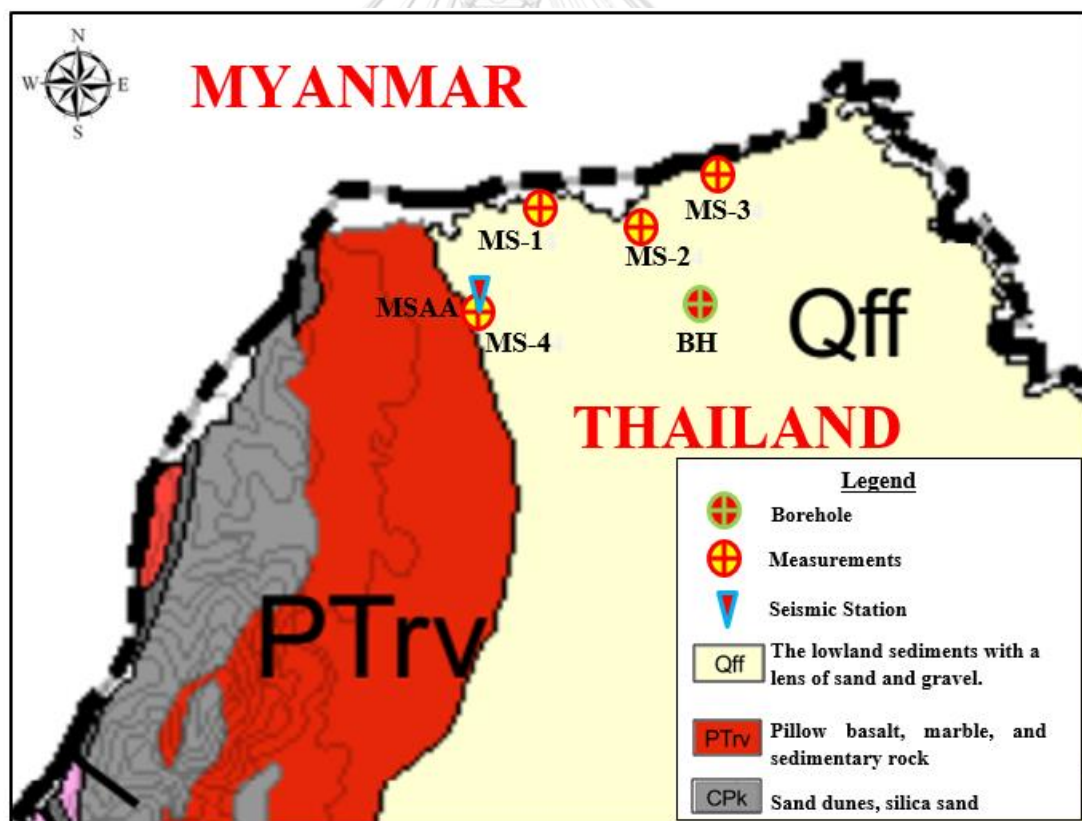


Figure 5.13. Geology map ([TDMR, 2016](#)) and investigated location.

Table 5.5. Location of investigated location and earthquake epicentre (TMD, 2015)

Sites	Location	Latitude (°)	Longitude (°)
MS-1	Tambo Mae Sai	20.447	99.907
MS-2	Reservoir of Child Development Centre	20.445	99.919
MS-3	Tambo Ko Chang	20.451	99.932
MS-4 (MSAA Station)	Mae Sai Seismic Station	20.289	99.881
Tarlay Earthquake Epicentre	Tarlay, Myanmar	20.705	99.949

5.2.3. Result and discussions for the local site investigation in Mae Sai

A. Measurement results

Figure 5.15 presents site investigation results. The result of microtremor measurement has fulfilled the criteria defined by [SESAME \(2004\)](#) for reliable curve and clear peak. Generally, the observed sites have peak of H/V ratio (A) ranging from 2.31 to 3.38, with f_0 ranging from 2.31 to 4.05 Hz. MS-1 shows predominant frequency (f_0) of 4.05 Hz with A of 2.32, which indicates the relative medium thickness sediment with the impedance contrast between bedrock and sediment. The presence of a lower peak H/V ratio of 1.25 at frequency of 1.1 Hz explains that the location of site is close to a valley edge. MS-2 has the f_0 of 3.56 with H/V ratio peak of 3.38 which indicates the medium thickness sediment in this area and is close to a valley edge as well. However, corresponding to H/V ratio peak, the impedance contrast between sediment and bedrock in this site is higher than MS-1. MS-3 has a low H/V peak of 2.31, with high a f_0 of 2.05. This indicates that the part has medium thickness sediment where the impedance contrast between bedrock and sediment is smaller. The relatively flat curve explains that this location seems to be located at the outcrop, which is overlain by thin sediment.

The vulnerability index of the investigated sites is compiled in Table 5.7. In general, the vulnerability index in the investigated area ranges from 3.21 to 1.83. Based on Table 5.7, it can be concluded that MS-2 is the most vulnerable area to undergo the amplification effect due to the seismic impact in the investigated areas. In general, the vulnerability index of each investigated location is slightly lower than other investigated areas, as reported by [Choobbasti et al. \(2015\)](#) and [Huang and Tseng \(2002\)](#) in studying the characteristic of liquefaction based on microtremor observation in Babol City and Yuanlin Areas, respectively. [Choobbasti et al. \(2015\)](#) showed that the

minimum K_g values of the liquefied site in Babol City was 5, whereas based on [Huang and Tseng \(2002\)](#), the values of K_g varied from 2 to 14. The different values of K_g from the result and other studies may be caused by the difference of geological condition. The result of this study and other studies show that the vulnerability indices are not always well matched with the liquefaction damage. It means that the liquefaction event is possible to be found on the locations having the low vulnerability index, even though in the location with a high vulnerability index, liquefaction damage is more generally found ([Huang and Tseng, 2002](#)).

B. Shear wave velocity profile

The inversion analysis was performed based on H/V ratio and the frequency corresponding to the modelling parameters in Table 5.6. The interpretation of inversed H/V and measured H/V in Figure 5.16 shows that each H/V curve is consistent each other.

From the inversion analysis, V_s profile is generated. V_s profile up to 30 m depth on each investigated location is presented in Figure 5.17. Generally, V_s profile on each investigated location increases with depth. The result also showed that generally the investigated sites are composed by 6 layers for 30 m depth.

V_{s30} in the investigated location ranges from 268 to 288 m/s. According to NEHRP, the site class of the investigated areas is categorised as Class D, which is also consistent with site class of BH site. The findings in this study confirms the previous studies performed by [Poovarodom and Pitakwong \(2010\)](#) and [Ruangrassamee et al. \(2012\)](#) where the Site Class D is dominant in Mae Sai basin area.

The tendency of V_{s30} and vulnerability index is shown in Figure 5.18. In the figure, the vulnerability index in the study area tends to be consistent with V_{s30} on each site. The lower V_{s30} tends to provide the higher vulnerability index. This is reasonable because the site, which has a lower V_{s30} seems to be under high-risk of seismic hazard. The result is also consistent with two other studies conducted by [Dikmen et al. \(2016\)](#) and [Yuliyanto et al. \(2016\)](#) in studying the site effect in Izmir (Turkey) and Wirogomo (Indonesia), where the vulnerability indices are in a good agreement with V_{s30} .

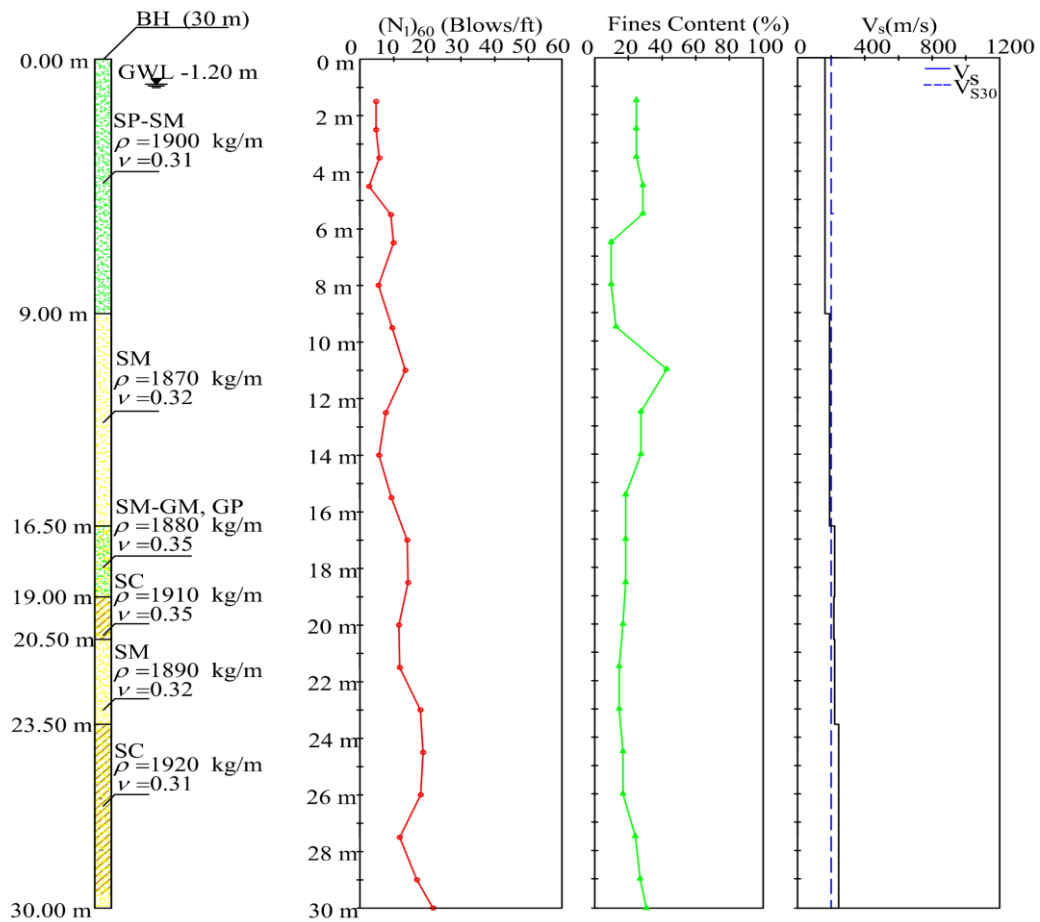


Figure 5.14. Typical subsoil condition of Mae Sai Basin.

Table 5.6. Modelling parameter of analysis

Layer	Soil Type	Thickness	V_p	V_s	Density	Poisson's Ratio
		(m)	(m/s)	(m/s)	(kg/m ³)	(ν)
1	SP-SM	1.00-20.00	180-350	100-200	1800-2000	0.2-0.4
2	SM	1.00-20.00	250-450	150-220	1800-2000	0.2-0.4
3	SM-GM	1.00-20.00	350-500	200-250	1800-2000	0.2-0.4
4	SC	1.00-20.00	400-600	220-300	1800-2000	0.2-0.4
5	SM	1.00-20.00	450-700	250-350	1800-2000	0.2-0.4
6	SC	1.00-20.00	550-800	300-400	1800-2000	0.2-0.4
Elastic Half Space	Rock	-	500-1250	500-760	2000-2200	0.1-0.3

Table 5.7. Vulnerability indices of investigated sites

Sites	A	f_0 (Hz)	K_g
MS-1	2.72	4.05	1.83
MS-2	3.38	3.56	3.21
MS-3	2.35	2.1	2.63

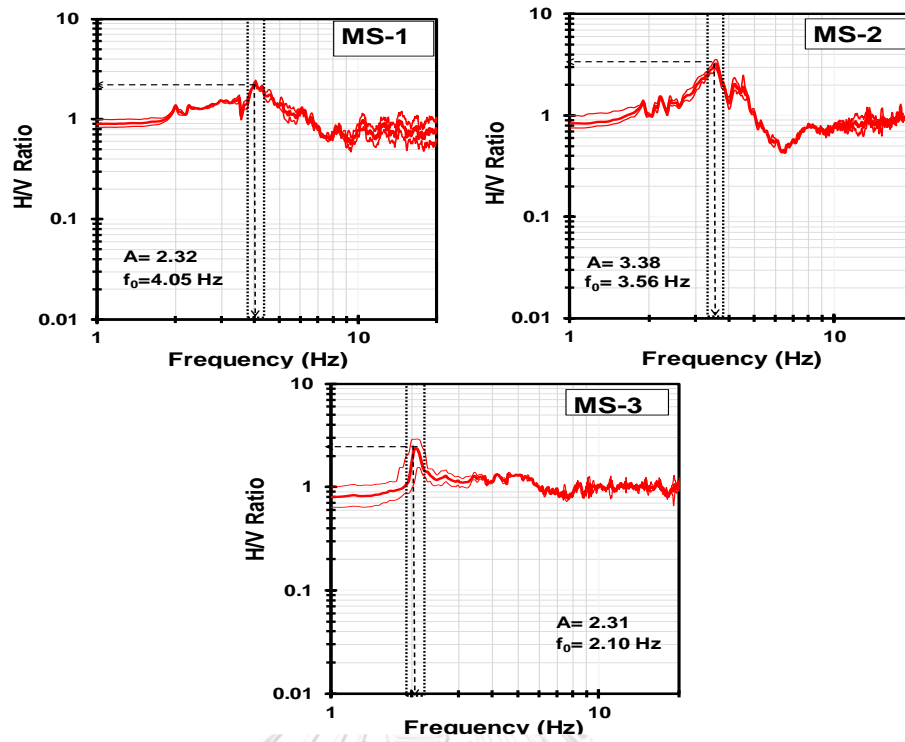


Figure 5.15. H/V ratio corresponding to frequency obtained from microtremor measurements.

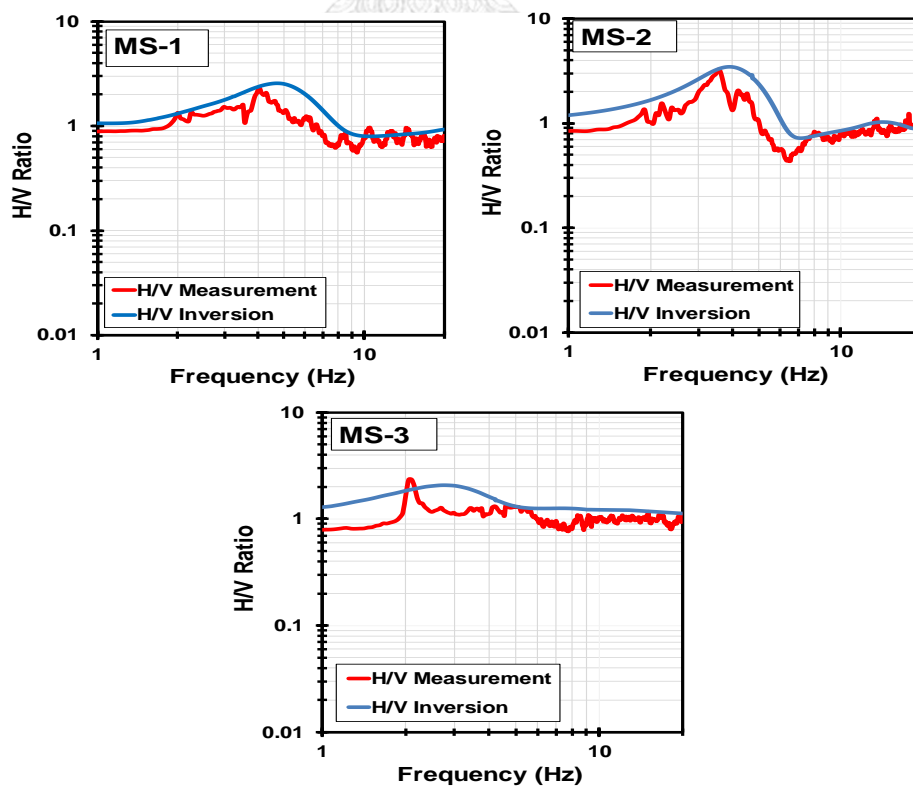


Figure 5.16. Comparison of H/V measured and H/V inversion.

C. Suspected liquefiable layer

Regarding to the geological condition of the study area, the investigated sites are dominated by Qff formation, which was dominated by sands and other granular materials, such as gravels, which was also found on the BH site. The sand layers with low resistance composed the subsoils structure in BH. In addition, the shallow ground water table was found. According to [Kramer \(1996\)](#), those conditions were ideal for the soil sites to undergo liquefaction, especially if the earthquake with magnitude larger than 5 M_w and PGA at least 0.1g shakes the area. That information had become the main factors which possibly triggered liquefaction at the border of Thailand-Myanmar during Tarlay Earthquake.

Corresponding to geological condition and subsoils in the study area, at shallow depth, the loose sandy soils possibly existed in the study area and possibly extruded out during Tarlay Earthquake. Linking to V_s profile, the $V_s \leq 180$ m/s exists at shallow depth of 0 to 9 m in the study area. According to [Stokoe et al. \(1988\)](#), the sandy layer with $V_s \leq 180$ m/s is vulnerable to undergo liquefaction. [Andrus et al. \(2004\)](#) suggested that stress corrected $V_s (V_{sI})$ less than 215 m/s could be vulnerable to undergo liquefaction. In this study, the V_{sI} of the sites estimated from [Sykora \(1987\)](#) and [Robertson et al. \(1992\)](#) studies ranges from 151 to 207 m/s, which confirms that the values are in the vulnerable range to liquefaction. Based on the results, it can be roughly predicted that the depth range of 0 to 9 m is vulnerable to undergo liquefaction.

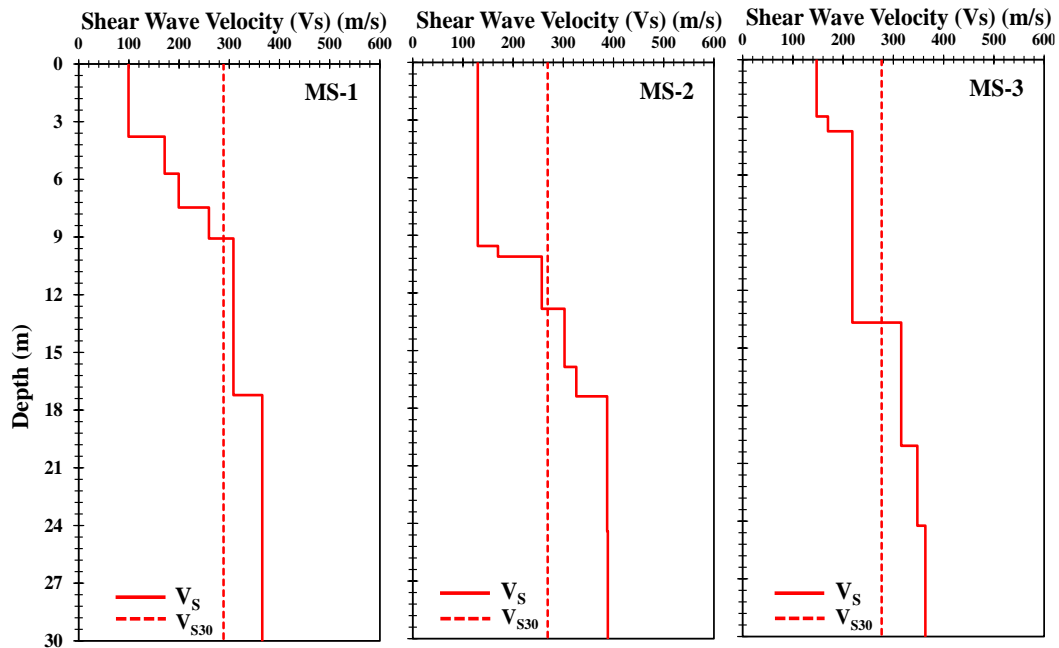


Figure 5.17. Shear wave velocity profile from inversion H/V ratio

D. The resonance prediction

In this study, the resonance effect between the ground structure and the earthquake shaking in MS-4 (Figure 5.19) is analysed. In Figure 5.19, the predominant frequency (f_0) of Tarlay Earthquake ground motion at Mae Sai (MSAA) Station and MS-4 are close, i.e. 1.82 Hz (predominant period, T_0 of 0.46 sec) and 2.1 Hz (T_0 of 0.55 sec), respectively. From the estimation of predominant frequency on both sites and earthquake H/V ratio, the resonance vulnerability between the ground structure and the earthquake motion can be predicted by the following equation (Gosar, 2010),

$$R = \frac{Abs[(f_0Site - f_0Earthquake)]}{f_0Earthquake} \quad (5.1)$$

where, R is the resonance vulnerability between ground structure and earthquake ground motion, f_0Site is the predominant frequency of site, and $f_0Earthquake$ is predominant frequency of earthquake ground motion.

According to the analysis, the resonance value of both ground structure and earthquake ground motion is about 15% where corresponding to Gosar (2010) recommendation, the resonance vulnerability is categorised as medium-high level.

The spectral acceleration of ground motion in Mae Sai station for NS, EW, Vertical directions compared with the spectral acceleration design of Thai Design

Seismic (TDS, 2009) for 2% probability of exceedance (return period of 2475 years) and 10% probability of exceedance (return period of 475 years) presents in Figure 5.20. At period of 0.1 second, the N-S spectral acceleration of 0.72g slightly touched the maximum design value of 10% probability of exceedance. The spectral acceleration is probably higher at the ground surface due to the amplification effect and results in the damage to the ground surface. This finding also confirms Ornthammarath (2013) study stated that the NS component of Mae Sai ground motion was more likely display the ground displacement caused by the Tarlay Earthquake.

About the resonance prediction, the frequency ranges from 1.8 to 2.1 Hz or period ranges 0.4 to 0.6 sec possibly had spectral acceleration of 0.28g to 0.33g. These values would significantly influence the buildings having the similar natural period (T_n) such as flexible low to medium high-rise buildings. It is noted that a simply estimation of $T_n = 0.1n$, where n is the number of stories is recommended by International Code Council or ICC (2009). In addition, these spectral acceleration values would be probably higher at the ground surface due to the seismic wave amplification. This confirms the study performed by Ruangrassamee et al. (2012) that generally, 2 to 4 stories buildings damage in the border of Thailand-Myanmar was found after the earthquake. However, in Figure 5.20, the design values of spectral acceleration are still sufficient in which if it was considered, the damage to the structures would be minimised.

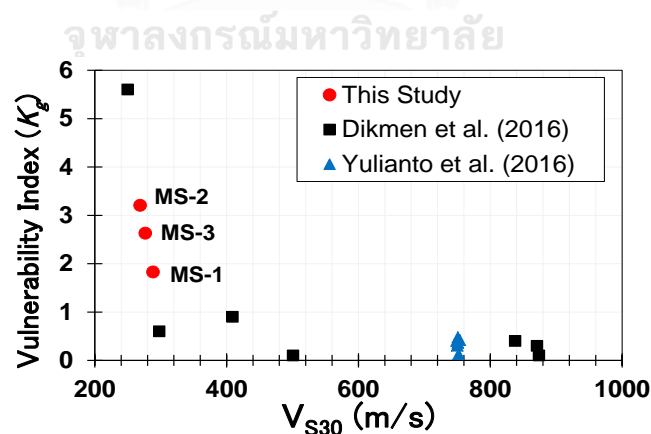


Figure 5.18. V_{s30} -vulnerability index (K_g) interpretation on each site

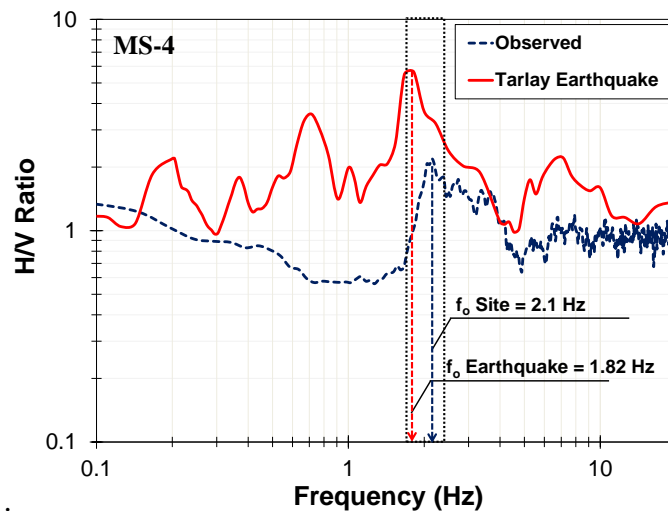


Figure 5.19. Comparison of predominant frequency between ground structure and Tarlay Earthquake ground motion

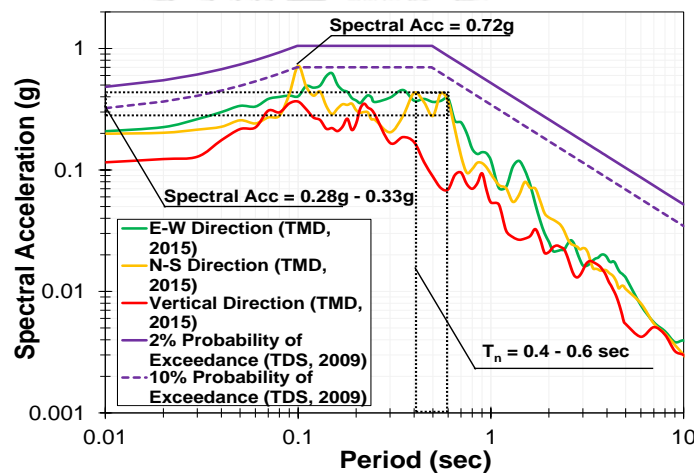


Figure 5.20. Spectral acceleration design between the recorded ground motion in Tarlay Earthquake and Thai Design Code for earthquake resistance building

5.3. Concluding Remarks

This chapter presents the local site investigation to the liquefiable spots found during the 6.1 M_w earthquake in Mae Lao District and the 6.8 M_w Tarlay Earthquake in Mae Sai District. The measurements including ambient noise-microtremor and SASW were performed to achieve the information of local site condition in the study area. Several conclusions can be drawn in the following,

1. The liquefaction points during Mae Lao earthquake were generally found at the geologic formation of alluvial deposits (Qa), which was dominated by gravel, sand, silt, and clay. The sand layers at shallow depth of this formation were extruded out during the liquefaction. The observed locations had peak H/V ratio (A) of 2.1 to 4.7 and predominant frequency (f_0) of 2 to 6.3 Hz, which indicated the existence of medium to thin sediment in the investigated area. The liquefied spots during Tarlay Earthquake were located at the geological formation of Qff, which was a low land sediment dominated by sands and other granular materials, such as gravels. The observed spots had H/V ratio peak of 2.31 to 3.38 and predominant frequency (f_0) of 2.05 to 4.05 Hz, which indicated the existence of medium to thin sediment in the investigated area.
2. The estimation of ground motion prediction in this area based on the NGA models revealed that the investigated area seemed to undergo the maximum acceleration (PGA) about 0.2 to 0.4g. It indicated that during Mae Lao earthquake, liquefaction could occur and was consistent with [Kramer \(1996\)](#) which suggested that liquefaction could happen under the minimum PGA of 0.1g and minimum magnitude of 5 M_w .
3. The analysis of V_{s30} showed that Mae Lao and Mae Sai sites are classified as Site Class D. The results were consistent with the other areas in Northern Thailand that were also classified as Site Class D, such as Mae Sai and Chiang Rai, as performed by the previous studies ([Poovarodom and Pitakwong \(2010\)](#), [Thitimakorn and Channoo \(2012\)](#) and [Ruangrassamee et al. \(2012\)](#)). In addition, the vulnerability index and V_{s30} comparison shows the strong relationship for Mae Sai site.
4. In Mae Lao site, the layers with V_s less than 180 m/s were found at the shallow depth in the study area, especially up to 3 m deep, which was dominated by granular soils. For Mae Sai site, The layers dominated by granular soils with V_s less than 180 m/s, were found at the shallow depth, especially up to 9 m deep. The result agreed with the studies i.e., [Stokoe et al. \(1988\)](#) and [Andrus et al. \(2004\)](#), which stated the sandy layer with $V_s \leq 180$ m/s can be vulnerable to undergo liquefaction. The existence of the low V_s at the shallow depth seemed to confirm the liquefaction evidence found in the study area.

5. During the Tarlay earthquake, the investigation of site and recorded ground motion showed that there was the resonance effect resulted during the earthquake. This effect seemed to contribute in the destructive damage found near the investigated sites, especially for low to medium high-rise buildings.
6. This study investigated the liquefied sites during the Mae Lao and Tarlay earthquakes by performing the passive and active measurement to obtain the shear wave velocity profile. The shear wave velocity profile could be used in the further analyses such as liquefaction potential analysis and ground response analysis.



CHAPTER VI. LIQUEFACTION SITE RESPONSE ANALYSIS

6.1. Introduction

In this chapter, the investigated location (Figure 4.1) presented in Chapter IV is picked up to perform one-dimensional liquefaction site response analysis due to the Tarlay Earthquake. The site investigation results in Chapter V (Mae Lao and Mae Sai sites), i.e. shear wave velocity profile, obtained from *H/V* inversion and SASW measurement are not considered in this chapter, since there are no other supporting data, such as SPT and CPT data for soil profiles and the soil resistances. To perform one-dimensional site response analysis in those locations, the supporting site investigation should be performed in the future.

Several local researchers ([Soralump and Feungaugsorn \(2013\)](#), [Tanapalungkorn and Teachavorasinskun \(2015\)](#), and [Mase et al. \(2015\)](#)) had investigated the liquefaction potential due to the earthquake in the northern provinces of Thailand. The previous studies were focused on liquefaction investigation by employing the empirical methods ([Seed and Idriss \(1971\)](#) and [Idriss and Boulanger \(2006\)](#)) based on site investigation data, such as standard penetration test (SPT) and cone penetration test (CPT). The previous studies reached to the conclusion that the Northern Thailand has potential to undergo liquefaction during the strong earthquake like Tarlay Earthquake. However, the detail explanation of the soil behaviour under the earthquake has not achieved yet.

The analysis aims to presents liquefaction potential under the earthquake shaking in Northern Thailand by conducting a non-linear site response analysis. Three sites in Chiang Rai and one site in Chiang Mai are selected. The NGA Models are employed to generate the ground motion input for each investigated site. Non-linear site response using effective stress model is used to observe soil behaviour under earthquake such as excess pore water pressure ratio time history, shear stress-shear strain hysteresis loop, and effective stress path. The analysis can provide the detail description of soil response during the earthquake. This analysis is also addressed to make an awareness of earthquake impacts to the Northern Thailand People for the possible major earthquake event in the future.

6.2. Site Location

The study is focused on the Northern Thailand (Figure 4.1), where four site investigations named BH-1 to BH-4 are performed. The results of site investigations including SPT and seismic downhole test i.e. shear wave velocity or V_s profile are presented in Figure 4.3.

6.3. Research Methodology

In this chapter, the analysis steps are performed based on the methodology presented in Chapter IV. However, in the ground response analysis, the analysis of liquefaction parameters should be firstly performed. In the analysis, to achieve the overview of liquefaction resistance of the soil layer especially sand layers, the element simulation based on multi-spring model element to demonstrate the laboratory test under the cyclic condition is performed. The material parameters, such as SPT value, FC , and σ'_v , are employed to determine the input parameters in the element simulation analysis, such as shear modulus (G_{ma}), bulk modulus (K_{ma}) and wet density (ρ). More detailed explanation of model can be found in [Morita et al. \(1997\)](#). After element simulation, the number of cyclic to generate liquefaction and corresponding cyclic stress ratio are depicted from the liquefaction resistance curve. From this analysis, the rough estimation of the susceptible layers to undergo liquefaction can be observed. The susceptible layers are then selected as the represented layers to describe the soil behaviour under one-dimensional site response analysis.

Furthermore, one-dimensional site response analysis is performed based on the assumption that waves generated from NGA from the analysis in Chapter IV are applied at the bottom of each borehole. The engineering bedrock of the site is assumed as same as the criteria implemented in Chapter IV. The bottom and the lateral boundaries are assumed as the impermeable layers. The soil column is assumed to be fully saturated, which is taken to consider the worst condition of soil column to undergo liquefaction, where liquefaction tends to more vulnerable to the soil with low ground water table ([Kramer \(1996\)](#) and [Day \(2002\)](#)). In one-dimensional analysis, the boundary condition is limited only on vertical direction of soil column. Once the input motion is applied

pore pressure would build up in the vertical direction; therefore, the excess pore pressure ratio (r_u) time history is presented. The shear stress-shear strain curve (τ - γ) and effective stress path (τ - σ'_v) are also discussed to achieve the description of soil behaviour of the investigated sites during Tarlay Earthquake. In this study, the information at the mid layer of the suspected liquefiable sand are selected to present.

6.3.1. Ground attenuation models

In the analysis, the results of NGA models analysis performed in Chapter IV are adopted. As presented in Chapter IV, [Boore and Atkinson \(2008\)](#) model is assigned as the suitable attenuation model during the Tarlay Earthquake; therefore, the Boore and Atkinson model is used to predict the ground motion in the investigated sites.

6.3.2. Liquefaction resistance curve

[Morita et al. \(1997\)](#) introduced the mechanism of pre-analysis before performing finite element analysis using FLIP program. The analysis aims to estimate the liquefaction behaviour based on simulation of single element. The analysis is performed to investigate the tendency of liquefaction characteristic, which is related to the liquefaction strength and number of cyclic to generate liquefaction under undrained cyclic shear test. The analysis is also addressed to set up the liquefaction parameters of multi-spring model used in the FLIP program, i.e. site response analysis of horizontally layered soils. The inputs of simulation are SPT value, FC (fines content), and effective vertical stress of soil layer (σ'_v). Furthermore, the simulation is performed under the referenced laboratory test results such as cyclic triaxial and cyclic simple shear tests. Therefore, the criteria of liquefaction threshold should be associated with the referred laboratory tests. In this study, the confining pressure is fixed at 100 kPa (equivalent to 10 m depth) to represent the maximum effective stress of the maximum vulnerable depth to undergo liquefaction and double amplitude axial strain (ε_a) of 5%, which is the liquefaction threshold in dynamic testing using cyclic triaxial. As the results, the initial required number of cyclic to generate liquefaction can be determined from the simulation.

6.4. Result and Discussions

6.4.1. Generated Wave Forms

The suitable attenuation model (i.e. Boore and Atkinson model) is used to estimate the ground motion prediction of the areas where the ground motion records are not available, since there is a limited seismic station in the investigated area. It should be noted that the ground motion record is only available at BH-1. The ground motions generated from the suitable attenuation model are used for BH-2, BH-3 and BH-4. The ground motion is generated by the scaling method to the maximum recorded peak ground motion (PGA of 0.207g), which in this case is recorded at MSA station. The generated ground motions for BH-2, BH-3, and BH-4 are depicted in Figure 6.1. Furthermore, those waves are applied at the bottom of each borehole to observe the site response through the 1D wave propagation analysis.

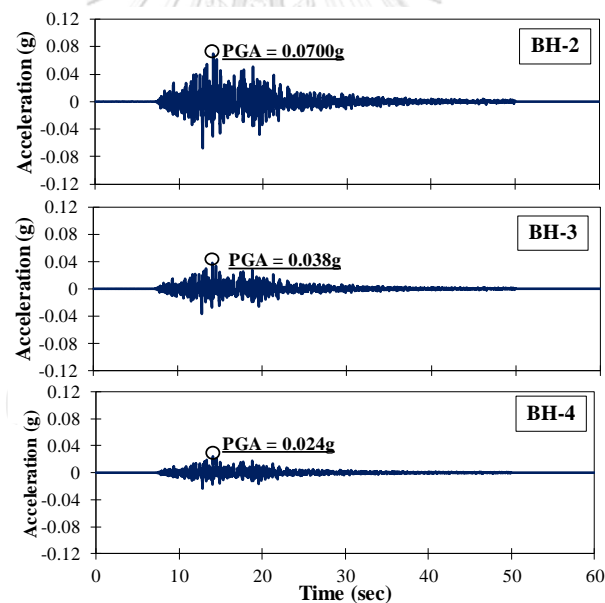


Figure 6.1. Generated input motion based on attenuation model analysis

6.5.2. Element Simulation Result

The element simulation result of the soil layers in the study area are presented in Figure 6.2. In general, the first two layers of each investigated location are possible to undergo liquefaction. The axial strain (ϵ_a) of 5% is used as the liquefaction criterion. These layers are dominated by sandy soils classified as SC-SM and SP-SM, with low

soil resistance ($(N_1)_{60}$) average ranging from 5 to 15 blows/ft. The existence of these soils layer at the shallow depths also provided the low effective stress. Those liquefiable layers are potentially to liquefy within 1 to 40 cyclic. The results are compared with the liquefaction resistance curves obtained from various experiment results under the same value of confining pressure and liquefaction criterion i.e. $\varepsilon_a \approx 5\%$ as shown in Figure 6.6. In general, the liquefaction resistance in the study area is higher than liquefaction resistance of Monterey Sand (Tatsuoka and Silver, 1981) and lower than Osaka Sand. However, the ranges of liquefaction resistance are quite close to liquefaction resistance of Toyoura Sand (Yang and Sze, 2011), Chiang Mai Sand (Gauchan, 1984), and Sacramento River Sand (Lee and Seed, 1960). Generally, the sands are initially undergone liquefaction within 1-70 cyclic. The liquefaction resistance of Chiang Mai sand shows the proximity to the liquefaction resistance of sands in the study area.

6.5.3. Cyclic Stress-strain Response from FLIP

The interpretation of soil behaviour at BH-1 is presented in Figure 6.6. At first sand layer, excess pore water pressure ratio rises significantly within a few seconds. The excess pore water pressure ratio almost reaches 1.00 which indicates that liquefaction possibly happens during wave propagation. The dynamic load of Tarlay earthquake with maximum PGA of 0.207g results in the decrease of shear modulus. It is shown by the flat curve of shear stress and axial strain. The reduction of shear modulus is highly influenced by the decrease of effective confining pressure during the dynamic load due to the excess pore water pressure build up. At the middle of this layer, the effective confining pressure decrease to almost zero due to excess pore pressure build up. The existence of low soil resistance seems to be sufficient to retain from soil liquefaction. At the second layer of BH-1, the excess pore water pressure also raised up shortly. The excess pore water pressure ratio is less than 0.5. Shear modulus decreases but not as much as the first sand layer. The effective confining pressure decreases from 75 kPa to 45 kPa. At the second layer, the effective stress is larger than the first sand layer, which provides the higher soil resistance. At the last layer, the excess pore water pressure builds up is very small.

Figure 6.7 presents the interpretation of soil behaviour under the PGA of 0.070g at BH-2 site. From this figure, both first and second layers undergo the decrease of effective confining pressure during the wave propagation. In those sand layers, the maximum excess pore water pressure ratio is very small (0.04 to 0.12, respectively). In addition, there is no significantly decreased excess pore water pressure ratio, which means the availability of soil resistance is still sufficient to retain the stability from the reduction of effective confining pressure. At the deeper depth, the increase of excess pore water pressure ratio is very small. There is no indication of liquefaction happening at BH-2.

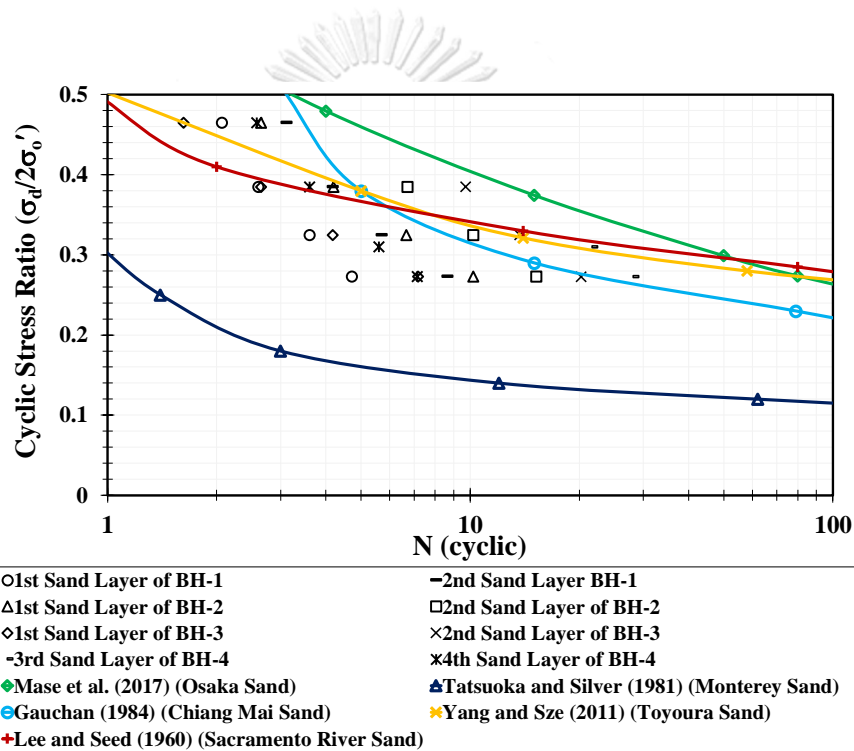


Figure 6.2. Liquefaction Resistance Curve.

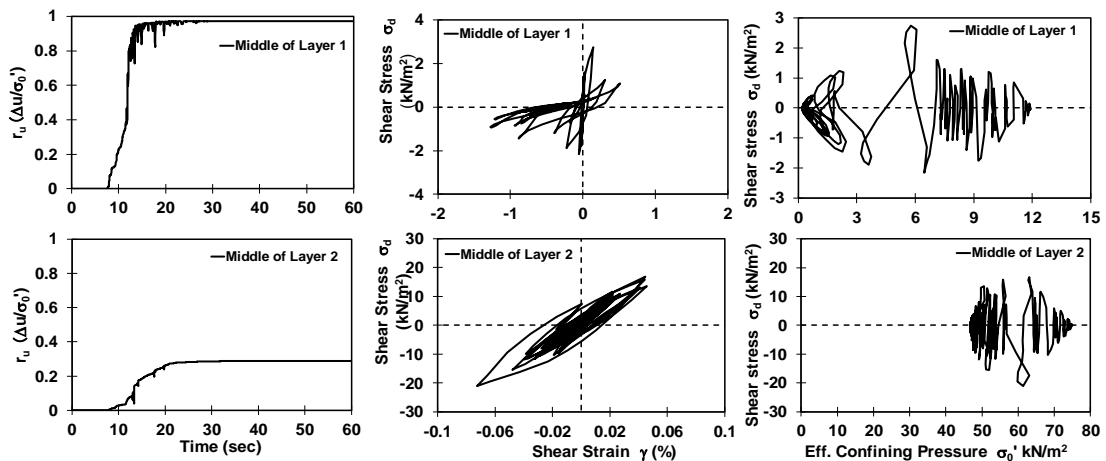


Figure 6.3. Soil behaviour of sand layers on BH-1

Soil behaviour under the propagated wave BH-3 is depicted in Figure 6.8. Similar with BH-2, the maximum excess pore water pressure ratio on the first and second sand layers in BH-3 are small. The excess pore water pressure increase seems to be not large enough to generate liquefaction. The shear modulus at the first two layers decreases insignificantly. This reflects that there is no significant effective stress reduction. At the deeper depths, the excess pore pressure build up is very small. Similar with the previous elaborated sites, the existence of large soil resistance at the deeper layers plays role to retain from the excess pore water pressure build up; therefore, no liquefaction indication occurred at BH-3.

The interpretation of soil behaviour at BH-4 under the PGA of 0.024g is presented in Figure 6.9. Like the previous site, the applied ground motion at BH-4 resulted in the relatively small excess pore water pressure at the first two layers. The excess pore pressure also decreases the effective stress insignificantly. This effect can be described in the hysteresis loop of shear stress-shear strain, which shows the insignificant shear modulus degradation. This indicates that the effective stress is not significantly decreased due to the excess pore pressure build up. During the wave propagation, there is the reduction of effective confining pressure. At the deeper depths, the excess pore pressure build up is very small, which reflects that no liquefaction occurs at BH-4. The existence of large soil resistance at the deeper layers plays role to retain from the excess pore water pressure build up.

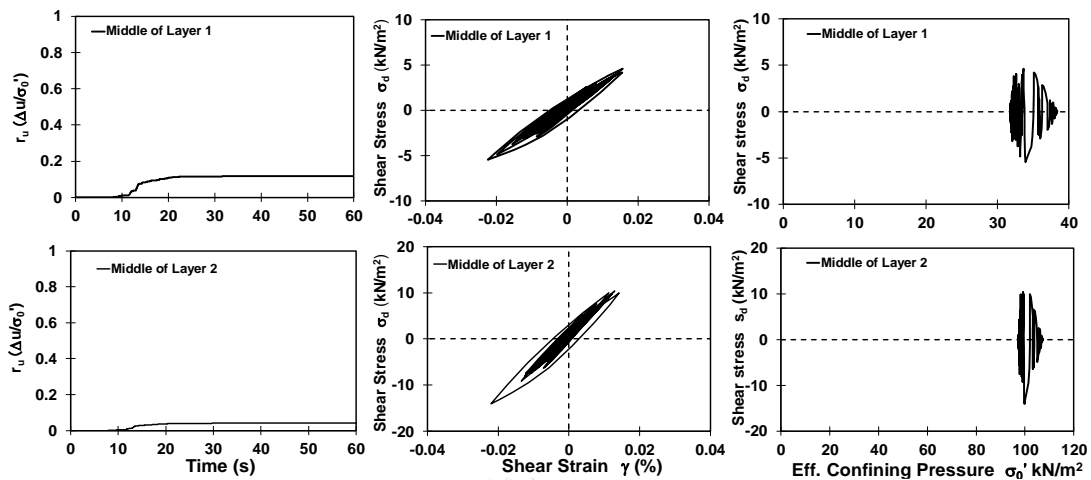


Figure 6.4. Soil behaviour of sand layers on BH-2.

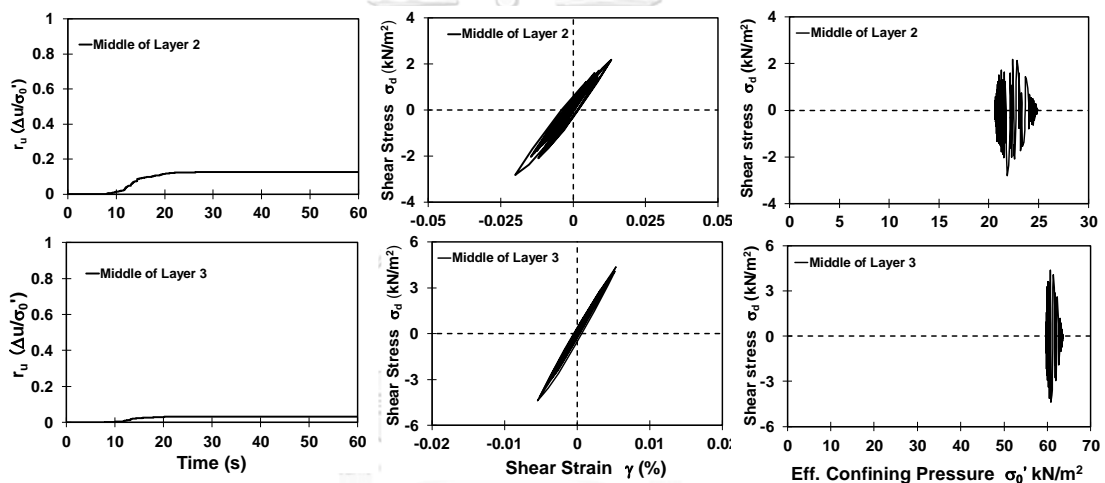


Figure 6.5. Soil behaviour of sand layers on BH-3

In general, the results show that the first sand layer of BH-1 is very vulnerable to undergo liquefaction during Tarlay Earthquake. In the other sites, liquefaction seems to be not occurred. The applied low ground motions and the larger soil resistance at the deeper depth play important roles to retain the bearing capacity from the excess pore pressure build up. Considering this result, it can be concluded that severe damage of liquefaction is only found on the first sand layer of BH-1. The result is consistent with [Soralump and Feungaosorn \(2013\)](#) and [Ruangrassamee et al. \(2012\)](#) who reported that the liquefaction was only found at shallow sandy layers in Mae Sai (the border of Thailand-Myanmar).

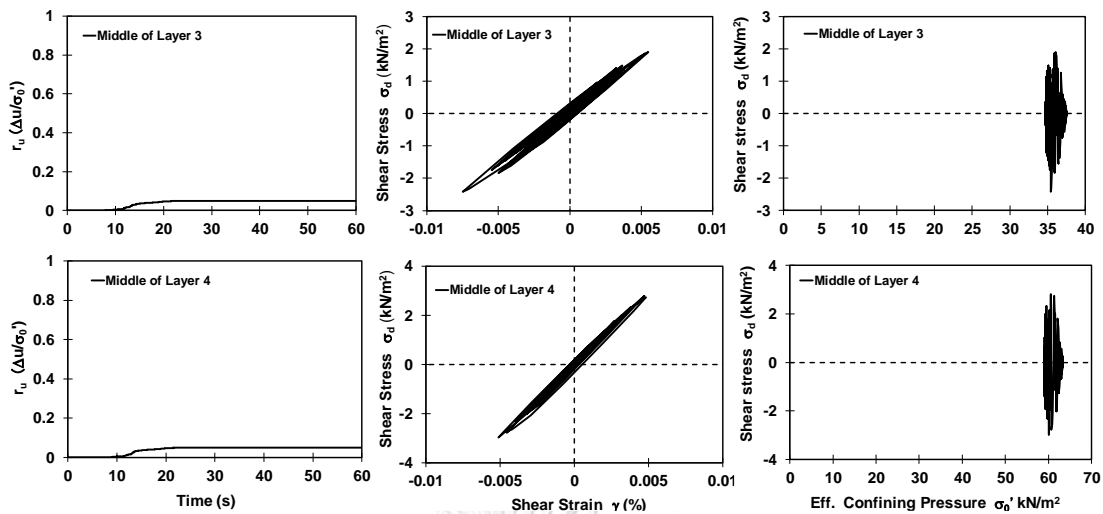


Figure 6.6. Soil behaviour of sand layers on BH-4.

6.6. Concluding Remarks

The research presents a non-linear site response analysis to soil sites in Northern Thailand during the Tarlay Earthquake. Attenuation model analysis and seismic wave propagation analysis to horizontally layered soils are performed to investigate soil behaviour of liquefiable layer during the earthquake. The attenuation model can be used to predict ground motion in the sites. Several concluding remarks can be drawn in the following points,

1. Based on the analysis, PGA at this particular site is less than 0.1g. Day (2002) noted that liquefaction could happen under the earthquake having the minimum PGA of 0.1g and the minimum magnitude of $5 M_w$.
2. From the attenuation model analysis, the BH-2, BH-3 and BH-4 locations are not undergoing the liquefaction during the Tarlay Earthquake. The prediction is then confirmed by the result of ground response analysis in Chapter IV.
3. During the earthquake, BH-1 is highly possible to undergo liquefaction at shallow depth, i.e. about 1 to 3 m deep, which is dominated by loose sand with a low soil resistance. The results agreed with the liquefaction evidences in Mae Sai District as reported by Soralump and Feungaugsorn (2013) and Ruangrassamee et al. (2012)
4. Generally, the result can help to describe the liquefaction potential and make an awareness of earthquake impacts to the Northern Thailand people.

CHAPTER VII. CONCLUSIONS AND RECOMMENDATIONS

7.1. Conclusions

A few studies performed in Northern Thailand to study the liquefaction potential had led to conduct the advanced study of liquefaction which do not only consider the preliminary analysis, but also the field test, experimental test, and numerical analysis. Those steps are performed to reach the more understanding of liquefaction potential and the earthquake aspect in general. This study also contributes to the earthquake field in Thailand, which are becoming the genuine issue within this decade. Several conclusions can be drawn as follows:

1. The Northern Thailand, especially Chiang Rai Province are vulnerable to undergo liquefaction. It is proven by the preliminary analysis, where mostly the investigated sites matched with the criteria of liquefaction. The low soil resistance, especially $(N_1)_{60}$ less than 15 blows/ft and shallow ground water table are the main factors causing this area vulnerable to undergo liquefaction.
2. One-dimensional seismic ground response analysis performed in the Northern Thailand showed that the Northern Thailand had been vulnerable to undergo significant impact during the Tarlay Earthquake, especially for the building structures. In addition, the ground motion prediction showed that the border of Thailand-Myanmar underwent the PGA more than 0.1g. PGA more than 0.1g are very possible to trigger liquefaction at the soil sites dominated by loose sandy soils with shallow ground water table that in majority were found in the Northern of Thailand. Besides, the method of scaled ground motion can be the alternative for seismic ground response analysis to the soil sites which has no actual record of ground motion. However, the study of attenuation model for the area should be firstly performed to determine the approaching PGA value. This method is called as the selection of attenuation model analysis. The method is also implemented to perform the liquefaction site response analysis in Northern Thailand during Tarlay Earthquake. The simulation showed that the border of Thailand-Myanmar is significantly impacted by liquefaction. In this area, the excess pore water pressure

ratio was very close to 1. It means that the area was highly possible to liquefy during the earthquake.

3. The field observation at the liquefied soils during Tarlay and Mae Lao Earthquakes using microtremor and SASW confirmed that the existence of sandy soil with low shear wave velocity at shallow depth in the basin areas of Mae Sai and Mae Lao. Those locations were composed by the alluvial deposits. The site class of both areas were generally categorised as Site Class D. In addition, those locations, based on attenuation model analysis, had possibly undergone the earthquake acceleration about 0.2 to 0.4g, which was possible to trigger liquefaction in those areas. This is consistent with the field evidences found in those locations, where loose sands were extruded out during both earthquakes. The resonance effect seemed to highly contribute to soil and structure damages during Tarlay Earthquake, especially for low to medium high-rise buildings, which has been already predicted by seismic response analysis study in Chapter IV.
4. The liquefaction site response analysis in the Northern Thailand showed that the possibility of liquefaction at the border of Thailand-Myanmar. During the wave propagation, the soil behaviour generally showed there was a reduction of shear modulus during the earthquake and the decrease the effective stress for the first and second sand layer with a maximum depth of 9 m. The results also strengthened the empirical study performed that the first and second soil layers are possible to undergo liquefaction in the border of Thailand-Myanmar.

7.2. Recommendations

Several recommendations for the further study can be drawn as follows:

1. Northern Thailand had been confirmed as the vulnerable area to undergo liquefaction. However, only a few studies have been performed to investigate liquefaction in that area. The limitation of investigation data becomes the challenging for the researchers to explore the liquefaction study there. Therefore, the site investigation data to the required standard of liquefaction evaluation should be performed to study the liquefaction in detail. The site investigation data would be valuable for the engineers or researchers to compose the liquefaction

vulnerability map. This study brings the recommendation to compose the map of liquefaction severity for the further study, which can probably interpret either liquefaction potential index or liquefaction severity index.

2. The Northern Thailand is considered as the most active tectonic region in Thailand. The necessity to study the seismic hazard analysis in that area is being the main issue for geotechnical engineering study. Site investigation data and geophysical survey to describe the geological formation in this area should be more increased.
3. The experimental study to model the soil behaviour under earthquake for the Northern Thailand subsoils can be performed. The further study can explore the description of soil behaviour under the earthquake in Northern Thailand. The further study for the experimental tests should be supported by the information of earthquake load design in the Northern Thailand. The experimental test using shaking table and centrifuge equipments can be implemented for the further study.
4. The study found that the recent strong earthquakes in Northern Thailand inclined to result in the destructive damage to the medium-high rise buildings in the Northern Thailand, since the design values of spectral acceleration were not generally sufficient to cover the spectral acceleration during wave propagation. This brings to the recommendation to reconsider the recent earthquakes in the building design for Northern Thailand.
5. The design countermeasures for the earthquake and liquefaction impacts should be composed, especially for the shallow foundation and building structures. The further study can be initiated by gaining the information from the local people about the earthquake and liquefaction impacts to the substructures.
6. This study only focused on the earthquake and liquefaction phenomenon in the northern border of Thailand-Myanmar. However, another area near the eastern border of Thailand and Myanmar has not yet deeply investigated. The eastern border is also the vulnerable area to earthquake. There are several active faults exist there. Therefore, the necessity to perform some analyses on earthquakes in this location can be recommended for the further study. To support this further study, the numerical analysis for the design countermeasure to the soil sites in Northern Thailand can be performed.

REFERENCES



จุฬาลงกรณ์มหาวิทยาลัย
CHULALONGKORN UNIVERSITY

- Abrahamson, N., and Silva, W., 2008, Summary of the Abrahamson & Silva NGA ground-motion relations: *Earthquake spectra*, v. 24, no. 1, p. 67-97.
- Abrahamson, N. A., and Silva, W. J., 1997, Empirical response spectral attenuation relations for shallow crustal earthquakes: *Seismological research letters*, v. 68, no. 1, p. 94-127.
- Adnan, A., Tiong, P. L. Y., and Chow, Y. E., 2012, Usability of the next generation attenuation equations for seismic hazard assessment in Malaysia: *Int J Eng Res Appl (IJERA)*, v. 2, p. 639-644.
- Ambraseys, N., Douglas, J., Sarma, S., and Smit, P., 2005, Equations for the estimation of strong ground motions from shallow crustal earthquakes using data from Europe and the Middle East: horizontal peak ground acceleration and spectral acceleration: *Bulletin of earthquake engineering*, v. 3, no. 1, p. 1-53.
- Ammon, C. J., Ji, C., Thio, H.-K., Robinson, D., Ni, S., Hjorleifsdottir, V., Kanamori, H., Lay, T., Das, S., and Helmberger, D., 2005, Rupture process of the 2004 Sumatra-Andaman earthquake: *Science*, v. 308, no. 5725, p. 1133-1139.
- Anderson, J. G., Lee, Y., Zeng, Y., and Day, S., 1996, Control of strong motion by the upper 30 meters: *Bulletin of the Seismological Society of America*, v. 86, no. 6, p. 1749-1759.
- Andrews, D. C., and Martin, G. R., Criteria for liquefaction of silty soils, *in Proceedings Proc., 12th World Conf. on Earthquake Engineering2000*, NZ Soc. for EQ Engrg. Upper Hutt, New Zealand.
- Andrus, R. D., Stokoe, K. H., and Hsein Juang, C., 2004, Guide for shear-wave-based liquefaction potential evaluation: *Earthquake Spectra*, v. 20, no. 2, p. 285-308.
- Atakan, K., 2009, The need for standardized approach for estimating the local site effects based on ambient noise recordings, *Increasing seismic safety by combining engineering technologies and seismological data*, Springer, p. 3-15.
- Bard, P., The SESAME project: an overview and main results, *in Proceedings Proc. of 13th World Conf. on Earthquake Engineering*, Vancouver, BC, Canada, August2004, p. 1-6.
- Bardet, J., Ichii, K., and Lin, C., 2000, EERA: a computer program for equivalent-linear earthquake site response analyses of layered soil deposits, University of Southern California, Department of Civil Engineering.
- Bardet, J., and Tobita, T., 2001, NERA, A computer program for Nonlinear Earthquake site Response Analyses of layered soil deposits. Univ. of Southern California.
- Bartlett, S. F., and Youd, T. L., 1992, Empirical analysis of horizontal ground displacement generated by liquefaction-induced lateral spreads.
- Baziar, M. H., Shahnazari, H., and Sharafi, H., 2011, A laboratory study on the pore pressure generation model for Firouzkooh silty sands using hollow torsional test: *International Journal of Civil Engineering*, v. 9, no. 2, p. 126-134.
- Blazquez, R., Krizek, R., and Bazant, Z., Site factors controlling liquefaction: *J Geotech Engng Div ASCE*, V106, NGT7, July 1980, P785-801, *in Proceedings International Journal of Rock Mechanics and Mining Sciences & Geomechanics Abstracts1981*, Volume 18, Pergamon, p. 7.
- Bonnefoy-Claudet, S., Cécile, C., Pierre-Yves, B., Fabrice, C., Peter, M., Jozef, K., and Fäh, D., 2006, H/V ratio: a tool for site effects evaluation. Results from 1-D noise simulations: *Geophysical Journal International*, v. 167, no. 2, p. 827-837.

- Boore, D. M., 2004, Estimating V_s (30)(or NEHRP site classes) from shallow velocity models (depths < 30 m): *Bulletin of the seismological society of America*, v. 94, no. 2, p. 591-597.
- Boore, D. M., and Atkinson, G. M., 2008, Ground-motion prediction equations for the average horizontal component of PGA, PGV, and 5%-damped PSA at spectral periods between 0.01 s and 10.0 s: *Earthquake Spectra*, v. 24, no. 1, p. 99-138.
- Boore, D. M., Joyner, W. B., and Fumal, T. E., 1997, Equations for estimating horizontal response spectra and peak acceleration from western North American earthquakes: a summary of recent work: *Seismological research letters*, v. 68, no. 1, p. 128-153.
- Boulanger, R. W., 2010, Sand plasticity model for nonlinear seismic deformation analyses: University of California, Davis, CA, 77 pp.
- Boulanger, R. W., and Idriss, I. M., 2004, Evaluating the potential for liquefaction or cyclic failure of silts and clays, Center for Geotechnical Modeling.
- Bray, J. D., Sancio, R. B., Riemer, M., and Durgunoglu, T., Liquefaction susceptibility of fine-grained soils, *in Proceedings Proc., 11th Int. Conf. on Soil Dynamics and Earthquake Engineering and 3rd Int. Conf. on Earthquake Geotechnical Engineering 2004*, Volume 1, Stallion Press, Singapore, p. 655-662.
- BSSC, N., 1997, Recommended provisions for seismic regulation for new buildings and other structures, 1997 edition, Part 2: Commentary FEMA 303: Washington, DC: Federal Emergency Management Agency.
- Byrne, P. M., Park, S.-S., Beaty, M., Sharp, M., Gonzalez, L., and Abdoun, T., 2004, Numerical modeling of liquefaction and comparison with centrifuge tests: *Canadian Geotechnical Journal*, v. 41, no. 2, p. 193-211.
- Campanella, R., and Lim, B., Liquefaction characteristics of undisturbed soils, *in Proceedings International Conferences on Recent Advances in Geotechnical Earthquake Engineering and Soil Dynamics*, Missouri, USA, 26 April-3 May 1981.
- Campbell, K. W., and Bozorgnia, Y., 2008, NGA ground motion model for the geometric mean horizontal component of PGA, PGV, PGD and 5% damped linear elastic response spectra for periods ranging from 0.01 to 10 s: *Earthquake Spectra*, v. 24, no. 1, p. 139-171.
- Casagrande, A., The determination of pre-consolidation load and its practical significance, *in Proceedings Proc. Int. Conf. Soil Mech. Found. Eng.* Cambridge, Mass., 1936-1936, Volume 3, p. 60.
- Castro, G., Empirical methods in liquefaction evaluation, *in Proceedings Proceedings of the 1st Annual Leonardo Zeevaert International Conference 1995*, Volume 1, p. 1-41.
- Cetin, K. O., Seed, R. B., Der Kiureghian, A., Tokimatsu, K., Harder Jr, L. F., Kayen, R. E., and Moss, R. E., 2004, Standard penetration test-based probabilistic and deterministic assessment of seismic soil liquefaction potential: *Journal of Geotechnical and Geoenvironmental Engineering*, v. 130, no. 12, p. 1314-1340.
- Chan, A. H.-C., 1988, A unified finite element solution to static and dynamic problems of geomechanics [Ph.D. Dissertation]: University College of Swansea.
- Chintanapakdee, C., Naguit, M., and Charoenyuth, M., Suitable attenuation model for Thailand, *in Proceedings Proc. 14th World Conf. Eqk. Eng 2008*.

- Chiou, B.-J., and Youngs, R. R., 2008, An NGA model for the average horizontal component of peak ground motion and response spectra: *Earthquake Spectra*, v. 24, no. 1, p. 173-215.
- Choobbasti, A., Naghizadehrokni, M., and Rezaei, S., Liquefaction assessment by microtremor measurements in Babol city, *in Proceedings Fifth International Conference on Geotechnique, Construction Materials and Environment 2015*.
- Clough, R. W., and Penzien, J., 1993, *Dynamics of structures*: Edn.: Singapore: McGraw Hill.
- Crouse, C., 1991, Ground-motion attenuation equations for earthquakes on the Cascadia subduction zone: *Earthquake spectra*, v. 7, no. 2, p. 201-236.
- Dafalias, Y. F., and Manzari, M. T., 2004, Simple plasticity sand model accounting for fabric change effects: *Journal of Engineering mechanics*, v. 130, no. 6, p. 622-634.
- Das, B., and Ramana, G., 2011, *Principles of soil dynamics*, 2nd edn. Cengage Learning, Stanford Google Scholar.
- Day, R. W., 2002, *Geotechnical earthquake engineering handbook*, McGraw-Hill.
- Dikmen, Ü., Hasancebi, N., Arisoy, M., and İ, D., 2016, Estimation of Source, Paht and Site Effect From S-Waves of Local Earthquakes in Izmir, Western Turkey: *Jeofizik*, v. 18, no. 1, p. 14-35.
- Duncan, J. M., and Chang, C.-Y., 1970, Nonlinear analysis of stress and strain in soils: *Journal of Soil Mechanics & Foundations Div.*
- El-Hady, S., Fergany, E. A.-A., Othman, A., and Mohamed, G. E. A., 2012, Seismic microzonation of Marsa Alam, Egypt using inversion HVSR of microtremor observations: *Journal of seismology*, v. 16, no. 1, p. 55-66.
- El Hosri, M., Biarez, J., and Hicher, P., Liquefaction characteristics of silty clay, *in Proceedings Proc. Eight World Conf. On Earthquake Eng. Prentice Hall, NJ1984*, p. 277-284.
- Elgamal, A., Yang, Z., and Lu, J., 2006, *Cyclic1D: a computer program for seismic ground response*, Department of Structural Engineering, University of California, San Diego.
- Elgamal, A., Yang, Z., Parra, E., and Ragheb, A., 2003, Modeling of cyclic mobility in saturated cohesionless soils: *International Journal of Plasticity*, v. 19, no. 6, p. 883-905.
- Fenton, C. H., Charusiri, P., and Wood, S., 2003, Recent paleoseismic investigations in Northern and Western Thailand: *Annals of Geophysics*, v. 46, no. 5.
- Fernández, J., Hermanns, L., Fraile, A., Alarcón, E., and Del Rey, I., 2011, Spectral-analysis-surface-waves-method in ground characterization: *Procedia Engineering*, v. 10, p. 3202-3207.
- Finn, W., Lee, M. K., and Martin, G. R., Comparison of dynamic analyses for saturated sands, *in Proceedings Earthquake Engineering and Soil Dynamics: 1978*, ASCE, p. 472-491.
- Finn, W. D. L., Lee, K. W., and Martin, G., 1977, An effective stress model for liquefaction: *Electronics Letter*, v. 103, no. ASCE 13008 Proceeding.
- Frankel, A., Harmsen, S., Mueller, C., Calais, E., and Haase, J., 2011, Seismic hazard maps for Haiti: *Earthquake Spectra*, v. 27, no. S1, p. S23-S41.

- García-Jerez, A., Piña-Flores, J., Sánchez-Sesma, F. J., Luzón, F., and Pertou, M., 2016, A computer code for forward calculation and inversion of the H/V spectral ratio under the diffuse field assumption: *Computers & Geosciences*, v. 97, p. 67-78.
- Gauchan, J., 1984, Liquefaction tests on sand using a cyclic triaxial apparatus [M.Eng Thesis]: Asian Institute of Technology.
- GERD, 2014, Liquefaction Evidences in the Northern Thailand: Faculty of Engineering.
- Gopalakrishna, G., and Namdar, A., 2009, Stability Analysis of the Embankment Model: *Buletinul Institutului Politehnic din Iasi. Sectia Constructii, Arhitectura*, v. 55, no. 4, p. 9.
- Gosar, A., 2010, Site effects and soil-structure resonance study in the Kobarid basin (NW Slovenia) using microtremors: *Natural hazards and earth system sciences*, v. 10, no. 4, p. 761.
- Gupta, M. K., 1977, Liquefaction of sands during earthquakes.
- Hardin, B. O., and Drnevich, V. P., 1972, Shear modulus and damping in soils: design equations and curves: *Journal of Soil Mechanics & Foundations Div*, v. 98, no. sm7.
- Hashash, Y., Musgrove, M., Harmon, J., Groholski, D., Phillips, C., and Park, D., 2015, DEEPSOIL 6.1, User manual: Board of Trustees of University of Illinois at Urbana-Champaign, Urbana.
- Hashash, Y. M., and Park, D., 2001, Non-linear one-dimensional seismic ground motion propagation in the Mississippi embayment: *Engineering Geology*, v. 62, no. 1, p. 185-206.
- Housner, T. J., Jennings, P., and Tsai, N., Simulated earthquake motions for design purposes, *in Proceedings Proc. 4th World Conference On Earthquake Engineering 1969*.
- Hsu, C.-C., and Vucetic, M., 2006, Threshold shear strain for cyclic pore-water pressure in cohesive soils: *Journal of Geotechnical and Geoenvironmental Engineering*, v. 132, no. 10, p. 1325-1335.
- Huang, H.-C., and Tseng, Y.-S., 2002, Characteristics of soil liquefaction using H/V of microtremors in Yuan-Lin area, Taiwan: *Terrestrial, Atmospheric and Oceanic Sciences*, v. 13, no. 3, p. 325-338.
- Hughes, T. J., 1987, *The finite element method: linear static and dynamic finite element analysis*, Courier Corporation.
- Hwang, J.-H., Yang, C.-W., and Juang, D., 2004, A practical reliability-based method for assessing soil liquefaction potential: *Soil Dynamics and Earthquake Engineering*, v. 24, no. 9, p. 761-770.
- Iai, S., 1993, Micromechanical background to a strain space multiple mechanism model for sand: *Soils and Foundations*, v. 33, no. 1, p. 102-117.
- Iai, S., Kameoka, T., and Matsunaga, Y., 1993, Numerical (Class A) prediction of Model No 1: Verification of Numerical Procedures for the Analysis of Soil Liquefaction Problems (VELACS), Balkema, p. 939-946.
- Iai, S., Matsunaga, Y., and Kameoka, T., 1992a, Analysis of undrained cyclic behavior of sand under anisotropic consolidation: *Soils and Foundations*, v. 32, no. 2, p. 16-20.
- , 1992b, Strain space plasticity model for cyclic mobility: *Soils and Foundations*, v. 32, no. 2, p. 1-15.

- ICC, 2009, International Code Council: International Building Code. International Code Council: Washington DC, United States.
- Idriss, I., 1993, Procedures for Selecting Earthquake Ground Motions at Rock Sites, US Department of Commerce, National Institute of Standards and Technology.
- , 1999, An update to the Seed-Idriss simplified procedure for evaluating liquefaction potential: Proc., TRB Workshop on New Approaches to Liquefaction, Publ. n. FHWA-RD-99-165, Federal Highway Administration.
- , 2008, An NGA empirical model for estimating the horizontal spectral values generated by shallow crustal earthquakes: *Earthquake Spectra*, v. 24, no. 1, p. 217-242.
- Idriss, I., and Boulanger, R., 2006, Semi-empirical procedures for evaluating liquefaction potential during earthquakes: *Soil Dynamics and Earthquake Engineering*, v. 26, no. 2, p. 115-130.
- , 2010, SPT-based liquefaction triggering procedures: Rep. UCD/CGM-10, v. 2.
- Idriss, I., and Boulanger, R. W., 2008, Soil liquefaction during earthquakes.
- Idriss, I., and Sun, J. I., 1992, SHAKE91: A computer program for conducting equivalent linear seismic response analyses of horizontally layered soil deposits: Center for Geotechnical Modeling, Department of Civil and Environmental Engineering, University of California, Davis, CA.
- Ishibashi, I., Sherif, M., and Tsuchiya, C., 1977, Pore-pressure rise mechanism and soil liquefaction: *Soils and Foundations*, v. 17, no. 2, p. 17-27.
- Ishihara, K., 1978, Introduction to dynamic soil mechanism, January.
- Ishihara, K., Tatsuoka, F., and Yasuda, S., 1975, Undrained deformation and liquefaction of sand under cyclic stresses: *Soils and foundations*, v. 15, no. 1, p. 29-44.
- Ishihara, K., Yoshida, N., and Tsujino, S., Modelling of stress-strain relations of soils in cyclic loading, *in* Proceedings International conference on numerical methods in geomechanics 1985, p. 373-380.
- Iwan, W. D., On a class of models for the yielding behavior of continuous and composite systems 1967, ASME.
- Iwasaki, T., 1986, Soil liquefaction studies in Japan: state-of-the-art: *Soil Dynamics and Earthquake Engineering*, v. 5, no. 1, p. 2-68.
- Jones, R., 1958, In-situ measurement of the dynamic properties of soil by vibration methods: *Geotechnique*, v. 8, no. 1, p. 1-21.
- Joshi, A., Kumar, A., Lomnitz, C., Castaños, H., and Akhtar, S., 2012, Applicability of attenuation relations for regional studies: *Geofísica internacional*, v. 51, no. 4, p. 349-363.
- Joyner, W. B., and Chen, A. T., 1975, Calculation of nonlinear ground response in earthquakes: *Bulletin of the Seismological Society of America*, v. 65, no. 5, p. 1315-1336.
- Juang, C. H., Ching, J., Luo, Z., and Ku, C.-S., 2012, New models for probability of liquefaction using standard penetration tests based on an updated database of case histories: *Engineering geology*, v. 133, p. 85-93.
- Juang, C. H., Li, D. K., Fang, S. Y., Liu, Z., and Khor, E. H., 2008, Simplified procedure for developing joint distribution of a max and M w for probabilistic liquefaction hazard analysis: *Journal of Geotechnical and Geoenvironmental Engineering*, v. 134, no. 8, p. 1050-1058.

- Kanai, K., 1951, Relation between the nature of surface layer and the amplitudes of earthquake motions: Bulletin Tokyo Earthquake Research Institute.
- Kazama, M., Yamaguchi, A., and Yanagisawa, E., 2000, Liquefaction resistance from a ductility viewpoint: *Soils and Foundations*, v. 40, no. 6, p. 47-60.
- Koçkar, M., and Akgün, H., 2012, Evaluation of the site effects of the Ankara basin, Turkey: *Journal of Applied Geophysics*, v. 83, p. 120-134.
- Kondner, R. L., 1963, A hyperbolic stress-strain formulation for sands, Northwestern University.
- Kramer, S. L., 1996, *Geotechnical earthquake engineering*, Pearson Education India.
- Kumar, S., 2001, Reducing liquefaction potential using dynamic compaction and construction of stone columns: *Geotechnical and Geological Engineering*, v. 19, no. 2, p. 169-182.
- Lachet, C., and Bard, P.-Y., 1994, Numerical and theoretical investigations on the possibilities and limitations of Nakamura's technique: *Journal of Physics of the Earth*, v. 42, no. 5, p. 377-397.
- Lachet, C., Hatzfeld, D., Bard, P.-Y., Theodulidis, N., Papaioannou, C., and Savvaidis, A., 1996, Site effects and microzonation in the city of Thessaloniki (Greece) comparison of different approaches: *Bulletin of the Seismological Society of America*, v. 86, no. 6, p. 1692-1703.
- Ladd, R. S., Dobry, R., Dutko, P., Yokel, F., and Chung, R., 1989, Pore-water pressure buildup in clean sands because of cyclic straining: *Geotechnical Testing Journal*, v. 1, no. 12, p. 77-86.
- Lai, C. G., 2000, Spectral analysis of surface waves active methods technical recommendations: *Rivista Italiana di geotecnica*, v. 4.
- Lai, S.-Y., Chang, W.-J., and Lin, P.-S., 2006, Logistic regression model for evaluating soil liquefaction probability using CPT data: *Journal of Geotechnical and Geoenvironmental Engineering*, v. 132, no. 6, p. 694-704.
- Laird, J., and Stokoe, K., 1993, Dynamic properties of remolded and undisturbed soil samples tested at high confining pressures: *Geotechnical Engineering Report GR93-6*, Electrical Power Research Institute, Palo Alto, California.
- Lee, K. L., and Albaisa, A., Earthquake induced settlements in saturated sands: 9F, 2T, 29R. *J. GEOTECH. ENGN. DIV. V100, N. GT4, APR. 1974, P387-406*, in *Proceedings International Journal of Rock Mechanics and Mining Sciences & Geomechanics Abstracts 1974*, Volume 11, Pergamon, p. A164.
- Lee, K. L., and Seed, H. B., 1960, Cyclic stress conditions causing liquefaction of sand.
- Lee, M. K., and Finn, W. L., 1978, DESRA-2: Dynamic effective stress response analysis of soil deposits with energy transmitting boundary including assessment of liquefaction potential, Department of Civil Engineering, University of British Columbia.
- Liou, C., Streeter, V., and Richart Jr, F., 1977, NUMREICAL MODEL FOR LIQUEFACTION: *Journal of Geotechnical and Geoenvironmental Engineering*, v. 103, no. ASCE 12998 Proceeding.
- Lukkunaprasit, P., Ruangrassamee, A., Boonyatee, T., Chintanapakdee, C., Jankaew, K., Thanasisathit, N., and Chandrangsu, T., 2016, Performance of Structures in the Mw 6.1 Mae Lao Earthquake in Thailand on May 5, 2014 and Implications for Future Construction: *Journal of Earthquake Engineering*, v. 20, no. 2, p. 219-242.

- Manzari, M. T., and Dafalias, Y. F., 1997, A critical state two-surface plasticity model for sands: *Geotechnique*, v. 47, no. 2, p. 255-272.
- Martin, G. R., Finn, W. L., and Seed, H. B., 1975, Fundamentals of liquefaction under cyclic loading: *Journal of Geotechnical and Geoenvironmental Engineering*, v. 101, no. ASCE# 11231 Proceeding.
- Mase, L. Z., 2017, Shaking Table Test of Soil Liquefaction in Southern Yogyakarta INTERNATIONAL JOURNAL OF TECHNOLOGY, v. 8, no. 4, p. 747-760.
- Mase, L. Z., Likitlersuang, S., Soralump, S., and Tobita, T., 2015, Empirical Study of Liquefaction Potential in Chiang Rai Province in the North of Thailand, The 28th KKHTCNN Symposium on Civil Engineering: Bangkok, 16-17 November.
- Mase, L. Z., Tobita, T., and Likitlersuang, S., 2016, Liquefaction Potential in Chiang Rai Province, Northern Thailand due to 6.8 Mw Earthquake On March 24, 2011, The 36th JSCE Conference on Earthquake Engineering: Kanazawa, Japan, JSCE.
- Masing, G., Eigenspannungen und verfestigung beim messing, *in* Proceedings Proceedings, second international congress of applied mechanics 1926, p. 332-335.
- Matasovic, N., 1993, Seismic Response of Composite Horizontally-layered Soil Deposits, Los Angeles, California: University of California at Los Angeles: Ph. D. thesis, 449p.
- McCaffrey, R., 1996, Slip partitioning at convergent plate boundaries of SE Asia: Geological Society, London, Special Publications, v. 106, no. 1, p. 3-18.
- McGuire, R. K., 1977, Seismic design spectra and mapping procedures using hazard analysis based directly on oscillator response: *Earthquake Engineering & Structural Dynamics*, v. 5, no. 3, p. 211-234.
- Miller, R. D., Xia, J., Park, C. B., Ivanov, J., and Williams, E., 1999, Using MASW to map bedrock in Olathe, Kansas, SEG Technical Program Expanded Abstracts 1999, Society of Exploration Geophysicists, p. 433-436.
- Morita, T., Iai, S., Liu, H., Ichii, K., and Sato, Y., 1997, Simplified method to determine parameter of FLIP: Technical note of the Port and Harbour Research Institute, no. 869.
- Mroz, Z., 1967, On the description of anisotropic workhardening: *Journal of the Mechanics and Physics of Solids*, v. 15, no. 3, p. 163-175.
- Mróz, Z., Norris, V., and Zienkiewicz, O., 1978, An anisotropic hardening model for soils and its application to cyclic loading: *International Journal for Numerical and Analytical Methods in Geomechanics*, v. 2, no. 3, p. 203-221.
- Naito, S., Azuma, H., Senna, S., Yoshizawa, M., Nakamura, H., Hao, K. X., Fujiwara, H., Hirayama, Y., Yuki, N., and Yoshida, M., 2013, Development and testing of a mobile application for recording and analyzing seismic data: *Journal of Disaster Research*, v. 8, no. 5.
- Nakamura, Y., 1989, A method for dynamic characteristics estimation of subsurface using microtremor on the ground surface: Railway Technical Research Institute, Quarterly Reports, v. 30, no. 1.
- , Seismic vulnerability indices for ground and structures using microtremor, *in* Proceedings World Congress on Railway Research in Florence, Italy 1997.

- Okamura, M., and Teraoka, T., 2006, Shaking table tests to investigate soil desaturation as a liquefaction countermeasure, *Seismic Performance and Simulation of Pile Foundations in Liquefied and Laterally Spreading Ground*, p. 282-293.
- Ornthammarath, T., 2013, A note on the strong ground motion recorded during the Mw 6.8 earthquake in Myanmar on 24 March 2011: *Bulletin of Earthquake Engineering*, p. 1-14.
- Ornthammarath, T., and Warnitchai, P., 2016, 5 May 2014 MW 6.1 Mae Lao (Northern Thailand) Earthquake: Interpretations of Recorded Ground Motion and Structural Damage: *Earthquake Spectra*, v. 32, no. 2, p. 1209-1238.
- Ornthammarath, T., Warnitchai, P., Worakanchana, K., Zaman, S., Sigbjörnsson, R., and Lai, C. G., 2011, Probabilistic seismic hazard assessment for Thailand: *Bulletin of Earthquake Engineering*, v. 9, no. 2, p. 367-394.
- Özener, P. T., Özyayın, K., and Berilgen, M. M., 2009, Investigation of liquefaction and pore water pressure development in layered sands: *Bulletin of Earthquake Engineering*, v. 7, no. 1, p. 199-219.
- Pailoplee, S., Channarong, P., and Chutakositkanon, V., 2013, Earthquake Activities in the Thailand-Laos-Myanmar Border Region: A Statistical Approach: *Terrestrial, Atmospheric & Oceanic Sciences*, v. 24, no. 4.
- Park, D., and Hashash, Y. M., 2004, Soil damping formulation in nonlinear time domain site response analysis: *Journal of Earthquake Engineering*, v. 8, no. 02, p. 249-274.
- Parra, E., 1996, Numerical modeling of liquefaction and lateral ground deformation including cyclic mobility and dilation response in soil systems [Ph.D. Dissertation]: Rensselaer polytechnic Institute.
- Pattararattanakul, P., 2003, Liquefaction resistance of sands in the northern part of Thailand [Ph.D. Dissertation]: Chulalongkorn University.
- Peacock, W. H., and Seed, H. B., 1968, Sand liquefaction under cyclic loading simple shear conditions: *Journal of Soil Mechanics & Foundations Div.*
- Pender, M., Orense, R., Wotherspoon, L., and Storie, L., 2016, Effect of permeability on the cyclic generation and dissipation of pore pressures in saturated gravel layers.
- Pongvithayapanu, P., and Teachavorasinskun, S., 2010, Local Site Response on Simulated Strong Earthquake Motion at Laem Chabang Port, Thailand: *Journal of Applied Geology*, v. 2, no. 3.
- Poovarodom, N., and Pitakwong, K., Microtremor observations for site characterization in Thailand, *in Proceedings Proceeding of the 3rd Asia conference on earthquake engineering (ACEE2010)2010*, p. 1-3.
- Prevost, J. H., 1985, A simple plasticity theory for frictional cohesionless soils: *International Journal of Soil Dynamics and Earthquake Engineering*, v. 4, no. 1, p. 9-17.
- , 1989, DYNA1D: a computer program for nonlinear seismic site response analysis technical documentation, National Center for Earthquake Engineering Research.
- Raptakis, D., Manakou, M., Chávez-García, F., Makra, K., and Pitilakis, K., 2005, 3D configuration of Mygdonian basin and preliminary estimate of its site response: *Soil Dynamics and Earthquake Engineering*, v. 25, no. 11, p. 871-887.

- Richart, F. E., Hall, J. R., and Woods, R. D., 1970, *Vibrations of soils and foundations*, New Jersey, USA, Prentice Hall.
- Robertson, P., Woeller, D., and Finn, W., 1992, Seismic cone penetration test for evaluating liquefaction potential under cyclic loading: *Canadian Geotechnical Journal*, v. 29, no. 4, p. 686-695.
- Robertson, P., and Wride, C., 1998, Evaluating cyclic liquefaction potential using the cone penetration test: *Canadian Geotechnical Journal*, v. 35, no. 3, p. 442-459.
- Roesset, J. M., and Whitman, R. V., 1969, *Theoretical background for amplification studies*, Massachusetts Institute of Technology.
- Ruangrassamee, A., Ornthammarath, T., and Lukkunaprasit, P., Damage due to 24 March 2011 M6. 8 Tarlay earthquake in Northern Thailand, *in Proceedings Proceeding of the 15th world conference in earthquake engineering (15WCEE)*: Lisbon, Portugal2012.
- Sabetta, F., and Pugliese, A., 1987, Attenuation of peak horizontal acceleration and velocity from Italian strong-motion records: *Bulletin of the Seismological Society of America*, v. 77, no. 5, p. 1491-1513.
- Sadigh, K., Chang, C.-Y., Egan, J., Makdisi, F., and Youngs, R., 1997, Attenuation relationships for shallow crustal earthquakes based on California strong motion data: *Seismological research letters*, v. 68, no. 1, p. 180-189.
- Salençon, J., 2012, *Handbook of continuum mechanics: general concepts thermoelasticity*, Springer Science & Business Media.
- Sawada, S., Ozutsumi, O., and Iai, S., Analysis of liquefaction induced residual deformation for two types of quay wall: analysis by "FLIP", *in Proceedings Proceedings of the 12th World Conference on Earthquake Eng. ; Auckland2000*, p. 2486.
- Schnable, P. B., Lysmer, J., and Seed, H. B., 1972, SHAKE-A computer program for earthquake response analysis of horizontally layered sites: *EERC Report*, v. 72, no. 12.
- Seed, H., and Idriss, I., 1970, Soil moduli and damping factors for dynamic analysis. Report No. EERC 70-10: University of California, Berkeley.
- Seed, H. B., and Booker, J. R., 1977, Stabilization of potentially liquefiable sand deposits using gravel drains: *Journal of Geotechnical and Geoenvironmental Engineering*, v. 103, no. ASCE 13050.
- Seed, H. B., and Idriss, I. M., 1971, Simplified procedure for evaluating soil liquefaction potential: *Journal of Soil Mechanics & Foundations Div.*
- , 1982, *Ground motions and soil liquefaction during earthquakes*, Earthquake Engineering Research Institute.
- Seed, H. B., Martin, P. P., and Lysmer, J., 1976, Pore-water pressure changes during soil liquefaction: *Journal of Geotechnical and Geoenvironmental Engineering*, v. 102, no. Proc. Paper# 12074.
- Seed, H. B., and Peacock, W. H., 1971, Test procedures for measuring soil liquefaction characteristics: *Journal of Soil Mechanics & Foundations Div.*
- Seed, H. B., Tokimatsu, K., Harder, L., and Chung, R. M., 1985, Influence of SPT procedures in soil liquefaction resistance evaluations: *Journal of Geotechnical Engineering*, v. 111, no. 12, p. 1425-1445.

- Seed, H. B., Wong, R. T., Idriss, I., and Tokimatsu, K., 1986, Moduli and damping factors for dynamic analyses of cohesionless soils: *Journal of Geotechnical Engineering*, v. 112, no. 11, p. 1016-1032.
- Seed, R. B., Cetin, K. O., Moss, R. E., Kammerer, A. M., Wu, J., Pestana, J. M., Riemer, M. F., Sancio, R. B., Bray, J. D., and Kayen, R. E., Recent advances in soil liquefaction engineering: a unified and consistent framework, *in Proceedings Proceedings of the 26th Annual ASCE Los Angeles Geotechnical Spring Seminar: Long Beach, CA2003.*
- SESAME, W., 2004, Guidelines for the implementation of the H/V spectral ratio technique on ambient vibrations-Measurements, processing and interpretation. SESAME European research project, Deliverable D23. 12., Project No: EVG1-CT-2000-00026 SESAME, 62 pp.
- Sherif, M. A., ISHIBASHI, I., and TSUCHIYA, C., 1978, Pore-pressure prediction during earthquake loadings: *Soils and Foundations*, v. 18, no. 4, p. 19-30.
- Shibata, T., and Soelarno, D. S., Stress-strain characteristics of sands under cyclic loading, *in Proceedings Proceedings of the Japan Society of Civil Engineers1975, Volume 1975, Japan Society of Civil Engineers*, p. 57-65.
- Shibata, T., Yukitomo, H., and Miyoshi, M., 1972, Liquefaction process of sand during cyclic loading: *Soils and Foundations*, v. 12, no. 1, p. 1-16.
- Silver, M. L., and Seed, H. B., 1971, Volume changes in sands during cyclic loading: *Journal of Soil Mechanics & Foundations Div.*
- Singh, H., Maheshwari, B., and Saran, S., Liquefaction Behavior of the Solani Sand using Small Shake Table, *in Proceedings The 12th International Conference of International Association for Computer Methods and Advances in Geomechanics [IACMAG]2008*, p. 2797-2803.
- Sonmez, H., and Gokceoglu, C., 2005, A liquefaction severity index suggested for engineering practice: *Environmental Geology*, v. 48, no. 1, p. 81-91.
- Soralump, S., and Feungaugorn, J., 2013, Probabilistic Analysis of Liquefaction Potential: The First Eyewitness Case In Thailand, *NCCE 18th: Chiang Mai. Thailand*, p. 301-307.
- Soralump, S., Feungaugorn, J., Yangsanphu, S., Jinagoolwipat, M., Thongthamchart, C., and Isaroranit, R., Impacts of 2014 Chiangrai earthquake from geotechnical perspectives, *in Proceedings EIT-JSCE joint international symposium on human resource development for disaster-resilient Countries, Bangkok, Thailand, 2014.*
- Spudich, P., Fletcher, J. B., Hellweg, M., Boatwright, J., Sullivan, C., Joyner, W., Hanks, T., Boore, D. M., McGarr, A., and Baker, L., 1997, SEA96—A new predictive relation for earthquake ground motions in extensional tectonic regimes: *Seismological Research Letters*, v. 68, no. 1, p. 190-198.
- Stafford, P. J., Strasser, F. O., and Bommer, J. J., 2008, An evaluation of the applicability of the NGA models to ground-motion prediction in the Euro-Mediterranean region: *Bulletin of earthquake Engineering*, v. 6, no. 2, p. 149-177.
- Stokoe, K. H., Roesset, J., Bierschwale, J., and Aouad, M., Liquefaction potential of sands from shear wave velocity, *in Proceedings Proceedings, 9nd World Conference on Earthquake1988, Volume 13*, p. 213-218.

- Sykora, D., 1987, Creating of a Data Base of Seismic Shear Wave Velocities For Correction Analysis. Geotechnical Laboratory Miscellaneous Paper GL 87-26: US Army Engineer Waterways Experiment Station, Vicksburg, MS.
- Sykora, D., and Stokoe, K., 1983, Correlations of in situ measurements in sands of shear wave velocity, soil characteristics, and site conditions, Report GR 83-33: Soil Dynamics and Earthquake Engineering v. 20, no. 1, p. 125–136.
- Tanapalungkorn, W., and Teachavorasinskun, S., 2015, Liquefaction Susceptibility Due To Earthquake In Northern Parts Of Thailand, the 20th National Convention of Civil Engineering (NCCE): Chonburi, Thailand.
- Tatham, R. H., 1982, V p/V s and lithology: Geophysics, v. 47, no. 3, p. 336-344.
- Tatsuoka, F., and Silver, M. L., 1981, Undrained stress-strain behavior of sand under irregular loading: Soils and Foundations, v. 21, no. 1, p. 51-66.
- TDMR, 2016, Thailand Geological Map, Thailand Department of Mineral Resources, Bangkok, Thailand.
- TDS, 2009, Seismic design code of Thailand. Department of Public Works and Town-Country Planning, *in* Ministry of Interior, T. i. T., ed.
- Teachavorasinskun, S., Pattararattanakul, P., and Pongvithayapranu, P., 2009, Liquefaction susceptibility in the Northern provinces of Thailand: American Journal of Engineering and Applied Sciences, v. 2, no. 1.
- Thitimakorn, T., and Channoo, S., 2012, Shear Wave Velocity of Soils and NEHRP Site Classification Map of Chiang Rai City, Northern Thailand: Electronic Journal of Geotechnical Engineering, v. 17, p. 2891-2904.
- TMD, 2015, Seismological Bureau (Earthquake Data of March 24, 2011 Earthquake), Thai Meteorological Department.
- Tobita, T., and Iai, S., 2007, Failure Mechanism of An Embankment Resting on Liquefiable Ground, The 4th International Conference on Earthquake Geotechnical Engineering: Thessaloniki, Greece.
- Tokimatsu, K., 1979, Generation and dissipation of pore water pressures in sand deposits during earthquakes: Dr. Eng. Thesis, Tokyo Institute of Technology.
- Toro, G. R., 2002, Modification of the Toro et al.(1997) attenuation equations for large magnitudes and short distances: Risk Engineering, Boulder, Colorado.
- Towhata, I., 2008, Geotechnical earthquake engineering, Springer Science & Business Media.
- Towhata, I., and Ishihara, K., Modelling soil behavior under principal stress axes rotation, *in* Proceedings International conference on numerical methods in geomechanics1985, p. 523-530.
- Tsuchida, H., Prediction and countermeasure against the liquefaction in sand deposits, *in* Proceedings Abstract of the seminar in the Port and Harbor Research Institute1970, p. 31-333.
- Ueda, K., Iai, S., Tobita, T., and Ozutsumi, O., Applicability of Multi-spring Model Based on Finite Strain Theory to Seismic Behavior of Embankment on Liquefiable Sand Deposit, *in* Proceedings The 15th World Conference on Earthquake Engineering, Portugal, 2012.
- Ukritchon, B., and Sangkhawilai, T., 2004, An Analysis of Liquefaction Potential For Bangkok First Sand Layer, The 14th National Convention of Civil Engineering: Thailand, NCCE.

- Unno, T., Kazama, M., Uzuoka, R., and Sento, N., 2008, Liquefaction of unsaturated sand considering the pore air pressure and volume compressibility of the soil particle skeleton: *Soils and Foundations*, v. 48, no. 1, p. 87-99.
- Vucetic, M., and Dobry, R., 1991, Effect of soil plasticity on cyclic response: *Journal of geotechnical engineering*, v. 117, no. 1, p. 89-107.
- Wang, L.-y., and Iai, S., 2014, Numerical Study on Seismic Performances of Geogrid Reinforced Soil Retaining Walls in Liquefiable Backfill Sand: *Journal of Engineering Science and Technology Review*, v. 7, no. 1, p. 109-115.
- Wang, M., Chen, G., and Iai, S., 2013, Seismic performances of dyke on liquefiable soils: *Journal of Rock Mechanics and Geotechnical Engineering*, v. 5, no. 4, p. 294-305.
- Wang, W., 1979, Some findings in soil liquefaction, Earthquake Engineering Department, Water Conservancy and Hydroelectric Power Scientific Research Institute.
- Wathelet, M., 2008, An improved neighborhood algorithm: parameter conditions and dynamic scaling: *Geophysical Research Letters*, v. 35, no. 9.
- Yang, J., and Sze, H., 2011, Cyclic behaviour and resistance of saturated sand under non-symmetrical loading conditions: *Géotechnique*.
- Yang, Z., 2000, Numerical modeling of earthquake site response including dilation and liquefaction [Ph.D. Dissertation]: Columbia University.
- Yasuhara, H., Okamura, M., and Kochi, Y., 2008, Experiments and predictions of soil desaturation by air-injection technique and the implications mediated by multiphase flow simulation: *Soils and Foundations*, v. 48, no. 6, p. 791-804.
- Yegian, M., and Vitelli, B., 1981, Analysis for liquefaction: empirical approach.
- Yılmaz, D., Babuçu, F., Batmaz, S., and Kavruk, F., 2008, Liquefaction analysis and soil improvement in Beydag dam: *Geotechnical and Geological Engineering*, v. 26, no. 2, p. 211-224.
- Yoshida, N., 2015, *Seismic Ground Response Analysis*, Springer.
- Youd, T., and Idriss, I., 2001, Liquefaction resistance of soils: summary report from the 1996 NCEER and 1998 NCEER/NSF workshops on evaluation of liquefaction resistance of soils: *Journal of geotechnical and geoenvironmental engineering*, v. 127, no. 4, p. 297-313.
- Youngs, R., Chiou, S.-J., Silva, W., and Humphrey, J., 1997, Strong ground motion attenuation relationships for subduction zone earthquakes: *Seismological Research Letters*, v. 68, no. 1, p. 58-73.
- Yuliyanto, G., Harmoko, U., and Widada, S., 2016, Identification of Potential Ground Motion Using the HVSR Ground Shear Strain Approach in Wirogomo Area, Banyubiru Subdistrict, Semarang Regency: *International Journal of Applied Environmental Sciences*, v. 11, no. 6, p. 1497-1507.
- Zienkiewicz, O., Chan, A., Pastor, M., Paul, D., and Shiomi, T., Static and dynamic behaviour of soils: a rational approach to quantitative solutions. I. Fully saturated problems, *in Proceedings Proceedings of the Royal Society of London A: Mathematical, Physical and Engineering Sciences* 1990, Volume 429, The Royal Society, p. 285-309.
- Zienkiewicz, O., Chang, C., and Hinton, E., 1978, Non-linear seismic response and liquefaction: *International Journal for Numerical and Analytical Methods in Geomechanics*, v. 2, no. 4, p. 381-404.

VITA

Lindung Zalbuin Mase was born in Bengkulu, a Province in Indonesia. He is currently a faculty member in Department of Civil Engineering, University of Bengkulu, Indonesia. He obtained a bachelor of engineering degree from the University of Bengkulu (Indonesia) in 2010 and master of engineering degree from Gadjah Mada University (Indonesia) in 2013. In 2014, he awarded the Ph.D. Sandwich scholarship under AUN/SEED-net JICA to study at Chulalongkorn University (Thailand) and Kyoto University (Japan). He started his Ph.D. course in January 2015, under Prof. Suched Likitlersuang as his advisor and Associate Prof. Dr. Tetsuo Tobita as his co-advisor. During his study, he had published some papers in international journals and international conference proceedings. His main research topic was to investigate the liquefaction potential, local site, and seismic response during the earthquakes in the Northern Thailand.





จุฬาลงกรณ์มหาวิทยาลัย
CHULALONGKORN UNIVERSITY